

TRACKING FLOWS ACROSS A METACOUPLED PLANET FOR SUSTAINABILITY

By

Yingjie Li

A DISSERTATION

Submitted to
Michigan State University
in partial fulfillment of the requirements
for the degree of

Fisheries and Wildlife – Doctor of Philosophy
Environmental Science and Policy—Dual Major

2022

ABSTRACT

TRACKING FLOWS ACROSS A METACOUPLED PLANET FOR SUSTAINABILITY

By

Yingjie Li

In an increasingly interconnected world, supply and demand are largely spatially segregated while reconnected through distant commodity trade and ecosystem service flows. Many of these transboundary flows can generate both positive and negative impacts and lead to trade-offs in achieving different sustainability goals. However, these impacts are largely neglected due to the inherent challenge in identifying and quantifying those transboundary flows. To better understand how the flows connect and impact different systems environmentally and socioeconomically, this dissertation aimed to provide a methodology synthesis for mapping different transboundary flows, and then exemplify the applications in coupled land-water systems (chapter 2), food-environment systems (chapter 3), and intercoupled global socio-environmental systems (chapter 4). This dissertation research applied the integrated framework of metacoupling (human-nature interactions within a system, between adjacent systems, and between distant systems) to systematically uncover the effects of transboundary flows on sustainability across multiple scales. Chapter 2 developed a typology of transboundary flows using six flow attributes (i.e., type, magnitude, direction, distance, time, and mode). Besides, this chapter provided a portfolio of multidisciplinary methods for characterizing transboundary flows, including trade analysis, big data analysis, and various modeling approaches. This synthesis will facilitate quantitative metacoupling research and inform flow-based governance. Chapter 3 revealed the spatiotemporal dynamics of coastal hypoxia (or dead zone) in the Gulf of Mexico across 20 years (2000-2019), and found chlor-a concentrations and sea surface temperatures are the top predictors

of hypoxia, indicating both excess nutrient inflows and climate warming fueled the consequence. This chapter laid a foundation for further linking nutrient hotspots in the watershed with the eutrophicated coasts to predict the timing and amount of nutrient flows for reduction strategies. Chapter 4 tracked the flow of virtual nitrogen (N) embedded in food trade among 132 U.S. regions, and found that 17.1% of the N surplus was induced by food consumption elsewhere but not local. The U.S. Midwest bore most of the N surplus burdens for the nation, with nearly one-third contributed by the lower Mississippi River basin and states other than the basin. This study revealed that downstream food consumers suffering from nutrient pollution are also part of contributors. Chapter 5 comprehensively evaluated a range of transnational flows and their effects on the performance of 17 SDGs for 189 countries globally. It found transnational connections and interactions (e.g., trade) are important for advancing countries' overall SDG performance (improving roughly 20%). Despite the overall benefit, high-income countries generally benefited more, while low-income countries benefited less and were occasionally disadvantaged. The analysis also found that transnational interactions more frequently occurred among distant countries with unequal economic levels. This study offered an integrated picture of the often-ignored transnational impacts on achieving sustainability. This dissertation advanced both theoretical and methodological understanding of transboundary flows in the metacoupled Planet. The cross-scale analysis of measuring multiple transboundary flows and their various socio-environmental impacts on achieving the SDGs will help develop proactive strategies for addressing transboundary challenges, mitigating SDG tradeoffs, and achieving co-benefits toward global sustainability.

This work is dedicated to my dear parents, Renjian Li and Xiaoqing Liu, as well as my beloved Luwen, without whose constant and unconditional support this dissertation was not possible.

ACKNOWLEDGEMENTS

The journey to complete this dissertation and Ph.D. study was full of challenges, happiness, excitement, and achievements. I would not reach this point without the tremendous support, encouragement, and guidance from my advisor, mentors, collaborators, friends, and family.

I would like to first thank my advisor, Dr. Jack Liu, for providing me with this great and unique platform to work with a brilliant team and giving me the full freedom to explore every possibility. He always puts students' work on his top priority list and offers as much help as he can. I still remember there are several times he sent comments back to me more than once a day. Even when he is extremely busy, he can still offer comments on my manuscripts in a week. As a research assistant, I feel I did not do much work for him, but he always worked for me. I have learned so much from him and will carry all the lessons forward in my career and life.

I also would like to thank my committee for their support and advice throughout my Ph.D. training process. I thank Dr. Anthony Kendall for always inviting me to his parties and helping extended my social network to his lab and department. His enthusiasm for science and passion for caring for students in various aspects are so invaluable to me. Thanks for cultivating a so supportive lab atmosphere, which I also benefited a lot directly or indirectly. Thanks, Dr. Emilio Moran, for the tremendous advice on how to be a better and more successful researcher. His experience and wise advice mean a lot to me, and I know he is there for help. Thanks, Dr. Scott Swinton, for admitting me to your class on Research Design and Writing in Applied Economics. This is one of my favorite classes so far, and I learned so much new from him and this class – ranging from how to do rigorous science, how to write a paper, how to do poster/oral

presentations, to how to use social media to disseminate research results. His comments are always critical, constructive, and intriguing.

Thank you also to the members of the Center for Systems Integration and Sustainability (CSIS) at MSU. Particularly, thanks to Zhenci, Hongbo, Min Gon, Anna, Kelly, Ciara, and Wei Liu for the helpful tips and resources, which made my Ph.D. journey so much easier. Thanks, Yuqian, Veronica, and Nan for devoting valuable time to help with my research projects. Thanks, Sue, James, Shuxin, and Jennifer, for the great support in science communication, software, and data management. Thanks, Jill, for the tremendous help throughout my Ph.D. program. She is the first person I talked to at MSU and the kindest person I've ever met. I appreciatively acknowledge the financial support from the Environmental Science and Policy Program (ESPP), State Scholarship Fund, Kellogg Biological Station Long-Term Ecological Research (KBS LTER) Program, William W. and Evelyn M. Taylor Endowed Fellowship, Dissertation Completion Fellowship, and other funds.

Huge thanks to Brain Fath and Ruishan Chen, who are mentors & friends, for providing me with many opportunities outside of MSU. Thanks to my dear friends, Yuqian, Veronica, Ming, Xutong, Yueyue, Kayleigh, and many others who brought so much fun to this journey.

Finally, I would like to thank my parents. They did not go to college, or high school, but they are the most open-minded parents I know. They respect and support any decisions I made, which made them very regretful right now because I fly thousands of miles away and they cannot see me often. I particularly would like to thank my best friend, excellent study pal, and cheerleader – Luwen – for more than 10 years. Thanks for being with me and helping me to be a better person.

PREFACE

The chapters in this dissertation were conceptualized as separate papers and written collaboratively with co-authors. While this research principally represents my own work, I use the pronoun we throughout the dissertation as an acknowledgement of the contributions of my collaborators, without whose contributions and guidance this dissertation would not be possible.

TABLE OF CONTENTS

LIST OF TABLES	xi
LIST OF FIGURES	xii
CHAPTER 1: INTRODUCTION	1
1.1 Background	1
1.2 Theoretical framework	1
1.3 Goal and objectives	2
CHAPTER 2: TRANSBOUNDARY FLOWS IN THE METACOUPLED ANTHROPOCENE: TYPOLOGY, METHODS, AND GOVERNANCE FOR GLOBAL SUSTAINABILITY	5
2.1 Abstract	5
2.2 Introduction	5
2.3 Typology of transboundary flows	8
2.3.1 Flow type	8
2.3.2 Flow magnitude	10
2.3.3 Flow directions	10
2.3.4 Flow distance	11
2.3.5 Flow time	12
2.3.6 Flow mode	12
2.4 Methods for quantifying flows	16
2.4.1 Trade-related flows	16
2.4.2 Passive biophysical flows	19
2.4.3 Human and animal flows	20
2.4.4 Non-material flows	21
2.4.5 Virtual flows	23
2.5 Governance of transboundary flows for global sustainability	27
2.5.1 Growing shocks to transboundary flows	28
2.5.2 System modeling and scenario analysis for understanding dynamic flows and metacouplings	30
2.5.3 Multi-sited, multi-stakeholder, multi-sector, and multi-scale flow-based governance	32
2.6 Concluding remarks	35
CHAPTER 3: MAPPING SPATIOTEMPORAL DYNAMICS OF COASTAL DEAD ZONES OVER 20 YEARS USING REMOTE SENSING	37
3.1 Abstract	37
3.2 Introduction	38
3.3 Materials and methods	41
3.3.1 Study area	41
3.3.2 Field data	42

3.3.3	Satellite data.....	43
3.3.4	Dead zone prediction using satellite imagery	44
3.4	Results	52
3.4.1	Temporal changes of dead zones	52
3.4.2	Spatial changes.....	55
3.5	Discussion	58
3.5.1	Strengths of and uncertainties of using satellite imagery for dead zone prediction	58
3.5.2	Important satellite predictors for dead zone mapping.....	62
3.5.3	Needs for long-term global studies on dead zones and telecoupled land-ocean systems	66
CHAPTER 4: FOOD DEMANDS ELSEWHERE ARE ALSO RESPONSIBLE FOR THE LOCAL FOOD-ENVIRONMENT TRADE-OFFS		69
4.1	Abstract	69
4.2	Introduction	70
4.3	Materials and methods	73
4.3.1	Study area.....	73
4.3.2	Agricultural food flows at subnational levels	74
4.3.3	Measure the shifted environmental burdens carried by food flows	76
4.4	Results	78
4.4.1	Food flows show food production for whom.....	78
4.4.2	Virtual nutrient flows reveal the displaced environmental responsibility	81
4.4.3	Change in food flows can lead to redistribution of N surplus	84
4.5	Discussion	85
4.5.1	Implications of tracking virtual nutrient flows	86
4.5.2	Uncertainty in virtual N surplus estimation	88
4.5.3	Future studies on tracking long-term and cross-scale food footprints.....	89
CHAPTER 5: METACOUPLING IMPACTS ON ACHIEVING NATIONAL SDGS		91
5.1	Abstract	91
5.2	Introduction	92
5.3	Materials and methods	96
5.3.1	SDG Indicators and SDG Index.....	96
5.3.2	Measuring the impacts of transnational interactions (TNIs) on national SDGs	97
5.3.3	Network analysis.....	103
5.4	Results	103
5.4.1	The overall impact of TNIs on SDGs	103
5.4.2	Dominant actors in the global TNIs networks	106
5.4.3	Telecouplings contributed more to SDGs than pericouplings	108
5.5	Discussion	109
CHAPTER 6: SYNTHESIS.....		115
APPENDICES		118
APPENDIX A SUPPORTING INFORMATION FOR CHAPTER 2		119

APPENDIX B SUPPORTING INFORMATION FOR CHAPTER 3	120
APPENDIX C SUPPORTING INFORMATION FOR CHAPTER 4	123
APPENDIX D SUPPORTING INFORMATION FOR CHAPTER 5	127
REFERENCES	153

LIST OF TABLES

Table 2.1. Types of transboundary flows, common spatial levels of analysis, and the quantification methods	15
Table 2.2. Summary of the main global MRIO databases	25
Table 3.1. Data sources	46
Table 4.1. The top 10 net flows of cereal grains (SCTG = 02) in 2017	80
Table A4.0.1. Parameters Used for Calculation of Biological N Fixation	123
Table A4.0.2. Parameters Used for Calculation of Crop N Uptake.....	124
Table A4.0.3. The top 10 net flows of live animals (SCTG = 01) in 2017	125
Table A5.0.4. SDG indicators impacted by transnational interactions	147
Table A5.0.5. Indicators for TNI impacts and detailed data sources.....	150
Table A5.0.6. Country list with country names, ISO3 country code, and income groups	152
Table A5.0.7. Countries and their adjacent neighbors (share land or maritime borders)	152

LIST OF FIGURES

Figure 1.1 Metacoupling framework (adapted from Liu 2017).....	2
Figure 1.2 The metacoupled systems: socioeconomic and environmental interactions within a coupled human-natural system (the watershed per se, e.g., the Mississippi River Basin in the US), between adjacent systems (e.g., the Mississippi River Basin and the Gulf of Mexico), and between distant systems (e.g., US and China).	4
Figure 2.1 Key attributes for characterizing transboundary flows: system boundaries, magnitude, directions, distance, time, and mode of flows. S – sending system, R – receiving systems, Sp – spillover system.....	13
Figure 2.2. Possible flow directions. (a) unidirectional, e.g., river flows; (b) bidirectional, bilateral trade or investment; (c) multidirectional, e.g., trade from one country to multiple countries; (d) omnidirectional – the flows diffuse to the surrounding regions (e.g., carbon emissions).....	14
Figure 2.3. An example of quantifying virtual flows of water, energy, nitrogen, and CO ₂ embedded in food trade by using life cycle assessment (LCA) of irrigated agricultural production. S – sending system, R – receiving systems. The subplot of LCA is adapted from (Xu et al., 2020b).	27
Figure 2.4. Shocks (red icons) and opportunities (blue icons on the top) that might impact transboundary flows and the metacoupled systems. S – sending system, R – receiving systems, Sp – spillover system.....	30
Figure 2.5. Scenario analysis for investigating dynamics of transboundary flows (left), and system sustainability under the UN SDG framework (right). S – sending system, R – receiving systems, Sp – spillover system.	32
Figure 2.6. Multiple interconnected flows across a transboundary river basin. Regions within a river basin are linked through their use of the water (for freshwater, food, and energy), and the impacts they cause through development and pollution (e.g., nutrient pollution, wastewater pollution, freshwater biodiversity, and reduction of sediment supply). Adapted from (UNEP-DHI and UNEP, 2016).	35
Figure 3.1. The geographic location of the water samples, Gulf of Mexico, and the adjacent Mississippi River basin in the US.	42
Figure 3.2. The number of DO sampling locations in the Gulf by years and by sources. Data sources: Louisiana Universities Marine Consortium (LUMCON), Southeast Area Monitoring and Assessment Program (SEAMAP), Texas A&M University (TAMU), University of Maryland Center for Environmental Sciences (UMCES), U.S. Environmental Protection Agency (EPA), and Nutrient Enhanced Coastal Productivity Program (NECOP), and the	

Louisiana Department of Wildlife and Fisheries (LDWF). The maps of sampling locations are shown in Figure A3.0.1.....	43
Figure 3.3. Multiple factors and processes contribute to coastal dead zone	47
Figure 3.4. Flowchart for dead zone prediction with Random Forest Regression (RFR) model. Satellite-derived variables (from MODIS and HYCOM) were integrated with water samples by considering a list of potential time lags.	49
Figure 3.5. Importance score of the selected variables in each lagged Random Forest Regression model. Each panel presents the results from the models with a range of time lags. For example, the panel named “0-5” shows the average variable importance from models with lagged satellite predictors at 1-day lag, 2-day lag, 3-day lag, 4-day lag, and 5-day lag. The error bars represent 95% confidence intervals. <i>Chlor_a</i> – Chlorophyll-a concentration; <i>nflh</i> – Normalized fluorescence line-height; <i>poc</i> – Particulate organic carbon, <i>temp</i> – Sea water temperature, <i>lon</i> – longitude, <i>lat</i> – latitude, <i>xxx_dif</i> – the difference between values on the surface and bottom water, <i>DOY</i> – day of the year. Refer to Table 3.1 for all other variable information. See Figure A3.0.3 for the importance scores of all the 24 pre-selected variables.	49
Figure 3.6. Model performance for DO prediction with satellite predictors at different time lags. Model performance is evaluated by R^2 , RMSE (mg/L), and MAE (mg/L) between estimated and observed DO. Lines represent mean values, and shaded areas around the lines represent 95% confidence intervals. The blue shaded area indicates the dates of satellite predictors that achieved relatively highest accuracy.....	51
Figure 3.7. Annual dead zone area from satellite predictions (2000 - 2019). Dead zone = bottom water hypoxia (< 2 mg/L of dissolved oxygen). The error bars indicate the standard error of predictions (n = 30 days). Because the area of dead zone is changing over time within a year, we used the top 30 maximum dead zone daily predictions during each summertime (note: dead zone usually peaks in summer) to show the standard error of yearly maximum dead zone predictions. The dashed horizontal red line denotes the goal of the Gulf Hypoxia Action Plan to reduce the five-year running average size to less than 5000 km ² . The light-gray line with dots shows the area of hypoxia reported by Rabalais et al (see https://gulfhypoxia.net/research/shelfwide-cruises , no data for 2016). Please note that the estimation by Rabalais et al was based on snapshot data of water measurement and the geospatial interpolation approach, which are not strictly comparable to our results. However, the trends from both studies show similarities.....	53
Figure 3.8. Intra-annual change of dead zones area over summer months. Dots show the estimated dead zone area each day, and darker red colors indicate larger areas of dead zones. Lines represent the smoothed conditional means by the local polynomial regression fitting method. The shaded areas around the lines represent 95% confidence intervals. The dashed horizontal red line denotes the goal of the Gulf Hypoxia Action Plan to reduce the five-year running average size to less than 5000 km ²	54

Figure 3.9. Inter-annual dead zone occurrence (%) during 2000–2019. All of the colored regions demote dead zone occurrence (dissolved oxygen < 2 mg/L).	55
Figure 3.10. The intra-annual dead zone occurrence (a), and the area with over 60% occurrence in each summer (b). All of the colored regions demote dead zone occurrence (dissolved oxygen < 2 mg/L). The dashed horizontal red line denotes the goal of the Gulf Hypoxia Action Plan to reduce the five-year running average size to less than 5000 km ²	56
Figure 3.11. Two demonstrations of the predicted dissolved oxygen (DO) levels in the bottom water. Pixels with DO less than 2 mg/L are classified as dead zones.	62
Figure 3.12. Importance score of the variables in the final Random Forest Regression model. The error bars represent 95% confidence intervals. Chlor_a – Chlorophyll-a concentration; nflh – Normalized fluorescence line-height; poc – Particulate organic carbon, temp – Sea water temperature, lon – longitude, lat – latitude, xxx_dif – the difference between values on the surface and bottom water, DOY – day of the year. Refer to Table 3.1 for all other variable information.	64
Figure 3.13. Temporal changes in chlor_a, (a) sea surface temperature (sst), and (b) nutrient loads (TN) from the Mississippi River basin (orange solid lines) and the Atchafalaya River basin (orange dashed lines)	65
Figure 4.1. Food flows and the embedded nitrogen (N) surplus flows (a), and a conceptual diagram showing N inputs and outputs in the agricultural food production systems (b). In (a), orange arrows represent the direction of food flows, while dashed purple arrows indicate the virtual N footprint (or more broadly known as the environmental impacts) a net food importer imposed on the food exporter regions. The adjacent directed-flows can be viewed as pericouplings, and distant ones can be viewed as telecouplings.	78
Figure 4.2. Top 100 net flows of cereal grains (a) and live animals (b) in 2017. The top 100 account for 84 % and 95% of the total interregional flows of cereal grains and animals, respectively. The deep-dark region represents the Mississippi River basin.	81
Figure 4.3. Top 100 net flows of virtual N surplus embedded in the flows of cereal grains (a) and live animals (b) in 2017. The deep-dark region represents the Mississippi River basin.	83
Figure 4.4. Total N surplus that displaced elsewhere by virtual N sending systems (a), and the total N surplus that is bore by virtual N receiving systems (b). Total N surplus is the sum of those in both cereal grains and animal flows.	83
Figure 4.5. Total N surplus in food production (a), and its change if food supply chains were disrupted (b, and c). NS – N surplus, MRB – Mississippi River basin, USA – United States of America.	85
Figure 4.6. N surplus rate of cereal grains (a) and animals (b) by county	87
Figure 5.1. The overall TNIs on SDG Index and individual SDG scores at the global and national scales in 2015. (a) The overall impacts on each country’s SDG Index (i.e., the aggregated	

mean of the 17 normalized SDG scores to characterize countries' overall SDG performance, see Methods). Positive values mean a country's SDG score benefited from TNIs. (b) The overall impacts on each Goal of the 189 countries. The error bars indicate the standard errors in the SDG scores across countries ($n = 189$). (c) The overall impact on each Goal by country income group. The income group categories are based on the World Bank's classification. The error bars indicate the standard errors in the SDG scores across countries in each income group. Figure A5.0.3 further shows the impacts of TNIs on each SDG at the country level. (d) Percent of improved SDGs from TNIs. SDG Icon images courtesy of the United Nations. . 105

Figure 5.2. Dominant influencer and affected in the global TNIs network. (a) Top 10 and bottom 10 influencers of the 189 countries in 2015, ranked by TNIs index (i.e., aggregated impact scores). Higher values mean larger overall negative impacts on the rest of the world, while lower values indicate smaller overall negative impacts (positive impacts could be offset by other negative impacts). (b) Map of TNIs index by country. Figure A5.0.5 further shows the impact of each TNI. (c) Network of the top 15 country pairs. Arrows point to dominant influencers; The width of the edges represents the magnitude of impact, and the size of each node represents the degree of centrality in the network. The colors indicate income-levels (blue – high-income, red – low-income). Full names of the country codes are listed in Table A5.0.3. (d) Distribution of the average distance of interactions between two countries. “Vertical flows” indicate the interactions between two economically unequal countries (e.g., resource flows from low-income countries to high-income countries), and “Horizontal flows” represent interactions between two countries with similar economic status. The red dash line indicates the average distance of interactions between each country pair. Figure A5.0.6 further illustrates the distance distribution by TNI types. 107

Figure 5.3. SDG Index (a) and the score of each SDG (b) by income group under four scenarios: the real world in 2015 (Real), only distant world connections (Only distant), only nearby world connections (Only nearby), and global lockdown with no connections (None). SDG 17 does not have all four scenarios due to the limited data for countries. 109

Figure A2.0.1. LCA tools, Carbon calculator, GREET (Greenhouse gases, Regulated Emissions, and Energy use in Transportation), GHGenius (focus on transportation fuels in Canada), GaBi Software, SimaPro, OPENLCA, Brightway2. Credits to Dr. Qingshi Tu at the University of British Columbia. 119

Figure A3.0.2. DO sampling locations from 2000 to 2019. 120

Figure A3.0.3. The number of sampling locations by year and by month. 121

Figure A3.0.4. Importance score of selected variables. The top 12 are the selected input variables. 122

Figure A4.0.5. The geographical locations of the Mississippi River Basin (MRB), non-MRB (states with gray shade), the MRB upper (states with green shade), and lower basins (states with red shade). 126

Figure A5.0.6. SDG Index under the baseline scenario (i.e., the current globally metacoupled system), and a hypothetical global lock-down scenario (i.e., no transnational interactions among countries but only domestic activities).....	130
Figure A5.0.7. TNIs on SDG Index by income group in 2015. A value above 0 means a positive impact on a nation's SDG Index, while a value less than 0 indicates a negative impact on a nation's SDG Index. In each boxplot, the central rectangle spans the first quartile Q1 to the third quartile Q3, while the segment inside the rectangle indicates the median. Each dot represents a country.....	131
Figure A5.0.8. Impacts of TNIs on each SDG at the country level.....	132
Figure A5.0.9. Impacts of TNIs by category and by the top 10 and bottom 10 influencers, ranked by TNI impact index (i.e., aggregated impact scores). The plot shows the overall impacts, which means some of the positive impacts could have been offset by other large negative impacts. High values mean larger negative impacts on the rest of the world. Full names of the countries are listed in Table A5.0.3.	133
Figure A5.0.10. Impact of TNIs by country. Refer to Table A5.0.2 for the full name of each impact. Asterisk (*) denotes the displaced footprint or net imported virtual footprint by a country.....	134
Figure A5.0.11. Distribution of the average distance of interactions between two countries, by and by TNI impact indicators.....	135
Figure A5.0.12. SDG scores by income group under four scenarios: the real world in 2015 (Real), only distant world connections (Only distant), only nearby world connections (Only nearby), and global lockdown with no connections (None).	136
Figure A5.0.13. Demonstration of the linkage between SDGs and TNIs. Shown are the 17 SDGs (center), 30 SDG targets (first ring), and 45 SDG indicators (second ring) that relate to 43 specific transnational footprint indicators (third ring). Two SDG indicators under SDG 8 and three SDG indicators for SDG 15 are presented in the figure for a demonstration purpose only. A full list of matched linkages between SDGs and TNIs can be found in Table A5.0.1.	137
Figure A5.0.14. Network for each TNI. Only the top 50 country pairs with the largest TNI flows are presented. The arrows point to the dominant influencers (or responsibility takers); The width of the edges represents the magnitude of impact.	138
Figure A5.0.15. Map of county income group.....	146

CHAPTER 1: INTRODUCTION

1.1 Background

In the increasingly interconnected world, many social and environmental challenges are interlinked not only within a single system but also coupled with adjacent and distal socio-environmental systems. For example, intensive farming in the US Midwest could cause coastal hypoxic zones 1000 miles away in the Gulf of Mexico (Li et al., in review; Rabalais and Turner, 2019), and beef consumption in Europe might lead to deforestation in Brazil (Ermgassen et al., 2020; Nepstad et al., 2014). Existing studies towards understanding these issues tend to be either static (discontinuous observation), isolated (only consider a single system and lack system thinking), or incomplete (focus on one or two aspects of sustainability). Failing to fill these gaps can result in unresolved issues, ineffective policy implementation, and tradeoffs in goal-achieving efforts.

1.2 Theoretical framework

To address the research gaps and often neglected but prominent interregional challenges nearby and faraway, this work aimed to implement the integrated framework of metacoupling.

Metacoupling aims to provide a holistic understanding of the socioeconomic-environmental interactions within a system (intracoupling), between adjacent systems (pericoupling), and between distant systems (telecoupling) (Figure 1.1) (Liu, 2017). These interactions are facilitated by agents and achieved through the flows of material, energy, capital, and information within and between systems. Many metacouplings generate complex and profound socioeconomic and

environmental impacts across local to global scales and impact the progress towards achieving the United Nations Sustainable Development Goals (Liu, 2018; Xu et al., 2020c).

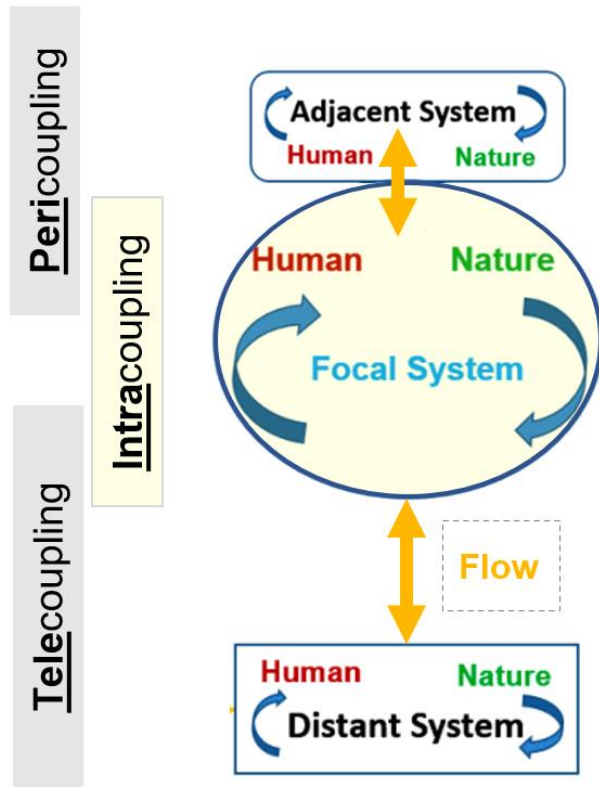


Figure 1.1 Metacoupling framework (adapted from Liu 2017).

1.3 Goal and objectives

The main goal of this dissertation is to exemplify the application of the metacoupling framework using multiple-scale case studies, ranging from local scale (the Gulf of Mexico), regional scale (Mississippi River Basin), national scale (the US), and global scale (Figure 1.2). Each tested different fundamental questions related to system complexity and interactions across systems, time, and scales.

Specifically, this dissertation includes four core chapters (i.e., chapter 2 to chapter 5), and the corresponding objectives are to:

- Develop a typology for transboundary flows and provide a methodologies synthesis for quantifying the flows across metacoupled Anthropocene (chapter 2).
- Investigate the long-term dynamics of the coastal hypoxic zone in the Gulf of Mexico, a major consequence of transboundary flows of excess nutrients from the US Midwest (chapter 3).
- Examine food flows and virtual nitrogen flows at the US subnational level to estimate the extent to which downstream food consumers contribute to and suffer from upstream excess fertilizer use for food, taking the Mississippi River basin as an example (Chapter 4).
- Quantify the impacts of multiple transboundary flows on nations' sustainability performance, covering both environmental and socioeconomic dimensions (chapter 5).

This research contributes to both methodology advances and novel findings in using the metacoupling framework to address pressing sustainability challenges. The chapters especially highlighted the critical role of transboundary flows in connecting and impacting each metacoupled system, and stress the use of system thinking and flow-based governance to inform policy and enhance global sustainability.

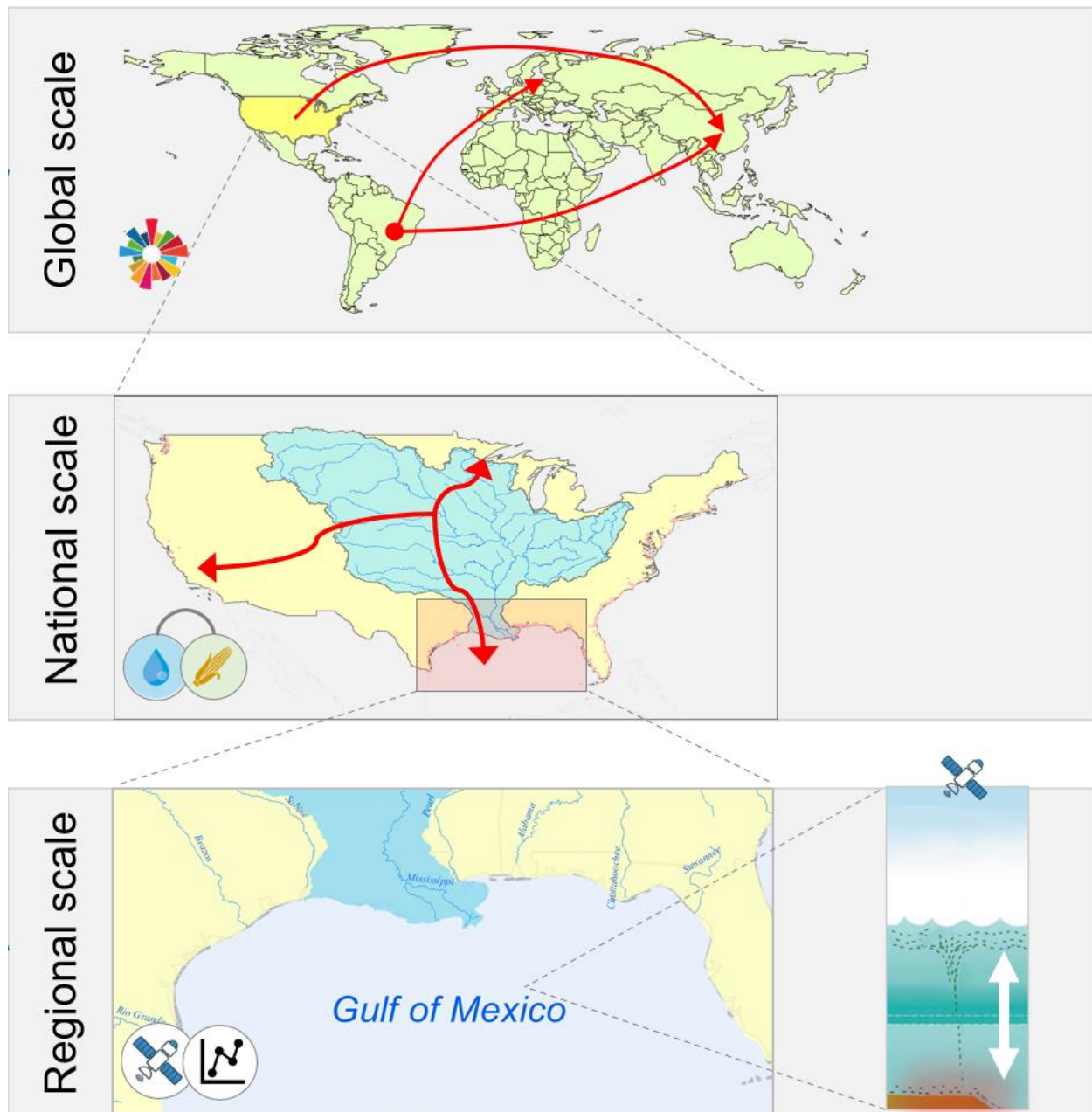


Figure 1.2 The metacoupled systems: socioeconomic and environmental interactions within a coupled human-natural system (the watershed per se, e.g., the Mississippi River Basin in the US), between adjacent systems (e.g., the Mississippi River Basin and the Gulf of Mexico), and between distant systems (e.g., US and China).

CHAPTER 2: TRANSBOUNDARY FLOWS IN THE METACOUPLED ANTHROPOCENE: TYPOLOGY, METHODS, AND GOVERNANCE FOR GLOBAL SUSTAINABILITY

2.1 Abstract

The world has become increasingly metacoupled through interregional flows of materials, energy, people, capital, and information. Transboundary flows, connecting adjacent and distant systems, are deemed the most critical indicators for measuring the intensity of interaction among systems. To advance metacoupling flow research and governance, this synthesis made the first attempt to develop a typology of transboundary flows using six flow attributes (i.e., type, magnitude, direction, distance, time, and mode). Furthermore, this chapter highlighted a portfolio of quantitative and practical methods for characterizing transboundary flows. To effectively govern flows for global sustainability and resilience, it highlighted the need to recognize the shared risks and goals, use system thinking, and enhance multilateral cooperation.

2.2 Introduction

Everything is connected to everything else (Barabási, 2014), and even things far away from each other become increasingly interconnected in the globalized Anthropocene (Kapsar et al., 2019; J. Liu et al., 2015a; Liu et al., 2019). Metacoupling is a newly developed integrated concept that encompasses a broad range of socioeconomic-environmental interactions within a place, between the place and adjacent places, and between the place and distant places (Liu, 2017). These interactions are achieved through the flows of material, energy, capital, and information within and between systems. Many metacouplings generate complex and profound socioeconomic and

environmental impacts across local to global scales and impact the progress towards achieving the United Nations Sustainable Development Goals (Liu, 2018).

The metacoupling framework offers a useful analytical lens for effective sustainability research and policy (Liu, 2017; Liu et al., 2018c; Tromboni et al., 2021). It explicitly views global interlinkages as flows among interconnected system units of analysis, for example, sending, receiving, and spillover systems (Liu, 2017). Sending and receiving systems are entities that send and receive flows of material, energy, products, humans, capital, and information. Spillover systems are entities that affect, or are affected by, interactions between sending and receiving systems. Recent studies have elaborated the key concepts and methodologies for characterizing agents (Dou et al., 2020, 2019), feedback (Hull et al., 2015), and spillover systems in the metacoupling framework (Liu et al., 2018a). These studies, therefore, provided an in-depth understanding of the framework and greatly facilitated the implementation in addressing the world's pressing socio-environmental challenges (Dou et al., 2018; Li, 2021; Yang et al., 2018). Flows, as the most critical component that connects adjacent and distant systems, have also drawn increasing attention. Schröter et al provided a typology for ecosystem service (ES) flows (Schröter et al. 2018), and Koellner et al further provided a guidance for assessing four types ES flows (Koellner et al., 2019). Their work laid a foundation for subsequent applications in investigating interregional flows of multiple ecosystem services (Y. Hou et al., 2020; Klapper and Schröter, 2021; Kleemann et al., 2020; Y. Wang et al., 2022; Wang et al., 2021). However, these studies only focus on a few key ecosystem services-related flows, there is still a lack of comprehensive synthesis for a broader range of transboundary flows across the metacoupled Anthropocene. A recent synthesis found around 40% of telecoupling research only used the

“telecoupling” concept or mentioned the keywords but lack of substantial and quantitative analysis of the telecoupling flows (Kapsar et al., 2019). The lack of corresponding methodologies could be a reason because “telecoupling” and “metacoupling” are still a rather novel framework to the broad scientific community. Another reason could be that traditional approaches such as using statistical data, field observations, and ecological modeling, or one single approach have become insufficient to address the complex metacoupling issues. Although a few new transdisciplinary approaches have been proposed (e.g., citizen science, and big data approaches), related methodologies have been published in dispersed literature (Koellner et al., 2019).

With growing bodies of researchers from different disciplines interested in applying the metacoupling framework to address real-world sustainability issues but encountering methodology challenges, there is a great need to provide methodological guidance for assessing transboundary flows. Closing the gap can have the potential to provide a generalized, quantitative understanding of different types of flows across the metacoupled Anthropocene. Armed with the knowledge, scientists could provide stakeholders with more quantitative and spatially explicit socio-environmental flow information that could be used for facilitating flow-based management and for achieving a range of sustainability goals. To advance the efforts for metacoupling flow research and governance, we aim to: (1) develop a typology of transboundary flows with illustrative examples; (2) highlight methods for investigating the flows; and (3) discuss the usefulness of flow-based governance.

2.3 Typology of transboundary flows

Flows are movements of materials, goods, energy, information, capital, and people between two or more coupled systems. To characterize and quantify the various transboundary flows, we synthesize the existing knowledge and develop a typology using six flow attributes (Figure 2.1). Although we focus on transboundary flows, the typology is also applicable for flows within a system.

Defining system boundaries is critical to disentangle the complexity of various connections among different systems. Depending on questions of interest, system boundary can be defined by political/administrative units (e.g., countries, states, counties, cities), socioeconomic and cultural units (e.g., conservation donor group, indigenous area), management units (e.g., protected areas), or geographical and ecological units (e.g., hydrological units, ecoregions) (Liu et al., 2019; Qin et al., 2022).

2.3.1 *Flow type*

Based on the nature of flows, we divide them into three broad categories.

(1) **Physical flows** include the trade of raw materials and products, interregional flows of energy, water, pollutants/waste, animal migration, species dispersal, as well as disease transmission (Table 2.1). Most of these material and organism flows are overlapped with ecosystem service flows (Schröter et al., 2018). Human flows (including tourism, human migration, and human trafficking) also belong to this category. Human flows can be used to investigate a variety of metacoupling effects. Apart from human flows related to tourism, migration of humans with high intelligence can be used to study the extent to which brain-drain (substantial emigration or

migration of valuable individuals, such as doctors, healthcare professionals, scientists, engineers, or financial professionals) can harm a country's economy and sustainable development (Brücker et al., 2013).

(2) **Non-material flows**, such as financial flows and information flows have emerged to generate unexpected large socio-environmental impacts (Eakin et al., 2014; Jiajia Liu et al., 2022; Qin et al., 2022). For example, the Belt and Road Initiative pledged to invest US\$1 trillion in 138 countries to boost infrastructure and economic development but led to the loss of natural land (Li et al., 2021). Information flows can be in the form of technology transfer, knowledge transfer, and other news or messages that could be spread through media channels or social ties.

(3) **Virtual flows** are also called the embedded resources (or footprints) “hidden” in products (Galli et al., 2012). For example, virtual water is the water “hidden” in the products, services, and processes people buy and use every day. Virtual water often goes unseen by the end-users of a product or service, but that water has been consumed throughout the value chain, which makes the creation of that product or service possible (Allan, 1998; Hoekstra and Hung, 2005). Virtual nitrogen is any nitrogen that was used in the food production process but is not physically contained in the final products (Galloway et al., 2007; Leach et al., 2012). Similarly, virtual flows also cover energy, GHG emissions, and phosphorus. Virtual flow is an important concept to unveil the indirect (or externalized) drivers of local resource problems and pave the way for analyzing what can be done ‘elsewhere’ than locally to improve the sustainability and equity of resource use (Hoekstra, 2017).

2.3.2 *Flow magnitude*

The magnitude of flows is the amount of flows and can be measured by weight (e.g., in kg), volume (e.g., in m³), value (e.g., in \$), and number count. Since sustainability depends on the size of humanity's footprint relative to the Planet's carrying capacity (Hoekstra and Wiedmann, 2014), flow magnitude is the key to estimating the potential impacts on sending systems, receiving systems, or spillover systems with consideration of each system's resource endowment. Data for quantifying the magnitude of flows usually come from the statistical database, field observations, and modeling. Recent developments in big data also provided a rich data source for mining and tracing human movements and information flows. Methodology for quantifying flows will be elaborated in Section 3.

2.3.3 *Flow directions*

Flows can be unidirectional, bidirectional, multidirectional, or omnidirectional (Figure 2.2). For unidirectional, bidirectional flows, and multidirectional it is relatively easy to track the exact direction because the flows usually follow certain pathways that proceed directly between sending and receiving systems, or indirectly between the two by passing through or leaking into the spillover systems (Liu et al., 2018a) (Figure 2.1). The direction of a specific flow determines which system is the sending system and which is the receiving system. For instance, in the case of food flows (food exports from country A to country B), country A is the sending system; while looking at money flows (country B pays country A for food), country A is the receiving system in terms of money. Conventionally, outwards flows are also termed “outflows”, and incoming flows are termed “inflows”. However, it is challenging to track the exact flow directions of omnidirectional diffusions, such as greenhouse gasses and air pollutants. One way

to determine the directions is based on atmospheric currents at broad spatial scales (Schröter et al., 2018). Another way is to identify the source of emissions and treat the surrounding regions as receiving systems without directional bias (Fisher et al., 2009).

2.3.4 *Flow distance*

Distances between systems can be geographical, political, institutional, social, or cultural (Boisso and Ferrantino, 1997; Eakin et al., 2014; Liu, 2017; Liu et al., 2018a; Tadesse and White, 2010; Tromboni et al., 2021). Geographic distance is the most used measurement and is determined by variables such as Euclidean space distance, or dummy variables such as whether sharing common borders (e.g., land border or water border), if having transportation or communication links, and differences in climates (Takayama, 2013). Geographic distance is useful to determine whether a trade flow is a telecoupling or pericoupling process (Xu et al., 2020c). Since geographic distance is usually linked with transportation, it has also been used to estimate environmental costs embedded in product transport. For example, the concept of “food miles” and “footprint distance” has been used to measure the impact of food transport on the environment (Coley et al., 2009; Li et al., 2022).

Other distance measurements, such as cultural distance and administrative distance, have been used for trade analysis and modeling and could be useful for future metacoupling studies beyond international trade. Cultural distance refers to differences in norms, beliefs, and values between countries (Hofstede, 2001). Increasing cultural distance between nations is expected to have a negative effect on trade flows between them since it complicates trade and leads to increased transaction costs (Söderström, 2008). Key attributes creating cultural distance include different

languages, different ethnicities, lack of connective ethnic or social networks (e.g., colony/colonizer), different religions, and different social norms. The administrative distance can be measured by the absence of colonial ties, absence of shared monetary or political association, political hostility, and government policies institutional weakness.

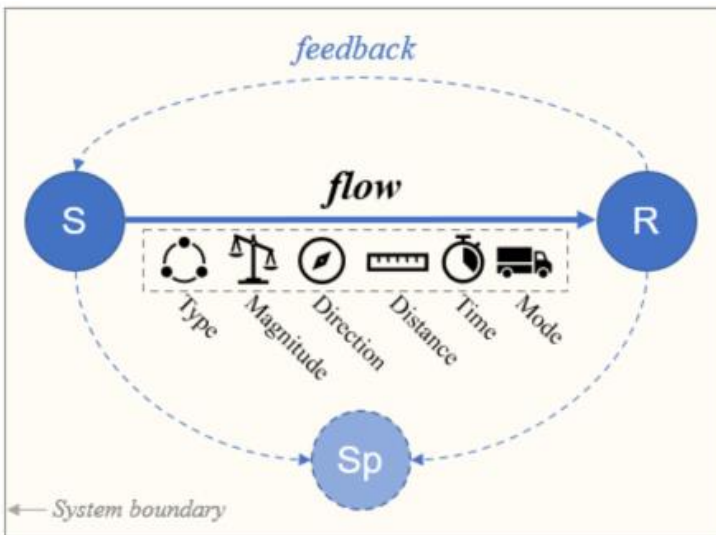
2.3.5 *Flow time*

Temporal dimension of flows describes the timing (e.g., when the flow starts), duration (i.e., from start to end), frequency, and change rate of a targeted flow. Knowing the temporal dynamics of flows can also help understand time lags in the metacoupled human-nature systems (Liu et al., 2007). For example, in a telecoupled system, the sending and receiving systems are usually far away from each other. Therefore, there are usually time lags between changes in the sending system and effects in the receiving system (Rau et al., 2018). For instance, excess fertilizer applied to agricultural land in the US Midwest cannot be immediately observed at the Mississippi River estuary, neither coastal eutrophication nor “dead zones” (Li et al., in review; Meter et al., 2018). Temporal scales of interregional flows vary and largely rely on certain types of flows. For instance, trade-related flows are usually recorded at the annual level, with some at the quarter or month level (USDA ERS, 2022). Physical water flows monitoring can be at daily level or even real-time.

2.3.6 *Flow mode*

Flow mode distinguishes different ways of movement, including several types: (1) trade-related flows depend on man-made carriers (e.g., boats, vehicles, airplanes, pipelines, and cable); (2) passive biophysical flow through ecological processes, for example, water and sediment flows

follow certain hydrological pathways. In some cases, water flow might also follow manmade channels after human intervention. For example, China implemented the South-to-North Water Transfer Project (SNWTP) to divert freshwater from water-abundant southern China to northern China to mitigate water shortages (Xu et al., 2020b; Zhao et al., 2015). (3) movement of people and animals for certain purposes (e.g., tourism, migration) (Chen et al., 2012; Hulina et al., 2017); (4) flows of information and knowledge through man-made communication channels (Schirpke et al., 2019; Schröter et al., 2018). Flow mode is important for characterizing flows and the interactions among systems. Particularly, the reliability of man-made transportation also depends on transport infrastructure networks and intergovernmental networks (Liu et al., 2013). Disruption of these networks, e.g., port disruptions, can have a large impact on international trade flows (Verschuur et al., 2022).



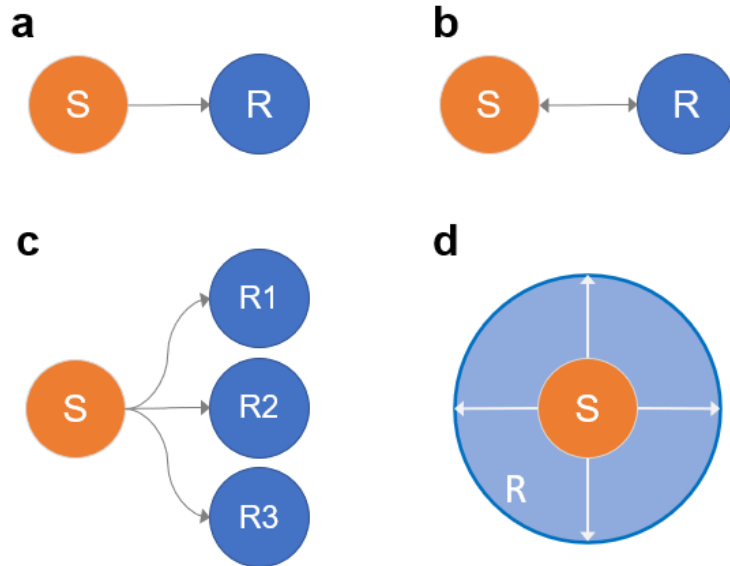









Figure 2.2. Possible flow directions. (a) unidirectional, e.g., river flows; (b) bidirectional, bilateral trade or investment; (c) multidirectional, e.g., trade from one country to multiple countries; (d) omnidirectional – the flows diffuse to the surrounding regions (e.g., carbon emissions).

Table 2.1. Types of transboundary flows, common spatial levels of analysis, and the quantification methods

Categories	Type of flows	Spatial levels	Methods
Physical flows	Trade of materials (raw, e.g., woods, minerals)	 National Subnational Finer grain Note: Darker colors indicate greater data availability	- Statistical data-based approach - Data mining & Crowdsourcing approaches - Modeling approaches (e.g., gravity model)
	Trade of goods (foods, illegal wildlife trade; trade of conventional weapons)		
	Embodied nutrients * (physical content)		
	Energy flows (biomass, fossil fuels, ...)		
	Water flows		- Statistical models - Process-based hydrological models - Air current models
	Pollutants/waste (Nutrients, GHG emissions, PM2.5, ...)		
	Human flows		- National visitor statistics - Big data approach (human mobility trajectory from mobile phone and social media)
	- Tourism		
	- Human migration (Refugees, brains drain, ...)		
	- Human trafficking		
	Animal migration		- Field observation - Animal tracking technologies - Citizen science - Modeling (Species distribution models)
	Species dispersal (e.g., species invasion)		
	Disease transmission (COVID19)		- Big data approach (human mobility trajectory from mobile phone and social media) - Modeling
Non-material flows	Flows of social services (International investments in conflict prevention and peacekeeping)		- Statistical data-based approach
	Investment/financial aids		- Statistical data-based approach
	Information, knowledge, technology		- Statistical data-based approach - Public surveys - Big data approach (geotagged text, photographs, and videos)
Virtual flows	Environmental footprints (virtual water/energy/land/emissions/phosphorus/nitrogen, biodiversity embedded in production **)		- Life cycle assessment - Input-output analysis
	Social footprints (social risks embodied in production)		

* Embodied nutrients are different from virtual nutrients (**). The former represents the matters or elements (e.g., protein, energy, zinc, calcium, iron, vitamin B12, folate, vitamin A, nitrogen, and phosphorus) that are physically contained in the trade products, while the latter represents the matters used in the production process but are not physically contained in the final products.

2.4 Methods for quantifying flows

Quantifying the flow magnitude is the key to describing the reciprocal interactions among systems and estimating the potential impacts. Depending on the study scale and flow types, we summarized the methods in four broad categories (Table 2.1).

2.4.1 *Trade-related flows*

For trade-related flows, there are three main ways to quantify flows: statistical data-based approach, data mining/crowdsourcing approach, and modeling approach.

(1) Statistical data are broadly available at the country level but are limited at subnational levels. National-level bilateral trade data can be acquired from either Food and Agriculture Organization Corporate Statistical Database (FAOSTAT) or the United Nations Commodity Trade Statistics Database (UN Comtrade). The former most focus on agricultural products while the latter includes more broad materials and product coverage. At the subnational level, the U.S. Economic Research Service (ERS) provides state agricultural trade that is estimated from farm production value and farm cash receipts for exported products (USDA ERS, 2022). In addition to the conventional goods, to study peace and global safety-related flows, the trade of weapons can be acquired from the Stockholm International Peace Research Institute Arms Transfers Database. Illegal wildlife trade can be acquired from the CITES (the shorter name for the Convention on International Trade in Endangered Species of Wild Fauna and Flora) (Koellner et al., 2019) and the Oxford Martin Programme on Wildlife Trade. Some agencies also keep records of trade-related information, such as Panda loans, which can be obtained from the giant panda registry managed by the China Conservation and Research Center for the Giant Panda (J. Liu et al., 2015a).

(2) Data mining & Crowdsourcing approaches are emerging in recent years, showing great potential to fill the data gap at the subnational level and even institution level (e.g., company level). For instance, the Land Matrix Initiative takes a decentralized data collection strategy by establishing a broad network in the different regions globally to obtain information on large-scale land acquisitions (LSLAs). They synthesize and cross-check data from multiple sources (such as research papers, policy reports, official government records, company websites, annual reports, media reports, and field-based research projects) to produce the data products on the global flow of transnational land acquisitions (Land Matrix, 2022). The rich information at very fine spatial and temporal scales has facilitated food-water-energy-land-related telecoupling studies across scales (Chiarelli et al., 2022; Liao et al., 2016; Liu et al., 2014). Similarly, the Trase Finance initiative takes a unique supply chain mapping approach to map in unprecedented detail subnational trade flows by combining self-disclosed data from companies with customs, shipping, tax, logistics, and other data (Godar et al., 2015). The approach is unique because it links consumer countries, and traders, with the patterns of ownership and investment in trading companies, as well as places of production down to the lowest level of government administrative unit (e.g., individual farms or production areas). This spatially explicit information can help trace multiple environmental impacts (e.g., deforestation, biodiversity loss) of supply chains in great detail (Ermgassen et al., 2020; Green et al., 2019; Reis et al., 2020; Schim van der Loeff et al., 2018; zu Ermgassen et al., 2022). While these two examples are focused on land deals and agricultural commodity supply chains respectively, the approach can be used for mining and mapping flows of other types of goods and services.

(3) Modelling and simulation approaches are especially useful when statistical data or public data are not sufficient. The gravity model is widely used for analyzing bilateral trade flows of various commodities at both national and subnational levels (Kabir et al., 2017; W. Liu et al., 2015). The concept of the gravity model is based on Newtonian physics, and trade volume between two areas is modeled as an increasing function of their sizes (often using GDP) and a decreasing function of the distance between the two (Anderson, 1979; Kepaptsoglou et al., 2010). Though geographic distance is the most commonly used distance variable, revised versions of gravity models have also considered other impedance factors (or flow distance variables described above in this paper) such as transportation costs, tariffs, quality of infrastructure, and common language (Kepaptsoglou et al., 2010). In addition to the gravity model, input-output (IO) and generalized equilibrium models have been exploited for simulating trade flows. Constructing interregional IO tables usually takes large financial and labor efforts, and running computable generalized equilibrium (CGE) models requires a considerable number of parameters (Boero et al., 2018). For application purposes, users usually resort to existing IO tables and datasets released by professional institutions and teams. For instance, the Food and Agriculture Biomass Input–Output (FABIO) tables provide a comprehensive flow of agriculture, food and forestry products of materials among 191 countries (Bruckner et al., 2019). The Chinagro model, a geographically detailed general equilibrium model, depicts the interregional trade of agricultural products among eight regions in China (Dalin et al., 2014; Fischer et al., 2007).

In addition to the aforementioned models focusing on national and subnational, freight flow models can be used to map trade flows at more spatially explicit scales (e.g., county, and pixel

level) (Karakoc et al., 2022; Kinnunen et al., 2020; Lin et al., 2019). For example, the U.S. Bureau of Transportation Statistics (BTS) and Federal Highway Administration (FHWA) integrate data from a variety of sources (e.g., Commodity Flow Survey, CFS) to create a freight movement database – Freight Analysis Framework (FAF) – among states and major metropolitan areas by all modes of transportation (Hwang et al., 2021). Lin et al and Karakoc et al further downscaled this data and produced the US county-level food flows (Karakoc et al., 2022; Lin et al., 2019). At finer spatial resolution, Kinnunen et al combined the foodsheds (self-sufficient areas with internal dependencies) approach and freight analysis and modeled food flow paths at 30 arcmin resolution (Kinnunen et al., 2020). Both examples are on food flows, but the approach can also be applied to other traded commodities. Other novel data such as the automatic identification system (AIS), which is an automatic tracking system that uses transceivers on ships, can provide rich and real-time ship locations and movement trajectories (Mou et al., 2020). In combination with auxiliary data, AIS can also be used for estimating maritime freight flows.

2.4.2 Passive biophysical flows

The methods for estimating the flows of water, sediments, and pollutants (e.g., nitrogen, phosphorus, GHG emissions, and PM_{2.5}) range from field observations to process-based modeling.

Water flows, such as streamflow, are usually publicly available from government-led or research institute-led observation stations (e.g., the U.S. Geological Survey). For human-intervened water flows, such as China’s South-to-North Water Transfer Project (SNWTP), the amount of transferred water across regions can be acquired from the management department or through public reports. According to the most recent report, 50 billion m³ of water has been transported

from southern to northern China from 2014 to 2021 (Xinhua News Agency, 2021). Researchers can also develop their own field observation stations to obtain related water flow data. However, the observed data have drawbacks either due to limited spatial coverage or temporal availability. Modeling approaches are often used for filling the data gaps. Hydrological models, such as Soil & Water Assessment Tool (SWAT), can be used to simulate the quantity and quality (e.g., nitrogen and phosphorus concentrations) of surface and groundwater in watersheds (Bieger et al., 2017). SWAT does not directly model flows, but the outputs can be used for estimation or as inputs for other flow models. The Model to Assess River Inputs of Nutrients to seas (MARINA) is a widely used flow model, which quantifies river export of nutrients (dissolved N and P) from land to sea by the source at the sub-basin scale (Strokal et al., 2016). For finer spatial scale, Bagstad et al developed an agent-based model termed “Service Path Attribution Networks” (SPANs) on the Artificial Intelligence for Ecosystem Services (ARIES) modeling platform (Bagstad et al., 2013). The SPAN initializes agents from spatially explicit source (i.e., sending systems), sink, and use data, and track the spatially explicit paths taken by carrier agents through the network (e.g., hydrologic or transportation networks, or the atmosphere) to determine the quantity of goods or services reaching final users (i.e., receiving systems). SPAN is a powerful tool to model the flows of freshwater, riverine flood, and sediments (Bagstad et al., 2013). The flows of emissions (e.g., GHG and PM_{2.5}) through the air are more volatile and can be stimulated by applying advanced air current models (Koellner et al., 2019).

2.4.3 Human and animal flows

Human migration data are recorded at multiple levels, such as the national level for international migration and the subnational level for interregional (within a nation) migration. Data can be

acquired from nation or state statistical administrations. For example, tourism flows, can be collected from national visitor statistics provided by World Tourism Organization (UNWTO). These data are usually collected through census surveys or self-reporting. Illegal human flows, however, are less accessible. Such data might be sourced from data initiatives. For example, the Counter-Trafficking Data Collaborative (CTDC) utilized a crowdsourcing approach and collected anonymized human trafficking data contributed by counter-trafficking organizations around the world. Recent development in big data using human mobility trajectory from mobile phone and social media provides alternative high-resolution and instant human flow data for investigations (SafeGraph, 2022). The human mobility data with detailed geospatial information can also be used to model tourism and disease transmission (e.g., COVID-19) (Chang et al., 2020; Grantz et al., 2020; Kang et al., 2020; Xiong et al., 2020).

Animal migration and species dispersal (e.g., species invasion) can be estimated based on field observation (e.g., birdwatching) (Koellner et al., 2019), citizen science, and crowdsourcing approach (e.g., iNaturalist), or animal tracking technologies. Since these approaches can only capture a sample of the whole population, species distribution models have often been used (Koellner et al., 2019).

2.4.4 Non-material flows

In an era of information, massive information flows everywhere. To quantify the interregional flows of particular information of interest, it is important to first identify the information sending systems and receiving systems. A sending system can be quickly identified based on the source and content of the information (such as when, where, and who), while the receiving systems can

be multiple or hundreds of thousands. Based on the scales or certain system boundaries, one can identify the receiving systems by examining the occurrence of news in local public media and social media. Further, the quantity of keywords, photos, and videos in geotagged social media (e.g., Twitter, Flickr, Sina Weibo) and digital search engines (e.g., Google Trends), or the number of newspaper articles, reports, and documentaries that report about the sending system in the receiving system could be used as a proxy to estimate the magnitude of information flow (Koellner et al., 2019; Li et al., 2021; J. Liu et al., 2015a). We must be aware that these proxies can serve as an approximation but might be biased in estimating the actual magnitude of information flows. The bias can be introduced by the representativeness of samples. For instance, social media participants are not a random sample of the population. Therefore, certain population groups with different demographic traits (e.g., age, education level, income) could be over- and under-represented in social media data (Li et al., 2021). Similarly, the heterogeneous coverage of social media platforms and devices across regions, as well as the uncertainties caused by potential noise of misinformation, can also bring bias in estimation. To accurately estimate information flow using social media data, there is a need to carefully handle the inherent bias in data.

Knowledge transfer and technology transfer can be quantified in the same way as information flows. Depending on the types of technology, the technology transfer could also be measurable by trade flow approach. For example, energy-related technology transfer can be measured by the trade quantity of high-tech energy equipment and materials (e.g., solar panels, and rare-earth metals) (Fang et al., 2016; Fishman and Graedel, 2019; J. Li et al., 2020).

Flows of investment and financial aid can be measured by data from public datasets, such as foreign direct investment. In addition, the AidData team at William & Mary used data mining approaches to produce project-level financial flow by coding over 1.5 million development finance activities (AidData, 2016; Custer et al., 2021). The Global Development Policy Center at Boston University also took a similar approach and produced a high-precision dataset for China's overseas finance investment (Ray et al., 2021). These financial flow data have been used for investigating international conservation interest (Qin et al., 2022), the risk to global biodiversity (Yang et al., 2021), and the social and environmental impact of large-scale overseas infrastructure development (Li et al., 2021).

2.4.5 *Virtual flows*

Virtual flows, or the embedded resources or footprints “hidden” in products, have emerged as a set of major indicators for evaluating the potential impacts of trade (Fang et al., 2014; Galli et al., 2012; Vanham et al., 2019; Xu et al., 2020c). Since the virtual resources are the portion that was used in the production process but are not physically contained in the final products, the end-users (or the product receiving systems) usually cannot see or be aware of their impacts on distant producing systems (or product sending systems). The concept of virtual flows can thus be used to inform final consumers to adjust their consumption behaviors (e.g., changing diets or sourcing products from more sustainable production systems). There are two widely used approaches for quantifying virtual flows: Multi-Regional Input Output (MRIO) analysis, and life cycle assessment (LCA).

(1) MRIO is a macroeconomic approach that tracks financial flows between countries' major economic sectors. Developed by the Nobel Prize Laureate Wassily Leontief, input-output analysis is an economic technique that relies on input-output tables. Monetary MRIO tables can be coupled with satellite accounts data on a range of environmental indicators (e.g., land, water, energy, emissions, biodiversity risk) to estimate environmental footprint flows (Lenzen et al., 2012; Li et al., 2022; Oita et al., 2016; Xu et al., 2019b; Zhao et al., 2015). The basic idea is to convert monetary values in the MRIO tables to physical or virtual footprint flows among sectors and countries based on independent data on the national price per physical unit of certain products, and on the physical resource or environmental intensity (e.g., CO₂ emissions in tonnes per monetary unit) by country and industry sector (Shapiro, 2020). In recent years, research has been extended from not just environmental indicators, but also incorporated social indicators (e.g., employment, child labor, and gender pay gap) to assess the social risk embedded in products and services (Alsamawi et al., 2017a; Malik et al., 2021b; Wiedmann and Lenzen, 2018; Xiao et al., 2017). MRIO analysis is suitable for macro-scale virtual flow analysis, and the data are broadly available at the global scale. Table 2.2 summarized a list of widely used MRIO databases, detailing country, sector, and year coverages, as well as the associated satellite accounts available for use. Countries, such as the US and China have subnational MRIO tables (i.e., IO between various sectors of multiple regions in a country). MRIO is more suitable for mapping virtual flows at aggregated sector level or economy level but usually not suitable for a single product.

Table 2.2. Summary of the main global MRIO databases

Database name	Countries	Sector details	Time	Extensions	Unit
EORA	World (190)	Full Eora: 20-500; Eora26: 26	1990-2021	GHG emissions, labour inputs, air pollution, energy use, water requirements, land occupation, N and P emissions, primary inputs to agriculture	USD
EXIOPOL-EXIOBASE	World (44 = 43+1RoW = 27EU+16+1)	163	1995-2021	30 emissions, 60 IEA energy carriers, water, land, 80 resources	EUR
World Input-Output Database (WIOD)	World (41 = 40+1RoW = 27EU+13+1)	35	1995-2009	Detailed socio-economic and environmental satellite accounts	USD
Global Trade Analysis Project (GTAP)	World (129 = 121+20R)	65	1990, 1992, 1995, 1997, 2001, 2004, 2007, 2011, 2014	5 (GWP), Land use (18 AEZ), energy volumes, migration	USD
Global Resource Accounting Model (GRAM)	World (62)	48	2000, 2004	CO2 emissions, material extraction, value-added, and employment	
IDE-JETRO	Asia-Pacific (8: 1975) (10: 1985-2005)	56 (1975); 78 (1985-1995); 76 (2000, 2005)	1975-2005	Employment matrices (2000, 2005)	YEN
Food and Agriculture Biomass Input-Output Model (FABIO)*	World (192 = 191 countries + 1RoW)	118 processes and 125 commodities	1986-2013	NA	Tonnes, Heads

* FABIO is a physical IO table, while others are all monetary tables.

(2) Life cycle assessment was initially developed to estimate environmental impacts associated with a product throughout its life cycle in the 1970s (Crawford et al., 2018; Guinée et al., 2011; ISO, 2006). Starting in the 2000s, social-LCA was proposed and developed to assess the social and sociological impacts (e.g., human rights, health, and safety) of products along the life cycle (Andrews, 2009; Guinée et al., 2011). LCA is a more comprehensive, high-resolution, and flexible approach compared to the MRIO approach. Combined with trade flow data, virtual flows of footprints at both macro-scale (e.g., country level) and micro-scale (e.g., corporation level and individual people level) can be quantified (Malik et al., 2021a; Xu et al., 2020b; Zhao et al., 2021). Figure 2.3 provides an example, illustrating the system boundaries and functional units for the life cycle assessment (LCA) of irrigated agricultural production. In this example, carbon, energy, and water footprints of producing per unit of winter wheat can be calculated through the LCA method in combination with unit process parameters (Xu et al., 2020b).

However, LCA relies heavily on data collection, either from onsite investigation, laboratory tests (Tu et al., 2021), or through questionnaire surveys and literature reviews (Poore and Nemecek, 2018). And different system boundary settings may result in very different results (Malik et al., 2021a). But still, by clearly defining the proper system boundaries and utilizing existing LCA tools (Figure A2.0.1), LCA is still a very powerful approach for virtual flow quantifications.

In practice, due to data limitations, MRIO and LCA scholars tend to use fixed parameters either borrowing average figures from studies at global scale or parameters examined in other regions at a certain time, but ignored the heterogeneity in terms of space and time. Accurate estimations should further consider the spatial variability (given the heterogeneity in climate, soils, resource

endowment, and other production conditions) and temporal variability (Hoekstra, 2017; Poore and Nemecek, 2018).

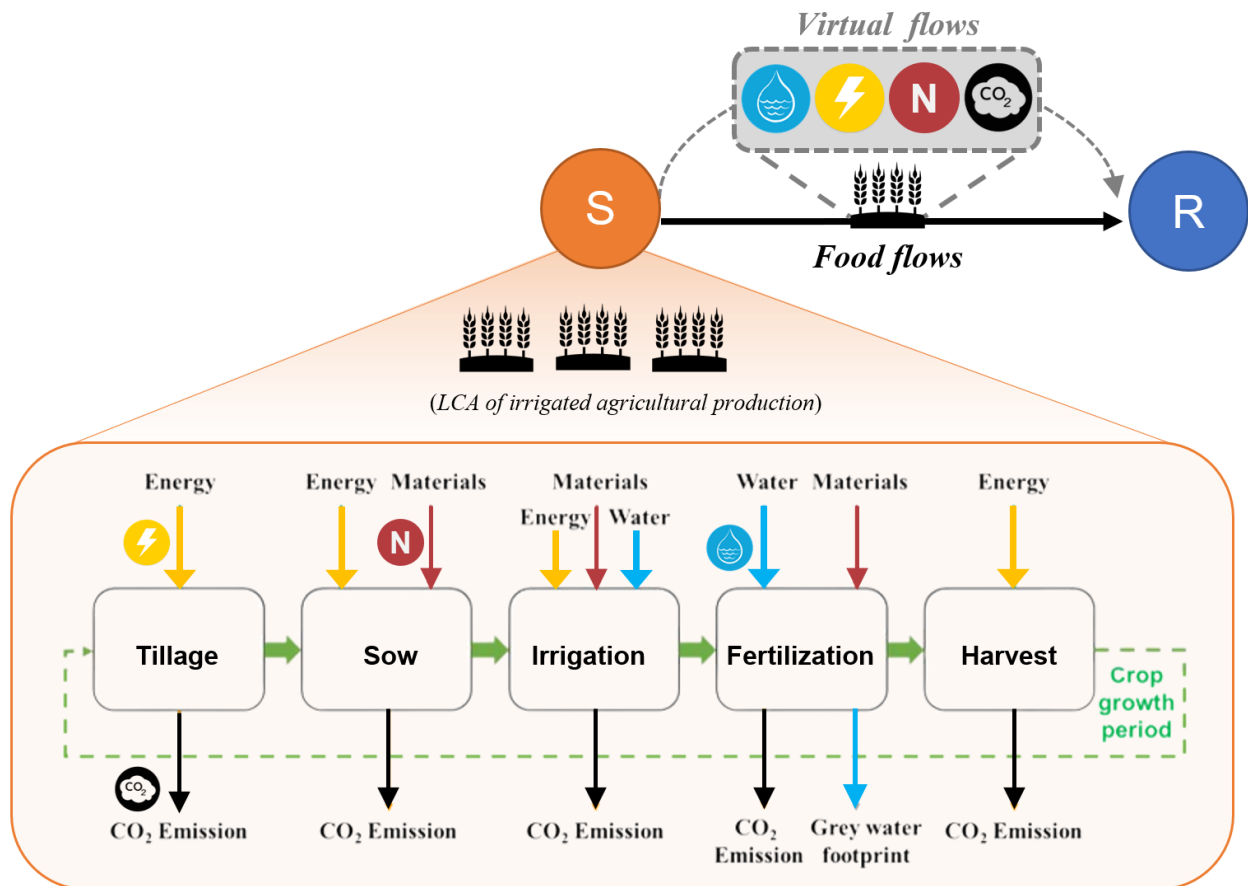


Figure 2.3. An example of quantifying virtual flows of water, energy, nitrogen, and CO₂ embedded in food trade by using life cycle assessment (LCA) of irrigated agricultural production. S – sending system, R – receiving systems. The subplot of LCA is adapted from (Xu et al., 2020b).

2.5 Governance of transboundary flows for global sustainability

In an increasingly metacoupled world, one place's actions can generate positive or negative impacts on others through various interregional linkages and flows (Chung and Liu, 2022; Li, 2021; Liu et al., 2018b; Sachs et al., 2017; Zhao et al., 2020). It is thus critical to understand, track, measure, and manage the transboundary flows across scales and over time.

Transboundary flows are particularly challenging for governance as they usually involve multiple states or multilateral governing authorities and regimes. Stakeholders under different governing systems can have very different interests and goals. Instead of providing a solution, we rather use transboundary flows as a scientific measurement and visual tool to inform multilateral stakeholders about the potential challenges and opportunities for sustainable development.

2.5.1 Growing shocks to transboundary flows

Changing climate (e.g., extreme climate events, global warming), emerging global pandemics (e.g., COVID-19), growing conflicts (e.g., Russia-Ukraine war), and volatile international relations (e.g., the recent US-China Trade war) have threatened the sustainable delivery of many flows (e.g., global supply chains) and global sustainability (Figure 2.4).

Global climate change is the most widespread risk, and can impact flows through many pathways, such as directly on flow transport, or impact production systems (often the sending systems). Research shows that 86% of ports globally are exposed to more than three natural hazards, potentially affecting global maritime trade flows (Verschuur et al., 2022). Research has revealed that each degree-Celsius increase in global mean temperature would reduce global yields of maize by 7.4%, wheat by 6.0%, rice by 3.2%, and soybean by 3.1% (Zhao et al., 2017). Large reduction in major food production regions could trigger systemic disruption – the soaring price of agricultural products and erratic food supply chains (Puma et al., 2015). In addition to trade-related flows, extreme climate events also impact passive flows, such as water flows, and cause disasters (e.g., floodings and drought), threatening human-nature systems.

The outbreak of epidemics (e.g., the recent COVID-19 pandemic) is another major threat to many transboundary flows. Global lockdown because of the pandemic has blocked more than 90% of the international human flows, and generated severe negative impacts on global supply chains (Falkendal et al., 2021; Guan et al., 2020). The African swine fever, another outbreak in East Asia and Europe, also caused a detrimental effect on food flows and threaten food security (Mason-D'Croz et al., 2020).

Growing conflicts and volatile international relations also impact various transboundary flows. For instance, since February 2022 after Russia's invasion of Ukraine, more than 9.1 million cross-border refugees have left Ukraine (UNHCR, 2022). The war also disrupted global flows of vital commodities such as food, energy, and fertilizer (Puma and Konar, 2022; Tollefson, 2022), which are expected to further affect biodiversity and the environment (Jianguo Liu et al., 2022). Another study on the impacts of the Syrian civil war revealed that refugees fleeing can also have unexpected impacts on transboundary water flows (Müller et al., 2016).

Being aware of these global impacts on transboundary flows, and assessing the system dynamics by applying the metacoupling framework can help stakeholders get a holistic picture and work together to address transboundary sustainability challenges.

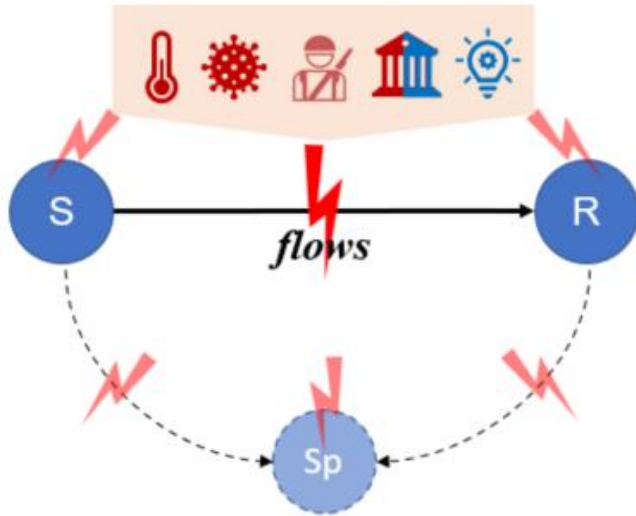


Figure 2.4. Shocks (red icons) and opportunities (blue icons on the top) that might impact transboundary flows and the metacoupled systems. S – sending system, R – receiving systems, Sp – spillover system.

2.5.2 System modeling and scenario analysis for understanding dynamic flows and metacouplings

In the age of metacoupled Anthropocene, system interactions become more complex than ever because of the growing number of interlinked systems, agents, linkages, causes, effects, and feedbacks. Network analysis is especially useful for visualizing the complex interactions between multiple flows and multiple systems (Carlson et al., 2021; Sonderegger et al., 2020), but is not sufficient for system modeling. Nexus approaches were highlighted to be highly useful in uncovering synergies, detecting harmful trade-offs, detecting harmful trade-offs among multiple sectors, and unveiling unexpected consequences (Liu et al., 2018b). In the five major steps of implementing nexus approaches (Liu et al., 2018b), we would like to elaborate on “simulate nexus dynamics” here, as this step is critical for quantitatively understanding changes in flows and dynamics of systems. Particularly, we recommend the integration of flow models (Section 3) and scenario analysis for simulation. Scientists can work with multi-stakeholders to develop

various scenarios. In addition to the common practice of including socioeconomic development and climate scenarios (Zhao et al., 2021), shocks on transboundary flows can also be included in developing scenarios. For instance, shocks can lead to different degrees of trade disruption. It would be better for countries or regions that rely on trade for goods and services to test the extent to which trade disruption might impact the supply for domestic needs.

Given the broad impacts each scenario might generate on a system's sustainable development, the Global indicator framework for the Sustainable Development Goals (SDGs) proposed by United Nations can be particularly helpful to provide a set of indicators for cross-sector or cross-region comparison (Figure 2.5) (UN, 2019). A fully integrated global social-environmental model – the Global Biosphere Management Model (GLOBIOM) – has shown great potential for application in global and regional agricultural trade and impact assessment (Havlík et al., 2018). For other types of flows, such as water and energy flows, the corresponding flow models can also be integrated with scenario analysis for simulations (Munia et al., 2020; Vinca et al., 2020). Although scenario analysis has often been criticized for not being able for validation, it is still useful for guiding policy making by revealing potential impacts. Not aiming at predicting the future, the analysis rather provides a big picture of what to avoid and how to adapt to an uncertain future.

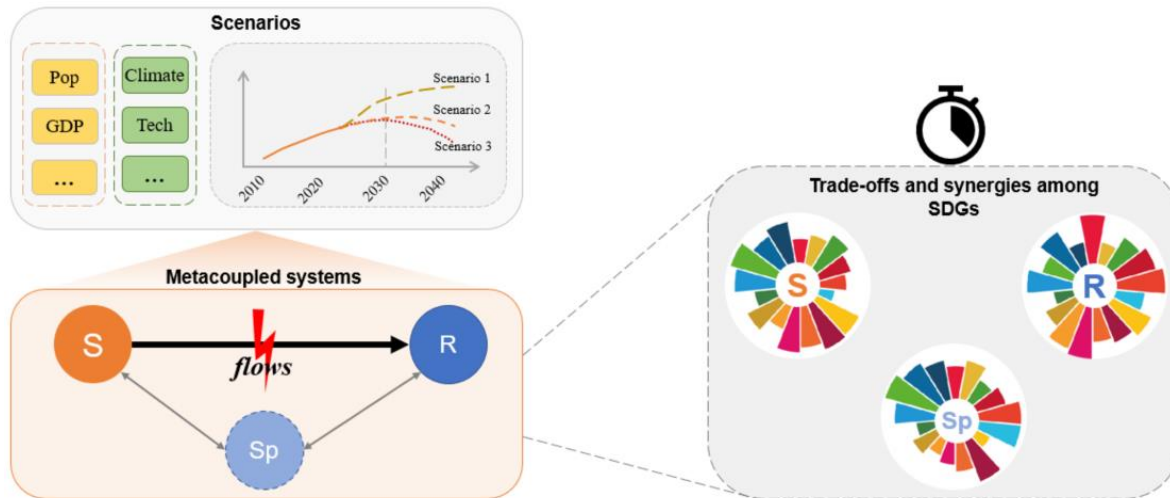


Figure 2.5. Scenario analysis for investigating dynamics of transboundary flows (left), and system sustainability under the UN SDG framework (right). S – sending system, R – receiving systems, Sp – spillover system.

2.5.3 Multi-sited, multi-stakeholder, multi-sector, and multi-scale flow-based governance

In an interconnected world, it is short-sighted to say that problems are caused and are to be solved where they occur (i.e., place-based governance or territorial-based governance) (Hoekstra and Wiedmann, 2014; Liu et al., 2018b; Munroe et al., 2019; Sikor et al., 2013). Such place-based governance might lead to well-intended but unexpected noneffective policy results. For instance, only focusing on emission target within the country might lead to displacement of carbon-intensive industries to other countries with lax environmental standards, resulting in “carbon leakage” (Xu et al., 2020c).

With the world becoming increasingly interconnected, there is a need for further facilitating flow-based governance, which considers governance in a place in light of its relationships with other places, by tracking and managing where flows start, progress, and end (Liu et al., 2018a; Sikor et al., 2013). Flow-based governance is not new if one considers, among others, colonial trading companies and transboundary river management (Sikor et al., 2013). Yet, the speed,

scale, and scope of transboundary flows have become arguably unprecedented under globalization and growing shocks (Section 4.1) in recent few decades (Munroe et al., 2019). New forms of flow-based governance are required and are emerging. Ample studies and practices have been implemented in global supply chain management, e.g., through certification schemes for products, environmental labeling and certification schemes along the global supply chains (OECD, 2016; Prag et al., 2016; Sikor et al., 2013). For biophysical flows, e.g., water and nutrient pollutants, many transboundary river basins are still suffering from conflicts between upstream and downstream regarding water quantity allocation and water quality control (De Stefano et al., 2017; UNEP-DHI and UNEP, 2016). Most of the transboundary river basins lack sufficient transboundary agreements, some exist but need more comprehensive coordination and modern cooperation among multi-stakeholders in addressing interlinked flow challenges among multiple sectors (e.g., climate, land, food, water, energy; Figure 2.6) induced by alarming warming trends, growing population demands, and emerging hydro-political tensions (e.g., caused by booming dam constructions) (UNEP-DHI and UNEP, 2016; Vinca et al., 2020).

Integrated governance of flows therefore requires the consideration of multi-site, multi-stakeholder, multi-sector, and multi-scale. It is essential to understand how different players contribute to forms of governance, and how different flows might interact and lead to potential trade-offs or synergies among sectors. There is also a need to understand how actions at different spatial levels can create the best synergies to make our production and consumption patterns more sustainable. Hoekstra et al used water governance as an example and illustrated the importance of interventions at different scale levels (from the field or production-line level to the farm or factory level, the river basin level, the country level, and the international level) and

bringing in new relevant players at different governance levels (e.g., from the individual water user to irrigation and water boards, governmental policy makers, and international agreements) (Hoekstra et al., 2019). Only by thinking holistically can we develop effective strategies to manage the flows and achieve co-benefits.

Flow-based governance also needs to view the metacoupled system as a whole and manage the flows in the system collectively. For example, focusing on a few key flows in supply chains might be efficient for short-term sustainability, but the whole system could be susceptible to unexpected shocks to these key flows. Preserving and promoting proper redundancy and diversity of the flows within the system can improve system resilience (Puma et al., 2015).

Furthermore, by utilizing the proposed system modeling and scenario analysis tools, flow-based governance should also pay attention to managing gradual changes and feedback impacting the metacoupled system.

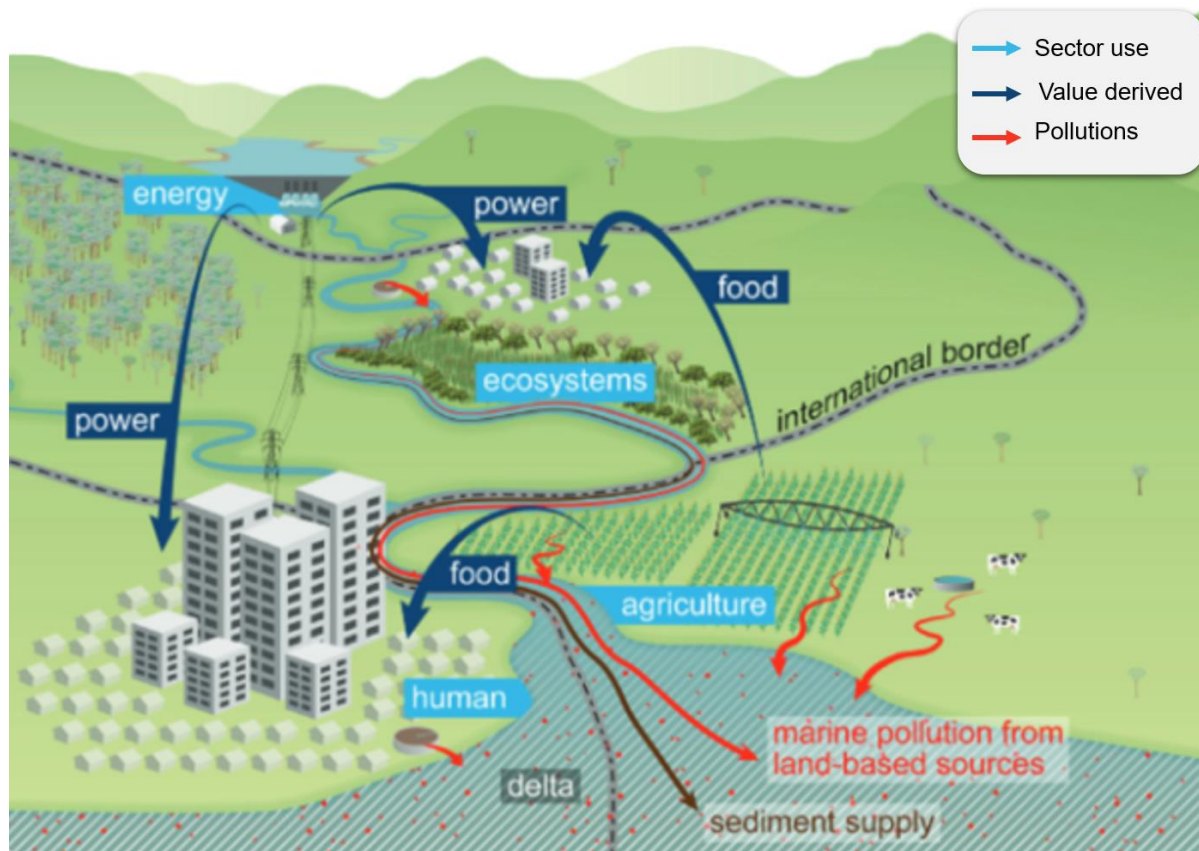


Figure 2.6. Multiple interconnected flows across a transboundary river basin. Regions within a river basin are linked through their use of the water (for freshwater, food, and energy), and the impacts they cause through development and pollution (e.g., nutrient pollution, wastewater pollution, freshwater biodiversity, and reduction of sediment supply). Adapted from (UNEP-DHI and UNEP, 2016).

2.6 Concluding remarks

Transboundary flows are the key component in the metacoupling framework, connecting adjacent and distant systems. Governance of transboundary flows is inherently challenging. To address the complexity and challenges, we made a first attempt to characterize them in different dimensions (e.g., type, magnitude, direction, distance, time, and mode), and summarized practical methodologies for characterizing them. Tracking and quantifying transboundary flows have profound implications for achieving co-benefits and minimizing trade-offs across sectors and places. Governing transboundary flows should recognize the shared risks and goals, use

system thinking, and enhance multilateral cooperation. To achieve global sustainability in the Anthropocene, transboundary flows must be explicitly recognized and systematically characterized in sustainability research and governance so that effective policies and practices can be developed and implemented to safeguard humankind and its planetary support systems.

CHAPTER 3: MAPPING SPATIOTEMPORAL DYNAMICS OF COASTAL DEAD ZONES OVER 20 YEARS USING REMOTE SENSING

3.1 Abstract

Spreading dead zones (hypoxia) are threatening coastal ecosystems and over three billion people's livelihoods globally. Traditional coastal dead zone models present a limitation on our ability to understand how dead zones change across time and space because they typically only used discrete ground measurements that are difficult to be applied over broad spatiotemporal scales. To fill this gap, this study proposed a workflow that integrates time-series remote sensing observations with field measurement archives and used Random Forest, a machine-learning algorithm, on the Google Earth Engine platform to characterize dead zone dynamics during 2000-2019. The chapter demonstrated this workflow using the Gulf of Mexico, the largest dead zone in North America, as a case study. The results show the Gulf dead zones peaked in 2009 ($17,699 \pm 679 \text{ km}^2$) and contracted afterward in terms of both size and persistence as measured by intra-annual occurrence. Despite the moderate contraction, the average size of the maximum dead zones in the recent 10 years (2010-2019) was still twice above the redline target (i.e., $< 5,000 \text{ km}^2$) set by the Interagency Mississippi River and Gulf of Mexico Hypoxia Task Force. Furthermore, dead zones occurred more frequently ($> 40\%$ of the 20 years) in the western Gulf, and nearly half of the region experienced dead zones annually. This research also detected dead zone occurrence at the Suwannee River estuary in the eastern Gulf, which was rarely studied. In addition to the interannual change, this analysis also depicted the intra-annual dead zone dynamics. In most of the studied years, dead zones started to grow in June and peaked during mid-August and September. The rich and fine temporal and spatial information on dead zone

dynamics will be helpful for policy-makers to develop targeted management plans and environmental policies. The demonstrated approach which incorporates remote sensing into long-term coastal dead zone monitoring can be used to monitor dead zones worldwide and help provide important information for moving toward the United Nations' Sustainable Development Goals.

3.2 Introduction

The past few decades have seen a massive increase in coastal eutrophication and growing dead zones (hypoxia and anoxia beneath the water) (Diaz and Rosenberg, 2008). Globally, at least 500 coastal dead zones have been reported, some of which have become exceedingly large ($>5,000$ km², hereby called mega dead zones) while a few others are growing rapidly (e.g., the Gulf of Oman) but lack sufficient and consistent monitoring (Breitburg et al., 2018). The lack of monitoring in many regions means the true number of dead zones may be much higher than currently estimated. Marine dead zones can lead to biodiversity loss and damage to ecosystem services (e.g., seafood, recreation fishing) that underpin human well-being (Breitburg et al., 2018). Given that more than three billion people depend on marine and coastal ecosystems for their livelihoods (IPBES, 2019), it is critical to improve the understanding and predictions of marine ecosystem change at large spatiotemporal scales to inform management plans and environmental policies for maintaining the sustainability of marine ecosystem services in a changing world.

Research towards understanding the marine dead zones has largely been based on cruise field observations. For example, in the Gulf of Mexico, shelfwide cruise hypoxia monitoring has been

persistent since 1985 (Rabalais et al., 2010; Smith et al., 2017). In the Baltic Sea, multinational monitoring programs and research cruises have collected water column measurements since 1900 (Carstensen et al., 2014; Conley et al., 2011; Murray et al., 2019). Monitoring efforts and data are more spatially sparse and temporally discrete in most other coastal systems (e.g., in the East China Sea) (Chen et al., 2007; Ning et al., 2011; Zhu et al., 2011). Despite substantial efforts to understand coastal hypoxia, existing studies are often limited in temporal and spatial extent because cruise field observations are usually labor-intensive, time-consuming, and costly. Unexpected shocks, such as storms, financial crises, and the recent pandemics have impacted cruise trips for continuous data collection efforts.

Hypoxia models thus have been developed to understand coastal hypoxia dynamics. Existing models are either process-based or statistical. Process-based models are useful to understand the hypoxia processes by accounting for biophysical and biogeochemical processes such as nutrient transport, primary production, and water stratification in order to predict dissolved oxygen (Del Giudice et al., 2020; Fennel et al., 2016; Obenour et al., 2015; Scavia et al., 2013; Wang and Justić, 2009). However, these models usually require tremendous parameter data for calibration and validation. Statistical models offer an alternative and more feasible way to approach hypoxia prediction by characterizing the empirical statistical relationship between the size of summertime hypoxia zones and nutrient loads along with river discharge (Forrest et al., 2011; Greene et al., 2009; Turner et al., 2012). Yet, existing hypoxia statistical models usually only predicted the hypoxia size but did not reveal the geospatial distribution of the hypoxic zones. In sum, existing modeling studies have contributed significantly to understanding coastal hypoxia issues.

However, few of them have produced spatially explicit information on hypoxia, partly because of the lack of sufficient water measurements (Matli et al., 2020, 2018).

Recent advancements in Earth observation satellites (e.g., NASA's Earth Observing System) provide an alternative way to acquire large-scale and consistent data for monitoring environmental changes both in terrestrial and marine ecosystems (Gorelick et al., 2017; Le et al., 2016). For example, remotely-sensed Chlorophyll a (Chl a) from satellite sensors such as MODIS (Moderate Resolution Imaging Spectroradiometer) and SeaWiFS (Sea-viewing Wide Field-of-view Sensor) have proved to be an efficient means for examining the marine eutrophication and dead zones (Chen et al., 2014; Klemas, 2011; Le et al., 2016). Time-series remotely-sensed imagery that covers a long-time span offers the potential to track historical marine ecosystem changes and even predict changes in the future. Yet, few studies have integrated remote sensing into investigating coastal dead zones over time and across large spatial scales. A recent study attempted to use a linear regression approach to characterize the relationship between surface dissolved oxygen and satellite-derived variables (Kim et al., 2020). They found that surface dissolved oxygen (DO) and water temperature shows a strong inverse relationship, demonstrating the potential of remote sensing data to model DO. However, very few studies have applied time-series of satellite imagery to predict bottom DO, which is more concerning as hypoxia zones usually occur in the bottom water and cause severe impacts on coastal marine ecosystems (Breitburg et al., 2018; Diaz and Rosenberg, 2008; Rabotyagov et al., 2014; Tomasetti and Gobler, 2020).

The objective of this study is to use freely available remote sensing imagery and documented field observation seawater data, combined with the machine-learning algorithm on the Google

Earth Engine (GEE) cloud computing platform, to investigate the spatiotemporal dynamics of dead zones in the Gulf of Mexico from 2000 to 2019. This research is the first to incorporate time-series remote sensing data in long-term coastal dead zone monitoring research. The demonstrated approach can be easily adapted to map dead zone dynamics in other coastal regions around the world. Findings from this research hold promise to provide urgently needed information for both terrestrial and marine conservation agencies to develop integrated solutions to optimize ecosystems management and to move toward the United Nations' Sustainable Development Goals (SDGs), especially SDG 14 (Life below water) and SDG15 (Life on land).

3.3 Materials and methods

3.3.1 *Study area*

Our study area is located in the Gulf of Mexico (Figure 3.1), and we chose it as a case study because (1) it is the largest hypoxic zone in North America and the second-largest worldwide; and more importantly, (2) there are the most abundant and consistent water samples that can be used for training and validating our models. Hypoxia in the Gulf is largely caused by excess nutrients from the adjacent human-dominated and agriculturally heavy Mississippi River basin (Diaz and Rosenberg, 2008; Pitcher et al., 2021). The Mississippi River basin drains approximately 41% of the land area of the conterminous United States, and the combined flows of the Mississippi and Atchafalaya Rivers account for 96% of the annual freshwater discharge and 98.5% of the total annual nitrogen load to the Gulf (Pitcher et al., 2021). Beginning from around the middle of the 20th century, there has been a marked increase in the concentration of nitrogen and phosphorus in the Lower Mississippi River, which has been attributed to agricultural activities, especially increased use of fertilizers, in the basin and surrounding regions

(Mitsch et al., 2001). The largest extent of the hypoxic zone was recorded in the summer of 2017 at 22,720 km², which is approximately the same size as the state of New Jersey (NOAA, 2017).

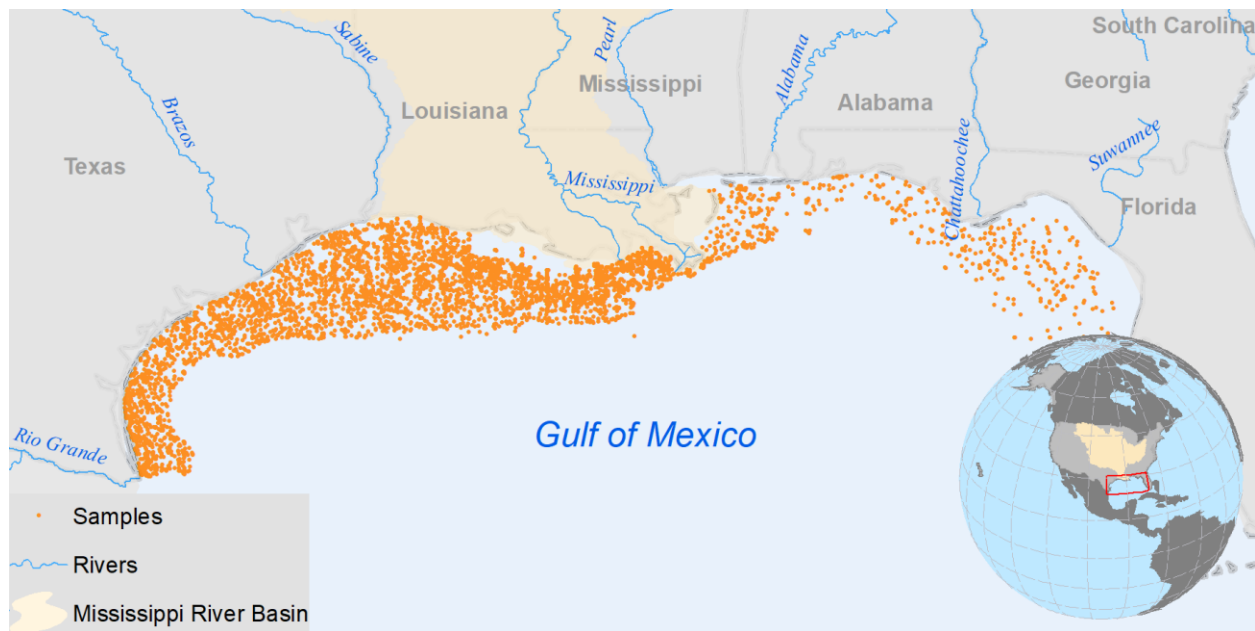


Figure 3.1. The geographic location of the water samples, Gulf of Mexico, and the adjacent Mississippi River basin in the US.

3.3.2 *Field data*

We compiled the coastal water quality dataset for the 2000-2019 period from multiple sources (Figure 3.2). Overall, this dataset includes 779,456 samples collected from 150 monitoring cruises at 8,117 locations (with latitude and longitude) in the Gulf area (Figure 3.2, Figure A3.0.1). The water sampling includes measurements of dissolved oxygen (DO), water temperature, sampling date, and depth. Detailed data description and assimilation can refer to Matli et al (Matli et al., 2020, 2018). We further filtered the dataset by keeping those collected between 3-80 m water depths because data beyond this range is sparse and hypoxia is extremely rare below 80 m (Matli et al., 2018). Additionally, we only used observations collected from May 1 to September 31 each year in the model development, as hypoxia occurs predominantly in

the summertime and most of the water samples were collected during this period (see Figure A3.0.2).

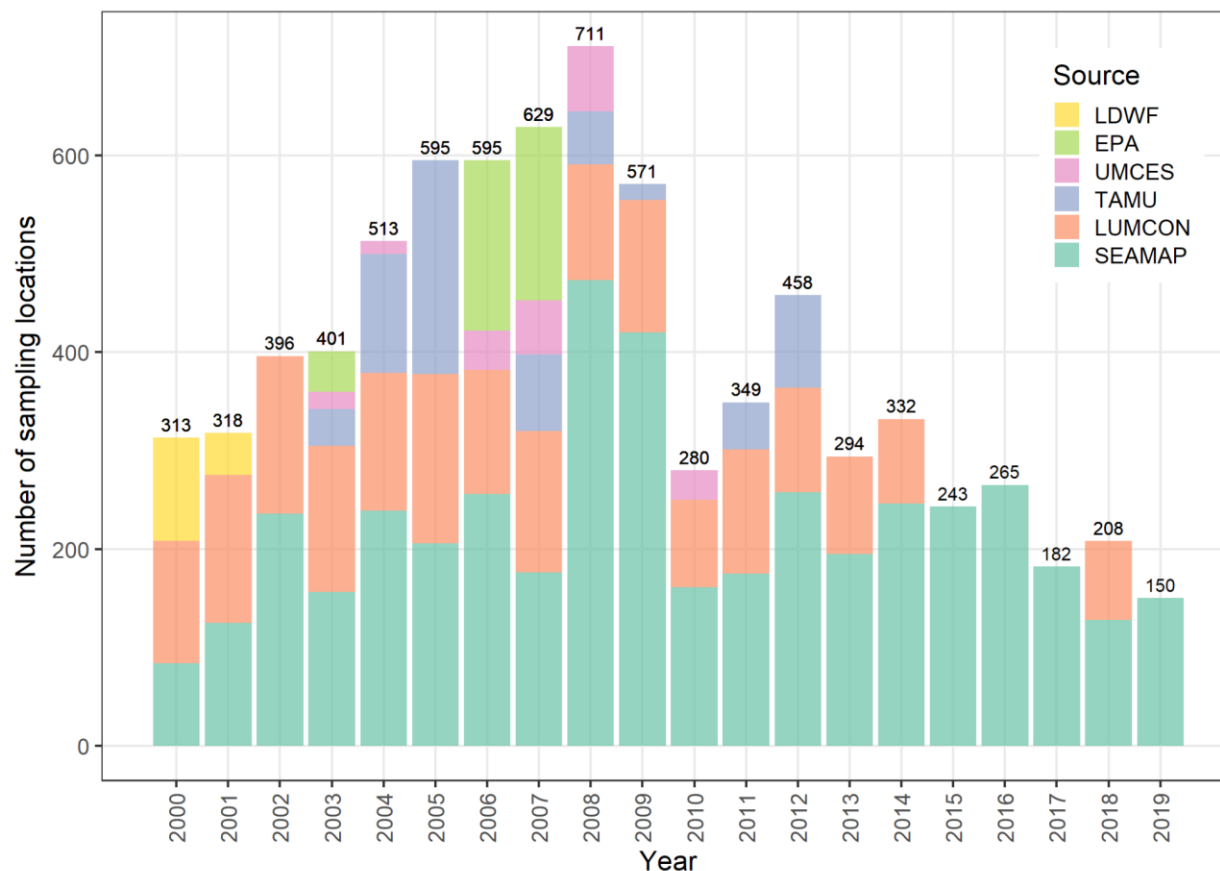


Figure 3.2. The number of DO sampling locations in the Gulf by years and by sources. Data sources: Louisiana Universities Marine Consortium (LUMCON), Southeast Area Monitoring and Assessment Program (SEAMAP), Texas A&M University (TAMU), University of Maryland Center for Environmental Sciences (UMCES), U.S. Environmental Protection Agency (EPA), and Nutrient Enhanced Coastal Productivity Program (NECOP), and the Louisiana Department of Wildlife and Fisheries (LDWF). The maps of sampling locations are shown in Figure A3.0.1.

3.3.3 Satellite data

Both the daily MODIS Aqua and Terra Ocean Color level-3 products were used in this study.

The data include global daily ocean color and satellite ocean biology data at approximately 4,500 m resolution. To predict hypoxia level, we considered all 14 available satellite-derived variables from the aforementioned MODIS dataset, including ten ocean color bands (412, 443, 469, 488,

531, 547, 555, 645, 667, and 678 nm) and four ocean biology variables (chlor_a - Chlorophyll-a concentration, nflh - Normalized fluorescence line-height, poc - Particulate organic carbon, and sst - Sea surface temperature) as inputs (see Table 3.1). Among these variables, Chlorophyll-a concentration is a key proxy of eutrophication and algae blooms, which have the most direct linkage with dead zones (Chen et al., 2014; Klemas, 2011, 2011; Le et al., 2016; Leming and Stuntz, 1984). We also included wind speed and sea surface temperature which are reported to play roles in the biophysical processes controlling hypoxia (e.g., photosynthesis, stratification) (Altieri and Gedan, 2015; Breitburg et al., 2018; Jane et al., 2021; Limburg et al., 2020). In addition, to capture the impact of water stratification on bottom water hypoxia, we used water salinity, water velocity, and water temperature in the depth profile of 0-5000 m. These gridded data were obtained from NOAA, the Hybrid Coordinate Ocean Model (HYCOM) consortium (Cummings and Smedstad, 2013). Here, we used the gridded bathymetry data from the General Bathymetric Chart of the Oceans (GEBCO) gridded bathymetric data set (GEBCO, 2019) to determine the depth of the water bottom. To ensure cloud-free or near-cloud-free wall-to-wall coverage, the imagery was composed by taking the median value of a given pixel every five days. All the gridded data were resampled to the same resolution as the MODIS Ocean Color products. In total, 24 satellite-derived variables were included in the initial analysis. More detailed information on data sources and variables is listed in Table 3.1.

3.3.4 Dead zone prediction using satellite imagery

To detect dead zones (hypoxia beneath the water) from remote space, it is important to understand the biological phenomena and underlying processes. Although the formation of dead zones involves multiple complex biophysical and chemical processes (Figure 3.3), it is clear that

in the Gulf of Mexico, hypoxia is usually preceded by coastal eutrophication and algae bloom caused by excessive nutrient runoffs from the adjacent river basin, especially the Mississippi River basin. Recent studies also reported global warming can also fuel the process of blooms and seawater thermal stratification) (Altieri and Gedan, 2015; Breitburg et al., 2018; Jane et al., 2021; Limburg et al., 2020). Satellite remote sensing is a powerful tool for capturing the related water surface changes, such as phytoplankton biomass (or chlorophyll concentration as a proxy), colored dissolved organic matter load, and sea surface temperature (Le et al., 2014; Pekel et al., 2016; Zhou et al., 2020), which can serve as important indicators for predicting dead zones (Demeke, 2016).

Table 3.1. Data sources

Data description	Variables	Resolution	Availability	Data source	GEE Collection
MODIS Aqua Ocean Color level 3 product	<i>chlor_a</i> , <i>nflh</i> , <i>poc</i> , <i>Rrs_412</i> , <i>Rrs_443</i> , <i>Rrs_469</i> , <i>Rrs_488</i> , <i>Rrs_531</i> , <i>Rrs_547</i> , <i>Rrs_555</i> , <i>Rrs_645</i> , <i>Rrs_667</i> , <i>Rrs_678</i> , <i>sst</i>	4616 m; Daily	2002-07-03 – Now	NASA Goddard Space Flight Center, Ocean Ecology Laboratory, Ocean Biology Processing Group	ee.ImageCollection("NASA/OCEANDATA/MODIS-Aqua/L3SMI")
MODIS Terra Ocean Color level 3 product	(Same as above)	(Same as above)	2000-02-24 – Now	(Same as above)	ee.ImageCollection("NASA/OCEANDATA/MODIS-Terra/L3SMI")
Pathfinder Version 5.3 AVHRR Sea Surface Temperature Data	<i>wind_speed</i>	4000 m; Twice-daily	1981-08-24 – Now	NOAA National Oceanographic Data Center	ee.ImageCollection("NOAA/CDR/SST_PATHFINDER/V53")
Hybrid Coordinate Ocean Model, Water Velocity	<i>velocity_u_x</i> (Eastward sea water velocity at <i>x</i> m); <i>velocity_v_x</i> (Northward sea water velocity at <i>x</i> m)	8905.6 m; Daily	1992-10-02 – Now	National Ocean Partnership Program (NOPP)	ee.ImageCollection("HYCOM/sea_water_velocity")
Hybrid Coordinate Ocean Model, Water Temperature and Salinity	<i>salinity_x</i> (Sea water salinity, in practical salinity units, at <i>x</i> m); <i>water_temp_x</i> (Sea water temperature at <i>x</i> m)	8905.6 m; Daily	1992-10-02 – Now	National Ocean Partnership Program (NOPP)	ee.ImageCollection('HYCOM/sea_temp_salinity')
Gridded Bathymetry Data	<i>Bathymetry</i>	~450 m; NA	2020	British Oceanographic Data Centre (BODC)	ee.ImageCollection("projects/sat-io/open-datasets/gebco/gebco_grid")

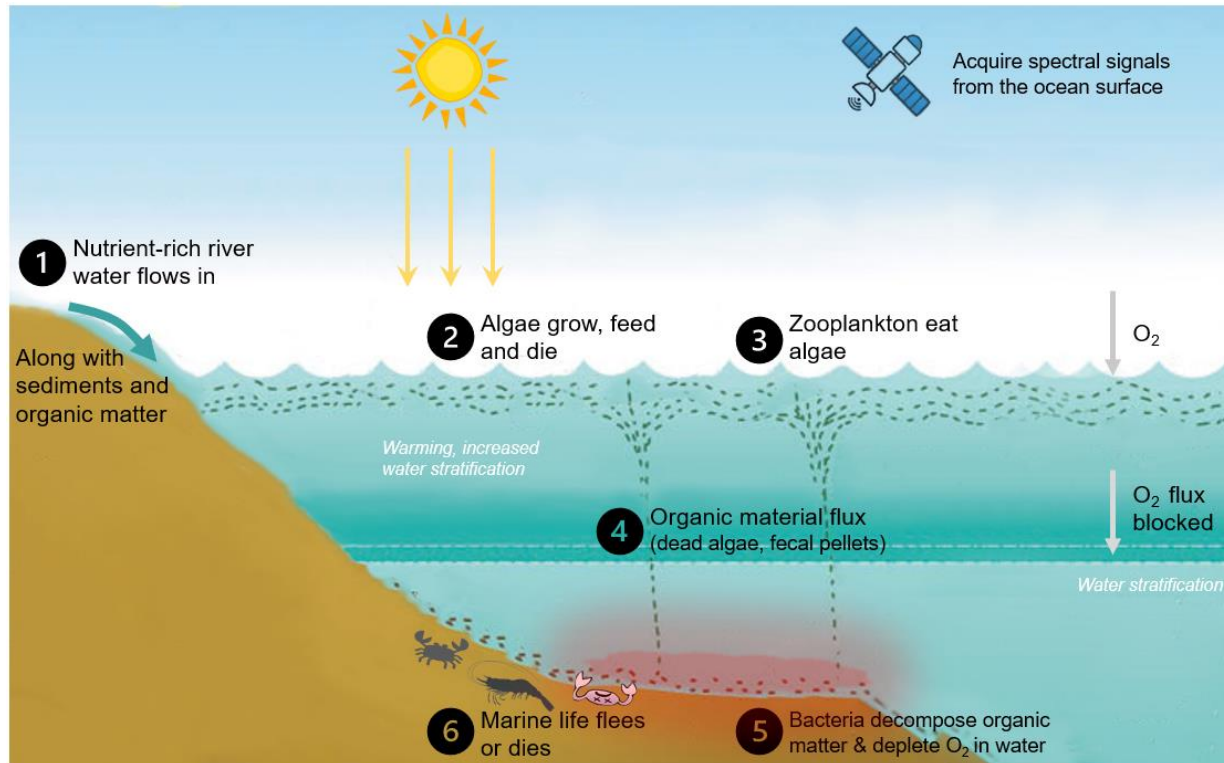


Figure 3.3. Multiple factors and processes contribute to coastal dead zone

(1) Random forests

We used the Random Forest Regression (RFR) model to fit the DO observations with the predictors mentioned above. Random Forest is well-known for its capability of capturing the hidden patterns and nonlinear interactions between features in large and complex data and enabling better predictions (Chen et al., 2019; Hutengs and Vohland, 2016). Besides, it can handle high data dimensionality and typically achieve high accuracy (Belgiu and Drăguț, 2016; Breiman, 2001; Lin, 2017; Teluguntla et al., 2018). Here, the built-in Random Forest algorithm in the GEE cloud computing platform was used, as it allowed us to develop a complete workflow on a single platform and facilitate the application at large spatial scales.

The flowchart for using RFR to estimate DO is illustrated in Figure 3.4. We first extracted features from multiple satellite data described above and used these features as initial predictor variables for RFR classifiers training. Water samples from 2000-2019 were used for developing the dead zone model. We randomly selected 70% of the 8117 water DO measurement locations (Figure 3.1) as training samples and the remaining 30% as testing samples (for validation). Through repeated experiments and following previous work (Pelletier et al., 2016; You et al., 2021), the “numberOfTrees” (i.g., the number of binary Classification and Regression Trees – CART – used to build a Random Forest model) in our study was set to 99 and other parameters were set by default in the GEE. Then, we selected 12 variables as the final predictor variables according to the importance score of each input feature (Figure 3.5 and Figure A3.0.3). The importance scores were derived from the RFR model and are often used to select important predictor variables in order to reduce the computational cost and ensure the stability of the classification results (Huang and Zhu, 2013; Xia et al., 2022).

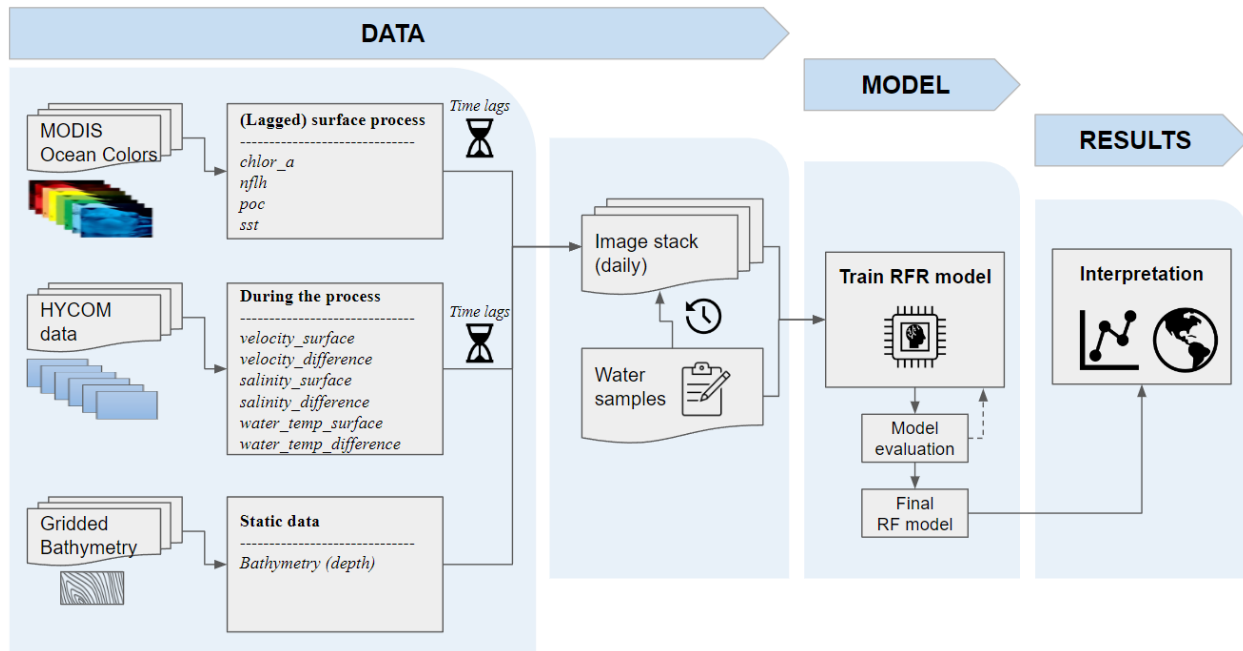


Figure 3.4. Flowchart for dead zone prediction with Random Forest Regression (RFR) model. Satellite-derived variables (from MODIS and HYCOM) were integrated with water samples by considering a list of potential time lags.

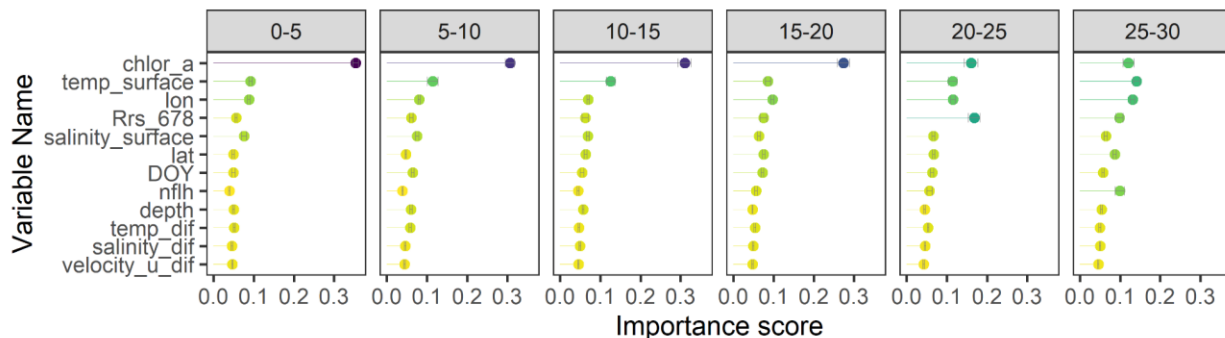


Figure 3.5. Importance score of the selected variables in each lagged Random Forest Regression model. Each panel presents the results from the models with a range of time lags. For example, the panel named "0-5" shows the average variable importance from models with lagged satellite predictors at 1-day lag, 2-day lag, 3-day lag, 4-day lag, and 5-day lag. The error bars represent 95% confidence intervals. *Chlor_a* – Chlorophyll-a concentration; *nflh* – Normalized fluorescence line-height; *poc* – Particulate organic carbon, *temp* – Sea water temperature, *lon* – longitude, *lat* – latitude, *xxx_dif* – the difference between values on the surface and bottom water, *DOY* – day of the year. Refer to Table 3.1 for all other variable information. See Figure A3.0.3 for the importance scores of all the 24 pre-selected variables.

(2) Prediction performance

The prediction performance of the RFR models was evaluated with the commonly used statistical metrics, including coefficient of determination (R^2 , equation 1), root mean square error (RMSE, equation 2), and the mean absolute error (MAE, equation 3). Similar to many other modeling studies (Linderman et al., 2005), we used a random 70% of the samples as the training dataset and the remaining 30% as the testing dataset (for model validation).

$$R^2 = 1 - \frac{\sum_{i=1}^n (\hat{y}_i - y_i)^2}{\sum_{i=1}^n (y_i - \bar{y})^2} \quad (1)$$

where y_i is the true values of DO observation, \hat{y}_i is the estimated DO values, and \bar{y} is the average value of y_i .

$$RMSE = \sqrt{\frac{\sum_{i=1}^n (y_i - \hat{y}_i)^2}{n-1}} \quad (2)$$

$$MAE = \frac{1}{n} \sum_{i=1}^n |y_i - \hat{y}_i| \quad (3)$$

where the n is the total number of testing samples, y_i is the true values of DO observation, \hat{y}_i is the estimated DO values.

(3) Time lags in satellite prediction of bottom DO

As described in Figure 3.3, there is likely a time lag between what can be detected on the surface (e.g., algae blooms, temperature variations) and hypoxia occurrence beneath the water. Although not well studied, a few studies indicate the lag can range from days up to two months (Chen et al., 2014; Justić et al., 1993; Zhou et al., 2020). To empirically determine the appropriate time lag for optimal prediction, we fitted DO with predictor variables collected at each different possible time lag (from 0 day to 80 days, in each model tested, only one lag was included), compared the model performance at each time lag, and chose the time window during which the

satellite-derived predictors can achieve the highest performance. We chose to examine the 0-80 days range because earlier studies suggest the time lag ranges from days to up to two months (Chen et al., 2014; Justić et al., 1993; Zhou et al., 2020).

Our analysis shows that satellite-derived predictors collected on 30-32 days achieved the highest prediction, with the highest R^2 , lowest RMSE, and MAE (Figure 3.6). Therefore, to implement the RFR for hypoxia mapping, we chose satellite imagery from these date ranges as model inputs.

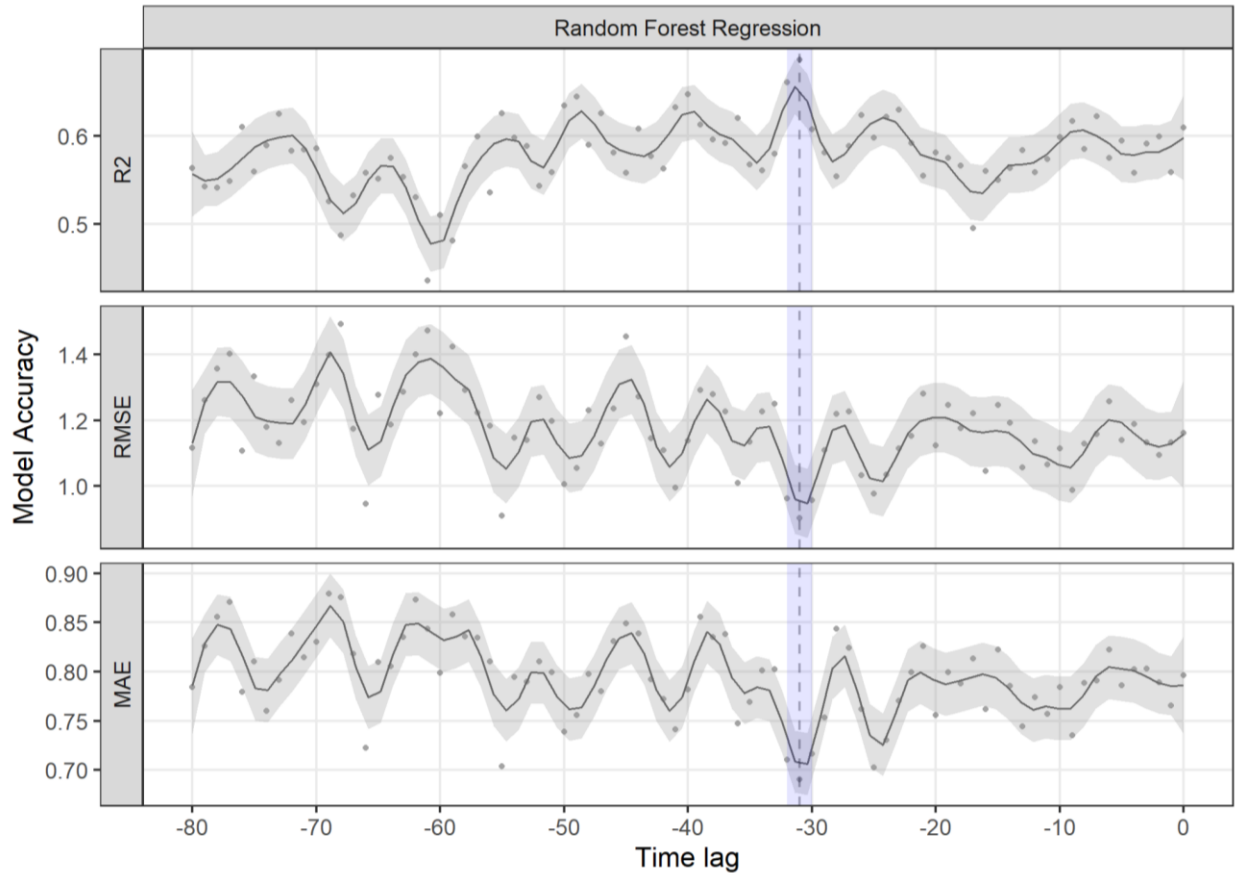


Figure 3.6. Model performance for DO prediction with satellite predictors at different time lags. Model performance is evaluated by R^2 , RMSE (mg/L), and MAE (mg/L) between estimated and observed DO. Lines represent mean values, and shaded areas around the lines represent 95% confidence intervals. The blue shaded area indicates the dates of satellite predictors that achieved relatively highest accuracy.

(4) Mapping intra- and inter-annual dead zone occurrence

We define the **annual maximum dead zone** as the total area of any locations that ever experienced hypoxia during the summer period (May - September) each year. This outcome can provide an estimation of the total affected areas, and our predictions can be also used to contrast with the reported dead zone area by other agencies. To show the persistence of dead zones each year, we used **intra-annual dead zone occurrence** (intra-DZO) to measure the frequency with which dead zones occurred during the summer period each year. Intra-DZO is computed at the pixel level, as the percentage of the number of days (d) with detected dead zone (DDZ) among the total days with valid observations (VO) during the same summer period in a certain year (y), as shown in equation 4.

$$intra\ DZO_y = (\Sigma DDZ_{dy} / \Sigma VO_{dy}) \times 100\% \quad (4)$$

$$inter\ DZO = (\Sigma DDZ_y / \Sigma VO_y) \times 100\% \quad (5)$$

Similarly, we used **inter-annual dead zone occurrence** (inter-DZO) to measure the variability in the presence of dead zones across years. Inter-DZO is also computed at the pixel level, as the percentage of the total years with detected dead zone (DDZ) among the total years with valid observations (VO) across the 20 years (2000-2019), as shown in equation 5.

3.4 Results

3.4.1 Temporal changes of dead zones

Satellite imagery, combined with random forest machine learning techniques, can well predict and map the Gulf hypoxic zones ($R^2 = 0.64 \pm 0.05$). We found that the hypoxic area increased steadily since 2000, peaking in 2009, then followed by a decreasing trend until 2013 and stayed at a fairly consistent level at $\sim 10,000\text{ km}^2$ afterward (Figure 3.7). The decrease since 2009 is

likely attributed to the Gulf Hypoxia Action Plan with the goal to reduce the size to less than 5000 km². Even with the ambitious reduction goal and substantial achievement, the average size was still persistently high beyond the red line (mean = 11245±3574 km², 2009-2019).

Most years, dead zones started to grow in June and peaked during mid-August and September (Figure 3.8). From the beginning of the 21st century until 2011, the dead zones were not only large in size but also persisted for over three months each year. Since 2011, the mega dead zones (area > 5,000 km²) usually persisted for around one month or a shorter period.

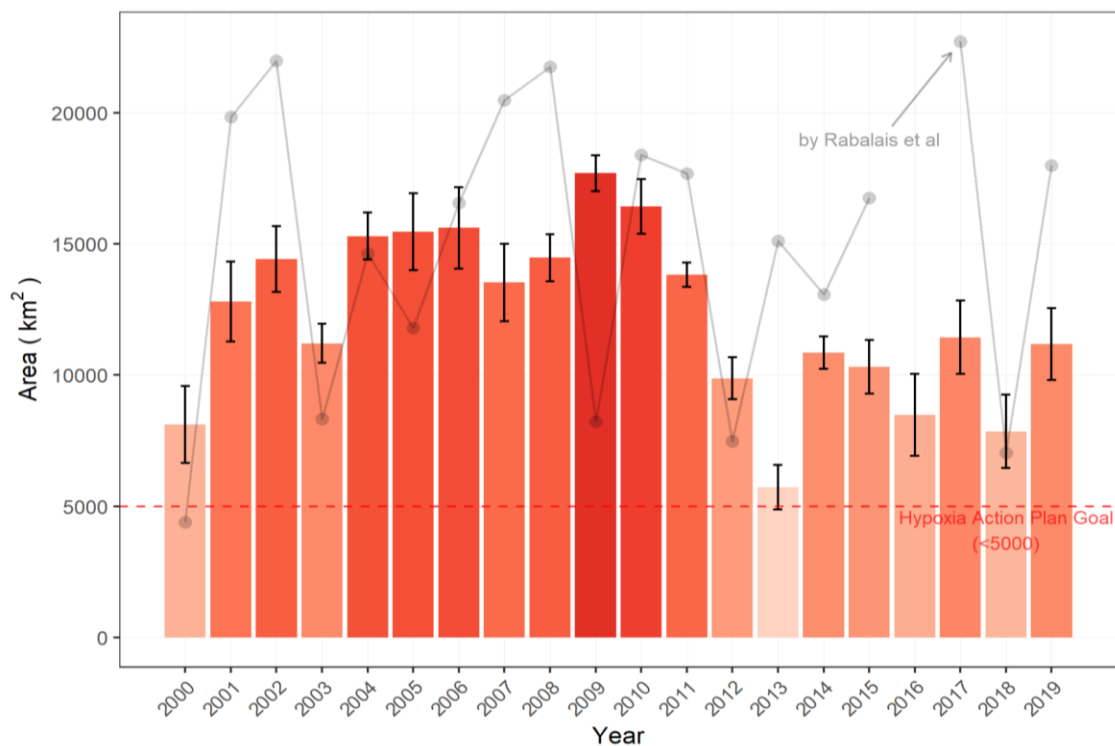


Figure 3.7. Annual dead zone area from satellite predictions (2000 - 2019). Dead zone = bottom water hypoxia (< 2 mg/L of dissolved oxygen). The error bars indicate the standard error of predictions (n = 30 days). Because the area of dead zone is changing over time within a year, we used the top 30 maximum dead zone daily predictions during each summertime (note: dead zone usually peaks in summer) to show the standard error of yearly maximum dead zone predictions. The dashed horizontal red line denotes the goal of the Gulf Hypoxia Action Plan to reduce the five-year running average size to less than 5000 km². The light-gray line with dots shows the area of hypoxia reported by Rabalais et al (see <https://gulfhypoxia.net/research/shelfwide-cruises>, no data for 2016). Please note that the estimation by Rabalais et al was based on snapshot data of water measurement and the geospatial interpolation approach, which are not strictly comparable to our results. However, the trends from both studies show similarities.

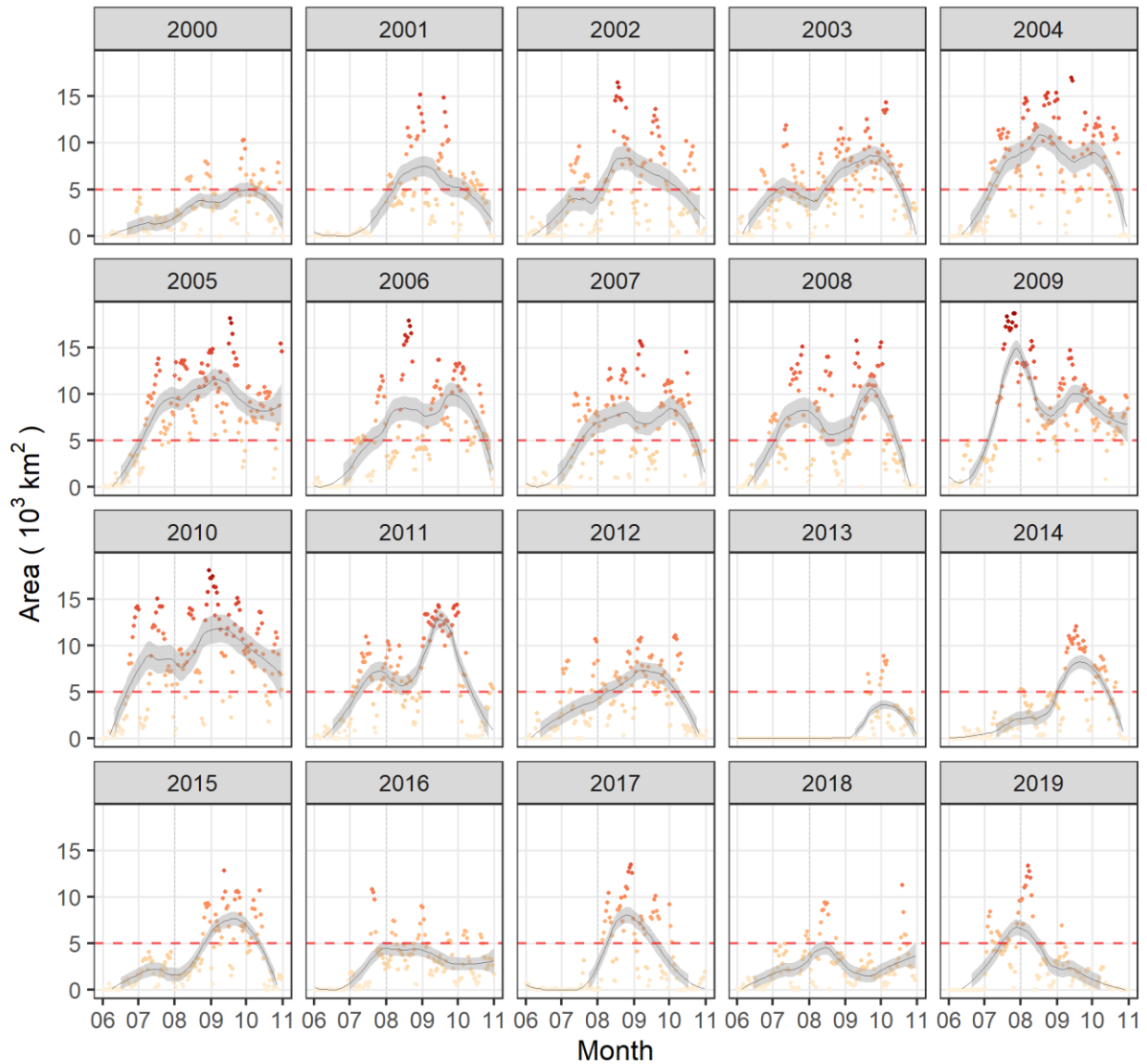


Figure 3.8. Intra-annual change of dead zones area over summer months. Dots show the estimated dead zone area each day, and darker red colors indicate larger areas of dead zones. Lines represent the smoothed conditional means by the local polynomial regression fitting method. The shaded areas around the lines represent 95% confidence intervals. The dashed horizontal red line denotes the goal of the Gulf Hypoxia Action Plan to reduce the five-year running average size to less than 5000 km².

3.4.2 Spatial changes

Most dead zones were detected in the nearshore waters over the summer. We found that dead zones occurred more frequently ($> 40\%$ of the 20 years) on the west side of the Mississippi-Atchafalaya Rivers bird-foot estuary than in other regions (Figure 3.9). Nearly half of the hotspot region experienced dead zones annually over the 20 years. In addition to the northern Gulf region, we also detected dead zone occurrences at the Suwannee River estuary in the eastern Gulf, which were rarely studied.

We further investigated the intra-annual dead zone occurrence each summer from 2000 to 2019 (Figure 3.10). Similar to the interannual dead zone occurrence, areas with high intra-annual dead zone occurrence are mostly located in the northern Gulf region and at the estuary of Suwannee River (Figure 3.10a). The area with over 60% dead zone occurrence over summertime (or over 3 months) exceeded the 5,000 km² redline from 2001 to 2012, while the subsequent years were below the line (Figure 3.10b). This indicates that dead zones became both smaller and less persistent after 2012 than in earlier years.

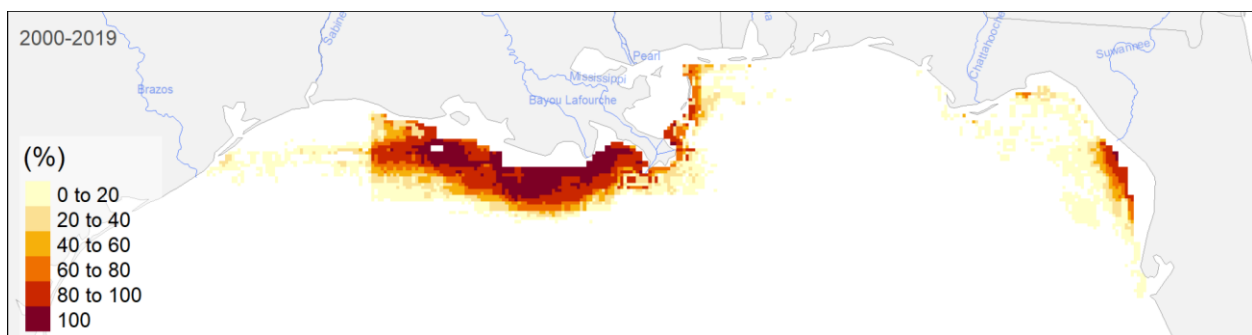


Figure 3.9. Inter-annual dead zone occurrence (%) during 2000–2019. All of the colored regions denote dead zone occurrence (dissolved oxygen < 2 mg/L).

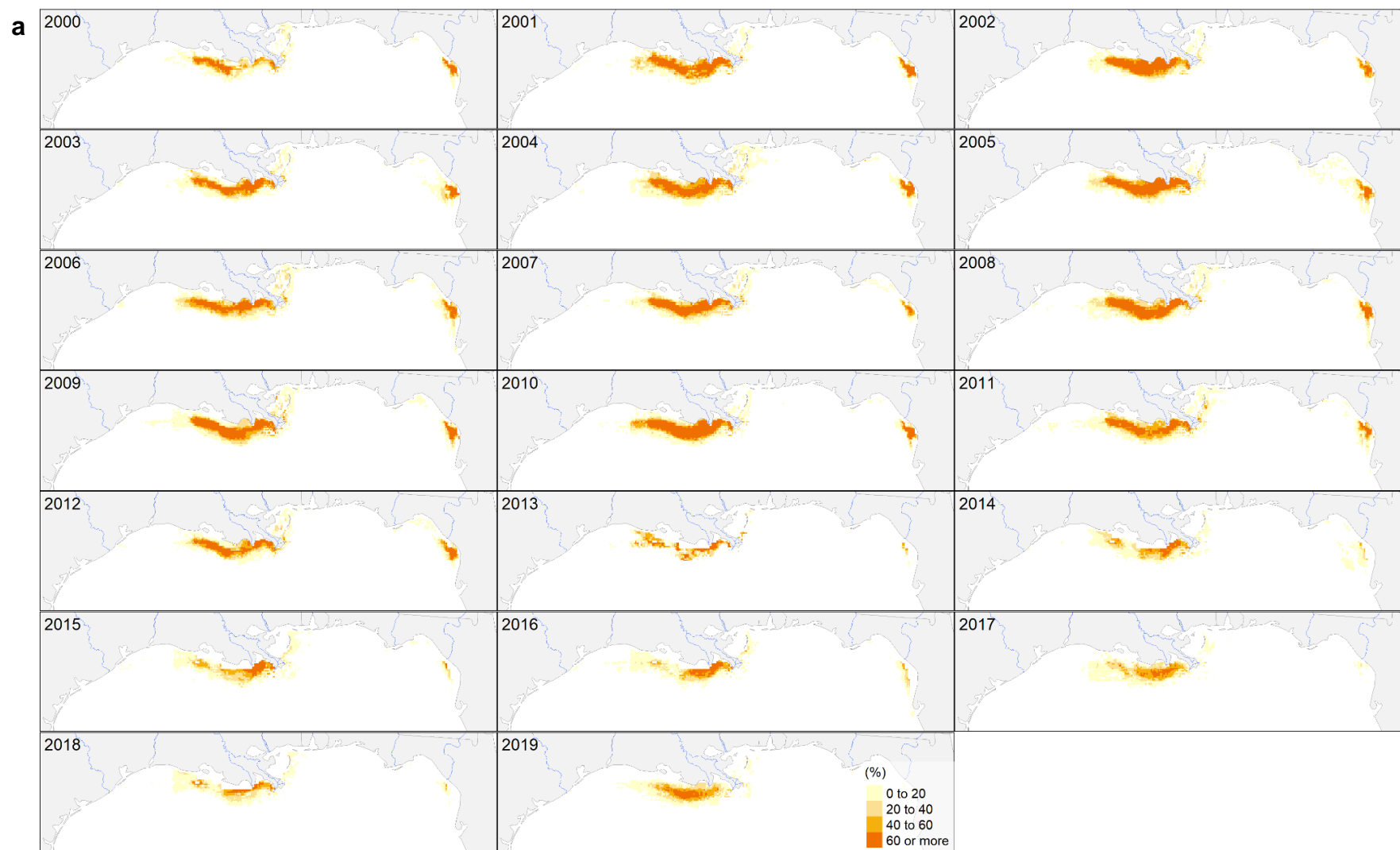
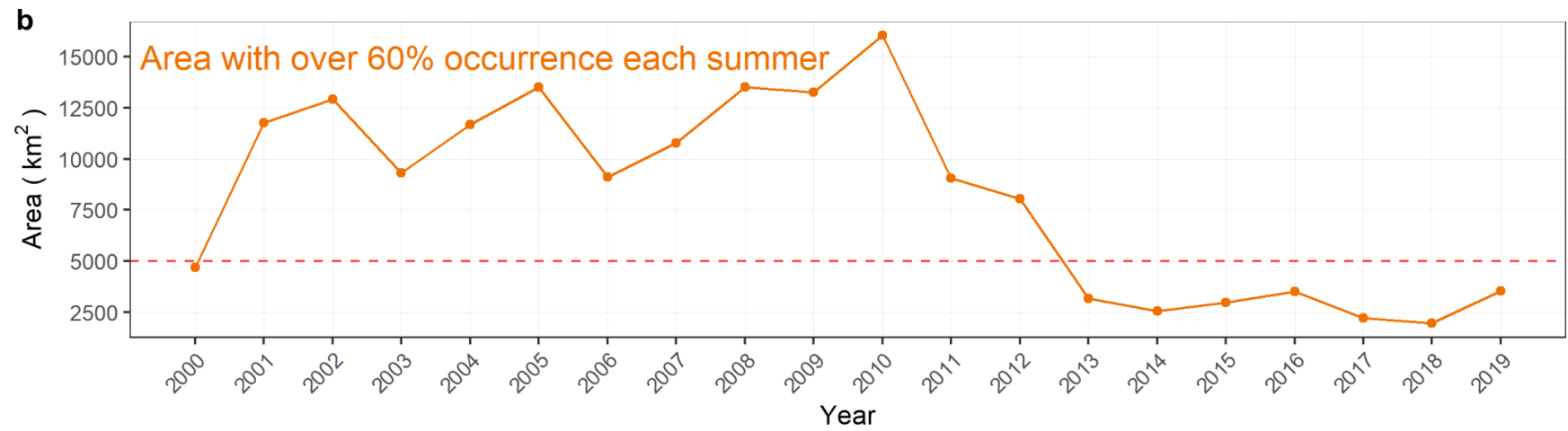


Figure 3.10. The intra-annual dead zone occurrence (a), and the area with over 60% occurrence in each summer (b). All of the colored regions demote dead zone occurrence (dissolved oxygen < 2 mg/L). The dashed horizontal red line denotes the goal of the Gulf Hypoxia Action Plan to reduce the five-year running average size to less than 5000 km².

Figure 3.10 (cont'd)



3.5 Discussion

This study presented the first spatiotemporal mapping of dead zones across 20 years using remotely sensed imagery. The spatially explicit dead zone maps from this study reveal not only the geospatial characteristic of the dead zones in the Gulf of Mexico but also the change over time at multiple temporal scales (e.g., from days to years). This research, therefore, advanced existing research by introducing and highlighting the usefulness of satellite imagery in modeling and predicting coastal hypoxia.

Our results show the Gulf dead zones peaked in 2009 and faded afterward in terms of both size and persistence (measured by intra-annual occurrence). Although the dead zone decreased in size that likely attributed to the achievement of the Gulf Hypoxia Task Force (US EPA, 2008), the average size was still twice beyond the targeted redline goal (targeting below 5,000 km²), highlighting the critical need for continual management and monitoring efforts

3.5.1 Strengths of and uncertainties of using satellite imagery for dead zone prediction

Our approach using remote sensing provides insight into selecting important satellite-derived variables and the appropriate time window for dead zone prediction. Previous research on dead zone modeling and prediction rarely used satellite data (Forrest et al., 2011; Matli et al., 2020; Murphy et al., 2011; NOAA, 2022; Scavia et al., 2017; Zhou et al., 2014), which might miss the important spatial and temporal changes in coastal monitoring. We found the satellite-derived variables can explain 64% ($\pm 5\%$) of the variance in bottom DO. Because traditional coastal hypoxia monitoring based on cruise trips is constrained by weather conditions, funding availability, and potential interruption of unexpected shocks, the ground measurements are

limited in space and time (usually a snapshot at a certain time point in a year). These constraints further limit the ability to estimate dead zone changes across space and over time. Ocean satellite imagery such as MODIS and SeaWiFS, can supplement the ground measurements, and provide long-term and large-scale information for coastal monitoring when integrated with ground measurements. For example, MODIS-Terra/L3SMI and MODIS-Aqua/L3SMI used in this study provide daily imagery since 2000. The SeaWiFS can provide similar satellite ocean biology data dating back to 1997 on a daily basis. These data with rich information can be very useful for an in-depth understanding of the coastal process. For instance, we used satellite imagery to explore the appropriate time lags between seawater surface characteristics captured by satellite and bottom hypoxia. Our analysis shows the time lag is most likely at 30-32 days on average. This partly aligns with previous estimations. For example, a study in the East China Sea by Zhou et al (2020) revealed a lag of 1–8 weeks, and Justić et al (1993) implied a lag of up to 8 weeks. Although our findings are supported by earlier studies, there is still a lack of sufficient and direct evidence to determine the exact time lag between surface processes and bottom hypoxia. One explanation could be that the time lag may vary across years due to changing climate and ocean environment. Future studies can use more continuous ground measurements (e.g., buoy) and more delicate process-based models to better examine the time lag issue.

Although satellite-based data are plentiful, they are prone to data gaps because of cloud and sun glint, and inter-orbit gaps. Like most other time-series analyses using remote sensing, our mapping also encountered missing pixel issues in our dead zone mapping (Figure 3.11). Those data gaps might lead to underestimation of the coastal dead zones, despite better spatial coverage than the traditional on-site measurements. Gap-filling using time series by taking the composite

median or mean is the conventional way to address the gap, but might not be appropriate for detecting time-sensitive changes, such as algae dynamics and the short-term dead zone consequences. In addition, unlike the terrestrial landscapes, the spatial movability of water requires that the ideal gap-filling techniques should consider the spatial dimension instead of only the temporal dimension. Some have used a soap-film smoothing approach (Li et al., in review; Wood et al., 2008) and deep learning approaches (L. Li et al., 2020; Shao et al., 2019), which incorporated both spatial and temporal dimensions for imputation. Unfortunately, these tools are either currently not available on the Google Earth Engine platform or require ancillary satellite imagery that is not available for this study. Future advances in these techniques and data fusion would promisingly address the data gaps. In addition to these data gaps in satellite imagery that might limit dead zone mapping, the accuracy and representativeness of satellite-derived variables might also influence model accuracy. For instance, the near-surface concentration of chlorophyll-a derived from remote sensing reflectances is a widely used proxy for detecting floating algae in open ocean environments (Hu, 2009), but still with some uncertainties. Taking the chlorophyll-a product by MODIS-Aqua as an example, the mean absolute error (MAE) is about 1.68 for a data range of 0.03 - 99.17 (Seegers et al., 2018). Furthermore, different algae species can impact the representativeness of using chlorophyll-a as the key variable for predicting dead zones. Not all algae are bad and lead to dead zones. For instance, Sargassum is considered critical for protecting marine habitats and associated marine species. While excessive Cyanobacteria, Dinoflagellates, Coccolithophores, and Diatom in coastal oceans are mainly responsible for causing significant adverse impacts on ocean ecosystems (Campbell et al., 2019). Our model did not tease out the “good” algae and thus might lead to an overestimation. Distinguishing the species will be critical for further improving model

accuracy and explanatory power. However, related algorithms for this effort have not been developed.

Existing dead zone predictions usually refer to the hypoxic area estimations by the Louisiana Universities Marine Consortium (LUMCON), which are based on water sampling by midsummer cruises. We also overlaid our predictions with the LUMCON results (Figure 3.7) and found both estimations show similar trends despite variations across years (Figure A3.0.2). The estimations of dead zone areas by LUMCON were largely based on snapshot data of water measurement and geospatial interpolation approaches, which are not strictly comparable to our results. This is because the LUMCON cruise sampling dates varied on each individual trip and also across years. As a consequence, it is possible that the measurements missed the timing for capturing important water information. It is therefore important we integrate the discrete ground measurements with the continuous satellite observations to construct models and characterize the relationships in order to better understand the spatial and temporal dynamics of the coastal dead zones.

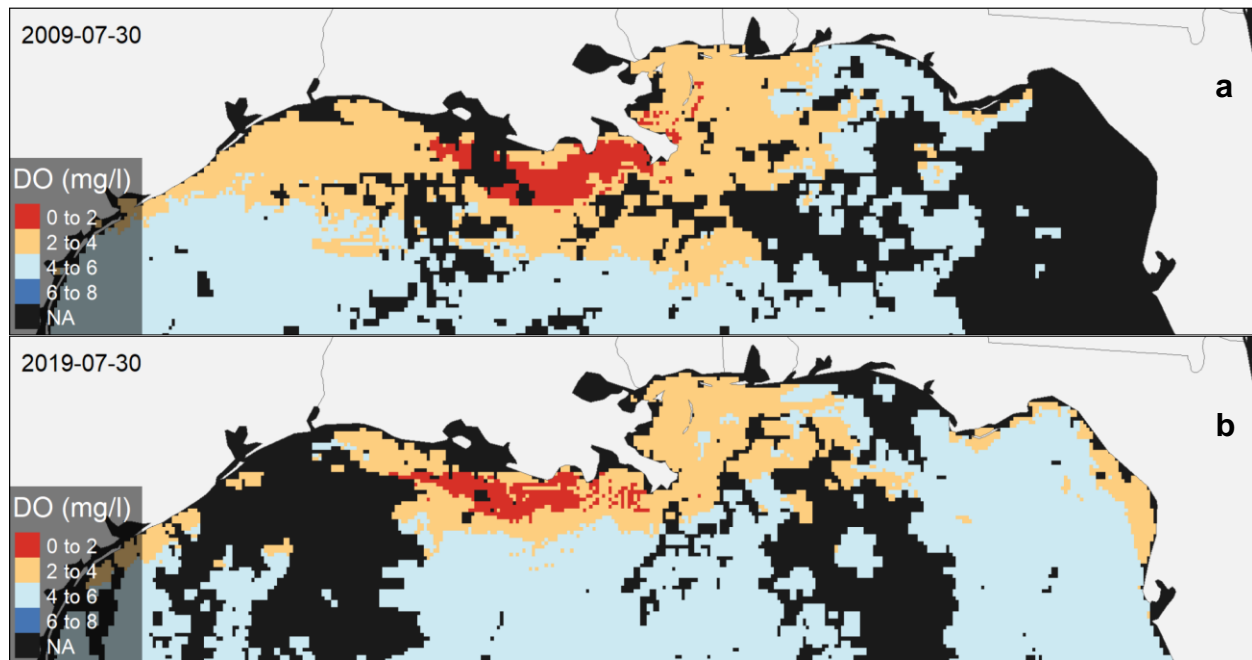


Figure 3.11. Two demonstrations of the predicted dissolved oxygen (DO) levels in the bottom water. Pixels with DO less than 2 mg/L are classified as dead zones.

3.5.2 Important satellite predictors for dead zone mapping

Our analysis found that sea surface temperatures, remote sensing reflectance at band 678 nm (the chlorophyll fluorescence emission spectrum), longitude, and chlorophyll a concentration are the most important predictors in the RFR model (Figure 3.12). This partly aligns with previous non-remote sensing studies, which demonstrated that algae bloom (or its equivalent net primary productivity) and climate warming are two important explanatory variables in hypoxia prediction models (Chen et al., 2014; Kim et al., 2020; Le et al., 2016). Climate warming has been well demonstrated in the literature that warming has become the dominant factor causing phytoplankton blooms and deoxygenation in both lakes and coasts (Altieri and Gedan, 2015; Breitburg et al., 2018; Ho et al., 2019; Jane et al., 2021; Kim et al., 2020). The main mechanism is that seawater warming can not only facilitate water stratification but also algae bloom (Dagg and Breed, 2003; Matli et al., 2020; Rabalais et al., 2009). Water stratification makes dead zones worse by preventing the water mixing that supplements oxygen to bottom water (Figure 3.3). In

the Gulf, the increase of algae often aligns with the temperature rise (Figure 3.13a). Chlorophyll a concentration and chlorophyll fluorescence (i.e., band 678 nm) both have been widely used as proxies of algae blooms. Specifically, Chlorophyll a is the predominant type of chlorophyll found in green plants and algae, and is used to measure the amount of phytoplankton in waterbody. Remote sensing reflectance at band 678 nm is often used for measuring normalized fluorescence height (nflh) – an important indicator of the physiological status of phytoplankton (Behrenfeld et al., 2009), and it is also used in the Red Band Difference algorithms for detecting algal blooms (El-habashi et al., 2016). Since algae have a short life span, and their growth and death infuse rich organic matter into the bottom water, where the decomposition by bacteria can lead to depletion of oxygen (Figure 3.3, <https://www.epa.gov/ms-htf/hypoxia-101>). Variables used as proxies of algae bloom therefore are important for modeling hypoxia. In addition, longitude is an important predictive variable, likely because longitude correlates with temperature and higher longitude also indicates more adjacent to the coastal line and river estuaries with relatively higher concentration of nutrients. We did not use nutrient loads as a predictor in our model for two reasons: (1) the lack of spatial information on nutrient loads, and these data were usually collected along river streams instead of in the coastal water; (2) there is a strong lagged correlation ($r = 0.60 \pm 0.15$, $p < 0.001$) between nutrient loads to the Gulf and the chlor_a levels (Figure 3.13b) (Walker and Rabalais, 2006), but the latter is a more direct driver of coastal water hypoxia and has spatial information from the satellite. Algal blooms (represented by chlor-a and fluorescence measurements) have been widely recognized as the dominant driver of hypoxia both in freshwater and oceans (Behrenfeld et al., 2009; Jane et al., 2021; Scavia et al., 2017; Shen et al., 2019). Other factors, such as water salinity, and three water

stratification-related variables (the difference between surface and bottom temperature, salinity, and velocity) are also among the top 12 most important predictors (Figure 3.12).

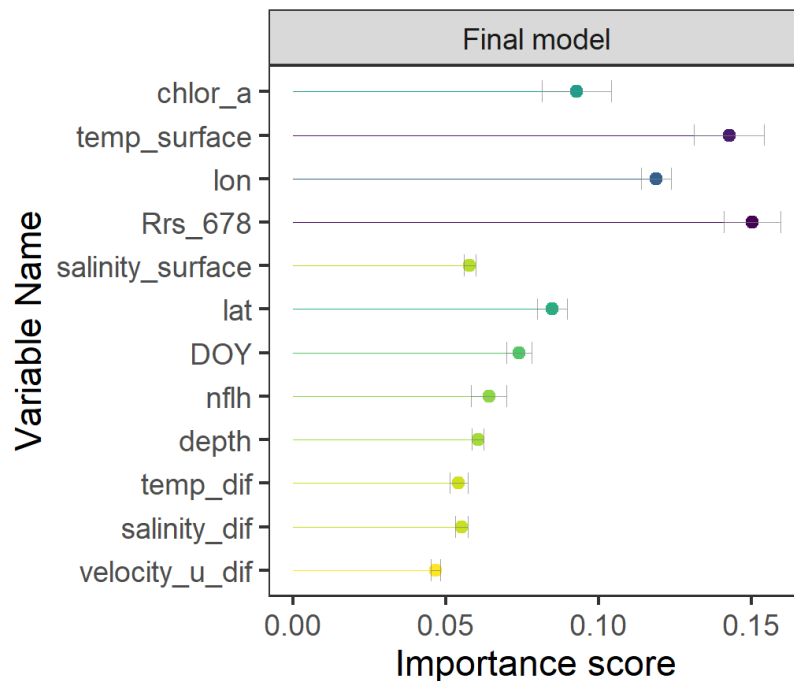


Figure 3.12. Importance score of the variables in the final Random Forest Regression model. The error bars represent 95% confidence intervals. Chlor_a – Chlorophyll-a concentration; nflh – Normalized fluorescence line-height; poc – Particulate organic carbon, temp – Sea water temperature, lon – longitude, lat – latitude, xxx_dif – the difference between values on the surface and bottom water, DOY – day of the year. Refer to Table 3.1 for all other variable information.

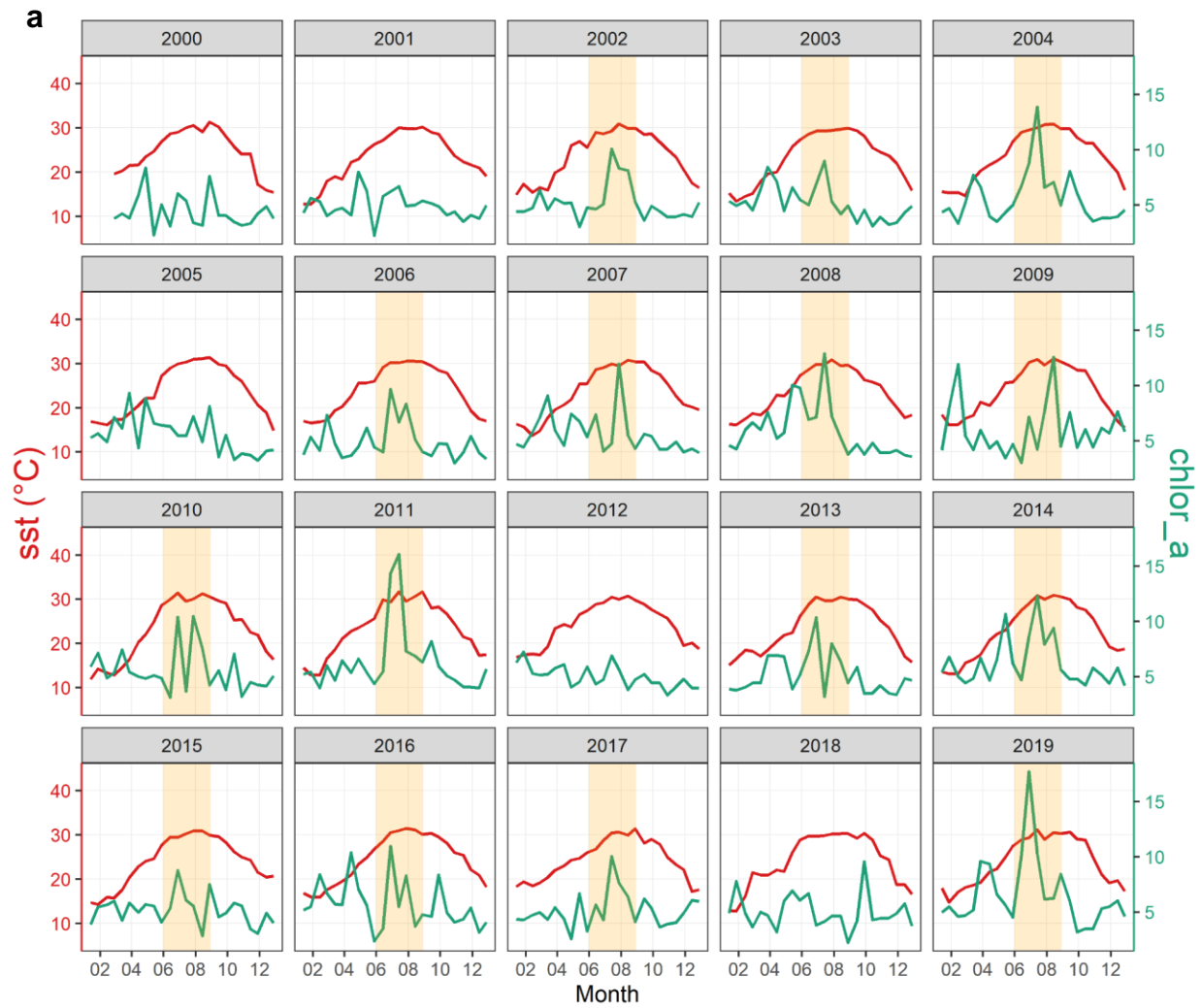
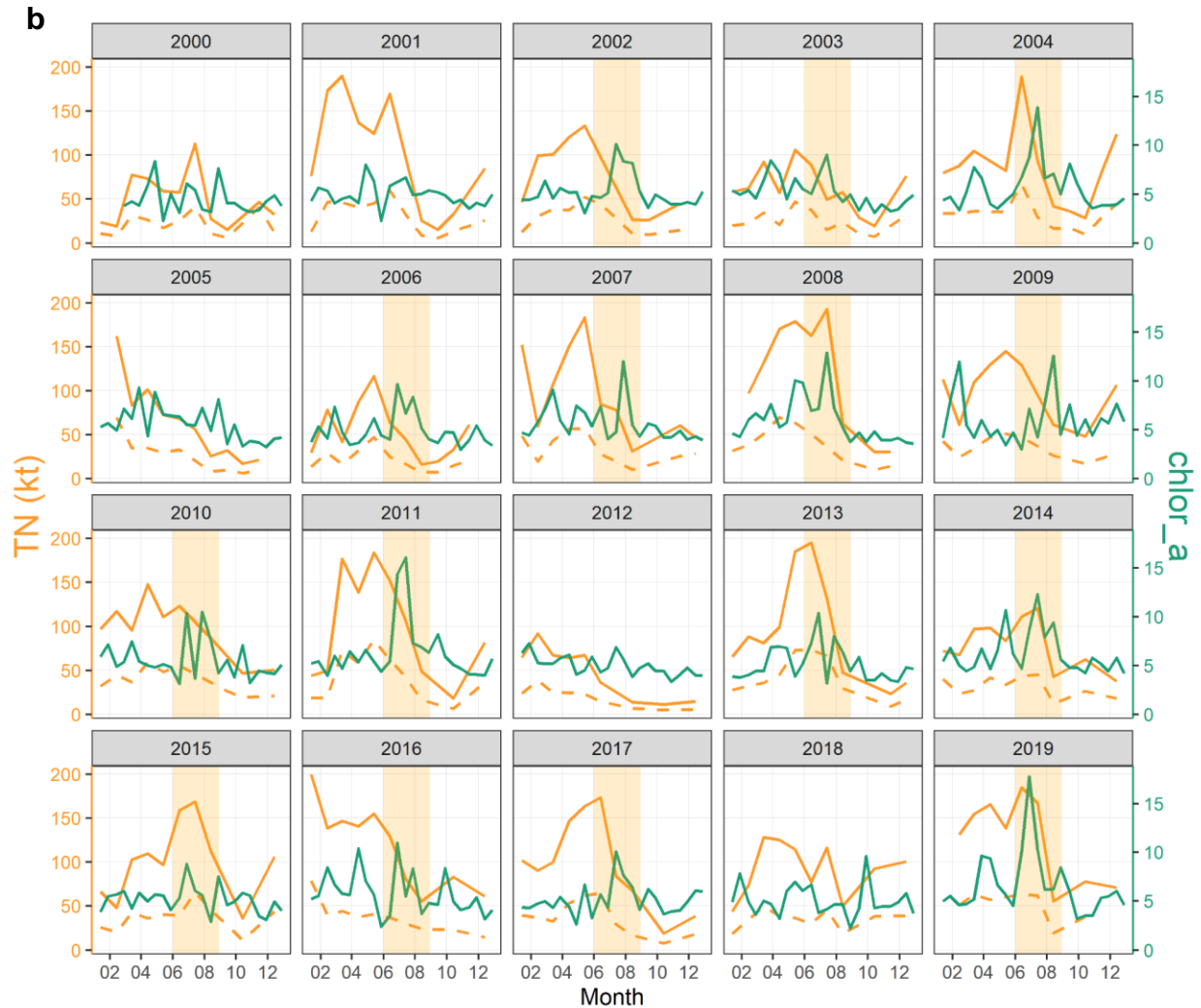


Figure 3.13. Temporal changes in chlor_a, (a) sea surface temperature (sst), and (b) nutrient loads (TN) from the Mississippi River basin (orange solid lines) and the Atchafalaya River basin (orange dashed lines)

Figure 3.13 (cont'd)



3.5.3 Needs for long-term global studies on dead zones and telecoupled land-ocean systems

In addition to the Gulf of Mexico, the United Nations Environment Programme (UNEP) and the Intergovernmental Oceanographic Commission also identified other 65 large marine coastal ecosystems across the globe that experienced similar human and natural stressors, which could potentially lead to interacting and cumulative environmental impacts and severe consequences on human well beings (IOC-UNESCO and UNEP, 2016; UNEP-DHI and UNEP, 2016). To address these widespread challenges, there is an urgent need for long-term, global-scale, and

consistent coastal monitoring efforts. Our research, taking one of the largest coastal ecosystems as a demonstration, provides a highly-reproducible approach (e.g., using freely available satellite data and open-source algorithms on the GEE cloud computing platform) that can be easily transferred to study other coastal ecosystems worldwide. The approach and data also provided a foundation for using system thinking approaches to examine the linkages between large river basins and the adjacent coastal ecosystems (Best, 2019; Breitburg et al., 2018), especially the ones that are undergone serve impacts of dead zones (e.g., the Black Sea, the Gulf of Oman, and the East China Sea). Studies show most of the coastal eutrophications leading to harmful dead zones are driven by human pollution inputs from terrestrial ecosystems (e.g., excessive use of chemical fertilizers from agriculture, and animal manure). The integrated framework of telecoupling thus can be used to link distant places in the watershed that apply excessive fertilizers with the coasts that are suffering hypoxia issues (Hull and Liu, 2018; Liu et al., 2018a). Building such linkages can help predict the timing and amount of the excessive fertilizers that reach global coasts based on the locations of fertilizer applications and leakages as well as the speed of river water flows. Such information can help policymakers develop more integrated strategies to tackle nutrient reduction challenges and coast dead zone issues.

Uncertain climate change and the growing global population are projected to increase the intensity, duration, and spatial extent of global dead zones (Fennel and Testa, 2019; IOC-UNESCO and UNEP, 2016; Sinha et al., 2017). Therefore, improving the understanding of both past and future dead zone dynamics under climate change is urgently needed for early conservation actions (Domínguez-Tejo et al., 2016; Ménesguen and Lacroix, 2018). Our study demonstrated that remote sensing with long-term, consistent, and global observation can help

track the spatiotemporal variation of large-scale coastal systems in combination with the traditional in-situ field measurements. Future studies can build on the data and approaches developed and used in this study to further integrate satellite imagery, climate, and socioeconomic scenarios to predict future trends of coastal dead zones across space and over time. Sustainably managing and protecting marine and coastal ecosystems from pollution is among the United Nations Sustainable Development Goals. This research demonstrated that remote sensing big data can provide a new way and critical data products for coastal ecosystem assessments and management.

CHAPTER 4: FOOD DEMANDS ELSEWHERE ARE ALSO RESPONSIBLE FOR THE LOCAL FOOD-ENVIRONMENT TRADE-OFFS

4.1 Abstract

Globalization and specification have distanced production and consumption, which makes it more challenging to track environmental responsibility associated with the traded goods and services. Particularly, the environmental impacts of food and agriculture are substantially large. For instance, intensive agriculture and excess nutrient use in the U.S. Midwest have caused severe waterway pollution in the Mississippi River basin and the dead zone in the Gulf of Mexico. Research and measures have mostly focused on the production systems, while few have considered the potential responsibility of remote consumers. For instance, downstream food consumers who suffer water pollution and eutrophicated coasts could also be the ones who contributed to excess fertilizer use in the upper streams. To better understand food system's environmental impacts and account for the associated environmental responsibility, this chapter investigated the flow of virtual nitrogen surplus embodied in food trade among 132 regions in the U.S. The analysis found that 17.1% of the N surplus is from food consumption elsewhere but not local. The U.S. Midwest bears most of the N surplus burdens for the nation, with 27% ($\pm 0.5\%$) contributed by the lower Mississippi River basin and states other than the basin. There are chances that restructuring food flows could reduce nutrients into the Mississippi River, but with the risk of causing spillover effect on other regions and increase the national total N surplus to the environment. Compared to existing studies that track physical nutrient flows across landscapes, this work offers a new perspective by tracking the embedded virtual nutrient flows in food across regions at the subnational level. The analysis thus can help identify who else other

than food producers should be responsible for the environmental impacts of food systems, and the findings (e.g., the displaced virtual N surplus) can serve as novel alternative indicators for determining the payment for ecosystem services.

4.2 Introduction

The world has become increasingly interconnected through trade among regions nearby and faraway. Large river basins span multiple states or regions can add more complexity to interregional interconnections (e.g., upstream-downstream relationships) through the natural interlinkages – river flows. For example, the U.S. Midwest in the upstream of the Mississippi River basin with intensive agricultural activities has long been blamed for leaking excess nutrients into waterways and leading to growing coastal "dead zones" in the Gulf of Mexico (Breitburg et al., 2018; Tian et al., 2020). Tremendous land conservation and nutrient reduction strategies have been taken, but the water quality issues across the watershed and subsequent eutrophication in the Gulf are still concerning (Murphy et al., 2013; Roy et al., 2021; Tian et al., 2020).

Past studies have provided in-depth and rich knowledge on how multiple socio-environmental factors (e.g., fertilizer use, atmospheric N deposition, land-use changes, climate variability) have affected the loading of total nitrogen in the Mississippi River basin. The data products (Byrnes et al., 2020; Cao et al., 2018) and findings (Meter et al., 2018; Roley et al., 2016) thus provided valuable information for identifying hotspots and implementing targeted nitrogen management strategies in the agricultural production systems (Roy et al., 2021). Despite the importance of sustainable production, recent studies have also highlighted the critical role of responsible

consumption in addressing environmental challenges and sustainable development goals (Li, 2021; Wiedmann and Lenzen, 2018; Xu et al., 2020c). The logic behind this claim is that demand could be a major driver of unsustainable production. While many studies have discussed the responsibilities of consumers, they generally do not explicitly state that the consumers could also be the victims of environmental pollution. Taking the river basin as an example, downstream consumers can be beneficiaries and victims of as well as contributors to food production upstream. Disentangling this paradox phenomenon is important to promote interregional environment governance and urge consumers to change consumption behaviors or switch to more sustainable and environmental-friendly food supply chain alternatives. To fully understand the coupled food and environment systems and explore alternative ways to address food-environment tradeoffs, it is important to approach the issue from both production-based and consumption-based accounting perspectives, especially the understudied consumption side.

In an increasingly interconnected world, production and consumption are largely spatially segregated while reconnected through distant commodity trade (Liu, 2020). It is thus challenging to accurately track how much environmental impact was imposed on the producer region by the distant consumers. Methods such as life-cycle assessment and environmental footprint approaches offer a feasible way to estimate the impacts by measuring the embedded environmental cost in commodity trade (Cucurachi et al., 2019; Fang et al., 2014; Galli et al., 2012). Related studies have mostly been carried out at the global scale (Lassaletta et al., 2014b; Schipanski and Bennett, 2012; Xu et al., 2019a), because international agencies, such as Food and Agriculture Organization Statistical Databases (FAOSTAT) and United Nations Commodity Trade Statistics Database (UN Comtrade), provide detailed bilateral international trade statistics

that can be used to measure the environmental footprints in traded commodities. However, few studies have been done at the subnational level due to the data availability, but see (Mahjabin et al., 2021; J. Wang et al., 2022). Think globally, act locally – a subnational analysis of environmental footprints can allow us to know which specific areas are susceptible to displaced environmental burdens and what targeted measures can be taken.

To narrow such knowledge gaps, the objective of this study aims to address the following questions. (1) Which regions' demand drove the food production in the U.S. Midwest? (2) How much virtual nitrogen surplus was displaced through food flows? And which regions contributed most to the nitrogen surplus in the environment? (3) How would the spatial pattern of N surplus change if the food supply chains were modified? To answer these questions, we compiled the U.S. interregional food trade information from the Commodity Flow Survey database, which covers commodity flows among 132 sub-regions (including 84 major metropolitan areas and the remainder of the states) in 50 states. In this study, we focus on major raw agricultural food, including seven cereal grains and seven livestock/poultry, because their productions are directly linked with land use and environmental impacts (see Methods 2.2). We are primarily interested in reactive nitrogen (i.e., all the nitrogen species except N_2) embedded in food production as reactive nitrogen is more mobile in the environment and is also the major cause of Gulf eutrophication and dead zones.

4.3 Materials and methods

4.3.1 *Study area*

The U.S. is one of the major agricultural suppliers as well as consumers in the global food supply chain networks (Chung and Liu, 2022). Many studies have examined its role in the international food trade networks (Berfin Karakoc and Konar, 2021; Dalin et al., 2017; Herzberger et al., 2019; Lassaletta et al., 2014b; Pastor et al., 2019), but much less on its domestic food systems (but see (Karakoc et al., 2022; J. Wang et al., 2022))). Studying food flows and the associated environmental impact at the sub-national scale has important implications because the U.S. Midwest, or most of the upper stream of the Mississippi River basin, has long been blamed for dumping excessive agricultural nutrients into the watershed systems, degrading water quality along the streams as well as contributing to the growing hypoxic dead zones in the Gulf of Mexico.

Considering both the socioeconomic interactions (e.g., food trade) and the embedded environmental interactions between systems, can help us have a holistic understanding of the coupled human-environment systems for interregional policy making. System thinking can help ignite new hypotheses, for instance, whether downstream food consumers who source food from upstream should be also responsible for the water pollution, although they do not physically involve in food production activities (Figure 4.1). This information could be useful for interregional watershed governance, such as through the payment for ecosystem services. We followed the integrated framework of metacoupling (socioeconomic-environmental interactions within a region, between the region and adjacent regions, and between the region and distant regions) (Liu, 2017), and viewed the food sending regions and receiving regions as well as

spillover regions (regions that are affected by the interactions between sending and receiving systems) as a metacoupled system. In this study, we are particularly interested in the interregional food flows and virtual N flows. We divided the U.S. into two major regions – the Mississippi River basin (MRB), and non-MRB (i.e., the remaining states). Since we focus on the MRB and the upper basin is the main food production region as well as the origin of nutrient pollutants, while the lower basin has more population and usually is the victim of nutrient run-offs, we further divided it into upper and lower MRB for convenient reference (Figure A4.0.1).

4.3.2 Agricultural food flows at subnational levels

We compiled sub-national level food trade data from the Commodity Flow Survey (U.S. Department of Transportation and U.S. Department of Commerce, 2020), which detailed the types of food commodities shipped among 132 Freight Analysis Framework locations (i.e., FAF Zones, including 84 major metropolitan areas and remainder of the states) in the U.S. The Commodity Flow Survey is conducted every five years as part of the Census Bureau’s economic census. Freight shipments within the Commodity Flow Survey dataset are grouped into 42 classes using the two-digit standard classification of transported goods (SCTG). For each class of commodities, the data provides information on the origin and destination, value, weight, mode of transportation, distance, and ton-miles of commodities shipped. This unique data enables us to understand the food flows and associated environment footprints at fine spatial scales.

In this study, we primarily focus on raw agricultural food goods because their production process is directly linked with environmental impacts and it is feasible to quantify these impacts with available data. Therefore, processed food products were excluded. Admittedly, this exclusion

likely underestimates the virtual N flows because much of the raw foods are likely processed in the nearby regions and then transported to distant consumers. However, there is no available data that can track the full food supply chains, i.e., from production, and processing, to final consumers. In this sense, the food users in this analysis represent a mix of food processors and final food consumers. Despite the limitation, our analysis focusing on interregional raw food flows is still a useful attempt, and the findings will be especially useful for food companies to be aware of the sustainability of their upper stream supply chains. Raw agricultural food goods, including SCTG 01 – live animals and fish (including cattle, hogs, chickens, broilers, turkeys, sheep, horses, and live fish) and SCTG 02 – cereal grains (including crops such as corn, wheat, rice, rye, barley, oats, sorghum), were subset from the Commodity Flow Survey dataset for analysis. This subset contains flows of cereal grains between 132 FAF Zones, with 32,952 potential links. The subnational food flows are similar to the international trade, and some regions serve as the “re-export transit stations”, but not the original producer of food. To reduce the complexity, we simplified the food flows by only retaining the net outflows.

We compiled data on production and fertilizer application for each crop at the county scale from the USDA’s Agriculture National Agricultural Statistics Service (NASS). For animal source foods production estimation, we used the number of animals in each livestock category (e.g., cows, hogs, poultry, sheep, and horses) in each county and the average animal weights from the U.S. Department of Agriculture (USDA, 2022), based on federally inspected averages of live-slaughter weights in pounds in the same year. In total, 3142 counties and county-equivalents are included in this analysis. Since the FAF Zones are clusters of U.S. counties, we linked the two datasets and aggregated county-level calculations to coarse FAF zone levels for analysis.

4.3.3 *Measure the shifted environmental burdens carried by food flows*

In the food trade networks, along with the agricultural products, there are also virtual environmental burdens (e.g., virtual nutrients) moving between the food sending systems and receiving systems. This study focuses on quantifying the nitrogen surplus embedded in food flows because the surplus is deemed as the proportion that leads to environmental pollution. Research finds that globally only around 35% of nitrogen fertilizer is used by crops, while almost two-thirds of the remaining become environmental pollutants by running off into our rivers, lakes, and natural environments (West et al., 2014). The US has high nitrogen use efficiency but still about one-third of the applied nitrogen is lost to the environment (Lassaletta et al., 2014a). We measured nitrogen surplus by multiplying the weight of a traded agricultural commodity by its NS rate, which is the nitrogen surplus generated by producing one unit of this agricultural commodity assuming producing each unit of food involves additional agricultural inputs (e.g., fertilizers), as well as extra environmental impacts. The equation for calculating the NS flows of a food flow is as follows (equation 1):

$$NS_i^{od} = FF_i^{od} \times NSR_i^o \quad (1)$$

where NS_i^{od} is the virtual nitrogen surplus embedded in the trade of product i flowed from origin region (o) to destination region (d), FF_i^{od} is the volume of food flow from origin region (o) to destination region (d), and NSR_i^o is the nitrogen surplus rate of product i originated from region o . Because nutrient inputs vary across regions, the use of NSR by origin can more accurately capture the shifted environmental burdens in food flows, thereby improving the traceability (Kastner et al., 2011; MacDonald et al., 2015).

Following previous studies (Byrnes et al., 2020), we used the difference between nutrient inputs and outputs to estimate NS. The nutrient inputs include the application of fertilizers, atmospheric deposition, and biological N fixation, and the output is mainly crop uptake (Figure 4.1). We calculated the NS for each crop by county using data from NASS. Detailed parameters for calculating the N inputs and output can be found in Table A4.0.1 and Table A4.0.2. Due to the lack of specific crop information in the food flow data, we used the average NSR for the cereal grain category (i). This average NSR was calculated as the total NS and the total production of the seven crops (PR_c) under the cereal grain category (equation 2). For animal-sourced nutrients, which are mostly from manure, we used the county-level estimates of kilograms of nitrogen from animal manure by the U.S. Geological Survey (USGS) (Falcone, 2021). Briefly, nitrogen from animal manure was calculated by multiplying the number of animals (in each county in each livestock category, e.g., cows, hogs, poultry, sheep, and horses) by the nutrient content formulas given in earlier studies and the animal-weight coefficient (Falcone, 2021; Gronberg and Arnold, 2017).

$$NSR_i^o = \frac{\sum_{c=1}^n NS_c}{\sum_{c=1}^n PR_c} \quad (2)$$

The total NS outflows of a region were calculated as the sum of all the net outflows from the region, and the total NS inflows of a region were calculated as the sum of all the net inflows to the region. The former can be viewed as the extra environmental burden bear by a net exporter of food, while the latter can be viewed as the environmental responsibility of a net importer of food. We further calculated each region's actual environmental responsibility by either subtracting the total outflow (for the net food exporters) or adding the total inflow (for the net food importers).

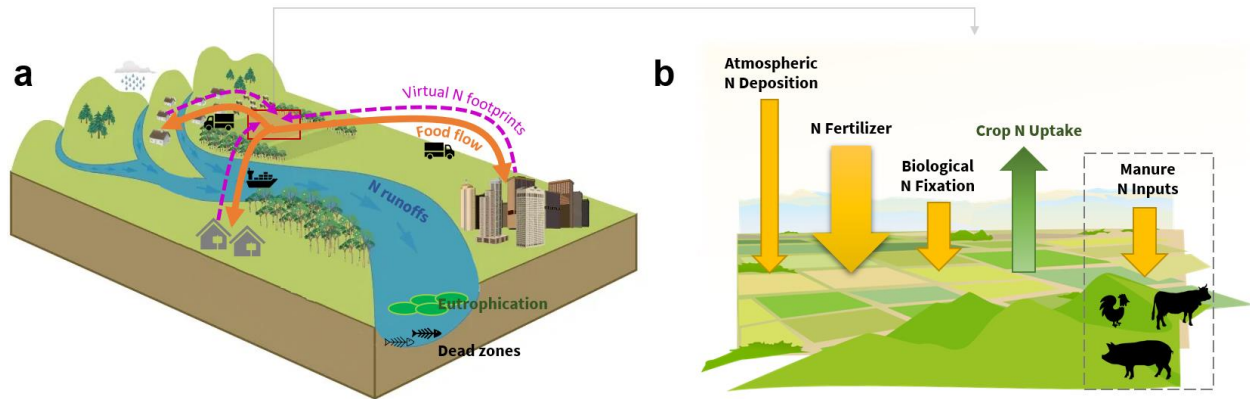


Figure 4.1. Food flows and the embedded nitrogen (N) surplus flows (a), and a conceptual diagram showing N inputs and outputs in the agricultural food production systems (b). In (a), orange arrows represent the direction of food flows, while dashed purple arrows indicate the virtual N footprint (or more broadly known as the environmental impacts) a net food importer imposed on the food exporter regions. The adjacent directed-flows can be viewed as pericouplings, and distant ones can be viewed as telecouplings.

4.4 Results

4.4.1 Food flows show food production for whom

40.2% of the cereal grain food flows by weight are interregional flows, and the remaining 59.8% are self-loops, i.e., foods were distributed to regions within the same FAF zone or states. The top 10, or 1.0%, of the food flows ($n = 32,952$) account for 42.7% of the total amount of flows. These top 10 are all food flows within a state (Table 4.1). Food flows within Iowa ranked on the top, with 56.9 million tons of cereal grains transported within the state.

If excluding self-loops, 53.4% of the cereal grains produced in the Midwest went downstream of the Mississippi River basin (27.5%) and regions outside of the basin (25.9%). Ranked by interregional flows, the top 10 accounts for 23.5% of the total interregional flows. We found most of the cereal grains flowed to the faraway regions, particularly, the State of Louisiana in the lower Mississippi River basin. Two large flows went to the western US – Portland-Vancouver-Salem FAF zone in Oregon and Washington (Table 4.1, Figure 4.2).

Different from cereal grains, the majority (66.3%) of the animal source foods flows are interregional flows, but most of which are relatively short-distance flows within the Mississippi River basin (83%) (Figure 4.2b). The exceptions are animal source foods flows from Pennsylvania to Philadelphia-Reading-Camden and New York-Newark, from Missouri to North Carolina, and from Kentucky to Texas (Table A4.0.3).

Table 4.1. The top 10 net flows of cereal grains (SCTG = 02) in 2017

Rank	From	To	Million Tons
1	Remainder of Iowa	Remainder of Iowa	56.9
2	New Orleans-Metairie-Hammond, LA-MS*	New Orleans-Metairie-Hammond, LA-MS	38.5
3	Remainder of Nebraska	Remainder of Nebraska	35.4
4	Remainder of Kansas	Remainder of Kansas	33.2
5	Remainder of Texas	Remainder of Texas	27.4
6	Remainder of Minnesota	Remainder of Minnesota	27.3
7	Remainder of Illinois	Remainder of Illinois	18.2
8	Remainder of South Dakota	Remainder of South Dakota	14.0
9	Remainder of North Dakota	Remainder of North Dakota	10.8
10	Remainder of Washington	Remainder of Washington	10.2
(Interregional flows, after excluding self-loop flows)			
1	Remainder of Illinois	St. Louis-St. Charles-Farmington, MO-IL	7.6
2	Remainder of Minnesota	Portland-Vancouver-Salem, OR-WA	7.2
3	Remainder of Illinois	Chicago-Naperville, IL-IN-WI	6.4
4	Remainder of Illinois	Baton Rouge, LA	6.3
5	Remainder of Illinois	New Orleans-Metairie-Hammond, LA-MS	6.2
6	Chicago-Naperville, IL-IN-WI	New Orleans-Metairie-Hammond, LA-MS	5.7
7	Remainder of Indiana	Atlanta-Athens-Clarke County-Sandy Springs, GA	5.0
8	Remainder of Indiana	New Orleans-Metairie-Hammond, LA-MS	4.5
9	Remainder of Montana	Portland-Vancouver-Salem, OR-WA	4.1
10	St. Louis-St. Charles-Farmington, MO-IL	New Orleans-Metairie-Hammond, LA-MS	3.9

* The two-uppercase-letter abbreviations denote the state names.

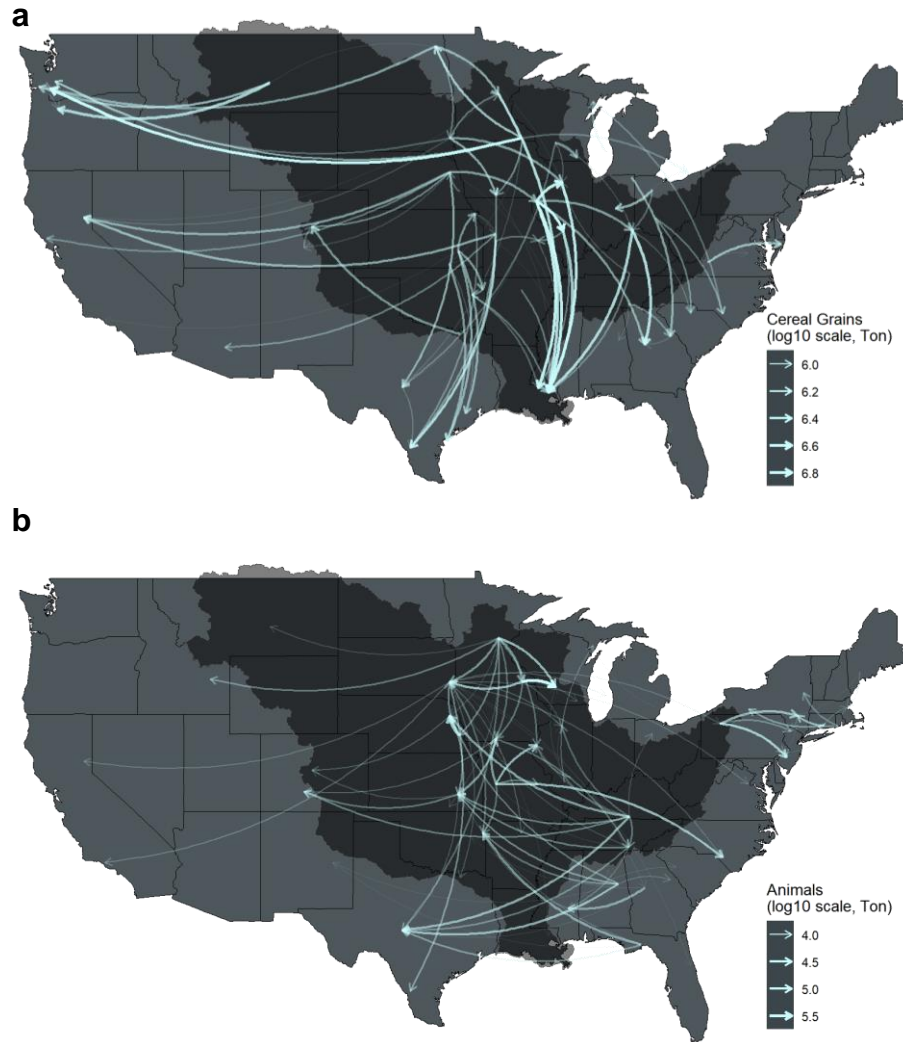


Figure 4.2. Top 100 net flows of cereal grains (a) and live animals (b) in 2017. The top 100 account for 84 % and 95% of the total interregional flows of cereal grains and animals, respectively. The deep-dark region represents the Mississippi River basin.

4.4.2 *Virtual nutrient flows reveal the displaced environmental responsibility*

Tracing the flows of virtual N surplus in food flows can reveal who is responsible for the distant environmental impacts, and by how much. In an opposite direction, large food receiving systems are usually the ones imposing a large amount of virtual N surplus on the food sending systems (Figure 4.3, Figure 4.4). For instance, New Orleans-Metairie-Hammond in Louisiana, Portland-Vancouver-Salem in Oregon, and Washington displaced the largest amount of N surplus to the

U.S. Midwest by importing cereal grains (Figure 4.3a). While for the animal source foods flows, North Carolina, New York, and Texas contributed almost 54.2% N surplus elsewhere regions in the U.S., such as Minnesota, Missouri, Nebraska, Pennsylvania, Alabama, and Kentucky (Figure 4.3b).

After totaling the N surplus displaced through the interregional flows of both cereal grains and animals, we found that coastal states are usually the large virtual N surplus pressure sending systems (Figure 4.4a), while states in the Midwest are the major virtual N surplus pressure receiving systems (Figure 4.4b). There are a few exceptions. A few metropolitan areas, such as Omaha-Council Bluffs-Fremont in Nebraska, Kansas City-Overland Park, Wichita-Arkansas City-Winfield in Kansas, and Tulsa-Muskogee-Bartlesville in Oklahoma, are both major sending and receiving systems of virtual N surplus (Figure 4.4).

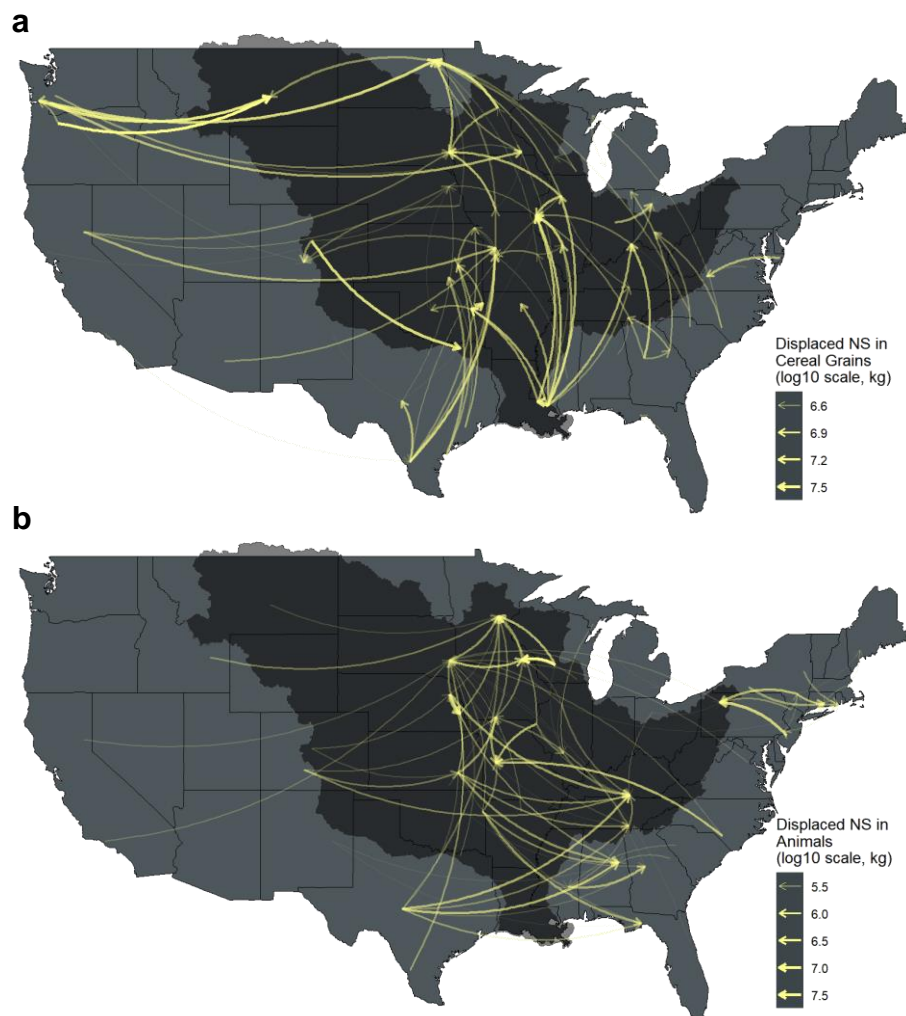


Figure 4.3. Top 100 net flows of virtual N surplus embedded in the flows of cereal grains (a) and live animals (b) in 2017. The deep-dark region represents the Mississippi River basin.

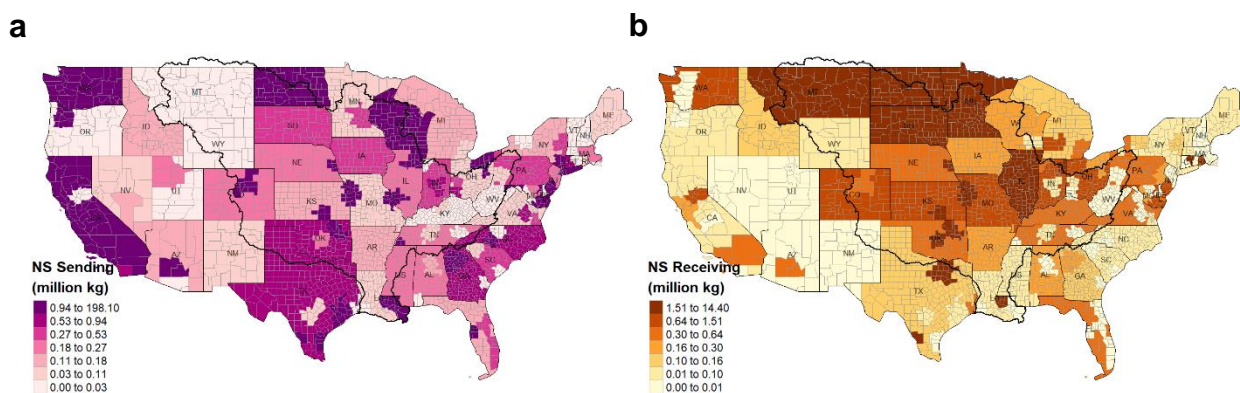


Figure 4.4. Total N surplus that displaced elsewhere by virtual N sending systems (a), and the total N surplus that is bore by virtual N receiving systems (b). Total N surplus is the sum of those in both cereal grains and animal flows.

4.4.3 Change in food flows can lead to redistribution of N surplus

Food production and supply are closely linked with nutrient use and surplus. Changes to food supply chains can not only lead to redistribution of food but also nutrient surplus to the environment. In 2017, the total virtual N surplus flows accounted for 17.1%, with the top 10 flows accounting for 3.6%, of the total N surplus from the U.S. agricultural production system. If the food supply chains were disrupted (i.e., no interregional food flows), and assuming each region must produce the same amount of food they used in 2017 and with the local nutrient use efficiency, the N surplus would be re-distributed across the U. S's landscape (Figures 4.5a, 4.5b).

This hypothetical scenario could potentially reduce the N surplus to a large area in the Mississippi River basin, especially the upper basin (reduce 0.61 billion kg, or 12%) (Figures 4.5b, and 5c). However, the whole basin would still suffer more N surplus (+0.6 billion kg, or +10%) (Figure 4.5c). This increase is mainly due to the likely surge of N surplus in the New Orleans-Metairie-Hammond, LA-MS CFS Area. Meanwhile, the U.S. as a whole would generate more N surplus (+1.68 billion kg, or +17%) into the environment, indicating environmental spillover effects.

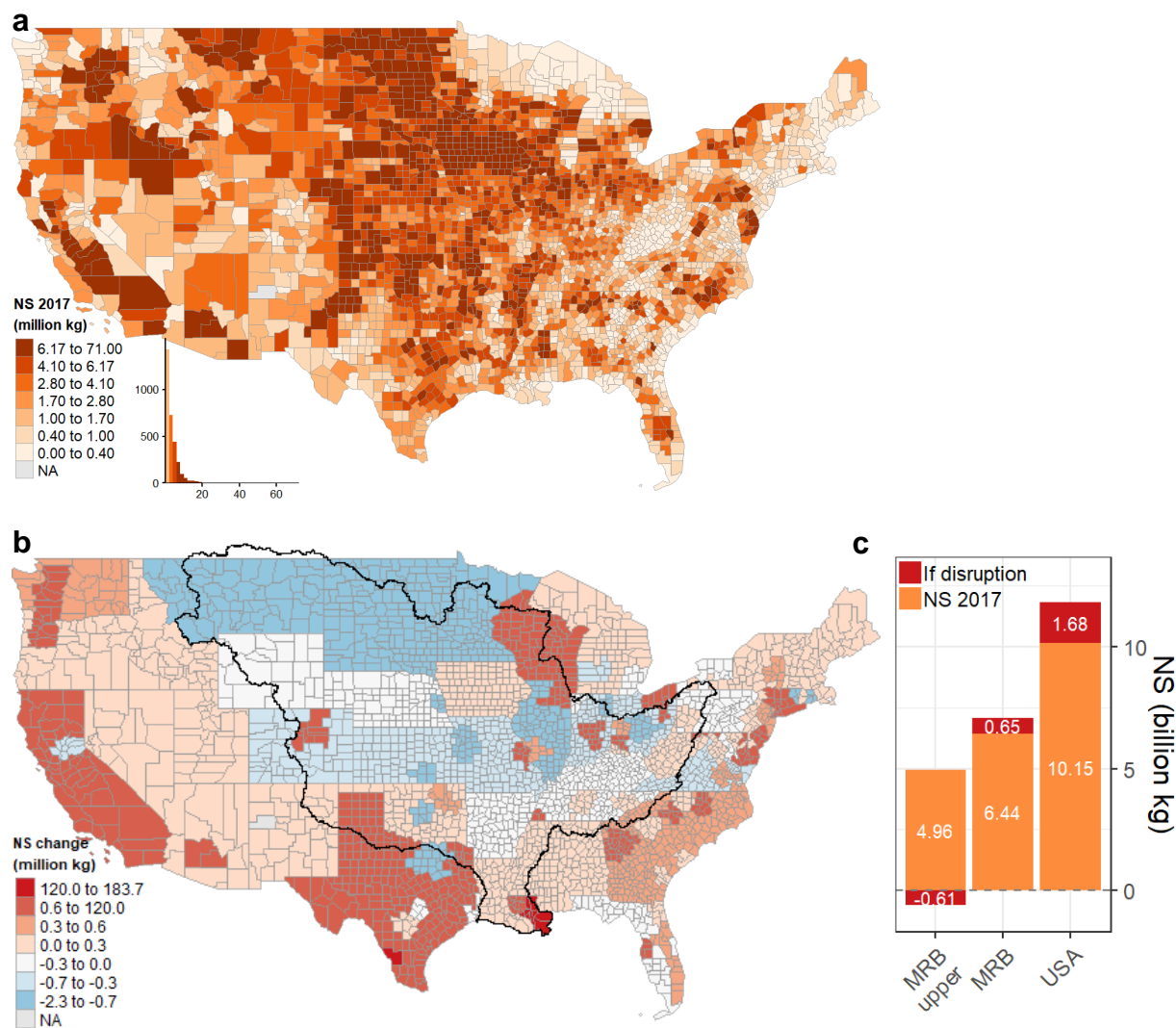


Figure 4.5. Total N surplus in food production (a), and its change if food supply chains were disrupted (b, and c). NS – N surplus, MRB – Mississippi River basin, USA – United States of America.

4.5 Discussion

In this study, we investigated the flow of virtual nitrogen surplus transferred through food flows at the subnational level. Compared to existing studies that track physical nutrient flows across landscapes, this work offers a different perspective to approach the excessive nutrient issue and the pathways to the environment.

4.5.1 Implications of tracking virtual nutrient flows

We found that 17.1% of the N surplus of the U.S. agricultural production is embedded in food flows to other regions, but not for local use. The U.S. Midwest bears most of the N surplus burdens for the nation. There are chances that restructuring food flows could reduce the excess nutrient in the Mississippi River, because regions with N surplus reduction potentials are largely located in the basin (Figure 4.5). In practice, it would be very challenging to modify food supply chain systems in order to reduce nutrient pollutants, while the quantitative measurement of virtual N surplus embedded in food flows could be useful for interregional watershed governance. For example, since importing food indicates the transfer of the environmental burden from food receiving systems to food sending systems, the transferred N surplus can thus serve as a novel alternative indicator for the payment for ecosystem services (Liu and Yang, 2013).

In addition, we constructed a food supply chain disruption scenario to estimate the potential impacts of food flow changes on N surplus redistribution. The scenario analysis revealed that if cutting off the existing food trade flows, the U.S. would be likely to generate an additional 17% N surplus to the environment. This demonstrated that the current US food supply-demand system is still environmentally efficient, i.e., the system as a whole can meet food demands through interregional trade and maintain a relatively overall low N surplus to the environment. This makes sense because the U.S. Midwest is characterized by great plains and fertile soils, which is an ideal place for agriculture. Additionally, both the N surplus rate (NSR) of cereal grains and livestock productions in the Midwest are lower than in other regions (Figure 4.6), indicating high N use efficiency. Alarmingly, we found the NSRs of both foods in the lower Mississippi river

basin are nearly twice or triple the rates in the U.S. Midwest. These regions are more adjacent to the estuary and more likely to cause nutrient leakage to the coastal system and fuel the hypoxic zone. The Mississippi River Basin Initiative (MRBI) has targeted the lower stream basin as the largest “MRBI Focus Area Watersheds” since 2010 (US EPA, 2015), but the NSR remained high in this region. More radical approaches and integrated policies might help. For instance, Liu et al (Jing Liu et al., 2022) suggest policy combinations (wetland restoration + improved N use efficiency + a leaching tax) could reduce the Mississippi River N load by 30-53%.

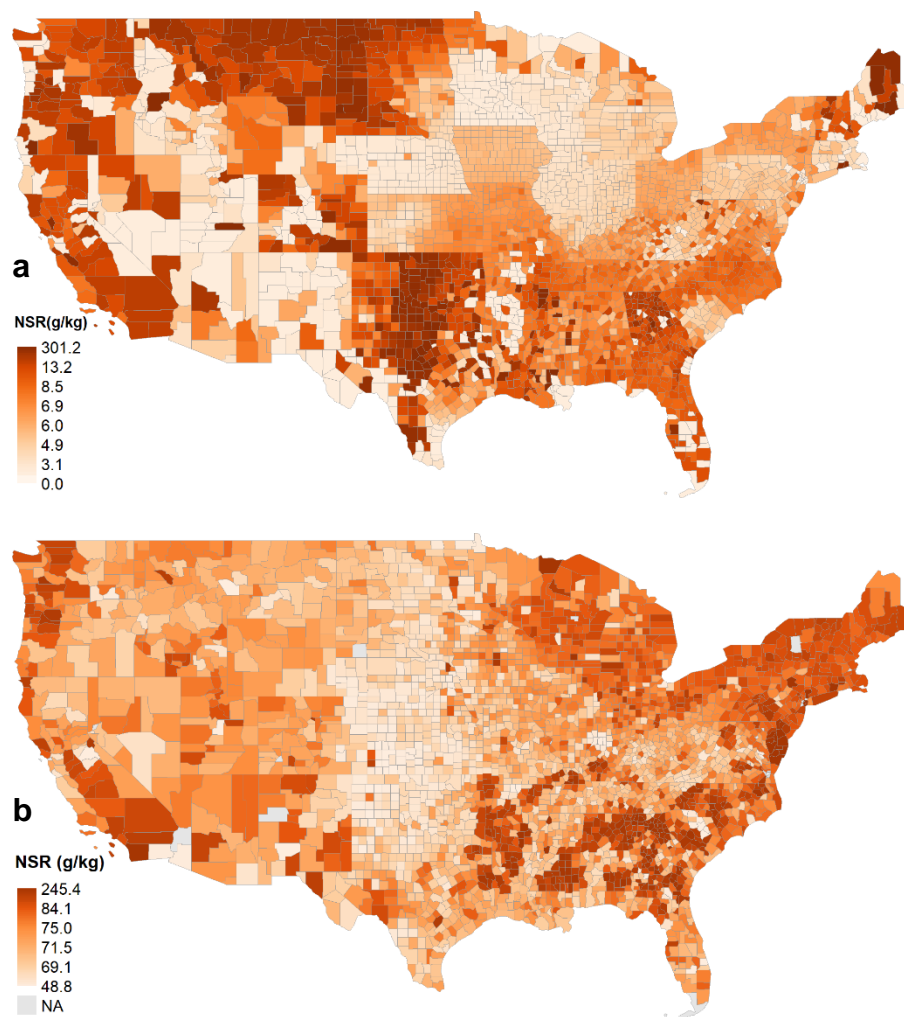


Figure 4.6. N surplus rate of cereal grains (a) and animals (b) by county

4.5.2 *Uncertainty in virtual N surplus estimation*

This study focuses on the flows of major cereal grains and animal source foods (livestock/poultry) for measuring the virtual N surplus flows. This is because the primary production of these foods is closely linked to nutrient inputs and outputs, and there are data available for the quantifications. We excluded processed food products mainly because there is no feasible way to trace their production origins and therefore making it challenging to measure the embedded N surplus in the products. Therefore, this analysis did not cover the full food supply chain (i.e., from production, to processing, and to final consumption), but largely food flows from “production to processing”, although part of which reached final consumers. In other words, the food users in this analysis represent a mix of food processors and final food consumers. Admittedly, the incomplete supply chain analysis likely leads to an underestimation of the virtual N flows because much of the primary foods are processed before reaching the final consumers. However, data limitation prevents such a thorough analysis. We also did not consider vegetables and fruits, which account for ~ 25% of the food production in the U.S., mainly because of the lack of sufficient and accurate information to link the production data with food flow data. We rather focus on the major food items with validated data to present a solid demonstration. Without including other food items can lead to an underestimation of the virtual N surplus because the N surplus rate of some vegetables can be higher than crops, although their production is much smaller compared to major crops (Sun et al., 2018). Despite these limitations, our analysis and findings will be useful for understanding the sustainability of one of the key processes of food supply chains.

Another uncertainty is inherited in the dataset itself. Noted that food flow estimation by the CFS relies on samplings and the survey covers about 710,500 establishments, mostly in the wholesale and retail industries (US Census Bureau, 2020). Consequently, the food flow estimation reported by CFS could be lower than the actual values. Nevertheless, this dataset provides by far the most comprehensive and accurate food flow information at the subnational level.

Finally, we use N surplus as an intuitive indicator to estimate the amount of pollutants that are most likely released into the environment. Since the process from N surplus to causing environmental impacts (e.g., water pollution) is also controlled by other factors, such as run-offs and adjacency to rivers, future studies need to use spatially explicit hydrological models (Wan et al., 2019) to better understand the extent to which N surplus redistribution due to food supply chain changes could reduce or increase the nutrient runoffs to rivers. This will be critical to understanding how food system transformations can help mitigate dead zone challenges in the Gulf of Mexico.

4.5.3 Future studies on tracking long-term and cross-scale food footprints

Our research took the most recent and available data year in 2017 as a case study, future research can include earlier years (2007 and 2012) for time-series analysis and test other interesting hypotheses and research topics. For example, 2012 is a drought year, researchers can use this year to examine the effects of natural shocks on food flows and associated virtual water use for food system resilience. The incoming 2022 Commodity Flow Survey data will be very useful to take COVID-19 as a natural experiment (Diffenbaugh et al., 2020; Liu et al., 2020; Yao et al.,

2021) and examining the effects of food flow disruption on nutrient surplus. This could be used to compare to the scenario analysis in this study and validate our findings.

This analysis focused on the interregional food flows within the contiguous U.S. but did not include the international food trade. An earlier study has found that the weakened food trade between US-China through the “trade war” can result in increases in nitrogen pollution in the United States (Yao et al., 2021). Future research can further integrate domestic food flows and international food trade data and use the telecoupling framework (J. Liu et al., 2015a) to investigate which specific regions in the U.S. would be most susceptible to disrupted international food supply chains and to what extent domestic food trade can buffer the impacts of the disturbance from the international market. A holistic understanding of the local and distant environmental impacts of agricultural food systems can facilitate synergically achieve multiple sustainable development goals, such as food security (SDG 2), clean water (SDG 6), responsible production and consumption (SDG 12), and coastal health (SDG 14).

CHAPTER 5: METACOUPLING IMPACTS ON ACHIEVING NATIONAL SDGS

5.1 Abstract

In an increasingly interconnected world, each country's ability to achieve the United Nations Sustainable Development Goals (SDGs) can be affected by external effects from other countries. For example, importing beef and soybeans to enhance domestic food security can lead to deforestation in exporting countries. Yet, little research has comprehensively evaluated these transnational effects in tracking countries' SDG progress. Ignoring these transnational effects may result in one country achieving the SDGs at the cost of others or missing positive synergies. To evaluate such effects, this chapter first quantified the international flows of resources and embedded socio-environmental footprints in trade, and used the amount of flows relative to country's resources and environment carrying capacity to quantify the transnational effects on each of the 17 SDGs for 189 countries. The analysis found that transnational interactions (e.g., trade) could help improve the national SDG Index by 19.4%. At the country level, 91% of countries (accounting for 94% world population) improved their SDG Index through transnational interactions. Despite the overall benefit, it found that, among the 17 SDGs, 16 benefited from international interactions while one (related to social fairness) was negatively impacted. Further, this research found that high-income countries generally benefited more, while low-income countries benefited less and were occasionally disadvantaged. Such negative transnational impacts were dominantly generated by a few powerful high-income countries, while impacted countries are mostly developing. Transnational impacts more frequently occurred among distant countries with unequal economic levels and benefited high-income countries more. Nevertheless, these distant interactions (known as "telecouplings") played a larger role in

advancing countries' SDG progress. This study quantified the often-ignored transnational impacts on achieving sustainability, therefore, informing how (inter)governmental agencies can target the negative transnational impacts and empower disadvantaged countries to achieve SDGs globally.

5.2 Introduction

Many global change challenges are transboundary and entwined to affect the progress towards the Sustainable Development Goals (SDGs) (Liu, 2018; Sachs et al., 2020; Xu et al., 2020c). However, SDG assessments have largely focused on evaluating the progress within administrative boundaries (e.g., individual countries or states) (Sachs et al., 2020; Xu et al., 2020a), and there is little knowledge about the transboundary impacts on SDGs across multiple systems. For instance, transnational flows of goods, services, capital, information, and people increased dramatically in recent decades, underpinning a world that is more interconnected than ever (J. Liu et al., 2015b; Liu et al., 2018b). As a consequence, one country's policies or actions can have expected and unexpected transnational impacts (TNIs) on other countries' efforts to achieve sustainable development goals. Studies have revealed that developed countries tend to transfer energy- and carbon-intensive industries to less developed countries, which hinders the progress towards goals such as climate and sustainable industries in those less developed countries (Sachs et al., 2021; Xu et al., 2020c). In addition to the prominent environmental TNIs such as carbon leakage (Feng et al., 2013) and biodiversity loss (Lenzen et al., 2012), recent studies have called for extended attention to the often ignored TNIs in the social dimension (e.g., vulnerable employment, child labor, and health risks) (Alsamawi et al., 2017b; Chung et al., 2021; Simas et al., 2014; Xiao et al., 2017) and the economic dimension (Malik et al., 2021a).

With the increasing frequency and intensity of transboundary interactions (e.g., trade) between countries (Tromboni et al., 2021), it is urgent to know the extent to which these transnational interactions shape national performance toward the 17 SDGs. Ignoring these TNIs may result in achieving one country's SDGs at the cost of others, or miss opportunities for synergistic co-actions.

Existing studies have attempted to use a spillover index, consisting of a list of indicators, to measure the external impacts one country may generate (Sachs et al., 2021, 2020; Schmidt-Traub et al., 2017; Zeng et al., 2021). Yet, it is still not clear to what extent the effects can impact SDG performance. With a recent study revealing that international trade can impact nine environment-related SDG targets (Xu et al., 2020c), it is also pressing to know how international trade can affect a broad spectrum of other SDG goals and targets (i.e., not only environmental, but also social, economic, and national security dimensions), as well as how other types of TNIs besides international trade may affect SDGs. Furthermore, most of these studies only examined the aggregated TNIs of one country on the rest of the world (Sachs et al., 2021; Xu et al., 2020c), while the information on how each country-pair influences each other is still missing. Such information is urgently needed for (inter)governmental agencies to target transnational impacts, and minimize their negative impacts (e.g., carbon leakage) while enhancing the positive ones (e.g., food security via trade) to achieve all SDGs globally. It is particularly important to identify such gaps now as the world is at the critical beginning stage of the UN Decade of Action to achieve its Sustainable Development Goals by 2030 for all.

Here, we report the first global analysis of the impacts of a range of TNIs on achieving national SDGs. Specifically, we address: (1) Which SDGs are most affected at the global scale, and to what extent? (2) How do the impacts vary across economic development levels and locations? (3) Which countries made the most impact, and which were most impacted by the TNIs? To address these questions, we compiled data and indicators on all 17 SDGs (with 103 indicators, listed in Table A5.0.1) for 189 countries for the year 2015, when the SDGs were adopted and the results provide a baseline for efforts in evaluating progress toward SDGs. We included the SDG indicators that can be quantitatively measured and are also directly influenced by transnational interactions (e.g., international trade). To quantitatively measure the impacts, we first estimated each country's performance in achieving the SDG targets in the current globally metacoupled system (Liu, 2017) (the baseline) and a hypothetical global lock-down scenario (i.e., no transnational interactions among countries but only domestic activities, e.g., no international trade but in "autarky"; the consequence caused by the recent COVID-19 global pandemic approximate some aspects of this scenario; see Methods). Comparing the difference in SDG target scores between the two scenarios can help estimate the impacts of transnational interactions on sustainable development (Xu et al., 2020c). Admittedly, this approach must be seen as an approximation given the complex socioeconomic dynamics that might unfold in the absence of transnational interactions. We used the quantity of goods and human flows to measure physical impacts (e.g., impacts of food trade on food security), and used virtual footprints, including virtual resources (e.g., virtual water), pollution, and risks (hereafter, virtual footprints) embedded in the trade flows, to measure the "virtual" impacts (see Methods and refer to Table A5.0.2 for a complete list of resource flows and virtual footprint indicators). To holistically analyze SDGs, we followed the integrated framework of metacoupling

(socioeconomic-environmental interactions within a country, between the country and adjacent countries, and between the country and distant countries), as metacoupling affects all SDGs (Liu, 2018). We first measured transnational impacts on each SDG, and then calculated the aggregated impacts on the SDG Index score of each country. Here, SDG Index is the aggregated score of the 17 SDGs for characterizing countries' overall SDG performance (see Methods). We further compared the difference in the extent to which the impacts on SDGs vary across countries, and income groups, as well as the difference in interactions between adjacent and distant countries. Here, we use "low-income" to refer to the low-income and low-middle income groups, and use "high-income" to refer to the upper-middle and high-income groups according to World Bank's income classification. Following (Anderson, 2003; Charney et al., 1993; Xu et al., 2020c), we classified country pairs into adjacent (countries sharing land or maritime boundaries) and distant pairs (countries that do not share land or maritime boundaries). This comparison can help test if distant interactions (telecouplings) are more prominent than adjacent interactions (pericouplings)(Liu, 2017) in influencing a nation's progress towards achieving SDGs. Finally, we use centrality in network analysis to identify key actors and characterize their interactions in the global interactive networks. This research is the first to integrate environmental-, social-, economic-, and security-related TNIs to investigate multifaceted transnational effects on SDGs by applying the framework of metacoupling (Liu, 2017). Our findings help identify the complex mechanisms behind goal-achieving efforts and improve the equality of intergovernmental conventions for achieving SDGs globally.

5.3 Materials and methods

5.3.1 *SDG Indicators and SDG Index*

We compiled data for 189 countries on 103 indicators (Table A5.0.1) that operationalize the 17 SDGs in the year 2015 using the best available data. Indicators were drawn primarily from the UN's "Global indicator framework for the Sustainable Development Goals and targets of the 2030 Agenda for Sustainable Development" (UN, 2019), supplemented with indicators from the "Sustainable Development Reports" (Sachs et al., 2020) and the UN's report on "Indicators and a Monitoring Framework for the Sustainable Development Goals" (Schmidt-Traub et al., 2017). These reports were published by the Sustainable Development Solutions Network (SDSN), which operates under the auspices of the UN to promote the implementation of the SDGs and the Paris Climate Agreement. In addition, we included SDG indicators that are used in existing literature (Sachs et al., 2020; Xu et al., 2020c, 2020a; Zeng et al., 2021) to cover as many SDG targets and goals as possible within the constraints of data availability across countries for the study period. Data were mainly obtained from the FAO (Food and Agriculture Organization of the United Nations), the World Bank, the ILOSTAT (International Labour Organization Database), EDGAR (the Electronic Data Gathering, Analysis, and Retrieval system), and other international agencies (See details in Table A5.0.1). We selected and included these 103 SDG indicators because they are measurable and are directly influenced by at least one of the 63 transnational impacts (measured by footprint indicators, listed in Table A5.0.2). This study provides by far the most comprehensive evaluation of the TNIs on SDGs. Readers should be aware of the uncertainties in our analysis because we excluded the SDG indicators that are either not measurable or have less attributable (or indirect) linkages with TNIs at this moment which leads to underestimation of TNIs on SDGs.

To make the evaluation comparable across countries and calculate the composite SDG Index, we follow SDSN and Xu et al.'s approach (Sachs et al., 2021; Xu et al., 2020a) and normalized all SDG indicators to values ranging from 0 (indicating the worst performance) to 100 (indicating the best performance). "Performance" refers to one country's progress toward achieving the SDGs. We further used an SDG Index score (0-100) consisting of individual normalized SDG scores (0-100) for characterizing countries' overall SDG performance. SDG Index score is an aggregate score composed of individual scores of the 17 SDGs, representing each country's overall performance in achieving all 17 SDGs (Sachs et al., 2020). We calculated each country's SDG Index score by using an equal-weight average approach, with the emphasis that the UN takes integrated solutions to address all 17 SDGs equally (Sachs et al., 2020). Within each goal, all indicators are also equally weighted. Therefore, theoretically, the SDG index could range from 0 to 1700, while we found a range of SDG Index between 0-100 is more intuitive for readers to know the gap from fully (100%) achieving the goals. For example, a country with a score of 50 indicates halfway towards achieving the best performance.

5.3.2 Measuring the impacts of transnational interactions (TNIs) on national SDGs

In an increasingly metacoupled world, one country's sustainability initiatives and actions can generate positive or negative transnational impacts on other countries, and sometimes in turn impact itself. Taking soybean trade as an example, importing soybean to enhance food security can not only cause deforestation in exporting countries but also environmental pollution in importing countries (Sun et al., 2018). Besides the commonly reported transnational environmental impacts (Dalin et al., 2017; Lenzen et al., 2012; Oita et al., 2016), there are also considerable social impacts embodied in international interactions (Dorninger et al., 2021;

Wiedmann and Lenzen, 2018). In addition to international trade, other types of international interactions are understudied. For example, international development finances play a big role (Galaz et al., 2018; Turner, 2019), as achieving the SDGs requires mobilizing resources from a variety of sources, including international partners, domestic budgets, foundations, and philanthropy, as well as the private sector. It is estimated that achieving the Sustainable Development Goals by 2030 will require a rough estimate of US\$5-7 trillion dollars (5.8% ~ 8.3% of global GDP) of annual investment across sectors and industries (UN, 2018).

The 2030 Agenda and the SDGs have recognized the importance of transnational impacts in several crucial ways. To comprehensively characterize the impacts on achieving sustainable development, we synthesized a list of 43 transnational impact indicators (see Table A5.0.2). In addition to the commonly used footprint indicators, including virtual resources (e.g., virtual water), pollution, and risks (hereafter, virtual footprints) that are embedded in the trade flows, we also included the physical flows of critical goods and people that can also have potential impacts on achieving SDGs (e.g., impacts of food trade on food security, international flows of students and scholars on education). In the context of the SDGs, we grouped the bulk list of transnational impacts (TNI) into four broad categories by referring to Sustainable Development Solutions Network's classification for international spillovers (Sachs et al., 2020): (1) Environmental TNIs, (2) Social and governance TNIs, (3) Economy and finance TNIs and (4) Security TNIs. Each TNI is associated with at least one specific SDG indicator. We then compiled global datasets for 189 countries and utilized well-developed models (see detailed description in the following) to measure these TNIs and estimate the extent to which one country may affect other countries' SDG performance (Figure A5.0.8).

Environmental impacts of TNIs cover the impacts related to trade of natural resources and embedded environmental footprints in trade. These transnational environmental impacts can be generated in two ways: 1) through virtual environmental footprints embodied in international trade, and 2) through direct transboundary flows of water resources or pollutants in air and water (Sachs et al., 2020). In this study, we focus on international trade-related environmental impacts, because trade is a major pathway of causing transnational environmental effects and the quantification approaches such as multi-region input-output (MRIO) analysis have been full-fledged and are ready to be used for tracking a range of transboundary environmental impacts (e.g., land use, water scarcity, energy use, carbon emissions, nitrogen emissions, and biodiversity) embodied in consumption and trade (Lenzen et al., 2012, 2013b; Oita et al., 2016; Sachs et al., 2020; Tukker and Dietzenbacher, 2013; Wiedmann and Lenzen, 2018). However, quantifying cross-border flows through air and water, such as transfer of pollutants, for each country at the global scale remains a great challenge, which are not included in this analysis. The exclusion of transboundary physical flows of water and pollutants would likely lead to an underestimation of the transnational environmental impacts.

The transnational environmental impacts on one country are measured by the amount of “exported” resources or embedded environmental footprints, comparing to the country’s total resources or total footprints. For example, to measure the transnational impacts on country A’s SDG 6.4.2 (Level of water stress: freshwater withdrawal as a proportion of available freshwater resources (UN, 2019); equation 1). We first calculated how much virtual water was embedded in its net exports using MRIO analysis. For a virtual water net exporter, it would use less domestic water (equivalent to the net exported virtual water) to only meet domestic demands if

international trade were interrupted or in a hypothetical autarky scenario, resulting in lower water stress (equation 2). This is because the virtual water net exporters can be viewed as the countries that extract local water resources to supply products (e.g., irrigated wheat) for other countries in the current trade world, but would be likely to consume less local water under the autarky scenario. The portion of net exported virtual water therefore can be used as a proxy to represent the impact of international trade on the country's water stress, and comparing the difference between $water\ stress_{trade}$ and $water\ stress_{no_trade}$ can help estimate the impact on the country's SDG 6.4.2.

$$water\ stress_{trade} = \frac{water\ use}{total\ water\ resources} \quad (1)$$

$$water\ stress_{no_trade} = \frac{water\ use + net\ imported\ virtual\ water}{total\ water\ resources} \quad (2)$$

We used the high-resolution global MRIO database, Eora (Lenzen et al., 2011), to calculate embedded environmental footprints. We chose the Eora MRIO database because it provides high-resolution IO tables documenting the inter-sectoral transfers amongst 15,909 sectors across 190 countries. It also includes a list of environmental satellite account indicators, covering GHG emissions, air pollution, energy use, water use, and land occupation, which can be directly used for quantifying the amount of embedded environmental footprints. The detailed methods for quantifying each environmental footprint have been well-documented in existing literature, and readers can refer to the key references listed in Table A5.0.2 and an example in Text S5.1 for more details.

Social impacts of TNIs cover occupational injuries and fatalities, health risks (e.g., noncommunicable diseases) related to consumption and other social supply chain impacts (Alsamawi et al., 2014, 2017b; Malik et al., 2021a; Xiao et al., 2017, 2018a). Directly measuring social impacts is extremely difficult, especially at the global scale. Here we use the potential social risk associated with the production and consumption to get an approximation. Following Xiao et al (Xiao et al., 2017), we combined the Eora MRIO with the novel Social Hot Spots Database (SHDB, a resource that assigns risk levels by impact category, and subcategory for each country and sector) (Norris and Norris, 2015), and used input-output analysis to measure the potential social risk footprints associated with the supply chain activities required to deliver a product to fulfill a country's needs. Taking SDG 8.8.1 (Fatal and non-fatal occupational injuries per 100,000 workers (UN, 2019)) as an example, fatal injuries in a country can be measured using employment-related national statistics data (equation 3). The embedded fatal injury cases in exports can be quantified by input-output analysis. For a net exporter, the fatal injury rate in a hypothetical autarky scenario can be estimated by equation 4, assuming fewer fatal injury cases with fewer production activities for exports. Admittedly, this approach must be seen as an approximation given the complex economic dynamics that might unfold in the absence of trade. Still, this approach can provide a useful approximation (Xu et al., 2020c).

$$fatal\ injury\ rate_{trade} = \frac{fatal\ injury\ cases}{total\ workers} \times 1000 \quad (3)$$

$$fatal\ injury\ rate_{no_trade} = \frac{fatal\ injury\ cases - embedded\ fatal\ injury\ cases\ in\ net\ exports}{total\ workers} \times 1000$$

(4)

Detailed methods for calculating each social footprint can be found in the references listed in Table A5.0.2.

Economy and finance impacts of TNIs cover international development finance (e.g., official development assistance; ODA), corruption footprints of nations, unfair tax competition, and banking secrecy (Sachs et al., 2020; Sethi et al., 2017; Turner, 2019). In this study, we used the official development assistance data by OECD (<https://data.oecd.org/oda/net-oda.htm>) and the international development finance data coded by AidData to measure the positive finance TNI (i.e., ODA). The AidData can supplement OECD ODA data by providing additional country coverage on estimating the contributions of international financials to the SDGs (and their associated targets) (DiLorenzo et al., 2017; Turner and Burgess, 2019). Every country's corruption footprint was measured by input-output analysis, the same approach for social footprints.

Security TNIs include negative TNIs – such as the exports of weapons and arms and organized international crime, and positive TNIs – such as investments in conflict prevention and peacekeeping (Béraud-Sudreau et al., 2020b, 2020a; Sachs et al., 2020; Wezeman et al., 2018). We compiled international arms transfers data from Stockholm International Peace Research Institute (SIPRI) Arms Transfers Database, and the Troop and Other Personnel (e.g., police) Contributions data from the UN Peacekeeping Open Data Portal and the SIPRI Multilateral Peace Operations Database. Following the approach by Sustainable Development Solutions Network (Sachs et al., 2020), we used the number of traded arms from country m to country n as an indicator of negative security TNIs, and the number of troops and other personnel (e.g., police) contributions from country m to country n as an indicator of positive security TNIs.

5.3.3 Network analysis

We use network analysis to reveal the relative importance of each country in impacting other countries' sustainable development. Each node in the network represents a country, and the node size tells us how central the node is in the complex network. The weighted in-degree centrality was computed using the *igraph* package (Csardi and Nepusz, 2006) to characterize the node size. The edge linking two country pairs demonstrates an impact relationship. The arrows point to the dominant influencers (or responsibility takers), the width of the edges represents the magnitude of impacts, and the colors indicate income levels (blue – high-income, red – low-income).

5.4 Results

5.4.1 The overall impact of TNIs on SDGs

Compared to the global lock-down scenario, TNIs improved the SDG Index of countries by 19.4% (or a score of 9.2) on average in 2015 (Index mean = 66.9, s.d. = 7.4, with scoring on a scale of 0 - 100; Figure 5.1a, Figure A5.0.1). At the country level, 91% of the 189 countries (accounting for 94% world population) benefitted from TNIs with their SDG Index improved. Only 9% of the countries ($n = 13$) decreased their SDG Index, over three-quarters of which are low-income countries (Figure 5.1a, Figure A5.0.2).

Among the 17 SDGs, 16 benefited from TNIs, with SDG 4 (Quality Education) and SDG 17 (Partnerships for the Goals) improving the most ($\Delta SDG_4 = 33.0$, $\Delta SDG_{17} = 32.1$), followed by SDG 15 (Life on Land), SDG 11 (Sustainable Cities and Communities), and SDG 9 (Industry, Innovation and Infrastructure). However, only SDG 10 (Reduce Inequality) was negatively impacted ($\Delta SDG_{10} = -4.4$) (Figure 5.1b). The global fairness issue is further reflected by the

different impacts of global interactions on the nation's SDGs across income groups (Figure 5.1c). High-income countries generally benefited more (on 14 of the 17 SDGs), while low-income countries benefited less and occasionally even reduced scores from TNIs. In addition, although TNIs improved most countries' SDG Index, not all Goals of a nation gained positive impacts. For instance, the SDG score of countries in the Global South, particularly countries in Africa and South Asia, declined in more than one-half of their 17 goals (Figure 5.1d). While countries in the Global North gained scores in more than half of their 17 goals, European countries and the US benefited in more than 80% of the 17 goals.

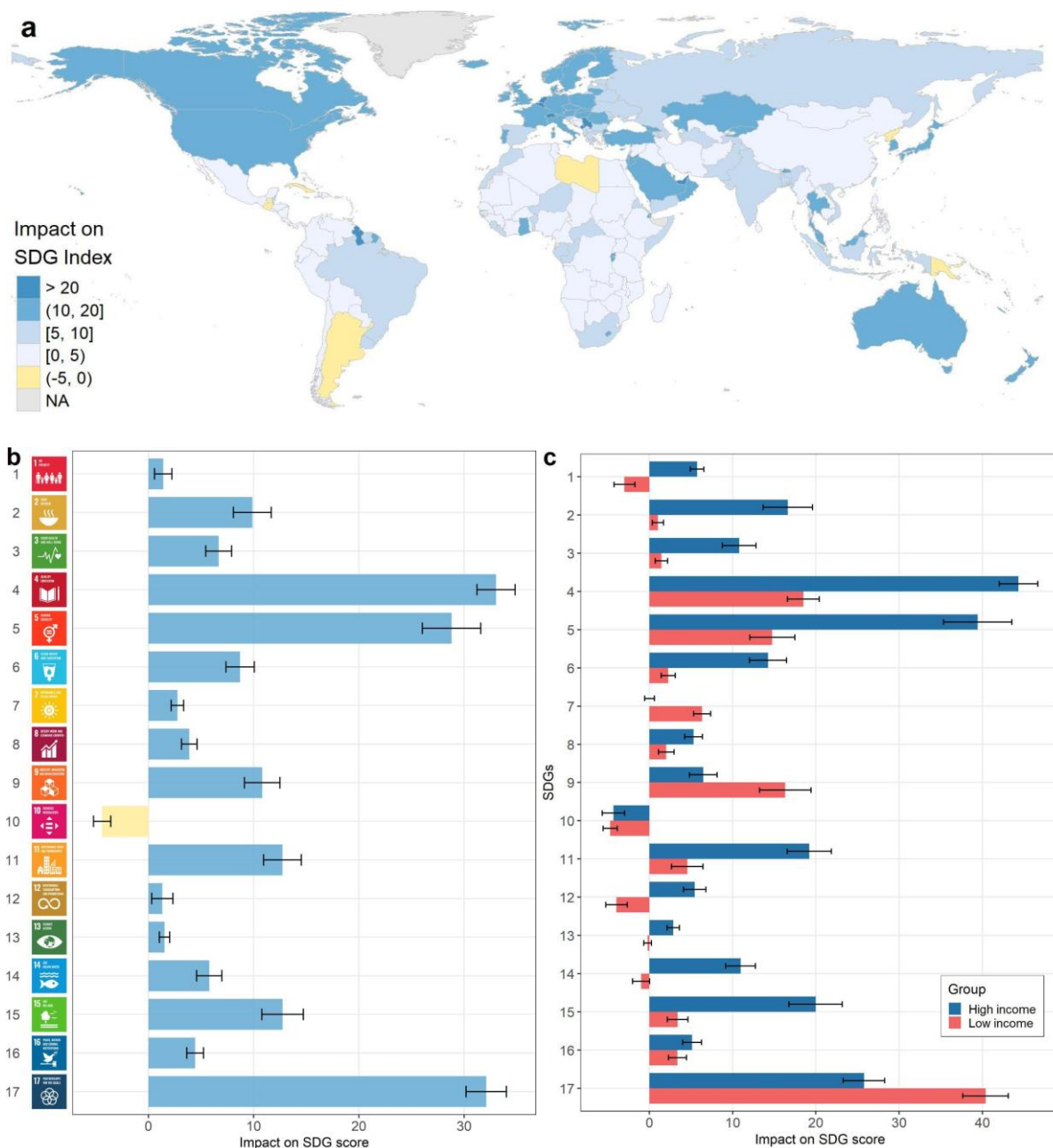
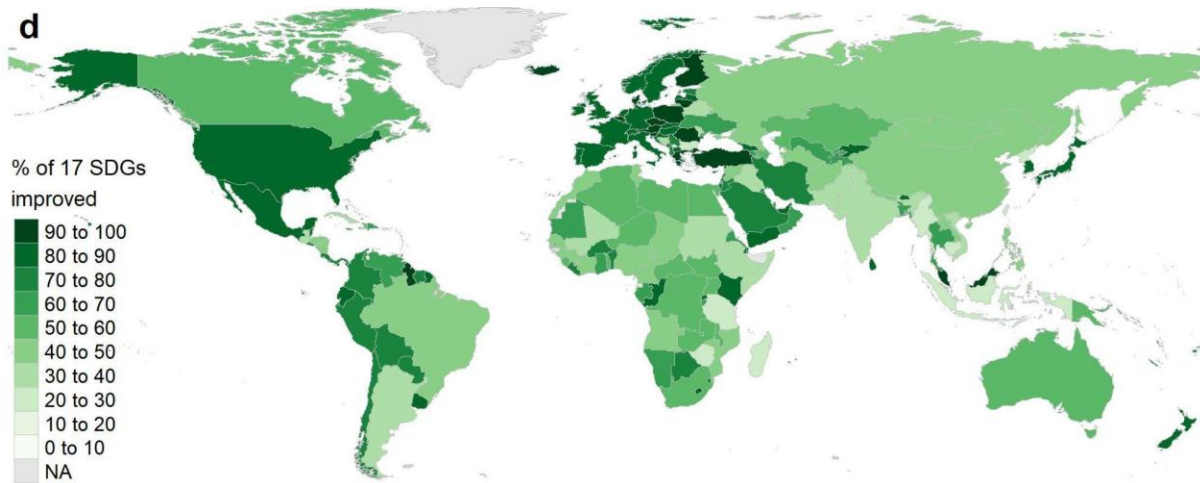


Figure 5.1. The overall TNIs on SDG Index and individual SDG scores at the global and national scales in 2015. (a) The overall impacts on each country's SDG Index (i.e., the aggregated mean of the 17 normalized SDG scores to characterize countries' overall SDG performance, see Methods). Positive values mean a country's SDG score benefited from TNIs. (b) The overall impacts on each Goal of the 189 countries. The error bars indicate the standard errors in the SDG scores across countries ($n = 189$). (c) The overall impact on each Goal by country income group. The income group categories are based on the World Bank's classification. The error bars indicate the standard errors in the SDG scores across countries in each income group. Figure A5.0.3 further shows the impacts of TNIs on each SDG at the country level. (d) Percent of improved SDGs from TNIs. SDG Icon images courtesy of the United Nations.

Figure 5.1 (cont'd)



5.4.2 Dominant actors in the global TNIs networks

Ranked by the aggregated TNIs (based on 45 TNI indicators), the top 10 countries that are responsible for the most negative impacts of TNIs on the rest of the world are the United States, Serbia, Germany, Japan, Italy, China, United Kingdom, UAE, Spain, and Singapore (Figure 5.2a, 2b). While the bottom 10 countries, including Indonesia, Argentina, Myanmar, Pakistan, Philippines, India, Ethiopia, Sudan, Angola, and Kazakhstan, are those that made the least negative impacts. All of the top 10 influencers are all in the high-income country group, while most of the bottom 10 are low-income countries. Notably, the impacts of TNIs on social-related SDGs can be as large as (or even larger than) the impacts on environmental-related SDGs but were rarely reported in existing literature (Figure A5.0.4).

When zooming into the complex TNIs network, most of the transnational responsibilities of impact point to the top influencers (Figure. 5.2c). For example, the USA, Serbia, Japan, and

China have the highest transnational impacts. Similarly, India, Indonesia, and Argentina are the bottom influencers in each specific global network (Figure 5.2c, Figure A5.0.1). Not only do high-income countries tend to impact low-income countries through TNIs, but also we found the impacts were more frequently generated between faraway trading countries with unequal economic levels (Figure 5.2d). That is, telecouplings lead to more socio-environmental inequality among countries in terms of achieving the national SDGs.

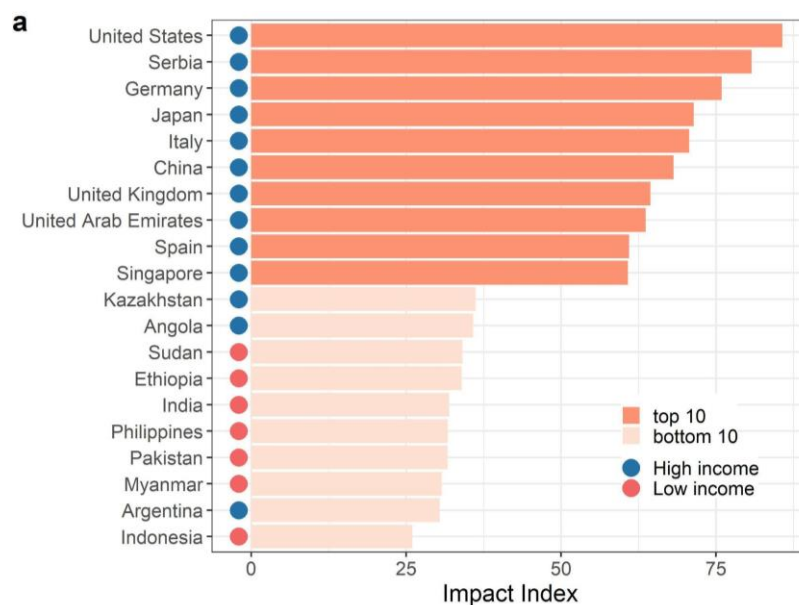
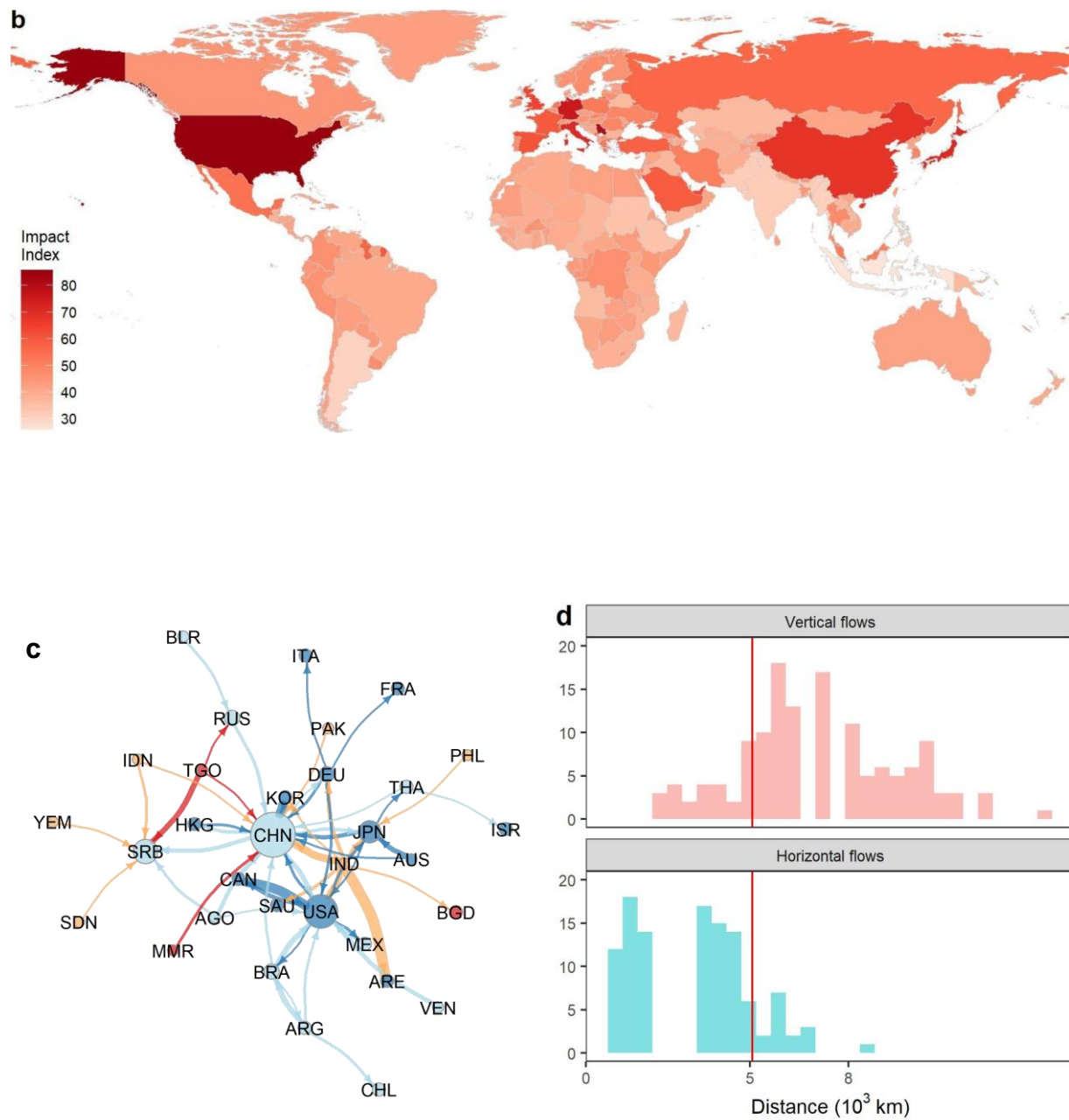


Figure 5.2. Dominant influencer and affected in the global TNIs network. (a) Top 10 and bottom 10 influencers of the 189 countries in 2015, ranked by TNIs index (i.e., aggregated impact scores). Higher values mean larger overall negative impacts on the rest of the world, while lower values indicate smaller overall negative impacts (positive impacts could be offset by other negative impacts). (b) Map of TNIs index by country. Figure A5.0.5 further shows the impact of each TNI. (c) Network of the top 15 country pairs. Arrows point to dominant influencers; The width of the edges represents the magnitude of impact, and the size of each node represents the degree of centrality in the network. The colors indicate income-levels (blue – high-income, red – low-income). Full names of the country codes are listed in Table A5.0.3. (d) Distribution of the average distance of interactions between two countries. “Vertical flows” indicate the interactions between two economically unequal countries (e.g., resource flows from low-income countries to high-income countries), and “Horizontal flows” represent interactions between two countries with similar economic status. The red dash line indicates the average distance of interactions between each country pair. Figure A5.0.6 further illustrates the distance distribution by TNI types.

Figure 5.2 (cont'd)



5.4.3 *Telecouplings contributed more to SDGs than pericouplings*

Interactions between distant countries (i.e., telecouplings) played a more important and larger role in advancing countries' overall SDG performance, as measured by SDG Index (Figure 5.3a

and 3b). Interestingly, telecouplings are especially critical in maintaining SDG performance for high-income countries, while having minimal contributions to low-income countries (Figure 5.3a and Figure A5.0.7).

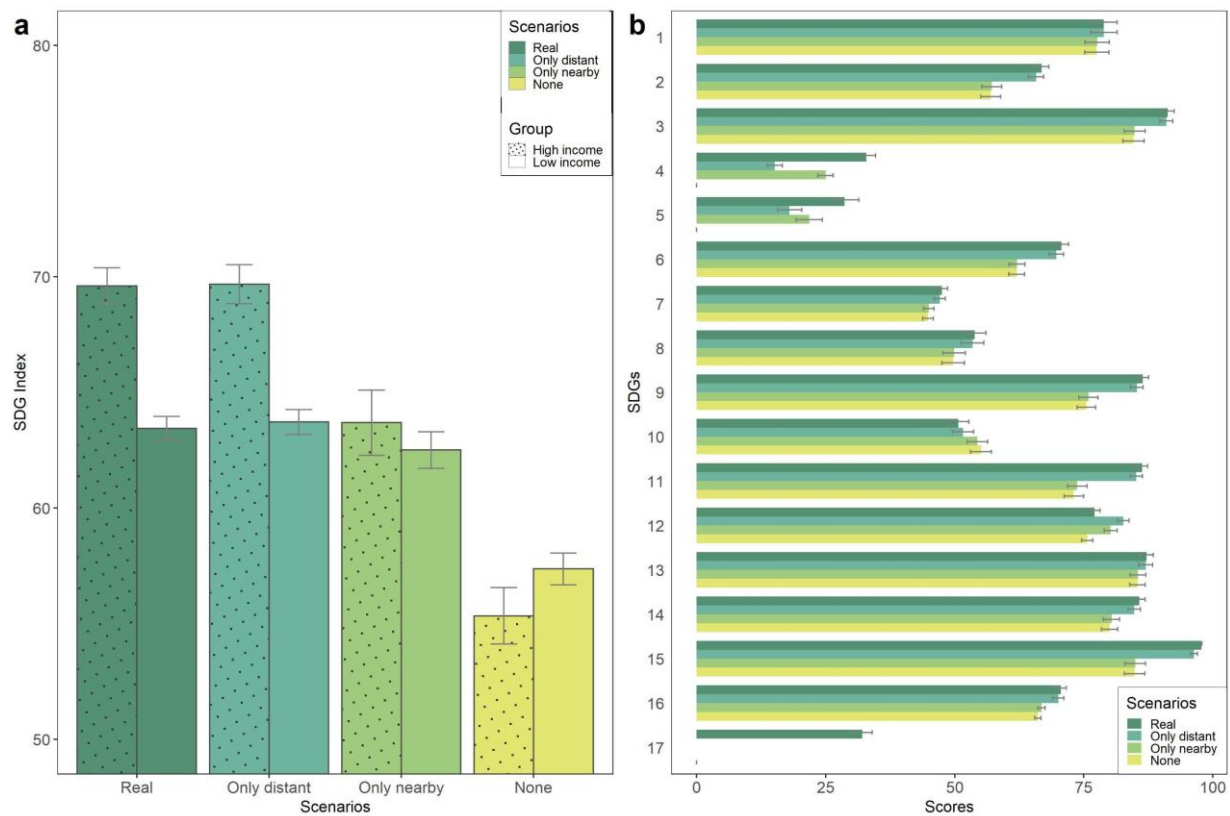


Figure 5.3. SDG Index (a) and the score of each SDG (b) by income group under four scenarios: the real world in 2015 (Real), only distant world connections (Only distant), only nearby world connections (Only nearby), and global lockdown with no connections (None). SDG 17 does not have all four scenarios due to the limited data for countries.

5.5 Discussion

This study presents the first quantitative assessment of the impacts of multiple TNIs on the performance of the 17 SDGs. Our approach advanced previous research by synthesizing the most comprehensive footprint indicators, including both environmental and social aspects to uncover the transboundary impacts on the global and national SDGs. Overall, our results indicated that the international interactions helped increase the national SDG Index by around 20% in 2015.

Given the important benefits of global connections, many SDGs might have been greatly affected due to the shutdown of critical supply chains (265 million people are likely to face acute food shortages), international development aid (could drop by US\$25 billion in 2021), and international tourism (could drop by 60%) because of global lockdown (Naidoo and Fisher, 2020; Verschuur et al., 2021). Research has warned that two-thirds of the goals are unlikely to be met due to the COVID-19 pandemic (Naidoo and Fisher, 2020). According to our analysis, 88% of the 17 goals would be held back by approximately 16% on average (Figure 5.1b). For post-pandemic recovery, it is especially urgent to rebuild the global connections and partnerships to keep countries on track toward the SDGs.

TNIs helped elevate 16 out of 17 SDGs, but undermined one SDG on “equality” (SDG 10). This finding expanded our previous research that revealed international trade improved seven environment-related SDGs at the global level (Xu et al., 2020c), but further revealed international interactions (including trade) improved the other eight SDGs. The negatively impacted SDG 10 was not covered in our previous research. This demonstrated that to have a holistic understanding of the transnational impacts on SDGs, it is important to take a wide range of transnational environmental and social interactions into consideration and cover all the 17 SDGs.

The difference in impacts also is reflected in another important finding that high-income countries generally benefited more while low-income countries benefited less or even lost scores from TNIs. As existing literature suggests, developed countries usually gain environmental benefits at the cost of developing countries (Sachs et al., 2020; Xu et al., 2020c), and developing

countries often bear most of the environmental burdens, such as resource depletion (Dalin et al., 2017), environmental degradation (Oita et al., 2016) and biodiversity loss (Lenzen et al., 2012). The inequality in environmental impacts is often embodied in international trade and global supply chains. Many have urged to initiate a World Environment Organization (WEO) (Biermann, 2020) because international trade supported by the World Trade Organization (WTO) disproportionately emphasizes more on achieving maximization of economic benefit while much less on the environment. Although existing multilateral and bilateral environmental agreements, such as CITES, UNFCCC, and IPCC have achieved a great deal and reduced the speed of environmental degradation, there still are pressing environmental problems prevailing throughout the world because many of the multilateral environmental agreements are regional in scope, some are conflicting with each other (Azizi et al., 2019; Kanie, 2018; Kim and Bosselmann, 2013), and many impacts beyond the countries involved in trade and other interactions such as investment were overlooked (Sachs et al., 2022).

In addition to the environmental impacts, transnational social impacts such as corruption (Xiao et al., 2018a), labor-related human rights (Alsamawi et al., 2017b), education, and gender inequality are also prominent but were much under-reported. This is particularly important because the overall transnational social impacts on a nation's SDGs were usually as large as the environmental ones, and were even larger in some countries (Figure A5.0.4). Future policy integration for sustainable development through multilateral environmental agreements needs to better integrate environmental concerns with social and economic issues. Policy conversations and coordination at the global level should also better empower less developed countries towards sustainability because stringent regulations in developed countries can lead to leakages of

pollution-intensive and high-social-risk industries to less-developed countries with lax regulations (Shapiro, 2020). A recent UN ban on plastic exports has been in effect in the European Union (Adyel, 2021), and this action can help countries in the global south to bear less environmental and health-related burdens that are embedded in the low-quality or difficult-to-recycle wastes. Other ways to empower less developed countries include promoting global green financing (Belhabib and Le Billon, 2018; Galaz et al., 2018) and knowledge/ technology transfer.

The SDGs are global in scope and emphasize ensuring no one is left behind. However, we found that the current world, being a metacoupled socio-environmental system, is dominated by a few powerful and affluent countries, such as the United States, Germany, Japan, Italy, and China. Most of the negative TNIs they exert on other countries are through their high footprints in consumption embedded in international trade, which is often structured in asymmetrical power relationships (e.g., in terms of affluence and military) between countries that give extra advantages to the more powerful nations and can sometimes be quite disadvantageous to the less powerful (Jorgenson, 2016). In addition, our analysis shows transnational impacts more commonly happening between faraway countries with unequal economic levels. Perhaps adjacent countries have more similar socio-economic and environmental conditions that determine the categories of resources and services for exchange, while distant exchanges can diversify the supplies (Xu et al., 2020c). Furthermore, the spatial segregation of countries by affluence levels (i.e., high-income countries are mostly located in the Global North, while low-income countries are in the Global South, see Figure A5.0.10) also makes telecouplings more prominent. Studies on ecological footprints and carbon emissions have shown that, when measured in terms of intensity of exports, the ecological unequal exchanges between developed

countries and less-developed countries are growing (Jorgenson, 2016, 2012), while in absolute terms, the opposite (Moran et al., 2013). With our finding that unequal exchanges are prominent both environmentally and socially in the context of the SDGs, future environmental justice and structural inequality scholars may also need to examine these aspects to provide more in-depth insights for international policymaking.

Our analysis on mapping the transnational multifaceted socio-economic, security, and environmental impacts on 17 SDGs for each country can help nations identify which countries impact their sustainability efforts and on which aspects. Such information will be useful for maximizing the positive impacts and minimizing the negative impacts to better achieve the SDGs. Practically, harmonizing regulation and standards among international trade partners (Lenzen et al., 2012), enhancing environmental labeling and certification schemes along the global supply chains (OECD, 2016; Prag et al., 2016), facilitating technical cooperation and knowledge transfer to support greater sustainability in producing countries, and implementing SDG financing (Sachs et al., 2022) might help address the negative transnational impacts. Due to the inherent complexity in the globally metacoupled networks, we estimated the transboundary impacts on SDGs by comparing the SDG scores under the current metacoupled world (the baseline) to a counterfactual global lock-down scenario, distant-interaction only, and adjacent-interaction only scenarios. Although this approach has been widely used in trade-scenario settings (Wood et al., 2018; Xu et al., 2020c) and was previously thought to be unlikely to happen, the recent global lockdown caused by the COVID-19 pandemic provided a factual case. Nevertheless, future research on better estimating and predicting the transboundary impacts on SDGs can adopt multiple scenarios and use more sophisticated models (e.g., the Global

Biosphere Management Model – GLOBIOM) (Havlík et al., 2018). This research also lays a foundation for further exploring the transboundary impacts on sustainable development at finer scales, such as at the sub-national level, corporation level (Malik et al., 2021a), and even pixel level by integrating satellite earth observation with supply chain data (Burke et al., 2021; Moran et al., 2020). With richer data available to fill the current data gaps in evaluating SDG performance, scientists would be able to have a better understanding of the complexity in the transboundary impacts and help achieve the SDGs around the world.

CHAPTER 6: SYNTHESIS

This dissertation facilitates the comprehensive understanding and application of metacoupling framework by developing and synthesizing advanced approaches for metacoupling quantification across scales. The main conclusions of each chapter are summarized as follows.

Chapter 2 made the first attempt to develop a typology of transboundary flows using six flow attributes (i.e., type, magnitude, direction, distance, time, and mode) to advance metacoupling flow research and governance. This study provided a portfolio of quantitative and practical methods for characterizing transboundary flows, ranging from trade analysis, and big data analysis, to various modeling approaches. This synthesis, covering multidisciplinary concepts and methodologies from geography, hydrology, industrial ecology, economy, and environmental science and policy, will be extremely useful for interdisciplinary research. This chapter highlighted the great need to recognize the critical but often neglected transboundary flows in impacting sustainability, be aware of the shared risks (e.g., climate change, global epidemic, and conflicts), use system thinking, and strengthen multilateral cooperation, so that effective policies can be developed for safeguarding humankind and planetary sustainability.

Chapter 3 mapped coastal hypoxia (or dead zone) dynamics across 20 years (2000-2019), which provides critical data and knowledge for linking excess nutrient flows from the US Midwest with the impact in the Gulf of Mexico region. This chapter integrated time-series remote sensing observations with field measurement archives, and developed a Random Forest model for predicting spatially explicit dead zone dynamics across time and space. The rich and fine temporal

and spatial information on dead zone dynamics will be also useful for policy-makers to develop targeted management plans and environmental policies. For example, the integrated framework of telecoupling can be used to link distant places in the watershed that apply excessive fertilizers with the coasts that are suffering hypoxia issues. Building such linkages can help predict the timing and amount of the excessive fertilizers that reach global coasts based on the locations of fertilizer applications and leakages as well as the speed of river water flows.

Chapter 4 tracked the flow of foods as well as the flow of virtual nitrogen (N) embedded in food trade among 132 U.S. regions. Compared to existing studies that track physical nutrient flows across landscapes, this work offers a different perspective to examining virtual nutrient flows across regions. The analysis can help identify who else other than food producers should be responsible for the environmental impacts of food systems. Here it found the downstream food consumers who suffer from excess fertilizer use in the upstream also contributed to the increase of pollutants. The analysis also identified the hotspot flows and hotspot regions that contributed most to the transboundary flows of virtual nitrogen. The findings (e.g., the displaced virtual N) therefore can be used to optimize food supply chains for nutrient reduction strategies, such as through improving N use efficiency in hotspot regions or using virtual N as a novel indicator for determining the payment for ecosystem services.

Chapter 5 comprehensively evaluated a range of transnational flows and their effects on the performance of 17 SDGs for 189 countries globally. This study quantitatively demonstrated that achieving SDGs in one country may enhance or compromise SDGs in other countries. It found transnational connections and interactions (e.g., trade) are important for advancing countries'

overall SDG performance (improving roughly 20%). Despite the overall benefit, high-income countries generally benefited more, while low-income countries benefited less and were occasionally disadvantaged. This chapter also found that transnational interactions more frequently occurred among distant countries with unequal economic levels. This study offered an integrated picture of the often-ignored transnational impacts on achieving sustainability. This work, therefore, is useful for (inter)governmental agencies to target the negative transnational impacts and empower disadvantaged countries for achieving SDGs globally.

To sum up, this dissertation research provided both theoretical and methodological synthesis, as well exemplifications for tracking transboundary flows in addressing sustainability challenges. In the context of rapid global environmental change (e.g., global warming, extreme climate, disease outbreaks) and erratic interregional relations (e.g., conflicts), the metacouplings among different socio-environmental systems are becoming more complex. Future research can take a similar analytical framework and conduct research in other regions and countries at different scales by utilizing local knowledge. There is also a great need to develop integrated models and use scenario analysis to simulate the dynamic metacoupled systems. This research also lays a foundation for further exploring the transboundary flows and their impacts on sustainable development at finer scales, such as at the sub-national level, corporation level, and even pixel level by integrating satellite earth observation with detailed supply chain data. A better understanding of the complexity of the transboundary impacts can shed light on more collaborative governance and policymaking and help facilitate the achievement of 17 SDGs by 2030.

APPENDICES

APPENDIX A

SUPPORTING INFORMATION FOR CHAPTER 2



Figure A2.0.1. LCA tools, Carbon calculator, GREET (Greenhouse gases, Regulated Emissions, and Energy use in Transportation), GHGenius (focus on transportation fuels in Canada), GaBi Software, SimaPro, OPENLCA, Brightway2. Credits to Dr. Qingshi Tu at the University of British Columbia.

APPENDIX B

SUPPORTING INFORMATION FOR CHAPTER 3

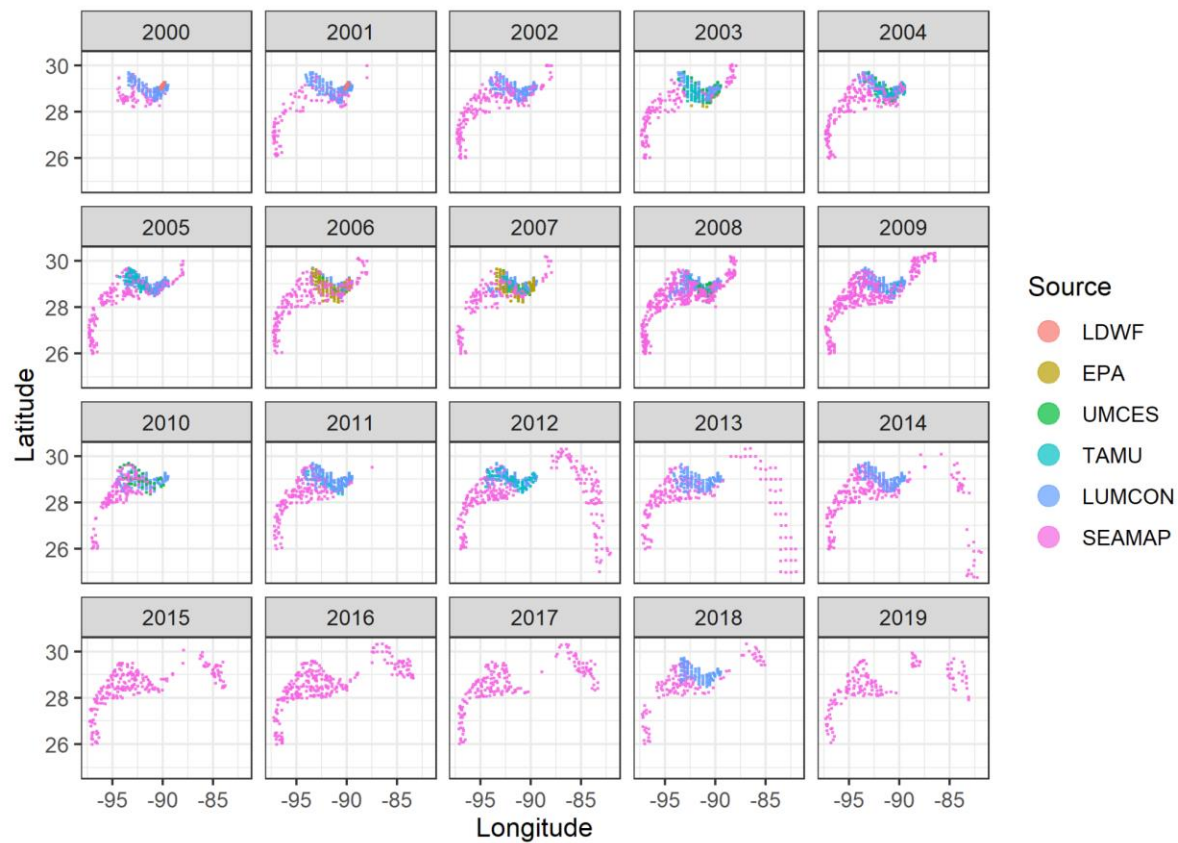


Figure A3.0.2. DO sampling locations from 2000 to 2019.

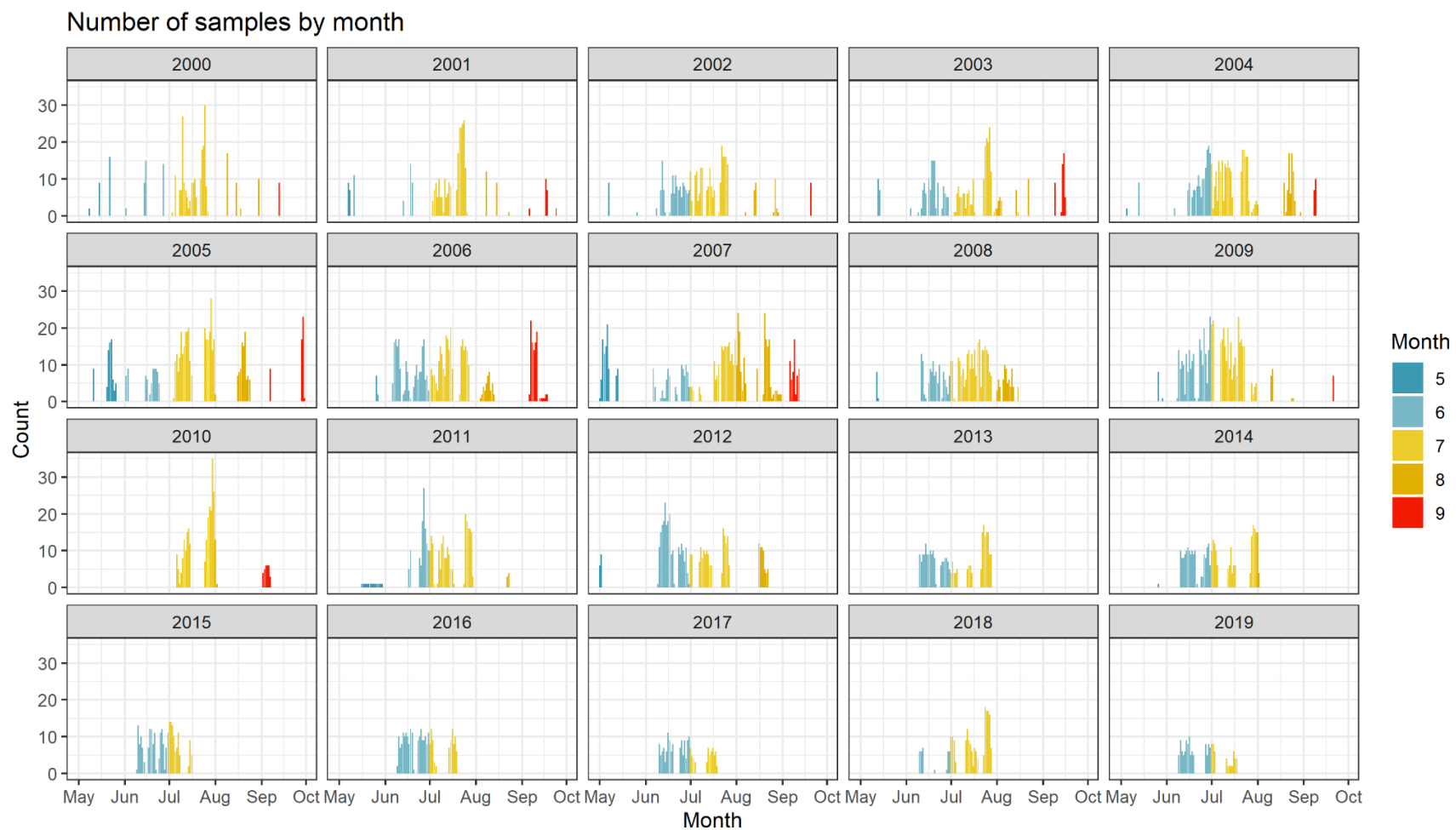


Figure A3.0.3. The number of sampling locations by year and by month.

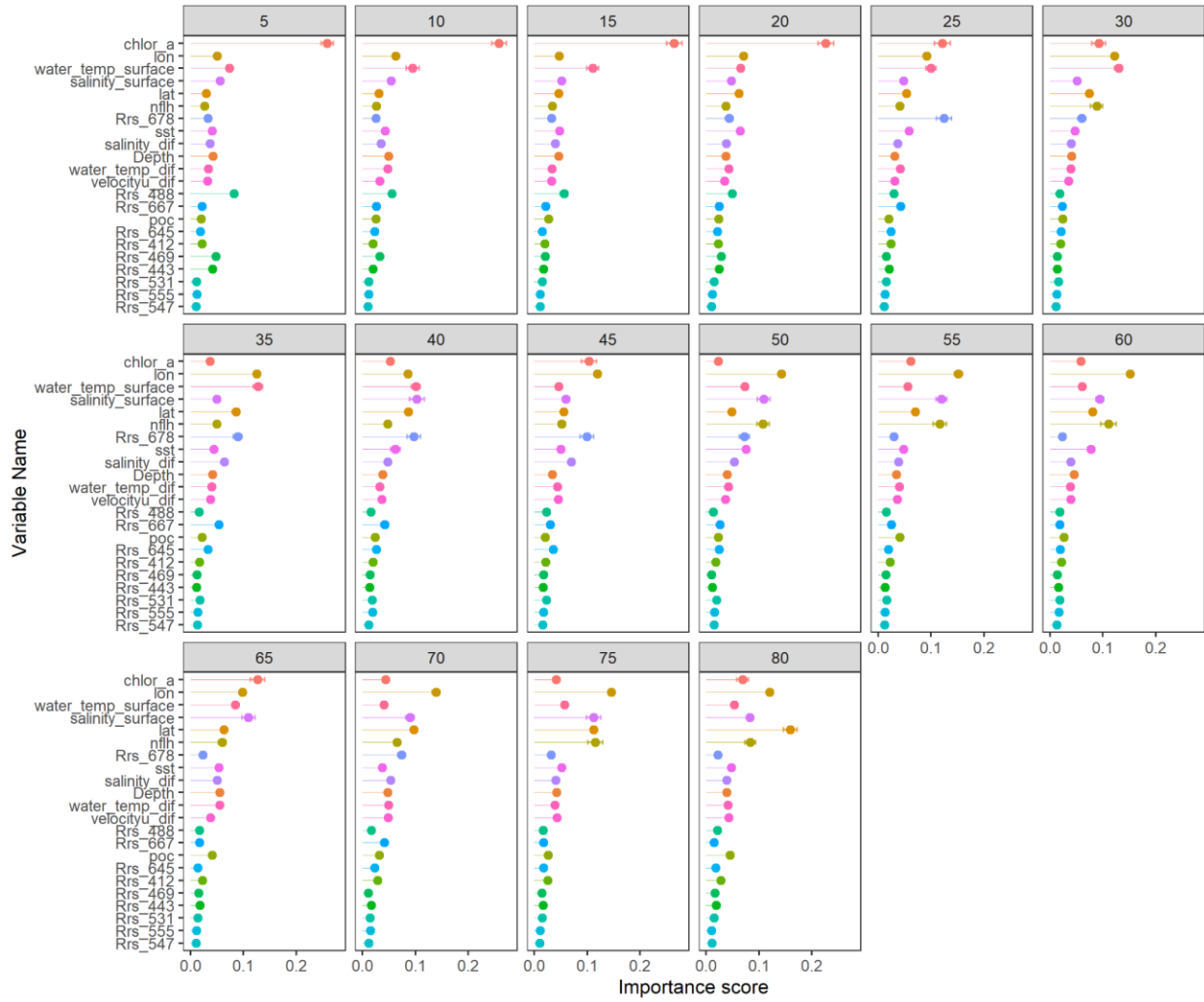


Figure A3.0.4. Importance score of selected variables. The top 12 are the selected input variables.

APPENDIX C

SUPPORTING INFORMATION FOR CHAPTER 4

Table A4.0.1. Parameters Used for Calculation of Biological N Fixation

Type	Reporting Unit	Unit conversion to	Unit conversion value	Fixation Rates unit	Fixation Rates value	Citation
Soybeans	Bushels	kg/reporting unit	27.2	kg-N/kg/yr	0.066	(Hong et al., 2011, 2013)
Alfalfa Hay	Dry tons	kg/reporting unit	907.2	kg-N/kg/yr	0.031	(Hong et al., 2011, 2013)
Peanuts	Pounds	kg/reporting unit	0.454	kg-N/kg/yr	0.045	(Hong et al., 2011, 2013)

Table A4.0.2. Parameters Used for Calculation of Crop N Uptake

Group	Type	Reporting Unit	Unit conversion to	Unit conversion value	N uptake unit	N uptake value	Citation
Crop	Barley	Bushels	kg/reporting unit	21.8	kg-N/kg	0.019	(Hong et al., 2011, 2013)
Crop	Corn, grain	Bushels	kg/reporting unit	25.4	kg-N/kg	0.013	(Hong et al., 2011, 2013)
Crop	Oats	Bushels	kg/reporting unit	14.515	kg-N/kg	0.018	(Hong et al., 2011, 2013; Lander et al., 1998)
Crop	Rice	Bushels	kg/reporting unit	20.3	kg-N/kg	0.013	(Hong et al., 2011, 2013; Lander et al., 1998)
Crop	Rye	Bushels	kg/reporting unit	25.4	kg-N/kg	0.019	(Hong et al., 2011, 2013; Lander et al., 1998)
Crop	Sorghum, grain	Bushels	kg/reporting unit	25.4	kg-N/kg	0.018	(Hong et al., 2011, 2013; Lander et al., 1998)
Crop	Wheat	Bushels	kg/reporting unit	27.2	kg-N/kg	0.019	(Hong et al., 2011, 2013; Lander et al., 1998)

Table A4.0.3. The top 10 net flows of live animals (SCTG = 01) in 2017

Rank	From	To	Million Tons
1	Remainder of Minnesota	Remainder of Wisconsin	0.69
2	Remainder of Nebraska	Remainder of Nebraska	0.49
3	Remainder of Iowa	Remainder of Iowa	0.21
4	Remainder of Kansas	Remainder of Kansas	0.19
5	Remainder of California	Remainder of California	0.18
6	Omaha-Council Bluffs-Fremont, NE-IA	Remainder of Nebraska	0.15
7	Remainder of Pennsylvania	Philadelphia-Reading-Camden, PA-NJ-DE-MD	0.12
8	Omaha-Council Bluffs-Fremont, NE-IA	Omaha-Council Bluffs-Fremont, NE-IA	0.10
9	Remainder of Missouri	Remainder of North Carolina	0.10
10	Remainder of Missouri	Remainder of Illinois	0.09
(Interregional flows, after excluding self-loop flows)			
1	Remainder of Minnesota	Remainder of Wisconsin	0.69
2	Omaha-Council Bluffs-Fremont, NE-IA	Remainder of Nebraska	0.15
3	Remainder of Pennsylvania	Philadelphia-Reading-Camden, PA-NJ-DE-MD	0.12
4	Remainder of Missouri	Remainder of North Carolina	0.10
5	Remainder of Missouri	Remainder of Illinois	0.09
6	Remainder of Minnesota	Remainder of South Dakota	0.09
7	Minneapolis-St. Paul, MN-WI	Remainder of Wisconsin	0.09
8	Remainder of Pennsylvania	New York-Newark, NY-NJ-CT-PA	0.07
9	Remainder of Alabama	Remainder of Texas	0.07
10	Remainder of Kentucky	Remainder of Texas	0.06

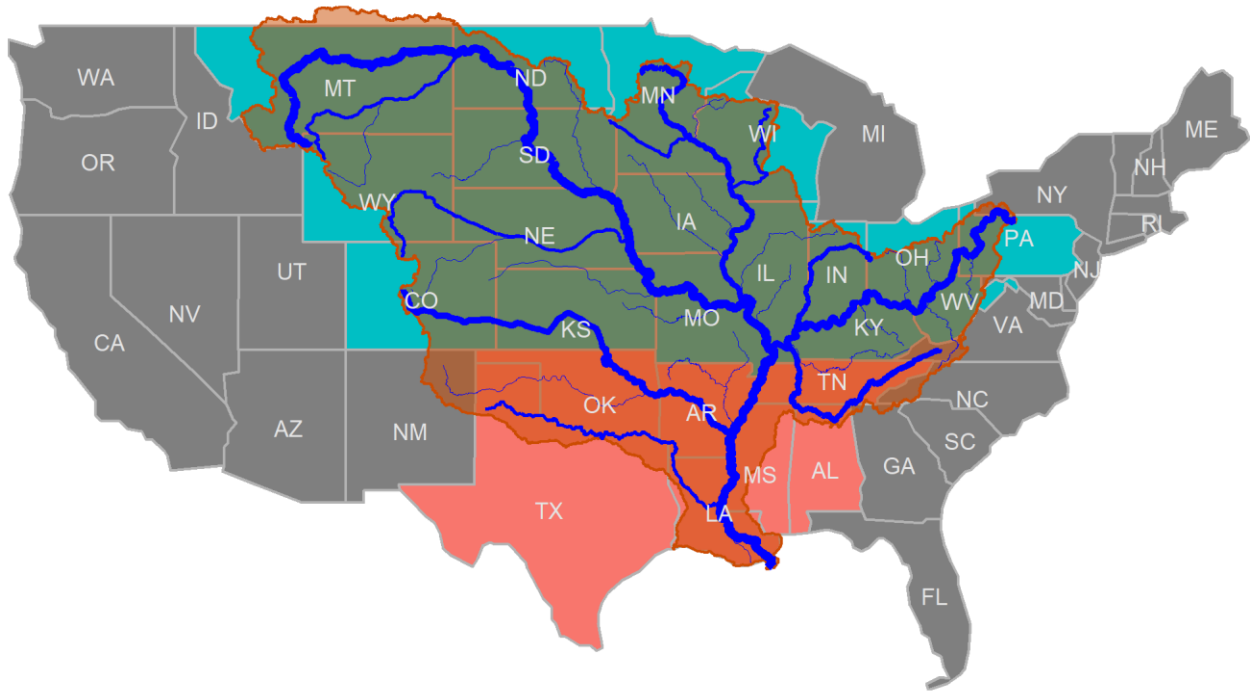


Figure A4.0.5. The geographical locations of the Mississippi River Basin (MRB), non-MRB (states with gray shade), the MRB upper (states with green shade), and lower basins (states with red shade).

APPENDIX D

SUPPORTING INFORMATION FOR CHAPTER 5

Text S5.1. MRIO analysis for quantifying effects of TNIs embodied in international trade

We applied multi-regional input-output analysis to quantify transnational impacts (such as virtual water, CO₂, energy, raw materials, and land) embodied in international trade. This footprint-based measurement can quantify the amount of natural resources required or social risks along the supply chain for the production of goods and services (Feng et al., 2013; Wiedmann et al., 2015; Zhao et al., 2015). For instance, CO₂ emissions are produced during the entire production and supply chain of goods and services.

MRIO has been widely used to study economic interdependencies between countries by tracking monetary flows. Assuming there are m countries and every country has n sectors, the monetary output of sector i in country R can be calculated using the following equation:

$$x_i^R = \sum_{S=1}^m \sum_{j=1}^n x_{ij}^{RS} + \sum_{S=1}^m y_i^{RS} \quad (1)$$

where x_{ij}^{RS} is the value of monetary flows from sector i of country R to sector j of country S , and y_i^{RS} represents country S 's final demand that is supported by sector i of country R .

The direct input coefficient a_{ij}^{RS} is derived from equation (2):

$$a_{ij}^{RS} = \frac{x_{ij}^{RS}}{x_j^S} \quad (2)$$

where a_{ij}^{RS} is the value of monetary flows from sector i of country R that contributes to one unit of monetary output in sector j of country S .

If we let $X=[x_i^R]$, $A=[a_{ij}^{RS}]$ and $Y=[y_i^{RS}]$, we can calculate the following matrix X based on equation (1):

$$X = A.X + Y \quad (3)$$

Then we rearranged and formulated the equation (3) as:

$$X = B.Y, B = (I - A)^{-1} \quad (4)$$

where $(I - A)^{-1}$ is the Leontief inverse matrix, suggesting both direct and indirect monetary value flow from other countries to meet one unit of final monetary demand.

To calculate the amount of virtual resources and social risks embodied in international trade, we first calculated the direct resource intensity coefficient. The direct resource intensity coefficient of sector i in country R is expressed as:

$$e_i^R = \frac{w_i^R}{x_i^R} \quad (5)$$

where w_i^R is the total resource/material intensity in sector i of country R ; therefore e_i^R is the amount of resource/material consumed/emitted to increase one monetary unit of output in sector i in country R .

If we let $E = [e_i^R]$, then we can calculate the virtual resource (VR) transfer matrix using the following equation.

$$VR = E.B.Y \quad (6)$$

The amounts of virtual water, energy, material, CO₂, and social risks embodied in yearly trade for each country/region therefore are calculated.

Text S5.2. Country list and country groups

The 189 countries were grouped into 112 “high income” countries (65 high-income countries and 47 upper-middle-income countries according to World Bank’s income classification), and 78 “low income” countries (or 48 lower-middle-income countries and 30 low-income countries according to World Bank) (Table A5.0.3). We then calculated the average SDG score for each country in each group, again without weighting for country population or gross domestic product. We also classified international interactions into “adjacent” ones and “distant” ones based on the geographical relationship between countries. Interactions between countries that share land or maritime borders were deemed as adjacent interactions. In all other cases, interactions between two countries or regions were deemed as distant ones (see Table A5.0.4 for a list of countries and territories by land and maritime borders) (Anderson, 2003; Charney et al., 1993; Xu et al., 2020c). This allowed us to assess the impacts of adjacent versus distant impacts on SDG scores in the metacoupled world system.

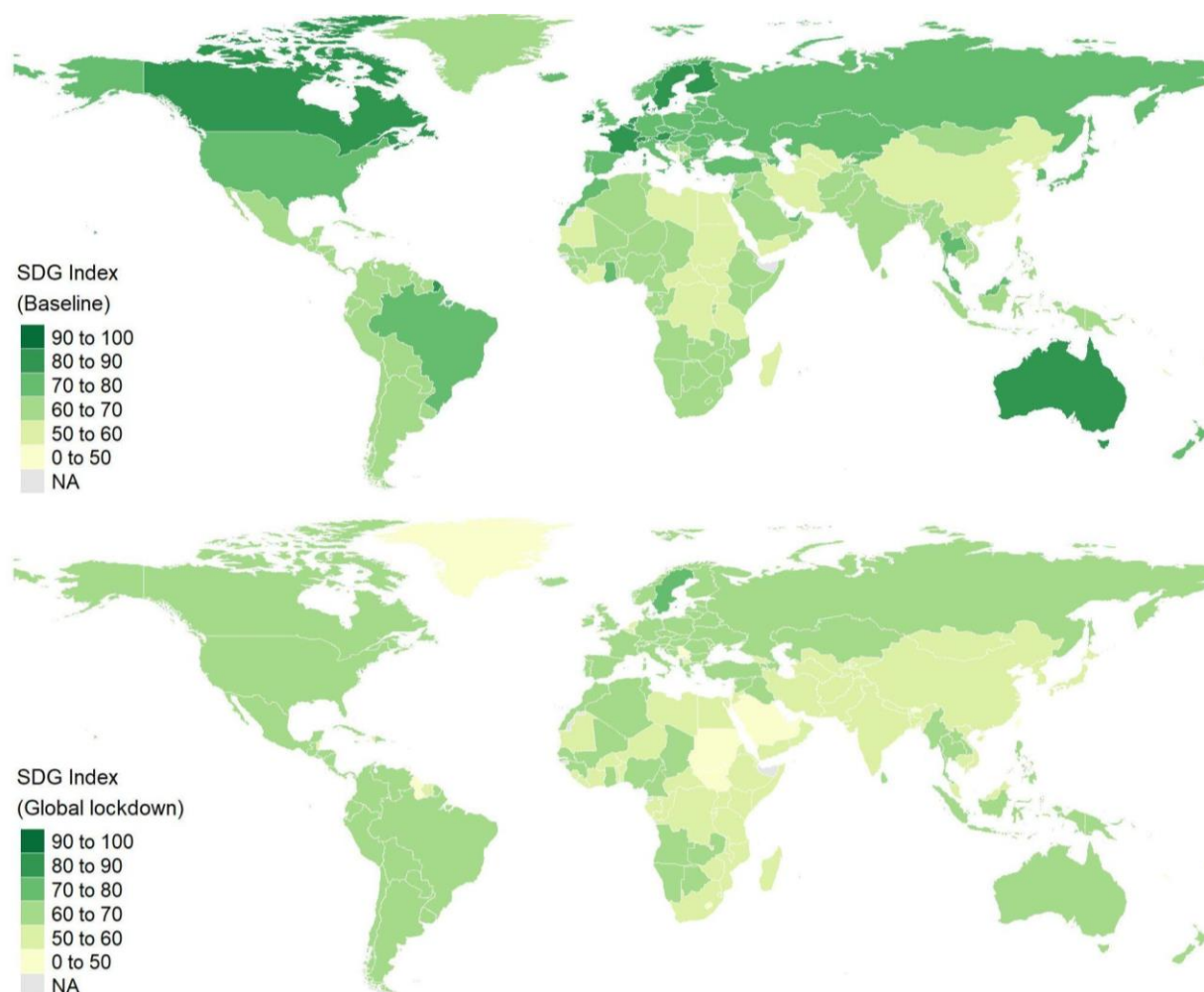


Figure A5.0.6. SDG Index under the baseline scenario (i.e., the current globally metacoupled system), and a hypothetical global lock-down scenario (i.e., no transnational interactions among countries but only domestic activities)

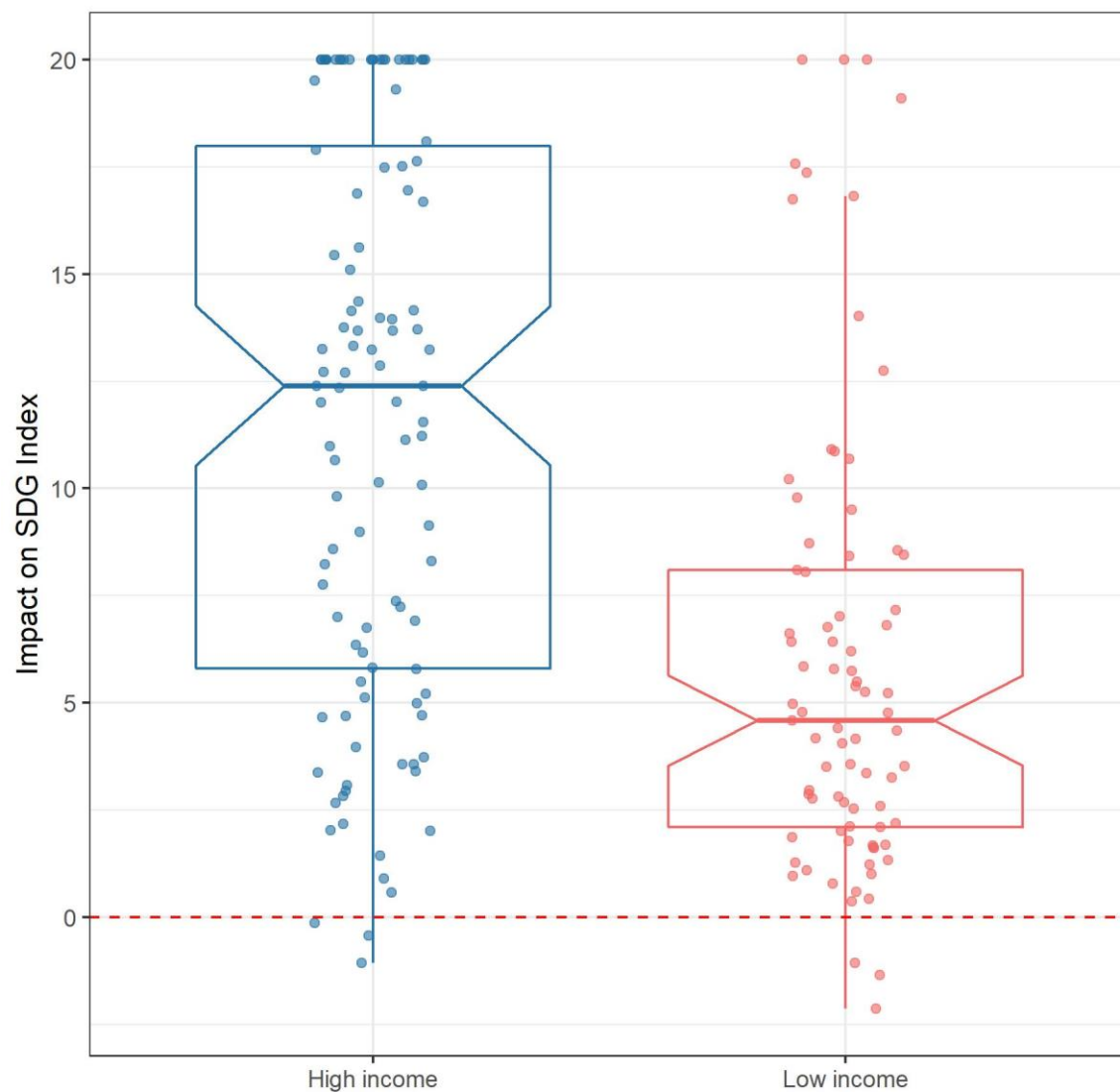


Figure A5.0.7. TNIs on SDG Index by income group in 2015. A value above 0 means a positive impact on a nation's SDG Index, while a value less than 0 indicates a negative impact on a nation's SDG Index. In each boxplot, the central rectangle spans the first quartile Q1 to the third quartile Q3, while the segment inside the rectangle indicates the median. Each dot represents a country.

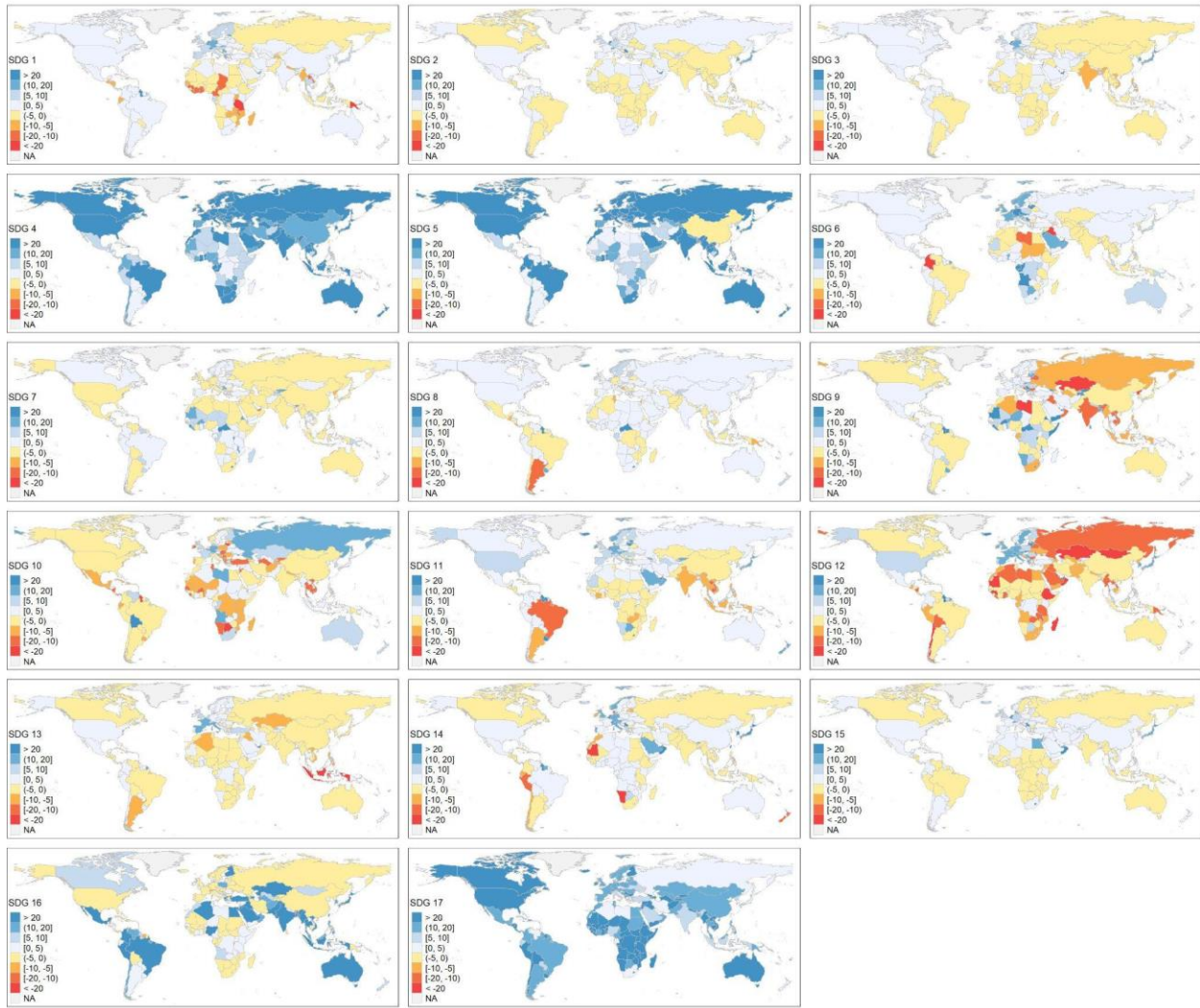


Figure A5.0.8. Impacts of TNIs on each SDG at the country level.

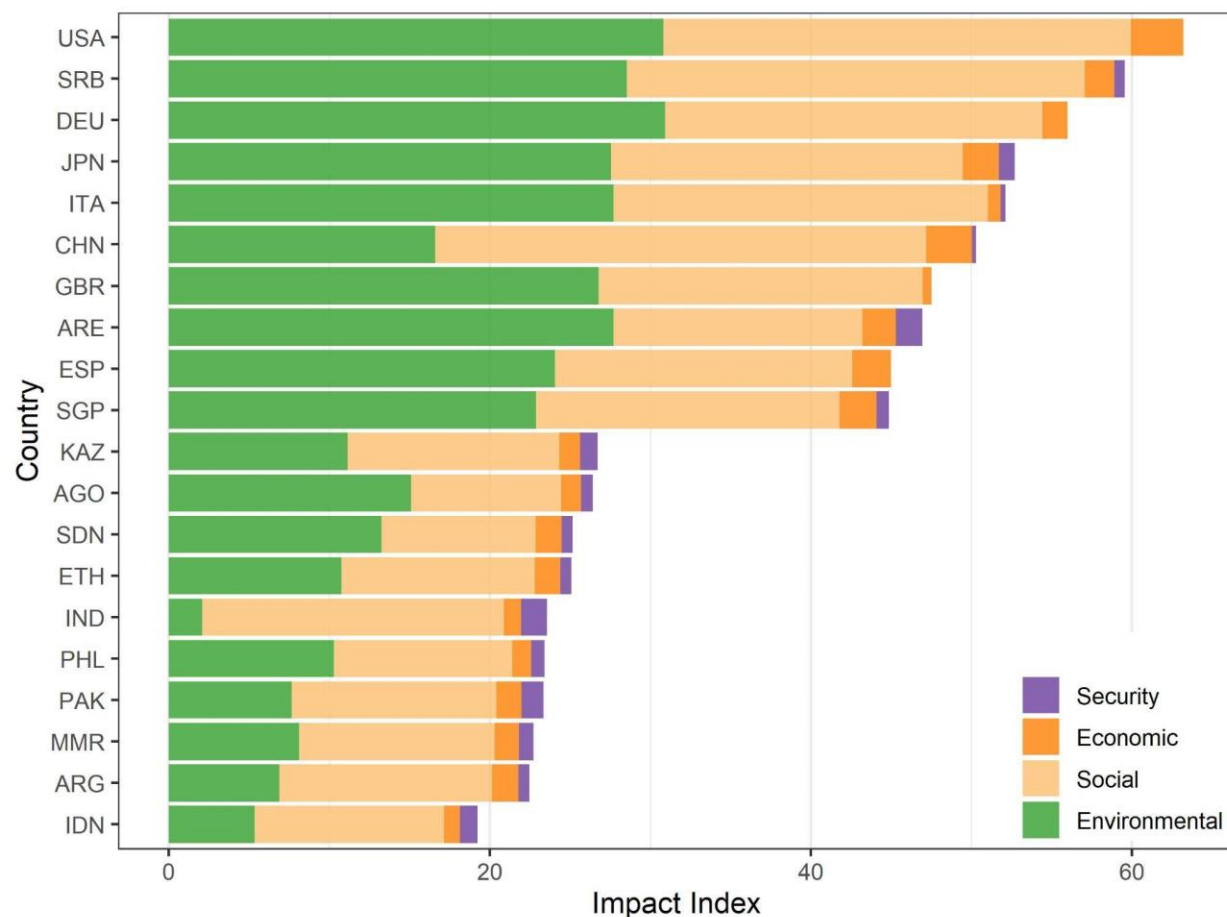


Figure A5.0.9. Impacts of TNIs by category and by the top 10 and bottom 10 influencers, ranked by TNI impact index (i.e., aggregated impact scores). The plot shows the overall impacts, which means some of the positive impacts could have been offset by other large negative impacts. High values mean larger negative impacts on the rest of the world. Full names of the countries are listed in Table A5.0.3.

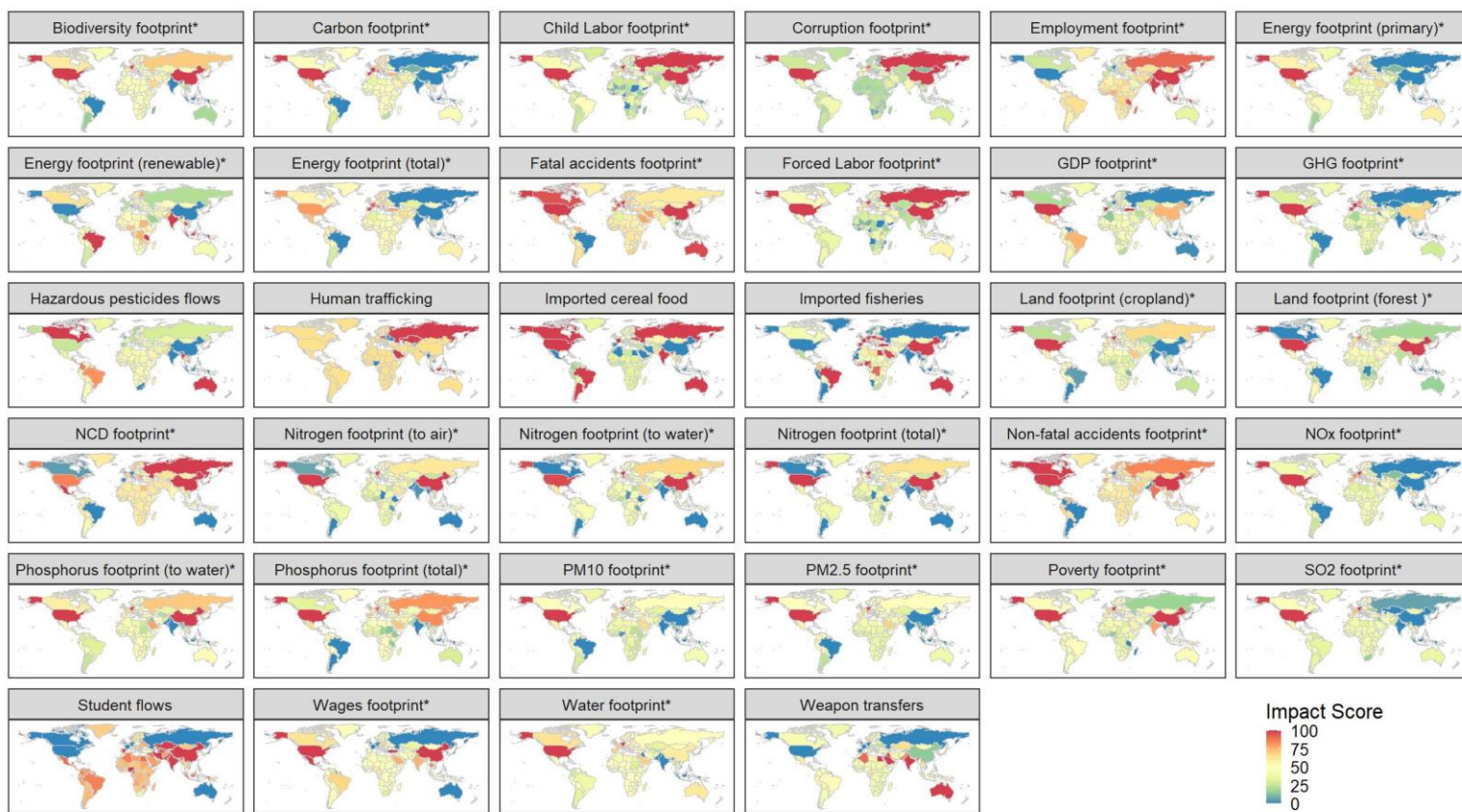


Figure A5.0.10. Impact of TNIs by country. Refer to Table A5.0.2 for the full name of each impact. Asterisk (*) denotes the displaced footprint or net imported virtual footprint by a country.



Figure A5.0.11. Distribution of the average distance of interactions between two countries, by and by TNI impact indicators.

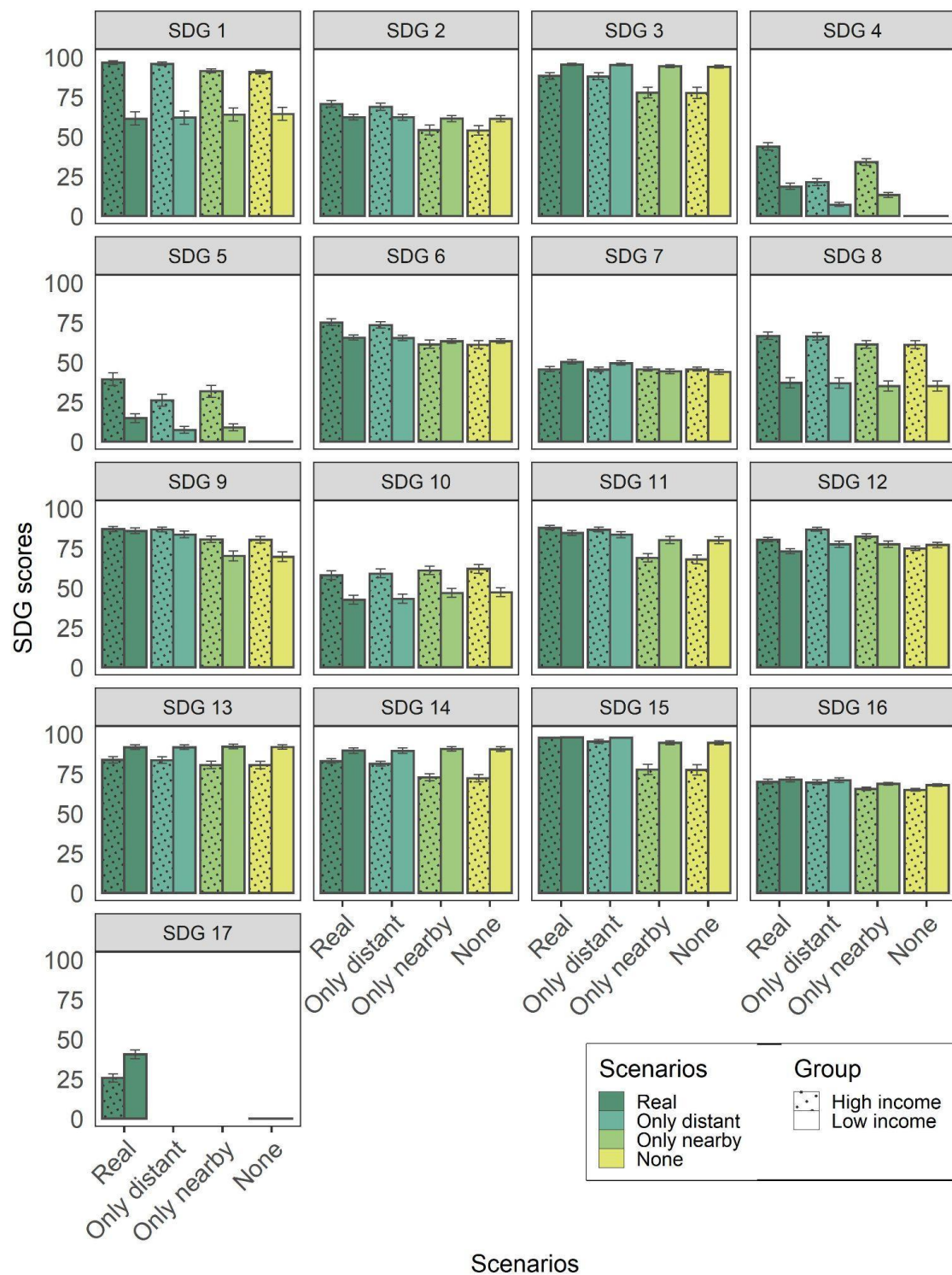


Figure A5.0.12. SDG scores by income group under four scenarios: the real world in 2015 (Real), only distant world connections (Only distant), only nearby world connections (Only nearby), and global lockdown with no connections (None).

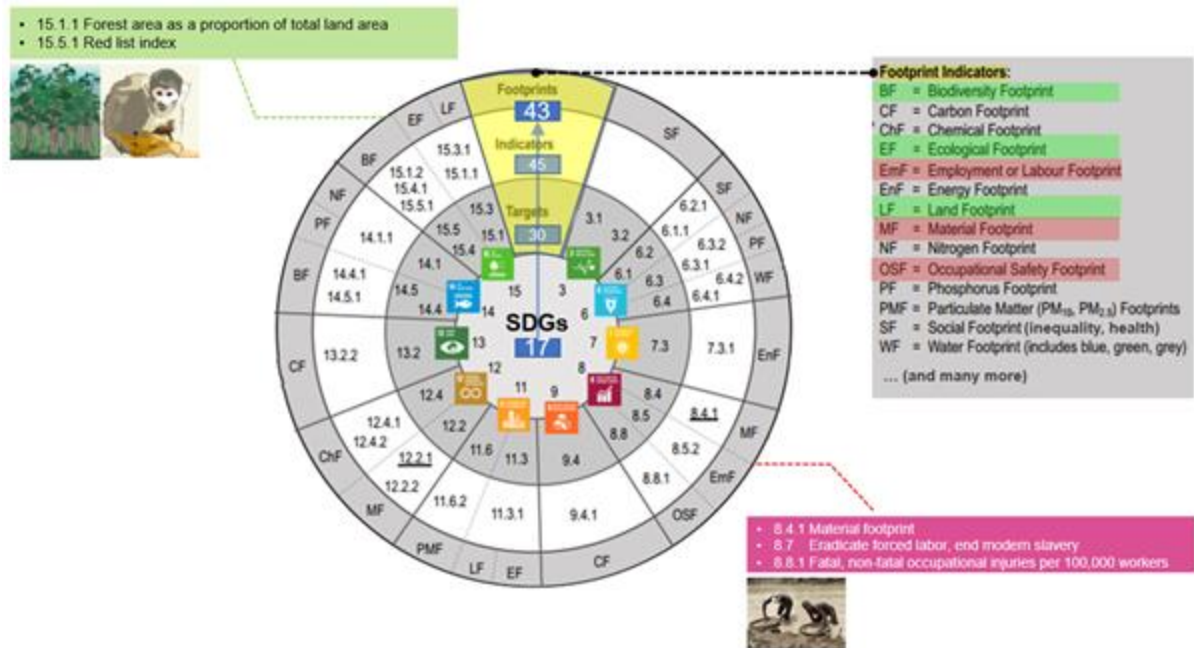
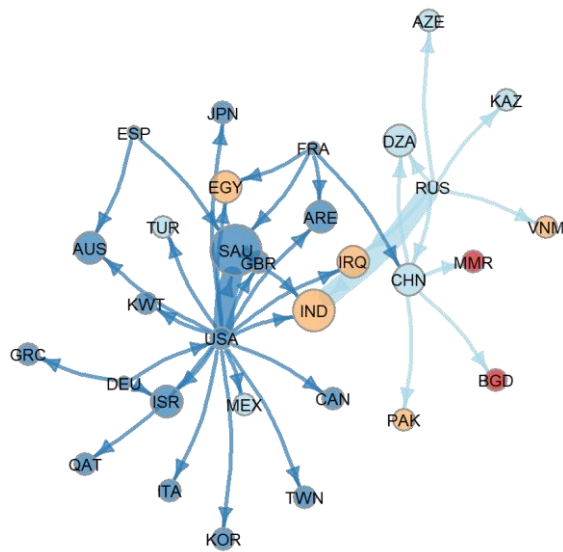
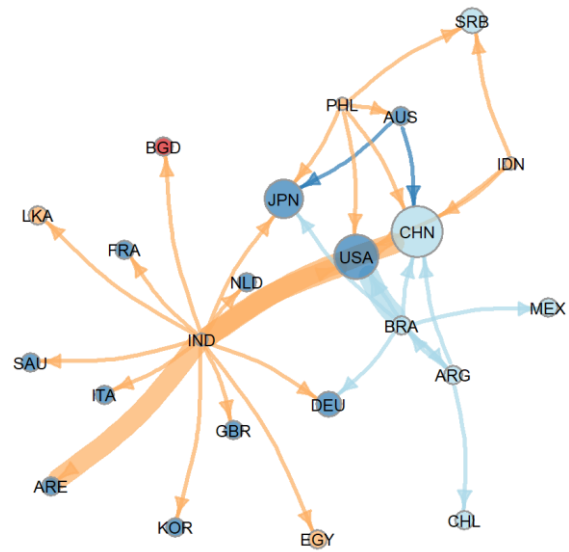


Figure A5.0.13. Demonstration of the linkage between SDGs and TNIs. Shown are the 17 SDGs (center), 30 SDG targets (first ring), and 45 SDG indicators (second ring) that relate to 43 specific transnational footprint indicators (third ring). Two SDG indicators under SDG 8 and three SDG indicators for SDG 15 are presented in the figure for a demonstration purpose only. A full list of matched linkages between SDGs and TNIs can be found in Table A5.0.1.

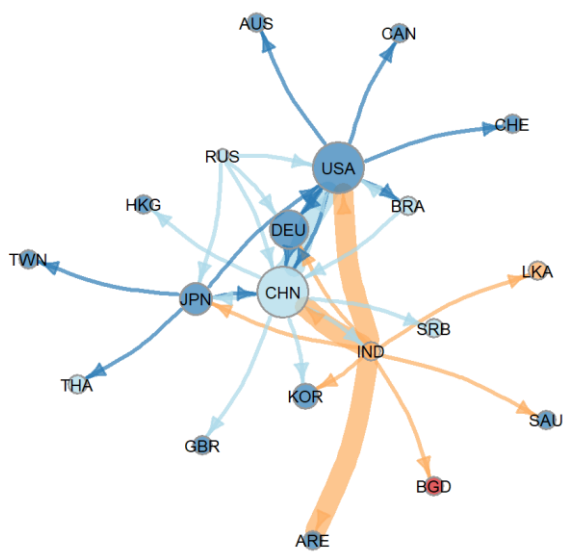
Weapon transfers



Biodiversity footprint



Carbon footprint



Corruption footprint

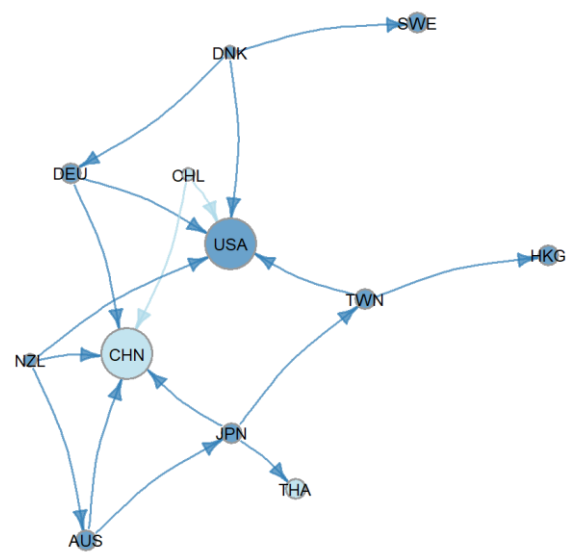
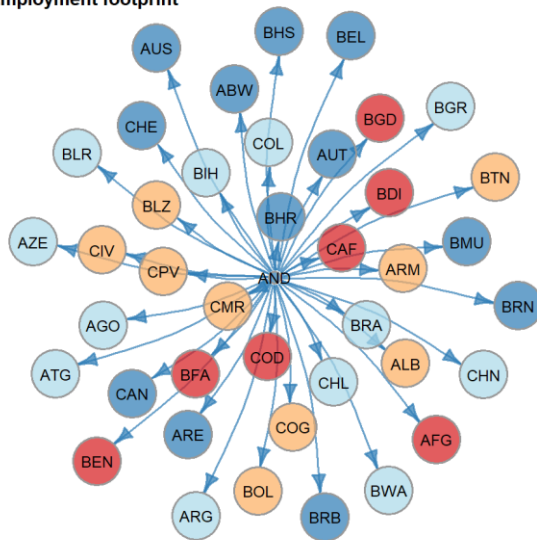
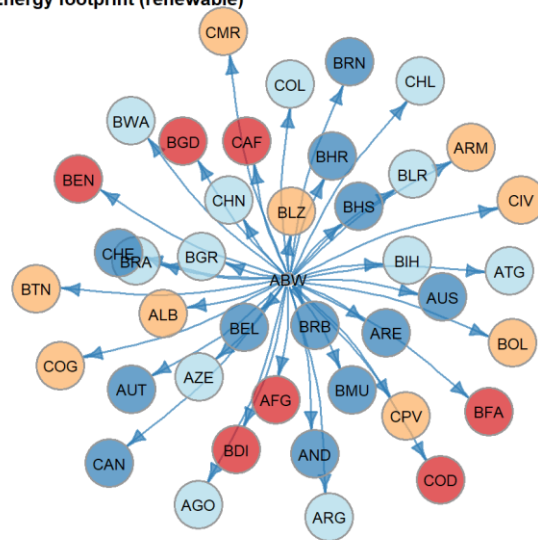


Figure A5.0.14. Network for each TNI. Only the top 50 country pairs with the largest TNI flows are presented. The arrows point to the dominant influencers (or responsibility takers); The width of the edges represents the magnitude of impact.

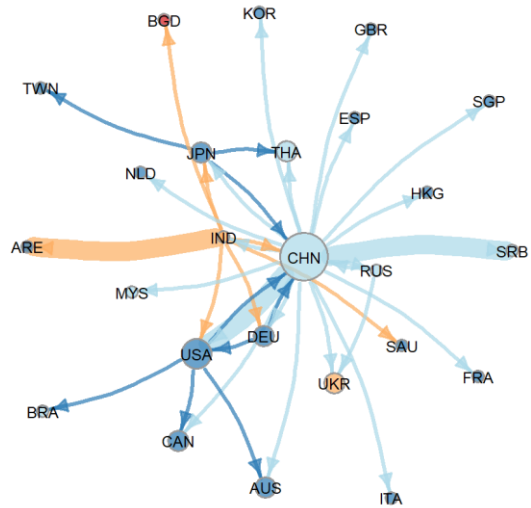
Employment footprint



Energy footprint (renewable)



Energy footprint (primary)



Energy footprint (total)

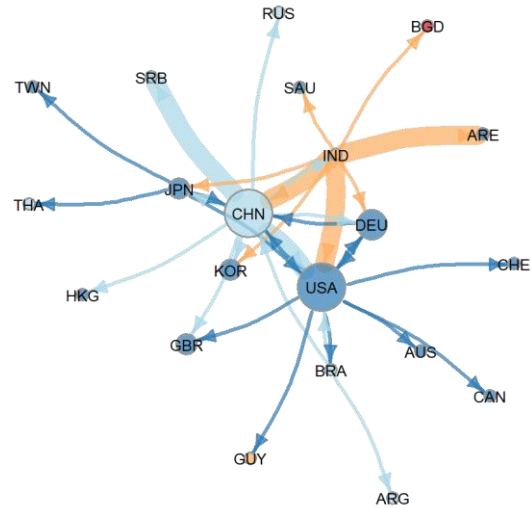


Figure A5.0.14 (cont'd)

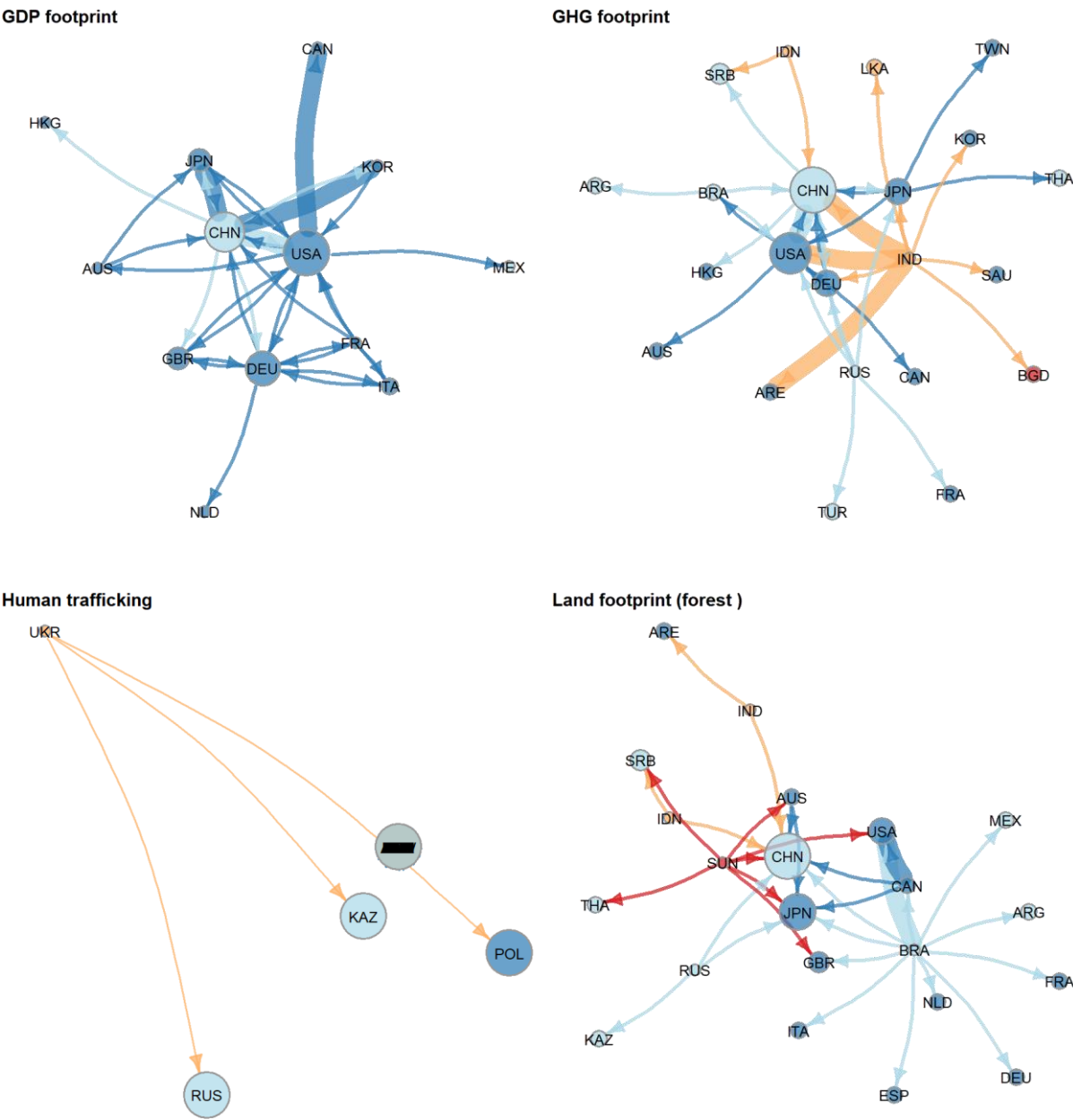
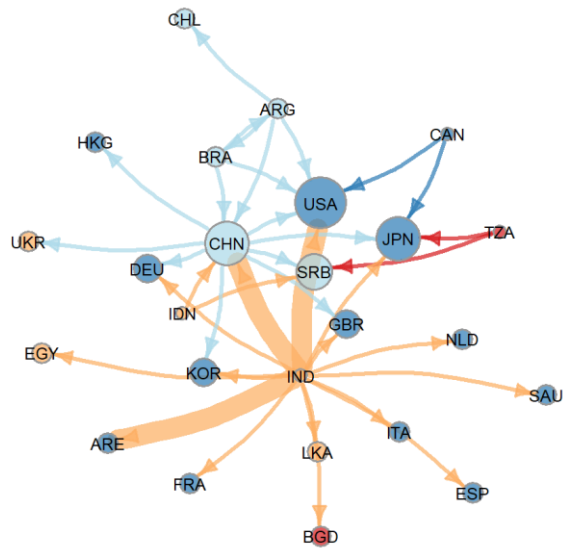
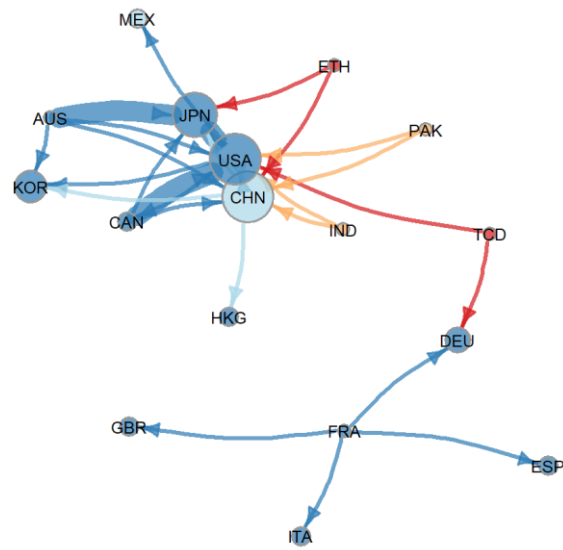


Figure A5.0.14 (cont'd)

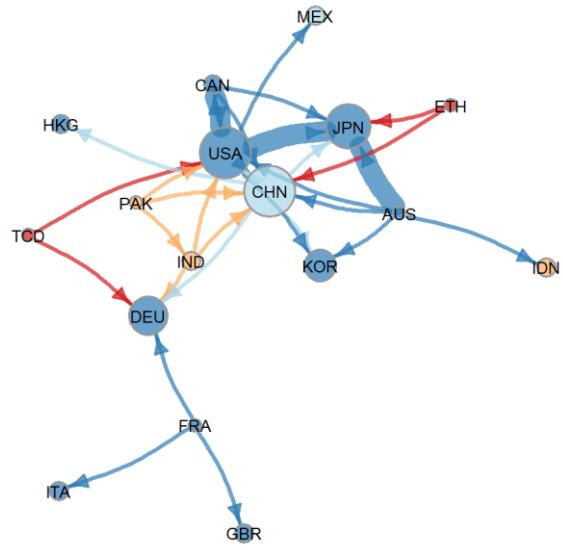
Land footprint (cropland)



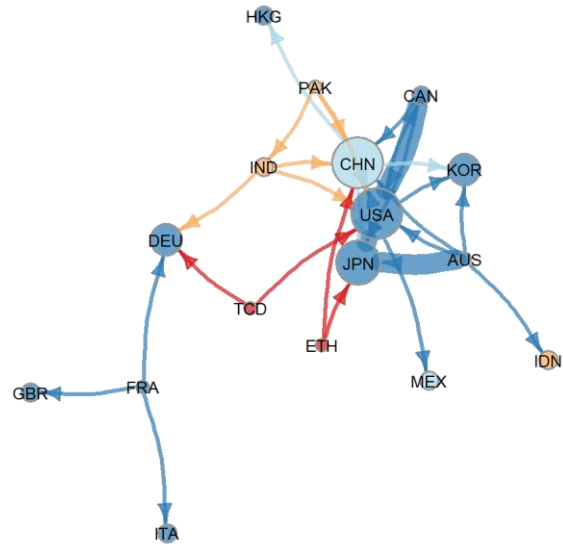
Nitrogen footprint (to air)



Nitrogen footprint (to water)



Nitrogen footprint (Total)



NOx footprint

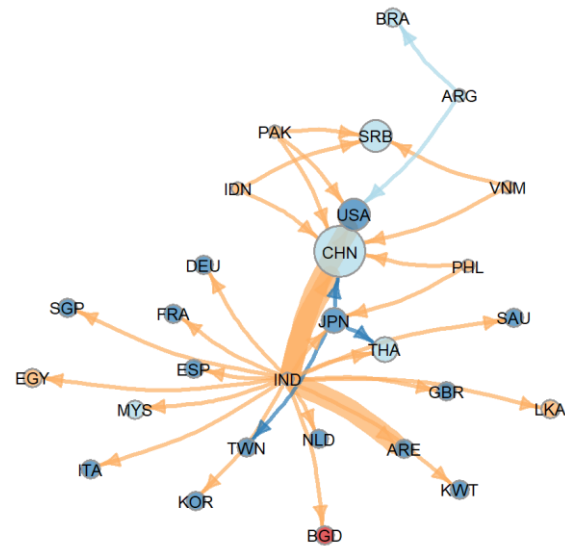
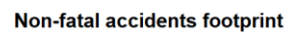
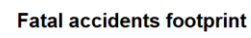
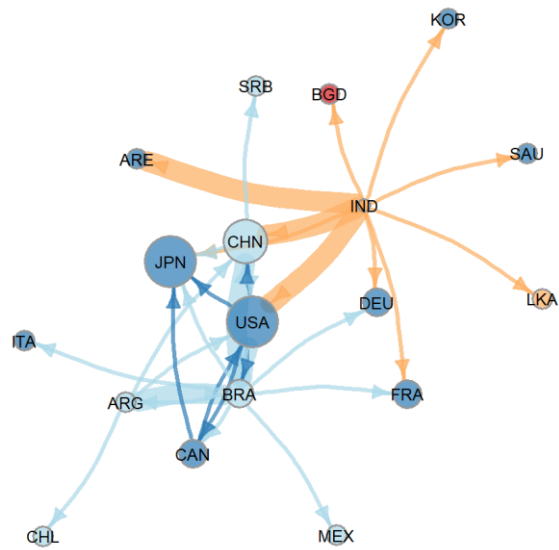
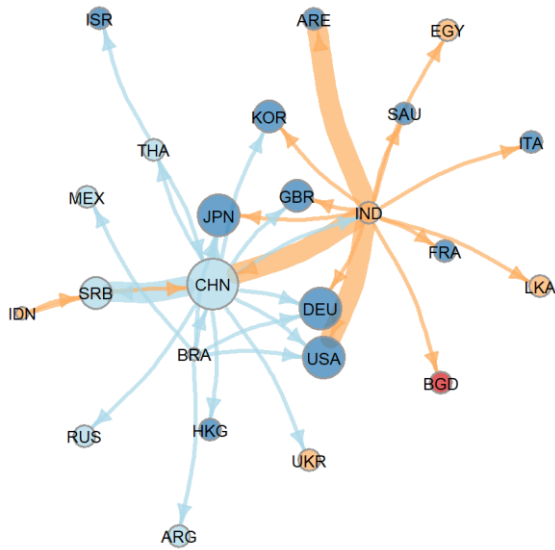


Figure A5.0.14 (cont'd)

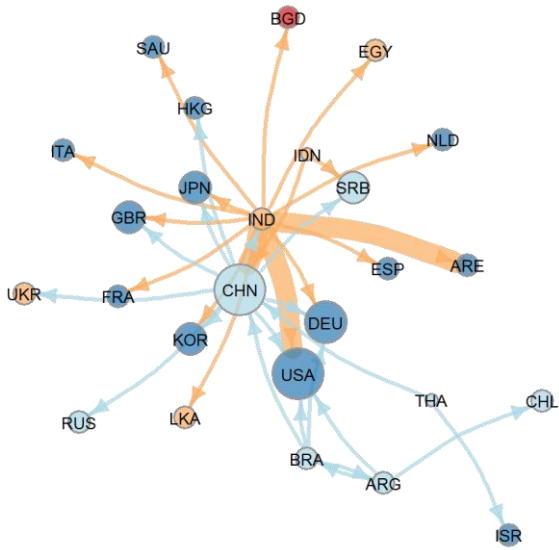
Phosphorus footprint (total)



PM10 footprint



PM2.5 footprint



Poverty footprint

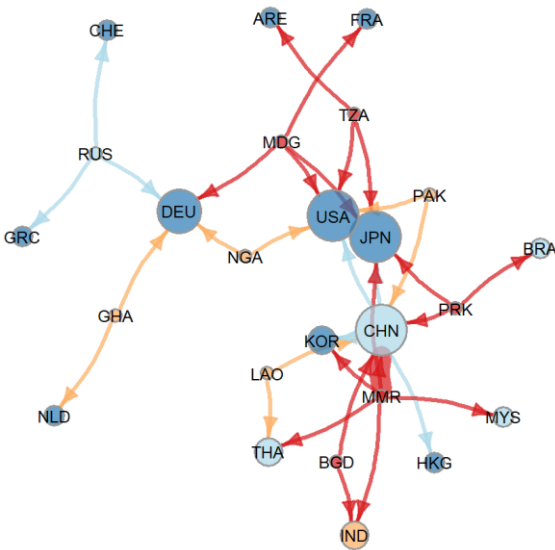
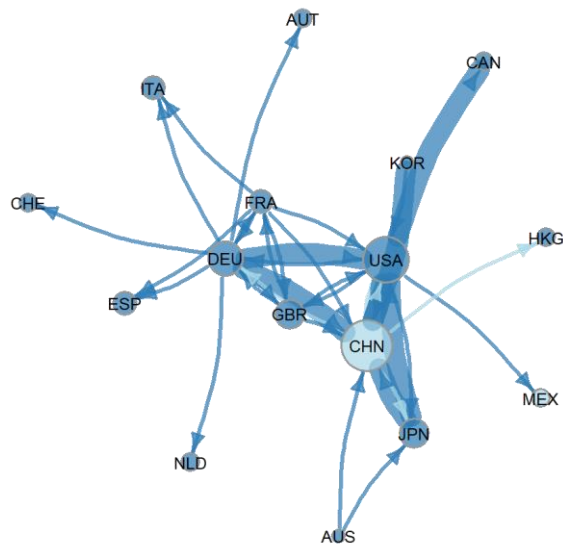
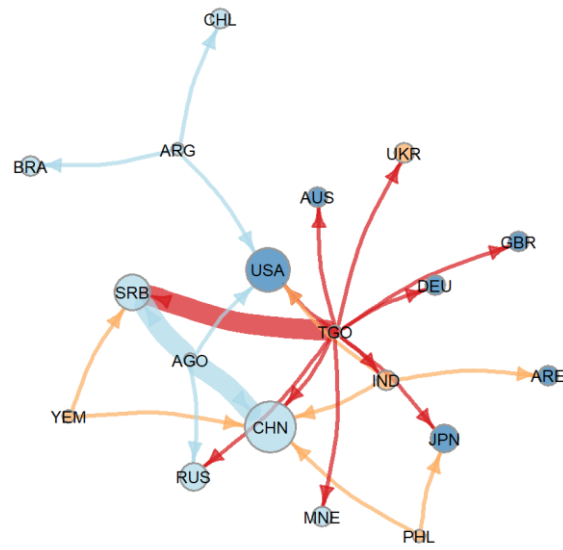


Figure A5.0.14 (cont'd)

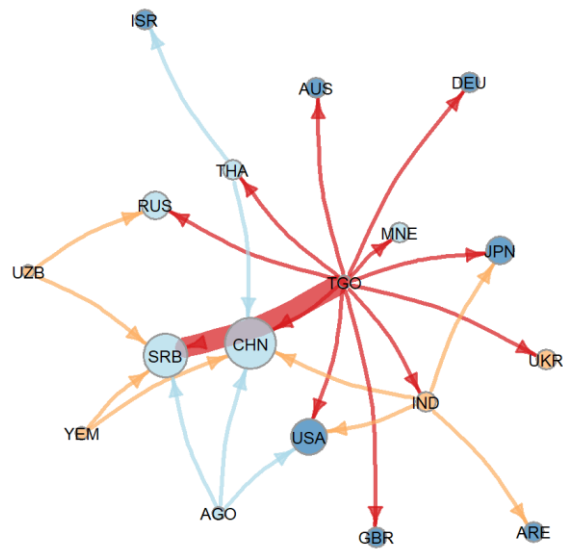
Wages footprint



Child Labor footprint



Forced Labor footprint



SO2 footprint

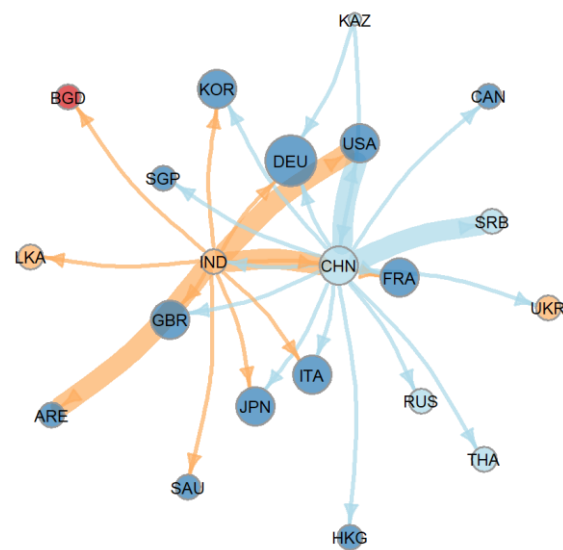
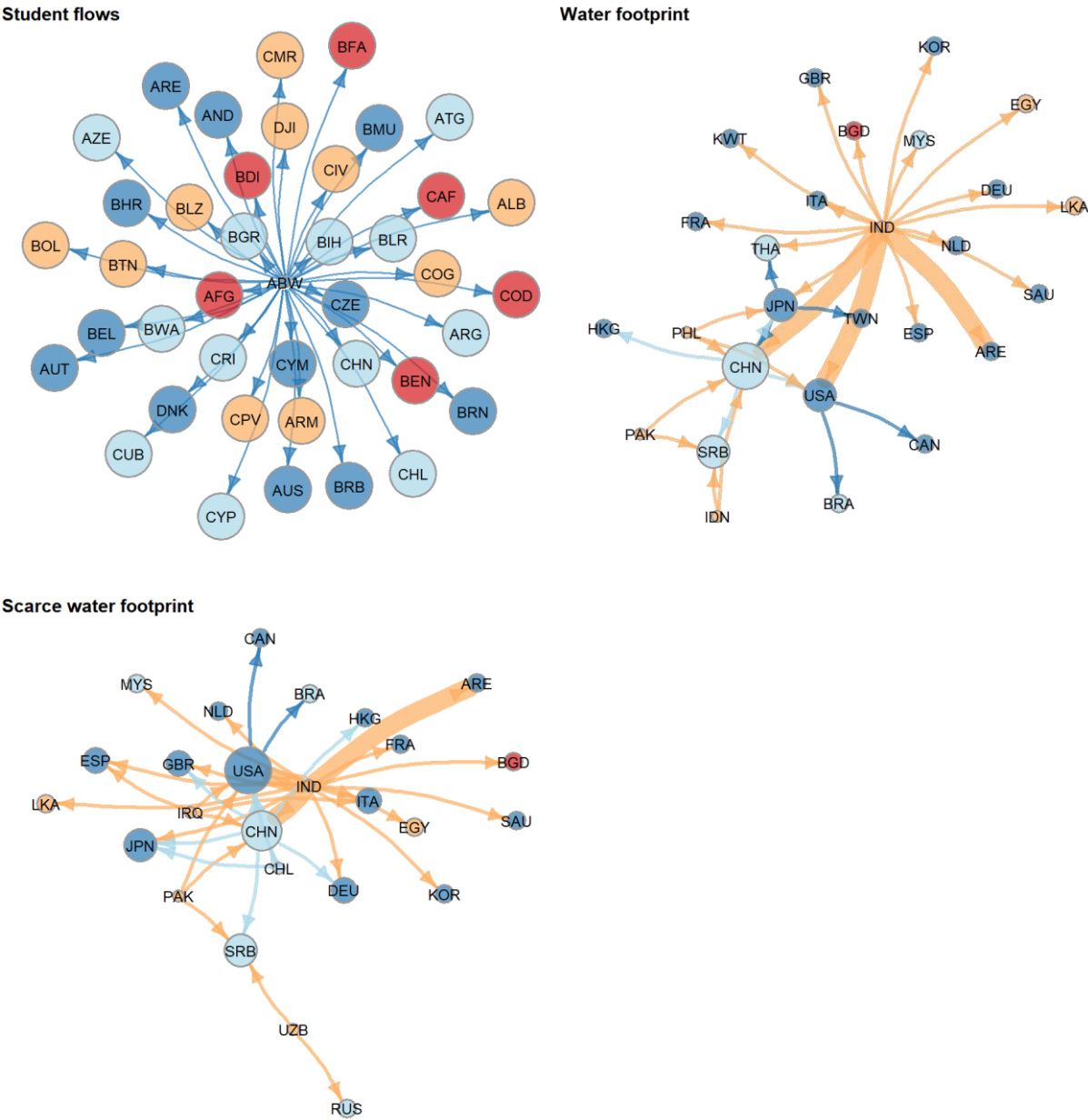


Figure A5.0.14 (cont'd)



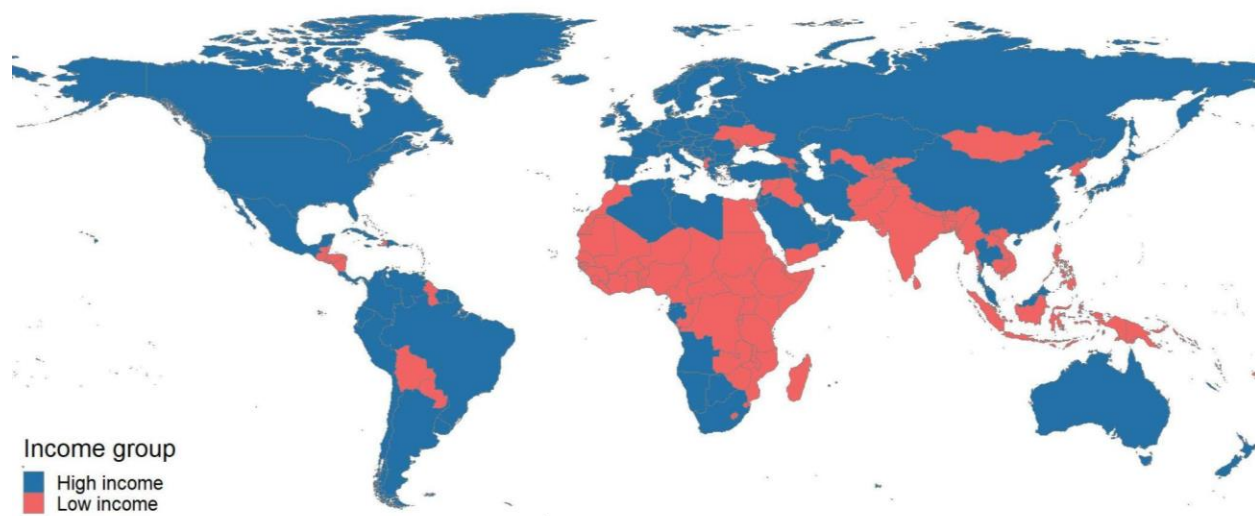


Figure A5.0.15. Map of county income group.

Table A5.0.4. SDG indicators impacted by transnational interactions

SDG	SDG Indicator	Indicators of TNI impacts*
1	1.1.1 Proportion of the population living below the international poverty line	Poverty footprint
2	2.4.1 Proportion of agricultural area under productive and sustainable agriculture	Land footprint (cropland)
2	2.1.2 Prevalence of moderate or severe food insecurity in the population (Cereal production per capita)	Imported cereal production
3	3.9.1 Mortality rate attributed to household and ambient air pollution (PM25 concentration)	PM2.5 footprint (air pollutants)
3	3.9.1 Mortality rate attributed to household and ambient air pollution (SO2 concentration)	SO2 footprint (air pollutants)
3	3.4.1 Mortality rate attributed to cardiovascular disease, cancer, diabetes or chronic respiratory disease	Noncommunicable diseases (NCD) attribute to net imported red and processed meat
4	4.7.1/12.8.1/13.3.1 Extent to which global citizenship education	International student flows (in tertiary education)
5	5.5.2 Proportion of women in managerial positions	Gender equity footprint
6	6.3.2 Proportion of bodies of water with good ambient water quality	Nitrogen footprint (nitrogen potentially exportable to water bodies)
6	6.4.1 Change in water-use (WU) efficiency over time	Water footprint
6	6.4.2 Level of water stress: freshwater consumption as a proportion of available freshwater resources (WR)	Water footprint
7	7.1.2 Proportion of population with primary reliance on clean fuels and technology	Energy footprint (Renewable)
7	7.2.1 Renewable energy share in the total final energy consumption	Energy footprint (Renewable)
7	7.3.1 Energy intensity measured in terms of primary energy and GDP (low energy intensity indicates high SDG indicator score)	Energy footprint (Primary)
8	8.1.1 Annual growth rate of real GDP per capita	GDP embodied in trade
8	8.8.1-1 Fatal occupational injuries per 100,000 workers	Occupational Safety and Health footprint (fatal accidents)
8	8.8.1-2 Non-fatal occupational injuries per 100,000 workers	Occupational Safety and Health footprint (non-fatal accidents)

Table A5.0.4 (cont'd)

9	9.4.1-1 CO2 emission per unit of value added	Carbon footprint
9	9.4.1-2 CO2 emissions from fuel combustion	Carbon footprint
10	10.4.1 Labour share of GDP, comprising wages and social protection transfers	Wages footprint
11	11.6.2-1 Annual mean levels of fine particulate matter (e.g., PM2.5 and PM10) in cities (population weighted)	PM2.5 footprint (air pollutants)
11	11.6.2-2 Annual mean levels of fine particulate matter (e.g., PM2.5 and PM10) in cities (population weighted)	PM10 footprint (air pollutants)
12	12.2.1 Material footprint per capita (SO2 footprint per capita)	SO2 footprint (air pollutants)
12	12.2.1 Material footprint per capita	Material footprint
12	12.2.1 Material footprint per GDP (low material intensity indicates high SDG indicator score)	Material footprint
12	12.2.1 Material footprint per GDP (Nitrogen footprint per GDP)	Nitrogen footprint (total, including NOx, NH3 and N2O emissions to air, and the direct nitrogen emissions to water)
13	13.2.2 Total greenhouse gas emissions per year	GHG footprint (emissions, including CO2, CH4, N2O)
13	13.2.s CO2 emissions intensity of areas under forest management (GtCO2-equivalent per ha)	Carbon footprint
14	14.1.1 Index of coastal eutrophication (Nitrogen footprint per ha of cropland as a proxy)	Nitrogen footprint (nitrogen potentially exportable to water bodies)
14	14.1.1 Index of coastal eutrophication (Phosphorus footprint per ha of cropland as a proxy)	Phosphorus footprint (to water bodies)
14	14.4.1 (Total fisheries production per capita) - Proportion of fish stocks within biologically sustainable levels	Imported fisheries
15	15.1.1 Forest area as a proportion of total land area (high value indicates high SDG indicator score)	Land footprint (forest land)
15	15.2.1 Progress towards sustainable forest management (forest area net change rate as a measure)	Land footprint (forest land)

Table A5.0.4 (cont'd)

16; 5	16.2.2 Number of victims of human trafficking per 100,000 population	Human trafficking
16	16.4.2 Proportion of seized, found or surrendered arms whose illicit origin or context has been traced or established by a competent authority in line with international instruments	Transfers of major conventional weapons
16	16.5 Substantially reduce corruption and bribery in all their forms	Corruption footprint
17	17.3.1 Foreign direct investment as a proportion of gross national income	Foreign direct investment
17	17.3.1 Official development assistance as a proportion of gross national income	Official development assistance

* Detailed data description and data source can be found in Table A5.0.2.

Table A5.0.5. Indicators for TNI impacts and detailed data sources

Indicators of TNI impacts	Source	Source link	References
Carbon footprint	Edgar_v5.0	https://edgar.jrc.ec.europa.eu/overview.php?v=50_GHG	
GHG footprint	Edgar_v5.0	https://edgar.jrc.ec.europa.eu/overview.php?v=50_GHG	
NOx footprint	Edgar_v5.0	https://edgar.jrc.ec.europa.eu/overview.php?v=50_AP	
PM10 footprint	Edgar_v5.0	https://edgar.jrc.ec.europa.eu/overview.php?v=50_AP	
PM2.5 footprint	Edgar_v5.0	https://edgar.jrc.ec.europa.eu/overview.php?v=50_AP	(Liang et al., 2017; Xiao et al., 2018b; Zhang et al., 2017)
SO2 footprint	Edgar_v5.0	https://edgar.jrc.ec.europa.eu/overview.php?v=50_AP	(Zhang et al., 2017)
Water footprint	Aquastat	http://www.fao.org/nr/water/aquastat/data/query/results.html	(Wiedmann and Lenzen, 2018)
Scarce water footprint	AWEAR	http://www.wulca-waterlca.org/aware.html	(Lenzen et al., 2013a)
Energy footprint (total)	IEA	https://stats.oecd.org/BrandedView.aspx?oecd_bv_id=enestats-data-en&doi=data-00510-en	(Chen et al., 2018)
Energy footprint (primary energy)	IEA	https://stats.oecd.org/BrandedView.aspx?oecd_bv_id=enestats-data-en&doi=data-00510-en	(Xu et al., 2020c)
Energy footprint (renewable energy)	IEA	https://stats.oecd.org/BrandedView.aspx?oecd_bv_id=enestats-data-en&doi=data-00510-en	(Xu et al., 2020c)
Land footprint (cropland)	FAOSTAT	http://www.fao.org/faostat/en/#data/RL	(Yu et al., 2013)
Land footprint (forest land)	FAOSTAT	http://www.fao.org/faostat/en/#data/RL	(Yu et al., 2013)
Employment footprint	ILOSTAT	https://ilostat.ilo.org	(Alsamawi et al., 2014)
Wage footprint	ILOSTAT	https://ilostat.ilo.org	(Alsamawi et al., 2014)
Nitrogen footprint - (Total, i.e., NOx, NH3 and N2O emissions to air, and the direct nitrogen emissions to water)	FAO and the International Fertilizer Industry Association (IFA)		(Oita et al., 2016)
Nitrogen footprint (NOx, NH3 and N2O emissions to air)	FAOSTAT	http://www.fao.org/faostat/en/#data/RL	(Oita et al., 2016)

Table A5.0.5 (cont'd)

Nitrogen footprint (nitrogen potentially exportable to water bodies)	FAOSTAT	http://www.fao.org/faostat/en/#data/RL	(Oita et al., 2016)
GINI footprint	World Bank	https://data.worldbank.org/indicator/SI.POV.GINI	(Alsamawi et al., 2014)
Corruption footprint	Corruption perceptions index; CCI; and IPB indices	https://www.transparency.org/research/cpi/overview	(Xiao et al., 2018a)
Occupational Safety and Health footprint (fatal accidents)	ILOSTAT	https://ilostat.ilo.org	(Alsamawi et al., 2017b)
Occupational Safety and Health footprint (non-fatal accidents)	ILOSTAT	https://ilostat.ilo.org	(Alsamawi et al., 2017b)
Material footprint		https://www.resourcepanel.org/global-material-flows-database	(Xu et al., 2019a)
Phosphorus footprint (total)			(Oita et al., 2020)
Phosphorus footprint (to water bodies)			(Oita et al., 2020)
GDP embodied in trade			(Xu et al., 2019a)
Biodiversity footprint			(Marques et al., 2017)
Poverty footprint	Based on employment and salary		(Alsamawi et al., 2014)
International concessional public finance, including official development assistance	OECD	https://data.oecd.org/oda/net-oda.htm	(Sachs et al., 2020)
Foreign direct investment	World Bank	https://data.worldbank.org/	/
Investments in conflict prevention and peacekeeping	Stockholm International Peace Research Institute (SIPRI)	https://www.sipri.org/databases/pko	(Sachs et al., 2020)
Transfers of major conventional weapons	Stockholm International Peace Research Institute (SIPRI)	https://www.sipri.org/databases/armstransfers	(Sachs et al., 2020)

Table A5.0.5 (cont'd)

Human trafficking	The Counter-Trafficking Data Collaborative (CTDC)	https://www.ctdatacollaborative.org/download-global-dataset	
International student flows	UNESCO	http://data.uis.unesco.org/	(C. Hou et al., 2020)
Child Labor footprint	SHDB	http://www.socialhotspot.org/purchase-shdb-licences.html	(Norris and Norris, 2015)
Forced Labor footprint	SHDB	http://www.socialhotspot.org/purchase-shdb-licences.html	(Norris and Norris, 2015)
Exports of hazardous pesticides	FAO	http://www.fao.org/faostat/en/#data/RT/metadata	(Sachs et al., 2020)
Chemical footprint (hazardous pesticides + PM2.5 + PM10)	Edgar_v5.0	https://edgar.jrc.ec.europa.eu/overview.php?v=50_AP	
Imported Cereal production	FAO	http://www.fao.org/faostat/	/
Noncommunicable diseases (NCD) deaths embodied in the meat trade	GHDx	http://ghdx.healthdata.org	(Chung et al., 2021)

Table A5.0.6. Country list with country names, ISO3 country code, and income groups
This large table has been deposited on [GitHub](#).

Table A5.0.7. Countries and their adjacent neighbors (share land or maritime borders)
This large table has been deposited on [GitHub](#).

REFERENCES

REFERENCES

- Adyel, T.M., 2021. Enforce ban on plastic exports or it could backfire. *Nature* 591, 34–34. <https://doi.org/10.1038/d41586-021-00541-x>
- AidData, 2016. AidDataCore_ResearchRelease_Level1_v3. 0 Research Releases Dataset.
- Allan, J.A., 1998. Virtual Water: A Strategic Resource Global Solutions to Regional Deficits. *Groundwater* 36, 545–546. <https://doi.org/10.1111/j.1745-6584.1998.tb02825.x>
- Alsamawi, A., McBain, D., Murray, J., Lenzen, M., Wiebe, K.S., 2017a. A Social Footprint of Nations: A Comparative Study of the Social Impact of Work, in: Alsamawi, A., McBain, D., Murray, J., Lenzen, M., Wiebe, K.S. (Eds.), *The Social Footprints of Global Trade, Environmental Footprints and Eco-Design of Products and Processes*. Springer, Singapore, pp. 35–52. https://doi.org/10.1007/978-981-10-4137-2_6
- Alsamawi, A., Murray, J., Lenzen, M., 2014. The Employment Footprints of Nations. *Journal of Industrial Ecology* 18, 59–70. <https://doi.org/10.1111/jiec.12104>
- Alsamawi, A., Murray, J., Lenzen, M., Reyes, R.C., 2017b. Trade in occupational safety and health: Tracing the embodied human and economic harm in labour along the global supply chain. *Journal of Cleaner Production* 147, 187–196. <https://doi.org/10.1016/j.jclepro.2016.12.110>
- Altieri, A.H., Gedan, K.B., 2015. Climate change and dead zones. *Global Change Biology* 21, 1395–1406. <https://doi.org/10.1111/gcb.12754>
- Anderson, E.W., 2003. *International boundaries: A geopolitical atlas*. Psychology Press, New York.
- Anderson, J.E., 1979. A Theoretical Foundation for the Gravity Equation. *The American Economic Review* 69, 106–116.
- Andrews, E.S., 2009. Guidelines for social life cycle assessment of products: social and socio-economic LCA guidelines complementing environmental LCA and Life Cycle Costing, contributing to the full assessment of goods and services within the context of sustainable development. UNEP/Earthprint.
- Azizi, D., Biermann, F., Kim, R.E., 2019. Policy Integration for Sustainable Development through Multilateral Environmental Agreements: An Empirical Analysis, 2007–2016. *Global Governance: A Review of Multilateralism and International Organizations* 25, 445–475. <https://doi.org/10.1163/19426720-02503005>
- Bagstad, K.J., Johnson, G.W., Voigt, B., Villa, F., 2013. Spatial dynamics of ecosystem service flows: A comprehensive approach to quantifying actual services. *Ecosystem Services*,

- Special Issue on Mapping and Modelling Ecosystem Services 4, 117–125.
<https://doi.org/10.1016/j.ecoser.2012.07.012>
- Barabási, A.-L., 2014. *Linked: How Everything Is Connected to Everything Else and What It Means for Business, Science, and Everyday Life*, Illustrated edition. ed. Basic Books, New York.
- Behrenfeld, M.J., Westberry, T.K., Boss, E.S., O'Malley, R.T., Siegel, D.A., Wiggert, J.D., Franz, B.A., McClain, C.R., Feldman, G.C., Doney, S.C., Moore, J.K., Dall'Olmo, G., Milligan, A.J., Lima, I., Mahowald, N., 2009. Satellite-detected fluorescence reveals global physiology of ocean phytoplankton. *Biogeosciences* 6, 779–794.
<https://doi.org/10.5194/bg-6-779-2009>
- Belgiu, M., Drăguț, L., 2016. Random forest in remote sensing: A review of applications and future directions. *ISPRS Journal of Photogrammetry and Remote Sensing* 114, 24–31.
<https://doi.org/10.1016/j.isprsjprs.2016.01.011>
- Belhabib, D., Le Billon, P., 2018. Tax havens are the tip of the iceberg. *Nature Ecology & Evolution* 2, 1679–1679. <https://doi.org/10.1038/s41559-018-0704-2>
- Béraud-Sudreau, L., Lopes da Silva, D., Kuimova, A., Wezeman, P.D., 2020a. Emerging Suppliers in the Global Arms Trade.
- Béraud-Sudreau, L., Marksteiner, A., Lopes da Silva, D., Tian, N., Kuimova, A., Wezeman, P.D., Wezeman, S.T., 2020b. Mapping the International Presence of the World's Largest Arms Companies.
- Berfin Karakoc, D., Konar, M., 2021. A complex network framework for the efficiency and resilience trade-off in global food trade. *Environ. Res. Lett.* <https://doi.org/10.1088/1748-9326/ac1a9b>
- Best, J., 2019. Anthropogenic stresses on the world's big rivers. *Nature Geoscience* 12, 7–21.
<https://doi.org/10.1038/s41561-018-0262-x>
- Bieger, K., Arnold, J.G., Rathjens, H., White, M.J., Bosch, D.D., Allen, P.M., Volk, M., Srinivasan, R., 2017. Introduction to SWAT+, A Completely Restructured Version of the Soil and Water Assessment Tool. *JAWRA Journal of the American Water Resources Association* 53, 115–130. <https://doi.org/10.1111/1752-1688.12482>
- Biermann, F., 2020. World Environment Organization, in: *Essential Concepts of Global Environmental Governance*. Routledge.
- Boero, R., Edwards, B.K., Rivera, M.K., 2018. Regional input–output tables and trade flows: an integrated and interregional non-survey approach. *Regional Studies* 52, 225–238.
<https://doi.org/10.1080/00343404.2017.1286009>
- Boisso, D., Ferrantino, M., 1997. Economic Distance, Cultural Distance, and Openness in International Trade: Empirical Puzzles. *Journal of Economic Integration* 12, 456–484.

- Breiman, L., 2001. Random forests. *Machine learning* 45, 5–32.
- Breitburg, D., Levin, L.A., Oschlies, A., Grégoire, M., Chavez, F.P., Conley, D.J., Garçon, V., Gilbert, D., Gutiérrez, D., Isensee, K., Jacinto, G.S., Limburg, K.E., Montes, I., Naqvi, S.W.A., Pitcher, G.C., Rabalais, N.N., Roman, M.R., Rose, K.A., Seibel, B.A., Telszewski, M., Yasuhara, M., Zhang, J., 2018. Declining oxygen in the global ocean and coastal waters. *Science* 359, eaam7240. <https://doi.org/10.1126/science.aam7240>
- Brücker, H., Capuano, S., Marfouk, A., 2013. Education, gender and international migration: insights from a panel-dataset 1980-2010. mimeo.
- Bruckner, M., Wood, R., Moran, D., Kuschnig, N., Wieland, H., Maus, V., Börner, J., 2019. FABIO — The Construction of the Food and Agriculture Biomass Input–Output Model. *Environ. Sci. Technol.* <https://doi.org/10.1021/acs.est.9b03554>
- Burke, M., Driscoll, A., Lobell, D.B., Ermon, S., 2021. Using satellite imagery to understand and promote sustainable development. *Science* 371. <https://doi.org/10.1126/science.abe8628>
- Byrnes, D.K., Van Meter, K.J., Basu, N.B., 2020. Long-Term Shifts in U.S. Nitrogen Sources and Sinks Revealed by the New TREND-Nitrogen Data Set (1930–2017). *Global Biogeochemical Cycles* 34, e2020GB006626. <https://doi.org/10.1029/2020GB006626>
- Campbell, L.G., Thrash, J.C., Rabalais, N.N., Mason, O.U., 2019. Extent of the annual Gulf of Mexico hypoxic zone influences microbial community structure. *PLOS ONE* 14, e0209055. <https://doi.org/10.1371/journal.pone.0209055>
- Cao, P., Lu, C., Yu, Z., 2018. Historical nitrogen fertilizer use in agricultural ecosystems of the contiguous United States during 1850–2015: application rate, timing, and fertilizer types. *Earth System Science Data* 10, 969–984. <https://doi.org/10.5194/essd-10-969-2018>
- Carlson, A.K., Young, T., Centeno, M.A., Levin, S.A., Rubenstein, D.I., 2021. Boat to bowl: Resilience through network rewiring of a community-supported fishery amid the COVID-19 pandemic. *Environ. Res. Lett.* <https://doi.org/10.1088/1748-9326/abe4f6>
- Carstensen, J., Andersen, J.H., Gustafsson, B.G., Conley, D.J., 2014. Deoxygenation of the Baltic Sea during the last century. *PNAS* 111, 13231–13236. <https://doi.org/10.1073/pnas.1323156111>
- Chang, S., Pierson, E., Koh, P.W., Gerardin, J., Redbird, B., Grusky, D., Leskovec, J., 2020. Mobility network models of COVID-19 explain inequities and inform reopening. *Nature* 1–8. <https://doi.org/10.1038/s41586-020-2923-3>
- Charney, J.I., Alexander, L.M., Smith, R.W., Colson, D.A., Lathrop, C.G., 1993. International maritime boundaries. M. Nijhoff, Dordrecht; Boston.
- Chen, B., Li, J.S., Wu, X.F., Han, M.Y., Zeng, L., Li, Z., Chen, G.Q., 2018. Global energy flows embodied in international trade: A combination of environmentally extended input–

- output analysis and complex network analysis. *Applied Energy* 210, 98–107. <https://doi.org/10.1016/j.apenergy.2017.10.113>
- Chen, C.-C., Gong, G.-C., Shiah, F.-K., 2007. Hypoxia in the East China Sea: One of the largest coastal low-oxygen areas in the world. *Marine Environmental Research* 64, 399–408. <https://doi.org/10.1016/j.marenvres.2007.01.007>
- Chen, Jianyu, Ni, X., Liu, M., Chen, Jianfang, Mao, Z., Jin, H., Pan, D., 2014. Monitoring the occurrence of seasonal low-oxygen events off the Changjiang Estuary through integration of remote sensing, buoy observations, and modeling. *Journal of Geophysical Research: Oceans* 119, 5311–5322. <https://doi.org/10.1002/2014JC010333>
- Chen, S., Hu, C., Barnes, B.B., Xie, Y., Lin, G., Qiu, Z., 2019. Improving ocean color data coverage through machine learning. *Remote Sensing of Environment* 222, 286–302. <https://doi.org/10.1016/j.rse.2018.12.023>
- Chen, X., Frank, K.A., Dietz, T., Liu, J., 2012. Weak Ties, Labor Migration, and Environmental Impacts: Toward a Sociology of Sustainability. *Organization & Environment* 25, 3–24. <https://doi.org/10.1177/1086026611436216>
- Chiarelli, D.D., D’Odorico, P., Müller, M.F., Mueller, N.D., Davis, K.F., Dell’Angelo, J., Penny, G., Rulli, M.C., 2022. Competition for water induced by transnational land acquisitions for agriculture. *Nat Commun* 13, 505. <https://doi.org/10.1038/s41467-022-28077-2>
- Chung, M.G., Li, Y., Liu, J., 2021. Global red and processed meat trade and non-communicable diseases. *BMJ Global Health* 6, e006394. <https://doi.org/10.1136/bmjgh-2021-006394>
- Chung, M.G., Liu, J., 2022. International food trade benefits biodiversity and food security in low-income countries. *Nat Food* 1–7. <https://doi.org/10.1038/s43016-022-00499-7>
- Coley, D., Howard, M., Winter, M., 2009. Local food, food miles and carbon emissions: A comparison of farm shop and mass distribution approaches. *Food Policy* 34, 150–155. <https://doi.org/10.1016/j.foodpol.2008.11.001>
- Conley, D.J., Carstensen, J., Aigars, J., Axe, P., Bonsdorff, E., Eremina, T., Haahti, B.-M., Humborg, C., Jonsson, P., Kotta, J., Lännegren, C., Larsson, U., Maximov, A., Medina, M.R., Lysiak-Pastuszek, E., Remeikaitė-Nikienė, N., Walve, J., Wilhelms, S., Zillén, L., 2011. Hypoxia Is Increasing in the Coastal Zone of the Baltic Sea. *Environ. Sci. Technol.* 45, 6777–6783. <https://doi.org/10.1021/es201212r>
- Crawford, R.H., Bontinck, P.-A., Stephan, A., Wiedmann, T., Yu, M., 2018. Hybrid life cycle inventory methods – A review. *Journal of Cleaner Production* 172, 1273–1288. <https://doi.org/10.1016/j.jclepro.2017.10.176>
- Csardi, G., Nepusz, T., 2006. The igraph software package for complex network research. *InterJournal Complex Systems*, 1695.

- Cucurachi, S., Scherer, L., Guinée, J., Tukker, A., 2019. Life Cycle Assessment of Food Systems. *One Earth* 1, 292–297. <https://doi.org/10.1016/j.oneear.2019.10.014>
- Cummings, J.A., Smedstad, O.M., 2013. Variational data assimilation for the global ocean, in: *Data Assimilation for Atmospheric, Oceanic and Hydrologic Applications (Vol. II)*. Springer, pp. 303–343.
- Custer, S., Dreher, A., Elston, T.-B., Fuchs, A., Ghose, S., Lin, J., Malik, A., Parks, B.C., Russell, B., Solomon, K., 2021. Tracking Chinese Development Finance: An Application of AidData’s TUFF 2.0 Methodology. Williamsburg, VA: AidData at William & Mary.
- Dagg, M.J., Breed, G.A., 2003. Biological effects of Mississippi River nitrogen on the northern gulf of Mexico—a review and synthesis. *Journal of Marine Systems* 43, 133–152. <https://doi.org/10.1016/j.jmarsys.2003.09.002>
- Dalin, C., Hanasaki, N., Qiu, H., Mauzerall, D.L., Rodriguez-Iturbe, I., 2014. Water resources transfers through Chinese interprovincial and foreign food trade. *PNAS* 111, 9774–9779. <https://doi.org/10.1073/pnas.1404749111>
- Dalin, C., Wada, Y., Kastner, T., Puma, M.J., 2017. Groundwater depletion embedded in international food trade. *Nature* 543, 700–704. <https://doi.org/10.1038/nature21403>
- De Stefano, L., Petersen-Perlman, J.D., Sproles, E.A., Eynard, J., Wolf, A.T., 2017. Assessment of transboundary river basins for potential hydro-political tensions. *Global Environmental Change* 45, 35–46. <https://doi.org/10.1016/j.gloenvcha.2017.04.008>
- Del Giudice, D., Matli, V.R.R., Obenour, D.R., 2020. Bayesian mechanistic modeling characterizes Gulf of Mexico hypoxia: 1968–2016 and future scenarios. *Ecological Applications* 30, e02032. <https://doi.org/10.1002/eap.2032>
- Demeke, A., 2016. Cyanobacteria blooms and biological control Methods. *Int. J. Fauna Boil. Stud* 3, 32–38.
- Diaz, R.J., Rosenberg, R., 2008. Spreading Dead Zones and Consequences for Marine Ecosystems. *Science* 321, 926–929. <https://doi.org/10.1126/science.1156401>
- Diffenbaugh, N.S., Field, C.B., Appel, E.A., Azevedo, I.L., Baldocchi, D.D., Burke, M., Burney, J.A., Ciais, P., Davis, S.J., Fiore, A.M., Fletcher, S.M., Hertel, T.W., Horton, D.E., Hsiang, S.M., Jackson, R.B., Jin, X., Levi, M., Lobell, D.B., McKinley, G.A., Moore, F.C., Montgomery, A., Nadeau, K.C., Pataki, D.E., Randerson, J.T., Reichstein, M., Schnell, J.L., Seneviratne, S.I., Singh, D., Steiner, A.L., Wong-Parodi, G., 2020. The COVID-19 lockdowns: a window into the Earth System. *Nature Reviews Earth & Environment* 1–12. <https://doi.org/10.1038/s43017-020-0079-1>
- DiLorenzo, M., Ghose, S., Turner, J., 2017. Estimating Baseline Aid to the Sustainable Development Goals. AidData at William & Mary, Williamsburg, VA.

- Domínguez-Tejo, E., Metternicht, G., Johnston, E., Hedge, L., 2016. Marine Spatial Planning advancing the Ecosystem-Based Approach to coastal zone management: A review. *Marine Policy* 72, 115–130. <https://doi.org/10.1016/j.marpol.2016.06.023>
- Dorninger, C., Hornborg, A., Abson, D.J., von Wehrden, H., Schaffartzik, A., Giljum, S., Engler, J.-O., Feller, R.L., Hubacek, K., Wieland, H., 2021. Global patterns of ecologically unequal exchange: Implications for sustainability in the 21st century. *Ecological Economics* 179, 106824. <https://doi.org/10.1016/j.ecolecon.2020.106824>
- Dou, Y., da Silva, R.F.B., Yang, H., Liu, J., 2018. Spillover effect offsets the conservation effort in the Amazon. *J. Geogr. Sci.* 28, 1715–1732. <https://doi.org/10.1007/s11442-018-1539-0>
- Dou, Y., Millington, J.D.A., Silva, R.F.B.D., McCord, P., Viña, A., Song, Q., Yu, Q., Wu, W., Batistella, M., Moran, E., Liu, J., 2019. Land-use changes across distant places: design of a telecoupled agent-based model. *Journal of Land Use Science* 14, 191–209. <https://doi.org/10.1080/1747423X.2019.1687769>
- Dou, Y., Yao, G., Herzberger, A., da Silva, R.F.B., Song, Q., Hovis, C., Batistella, M., Moran, E., Wu, W., Liu, J., 2020. Land-Use Changes in Distant Places: Implementation of a Telecoupled Agent-Based Model. *JASSS* 23, 11.
- Eakin, H., DeFries, R., Kerr, S., Lambin, E.F., Liu, J., Marcotullio, P.J., Messerli, P., Reenberg, A., Rueda, X., Swaffield, S.R., 2014. Significance of telecoupling for exploration of land-use change, in: *Rethinking Global Land Use in an Urban Era*. MIT Press, pp. 141–161.
- El-habashi, A., Ioannou, I., Tomlinson, M.C., Stumpf, R.P., Ahmed, S., 2016. Satellite Retrievals of *Karenia brevis* Harmful Algal Blooms in the West Florida Shelf Using Neural Networks and Comparisons with Other Techniques. *Remote Sensing* 8, 377. <https://doi.org/10.3390/rs8050377>
- Ermgassen, E.K.H.J. zu, Godar, J., Lathuillière, M.J., Löfgren, P., Gardner, T., Vasconcelos, A., Meyfroidt, P., 2020. The origin, supply chain, and deforestation risk of Brazil's beef exports. *PNAS* 117, 31770–31779. <https://doi.org/10.1073/pnas.2003270117>
- Falcone, J.A., 2021. Estimates of county-level nitrogen and phosphorus from fertilizer and manure from 1950 through 2017 in the conterminous United States (Report No. 2020–1153), Open-File Report. Reston, VA. <https://doi.org/10.3133/ofr20201153>
- Falkendal, T., Otto, C., Schewe, J., Jägermeyr, J., Konar, M., Kummu, M., Watkins, B., Puma, M.J., 2021. Grain export restrictions during COVID-19 risk food insecurity in many low- and middle-income countries. *Nature Food* 2, 11–14. <https://doi.org/10.1038/s43016-020-00211-7>
- Fang, B., Tan, Y., Li, C., Cao, Y., Liu, J., Schweizer, P.-J., Shi, H., Zhou, B., Chen, H., Hu, Z., 2016. Energy sustainability under the framework of telecoupling. *Energy* 106, 253–259. <https://doi.org/10.1016/j.energy.2016.03.055>

- Fang, K., Heijungs, R., de Snoo, G.R., 2014. Theoretical exploration for the combination of the ecological, energy, carbon, and water footprints: Overview of a footprint family. *Ecological Indicators* 36, 508–518. <https://doi.org/10.1016/j.ecolind.2013.08.017>
- Feng, K., Davis, S.J., Sun, L., Li, X., Guan, D., Liu, W., Liu, Z., Hubacek, K., 2013. Outsourcing CO₂ within china. *Proceedings of the National Academy of Sciences* 110, 11654–11659.
- Fennel, K., Laurent, A., Hetland, R., Justić, D., Ko, D.S., Lehrter, J., Murrell, M., Wang, L., Yu, L., Zhang, W., 2016. Effects of model physics on hypoxia simulations for the northern Gulf of Mexico: A model intercomparison. *Journal of Geophysical Research: Oceans* 121, 5731–5750. <https://doi.org/10.1002/2015JC011577>
- Fennel, K., Testa, J.M., 2019. Biogeochemical Controls on Coastal Hypoxia. *Annual Review of Marine Science* 11, 105–130. <https://doi.org/10.1146/annurev-marine-010318-095138>
- Fischer, G., Huang, J., Keyzer, M., Qiu, H., Sun, L., van Veen, W., 2007. China’s agricultural prospects and challenges: Report on scenario simulations until 2030 with the Chinagro welfare model covering national, regional and county level.
- Fisher, B., Turner, R.K., Morling, P., 2009. Defining and classifying ecosystem services for decision making. *Ecological Economics* 68, 643–653. <https://doi.org/10.1016/j.ecolecon.2008.09.014>
- Fishman, T., Graedel, T.E., 2019. Impact of the establishment of US offshore wind power on neodymium flows. *Nat Sustain* 2, 332–338. <https://doi.org/10.1038/s41893-019-0252-z>
- Forrest, D.R., Hetland, R.D., DiMarco, S.F., 2011. Multivariable statistical regression models of the areal extent of hypoxia over the Texas–Louisiana continental shelf. *Environ. Res. Lett.* 6, 045002. <https://doi.org/10.1088/1748-9326/6/4/045002>
- Galaz, V., Crona, B., Dauriach, A., Jouffray, J.-B., Österblom, H., Fichtner, J., 2018. Tax havens and global environmental degradation. *Nature Ecology & Evolution* 2, 1352–1357. <https://doi.org/10.1038/s41559-018-0497-3>
- Galli, A., Wiedmann, T., Ercin, E., Knoblauch, D., Ewing, B., Giljum, S., 2012. Integrating Ecological, Carbon and Water footprint into a “Footprint Family” of indicators: Definition and role in tracking human pressure on the planet. *Ecological Indicators, The State of the Art in Ecological Footprint: Theory and Applications* 16, 100–112. <https://doi.org/10.1016/j.ecolind.2011.06.017>
- Galloway, J.N., Burke, M., Bradford, G.E., Naylor, R., Falcon, W., Chapagain, A.K., Gaskell, J.C., McCullough, E., Mooney, H.A., Oleson, K.L.L., Steinfeld, H., Wassenaar, T., Smil, V., 2007. International Trade in Meat: The Tip of the Pork Chop. *ambi* 36, 622–629. [https://doi.org/10.1579/0044-7447\(2007\)36\[622:ITIMTT\]2.0.CO;2](https://doi.org/10.1579/0044-7447(2007)36[622:ITIMTT]2.0.CO;2)
- GEBCO, 2019. The GEBCO_2019 grid—A continuous terrain model of the global oceans and land. Liverpool, UK, British Oceanographic Data Centre, National Oceanography Centre, NERC.

- Godar, J., Persson, U.M., Tizado, E.J., Meyfroidt, P., 2015. Towards more accurate and policy relevant footprint analyses: Tracing fine-scale socio-environmental impacts of production to consumption. *Ecological Economics* 112, 25–35. <https://doi.org/10.1016/j.ecolecon.2015.02.003>
- Gorelick, N., Hancher, M., Dixon, M., Ilyushchenko, S., Thau, D., Moore, R., 2017. Google Earth Engine: Planetary-scale geospatial analysis for everyone. *Remote Sensing of Environment, Big Remotely Sensed Data: tools, applications and experiences* 202, 18–27. <https://doi.org/10.1016/j.rse.2017.06.031>
- Grantz, K.H., Meredith, H.R., Cummings, D.A.T., Metcalf, C.J.E., Grenfell, B.T., Giles, J.R., Mehta, S., Solomon, S., Labrique, A., Kishore, N., Buckee, C.O., Wesolowski, A., 2020. The use of mobile phone data to inform analysis of COVID-19 pandemic epidemiology. *Nature Communications* 11, 4961. <https://doi.org/10.1038/s41467-020-18190-5>
- Green, J.M.H., Croft, S.A., Durán, A.P., Balmford, A.P., Burgess, N.D., Fick, S., Gardner, T.A., Godar, J., Suavet, C., Virah-Sawmy, M., Young, L.E., West, C.D., 2019. Linking global drivers of agricultural trade to on-the-ground impacts on biodiversity. *PNAS* 116, 23202–23208. <https://doi.org/10.1073/pnas.1905618116>
- Greene, R.M., Lehrter, J.C., Iii, J.D.H., 2009. Multiple regression models for hindcasting and forecasting midsummer hypoxia in the Gulf of Mexico. *Ecological Applications* 19, 1161–1175. <https://doi.org/10.1890/08-0035.1>
- Gronberg, J.M., Arnold, T., 2017. County-level estimates of nitrogen and phosphorus from animal manure for the conterminous United States, 2007 and 2012 (USGS Numbered Series No. 2017–1021), County-level estimates of nitrogen and phosphorus from animal manure for the conterminous United States, 2007 and 2012, Open-File Report. U.S. Geological Survey, Reston, VA. <https://doi.org/10.3133/ofr20171021>
- Guan, D., Wang, D., Hallegatte, S., Davis, S.J., Huo, J., Li, S., Bai, Y., Lei, T., Xue, Q., Coffman, D., Cheng, D., Chen, P., Liang, X., Xu, B., Lu, X., Wang, S., Hubacek, K., Gong, P., 2020. Global supply-chain effects of COVID-19 control measures. *Nature Human Behaviour* 1–11. <https://doi.org/10.1038/s41562-020-0896-8>
- Guinée, J.B., Heijungs, R., Huppes, G., Zamagni, A., Masoni, P., Buonamici, R., Ekvall, T., Rydberg, T., 2011. Life Cycle Assessment: Past, Present, and Future. *Environ. Sci. Technol.* 45, 90–96. <https://doi.org/10.1021/es101316v>
- Havlík, P., Valin, H., Mosnier, A., Frank, S., Lauri, P., Leclère, D., Palazzo, A., Batka, M., Boere, E., Brouwer, A., Deppermann, A., Ermolieva, T., Forsell, N., Fulvio, F. di, Obersteiner, M., 2018. GLOBIOM documentation.
- Herzberger, A., Chung, M.G., Kapsar, K., Frank, K.A., Liu, J., 2019. Telecoupled Food Trade Affects Pericoupled Trade and Intracoupled Production. *Sustainability* 11, 2908. <https://doi.org/10.3390/su11102908>

- Ho, J.C., Michalak, A.M., Pahlevan, N., 2019. Widespread global increase in intense lake phytoplankton blooms since the 1980s. *Nature* 1–17. <https://doi.org/10.1038/s41586-019-1648-7>
- Hoekstra, A.Y., 2017. Water Footprint Assessment: Evolvement of a New Research Field. *Water Resour Manage* 31, 3061–3081. <https://doi.org/10.1007/s11269-017-1618-5>
- Hoekstra, A.Y., Chapagain, A.K., van Oel, P.R., 2019. Progress in Water Footprint Assessment: Towards Collective Action in Water Governance. *Water* 11, 1070. <https://doi.org/10.3390/w11051070>
- Hoekstra, A.Y., Hung, P.Q., 2005. Globalisation of water resources: international virtual water flows in relation to crop trade. *Global Environmental Change* 15, 45–56. <https://doi.org/10.1016/j.gloenvcha.2004.06.004>
- Hoekstra, A.Y., Wiedmann, T., 2014. Humanity’s unsustainable environmental footprint. *Science* 344, 1114–1117. <https://doi.org/10.1126/science.1248365>
- Hofstede, G.H., 2001. *Culture’s Consequences: Comparing Values, Behaviors, Institutions and Organizations Across Nations*. SAGE.
- Hou, C., DU, D., Liu, C., Gui, Q., Liu, S., Qin, X., 2020. Spatio-temporal evolution and factors influencing international student mobility networks in the world. *ACTA GEOGRAPHICA SINICA* 75, 681–694. <https://doi.org/10.11821/dlxb202004002>
- Hou, Y., Ding, S., Chen, W., Li, B., Burkhard, B., Bicking, S., Müller, F., 2020. Ecosystem service potential, flow, demand and their spatial associations: a comparison of the nutrient retention service between a human- and a nature-dominated watershed. *Science of The Total Environment* 748, 141341. <https://doi.org/10.1016/j.scitotenv.2020.141341>
- Hu, C., 2009. A novel ocean color index to detect floating algae in the global oceans. *Remote Sensing of Environment* 113, 2118–2129. <https://doi.org/10.1016/j.rse.2009.05.012>
- Huang, R., Zhu, J., 2013. Using Random Forest to integrate lidar data and hyperspectral imagery for land cover classification, in: *2013 IEEE International Geoscience and Remote Sensing Symposium - IGARSS*. pp. 3978–3981. <https://doi.org/10.1109/IGARSS.2013.6723704>
- Hulina, J., Bocetti, C., Iii, H.C., Hull, V., Yang, W., Liu, J., 2017. Telecoupling framework for research on migratory species in the Anthropocene. *Elem Sci Anth* 5. <https://doi.org/10.1525/elementa.184>
- Hull, V., Liu, J., 2018. Telecoupling: A new frontier for global sustainability. *Ecology and Society* 23. <https://doi.org/10.5751/ES-10494-230441>
- Hull, V., Tuanmu, M.-N., Liu, J., 2015. Synthesis of human-nature feedbacks. *Ecology and Society* 20. <https://doi.org/10.5751/ES-07404-200317>

- Hutengs, C., Vohland, M., 2016. Downscaling land surface temperatures at regional scales with random forest regression. *Remote Sensing of Environment* 178, 127–141. <https://doi.org/10.1016/j.rse.2016.03.006>
- Hwang, H.-L., Lim, H., Chin, S.-M., Uddin, M., Biehl, A., Xie, F., Hargrove, S., Liu, Y., Wang, R., 2021. Freight Analysis Framework Version 5 (FAF5) Base Year 2017 Data Development Technical Report. Oak Ridge National Lab.(ORNL), Oak Ridge, TN (United States).
- IOC-UNESCO, U.N.E., UNEP, U., 2016. Transboundary Waters Assessment Programme (TWAP) Vol. 4: Large Marine Ecosystems: Status and trends - Summary for Policy Makers.
- IPBES, 2019. Global assessment report on biodiversity and ecosystem services of the Intergovernmental Science-Policy Platform on Biodiversity and Ecosystem Services. Zenodo. <https://doi.org/10.5281/zenodo.3831674>
- ISO, I., 2006. ISO 14040 international standard. Environmental Management-Life Cycle Assessment-Principles and Framework. International Organisation for Standardization.
- Jane, S.F., Hansen, G.J.A., Kraemer, B.M., Leavitt, P.R., Mincer, J.L., North, R.L., Pilla, R.M., Stetler, J.T., Williamson, C.E., Woolway, R.I., Arvola, L., Chandra, S., DeGasperi, C.L., Diemer, L., Dunalska, J., Erina, O., Flaim, G., Grossart, H.-P., Hambright, K.D., Hein, C., Hejzlar, J., Janus, L.L., Jenny, J.-P., Jones, J.R., Knoll, L.B., Leoni, B., Mackay, E., Matsuzaki, S.-I.S., McBride, C., Müller-Navarra, D.C., Paterson, A.M., Pierson, D., Rogora, M., Rusak, J.A., Sadro, S., Saulnier-Talbot, E., Schmid, M., Sommaruga, R., Thiery, W., Verburg, P., Weathers, K.C., Weyhenmeyer, G.A., Yokota, K., Rose, K.C., 2021. Widespread deoxygenation of temperate lakes. *Nature* 594, 66–70. <https://doi.org/10.1038/s41586-021-03550-y>
- Jorgenson, A.K., 2016. The sociology of ecologically unequal exchange, foreign investment dependence and environmental load displacement: summary of the literature and implications for sustainability. *Journal of Political Ecology* 23. <https://doi.org/10.2458/v23i1.20221>
- Jorgenson, A.K., 2012. The sociology of ecologically unequal exchange and carbon dioxide emissions, 1960–2005. *Social Science Research* 41, 242–252. <https://doi.org/10.1016/j.ssresearch.2011.11.011>
- Justić, D., Rabalais, N.N., Eugene Turner, R., Wiseman, W.J., 1993. Seasonal coupling between riverborne nutrients, net productivity and hypoxia. *Marine Pollution Bulletin* 26, 184–189. [https://doi.org/10.1016/0025-326X\(93\)90620-Y](https://doi.org/10.1016/0025-326X(93)90620-Y)
- Kabir, M., Salim, R., Al-Mawali, N., 2017. The gravity model and trade flows: Recent developments in econometric modeling and empirical evidence. *Economic Analysis and Policy* 56, 60–71. <https://doi.org/10.1016/j.eap.2017.08.005>

- Kang, Y., Gao, S., Liang, Y., Li, M., Rao, J., Kruse, J., 2020. Multiscale dynamic human mobility flow dataset in the U.S. during the COVID-19 epidemic. *Scientific Data* 7, 390. <https://doi.org/10.1038/s41597-020-00734-5>
- Kanie, N., 2018. Governance with multilateral environmental agreements: a healthy or ill-equipped fragmentation?, in: *Green Planet Blues: Critical Perspectives on Global Environmental Politics*. Taylor and Francis, pp. 137–153.
- Kapsar, K.E., Hovis, C.L., Bicudo da Silva, R.F., Buchholtz, E.K., Carlson, A.K., Dou, Y., Du, Y., Furumo, P.R., Li, Y., Torres, A., Yang, D., Wan, H.Y., Zaehring, J.G., Liu, J., 2019. Telecoupling Research: The First Five Years. *Sustainability* 11, 1033. <https://doi.org/10.3390/su11041033>
- Karakoc, D.B., Wang, J., Konar, M., 2022. Food flows between counties in the United States from 2007 to 2017. *Environ. Res. Lett.* 17, 034035. <https://doi.org/10.1088/1748-9326/ac5270>
- Kepaptsoglou, K., Karlaftis, M.G., Tsamboulas, D., 2010. The Gravity Model Specification for Modeling International Trade Flows and Free Trade Agreement Effects: A 10-Year Review of Empirical Studies. *The Open Economics Journal* 3.
- Kim, R.E., Bosselmann, K., 2013. International Environmental Law in the Anthropocene: Towards a Purposive System of Multilateral Environmental Agreements. *Transnational Environmental Law* 2, 285–309. <https://doi.org/10.1017/S2047102513000149>
- Kim, Y.H., Son, S., Kim, H.-C., Kim, B., Park, Y.-G., Nam, J., Ryu, J., 2020. Application of satellite remote sensing in monitoring dissolved oxygen variabilities: A case study for coastal waters in Korea. *Environment International* 134, 105301. <https://doi.org/10.1016/j.envint.2019.105301>
- Kinnunen, P., Guillaume, J.H.A., Taka, M., D’Odorico, P., Siebert, S., Puma, M.J., Jalava, M., Kumm, M., 2020. Local food crop production can fulfil demand for less than one-third of the population. *Nature Food* 1, 229–237. <https://doi.org/10.1038/s43016-020-0060-7>
- Klapper, J., Schröter, M., 2021. Interregional flows of multiple ecosystem services through global trade in wild species. *Ecosystem Services* 50, 101316. <https://doi.org/10.1016/j.ecoser.2021.101316>
- Kleemann, J., Schröter, M., Bagstad, K.J., Kuhlicke, C., Kastner, T., Fridman, D., Schulp, C.J.E., Wolff, S., Martínez-López, J., Koellner, T., Arnhold, S., Martín-López, B., Marques, A., Lopez-Hoffman, L., Liu, J., Kissinger, M., Guerra, C.A., Bonn, A., 2020. Quantifying interregional flows of multiple ecosystem services – A case study for Germany. *Global Environmental Change* 61, 102051. <https://doi.org/10.1016/j.gloenvcha.2020.102051>
- Klemas, V., 2011. Remote Sensing of Algal Blooms: An Overview with Case Studies. *Journal of Coastal Research* 34–43. <https://doi.org/10.2112/JCOASTRES-D-11-00051.1>

- Koellner, T., Bonn, A., Arnhold, S., Bagstad, K.J., Fridman, D., Guerra, C.A., Kastner, T., Kissinger, M., Kleemann, J., Kuhlicke, C., Liu, J., López-Hoffman, L., Marques, A., Martín-López, B., Schulp, C.J.E., Wolff, S., Schröter, M., 2019. Guidance for assessing interregional ecosystem service flows. *Ecological Indicators* 105, 92–106. <https://doi.org/10.1016/j.ecolind.2019.04.046>
- Land Matrix, 2022. Land Matrix [WWW Document]. URL <https://landmatrix.org/> (accessed 7.15.22).
- Lassaletta, L., Billen, G., Grizzetti, B., Anglade, J., Garnier, J., 2014a. 50 year trends in nitrogen use efficiency of world cropping systems: the relationship between yield and nitrogen input to cropland. *Environ. Res. Lett.* 9, 105011. <https://doi.org/10.1088/1748-9326/9/10/105011>
- Lassaletta, L., Billen, G., Grizzetti, B., Garnier, J., Leach, A.M., Galloway, J.N., 2014b. Food and feed trade as a driver in the global nitrogen cycle: 50-year trends. *Biogeochemistry* 118, 225–241. <https://doi.org/10.1007/s10533-013-9923-4>
- Le, C., Lehrter, J.C., Hu, C., Murrell, M.C., Qi, L., 2014. Spatiotemporal chlorophyll-a dynamics on the Louisiana continental shelf derived from a dual satellite imagery algorithm. *Journal of Geophysical Research: Oceans* 119, 7449–7462. <https://doi.org/10.1002/2014JC010084>
- Le, C., Lehrter, J.C., Hu, C., Obenour, D.R., 2016. Satellite-based empirical models linking river plume dynamics with hypoxic area and volume. *Geophysical Research Letters* 43, 2693–2699. <https://doi.org/10.1002/2015GL067521>
- Leach, A.M., Galloway, J.N., Bleeker, A., Erisman, J.W., Kohn, R.A., Kitzes, J., 2012. A nitrogen footprint model to help consumers understand their role in nitrogen losses to the environment. *Environmental development* 1, 40–66. <https://doi.org/10.1016/j.envdev.2011.12.005>
- Leming, T.D., Stuntz, W.E., 1984. Zones of coastal hypoxia revealed by satellite scanning have implications for strategic fishing. *Nature* 310, 136–138. <https://doi.org/10.1038/310136a0>
- Lenzen, M., Kanemoto, K., Moran, D., Geschke, A., 2011. The Eora global multi-region input-output tables. ISA, Univ. Sydney, Australia <http://www.worldmrio.com>.
- Lenzen, M., Moran, D., Bhaduri, A., Kanemoto, K., Bekchanov, M., Geschke, A., Foran, B., 2013a. International trade of scarce water. *Ecological Economics* 94, 78–85. <https://doi.org/10.1016/j.ecolecon.2013.06.018>
- Lenzen, M., Moran, D., Kanemoto, K., Foran, B., Lobefaro, L., Geschke, A., 2012. International trade drives biodiversity threats in developing nations. *Nature* 486, 109–112. <https://doi.org/10.1038/nature11145>

- Lenzen, M., Moran, D., Kanemoto, K., Geschke, A., 2013b. Building Eora: A Global Multi-Region Input–Output Database at High Country and Sector Resolution. *Economic Systems Research* 25, 20–49. <https://doi.org/10.1080/09535314.2013.769938>
- Li, J., Peng, K., Wang, P., Zhang, N., Feng, K., Guan, D., Meng, J., Wei, W., Yang, Q., 2020. Critical Rare-Earth Elements Mismatch Global Wind-Power Ambitions. *One Earth* 3, 116–125. <https://doi.org/10.1016/j.oneear.2020.06.009>
- Li, L., Franklin, M., Girguis, M., Lurmann, F., Wu, J., Pavlovic, N., Breton, C., Gilliland, F., Habre, R., 2020. Spatiotemporal imputation of MAIAC AOD using deep learning with downscaling. *Remote Sensing of Environment* 237, 111584. <https://doi.org/10.1016/j.rse.2019.111584>
- Li, M., Jia, N., Lenzen, M., Malik, A., Wei, L., Jin, Y., Raubenheimer, D., 2022. Global food-miles account for nearly 20% of total food-systems emissions. *Nat Food* 1–9. <https://doi.org/10.1038/s43016-022-00531-w>
- Li, Y., 2021. International socio-environmental spillover effects on achieving the national SDGs. IIASA, Laxenburg, Austria.
- Li, Y., Robinson, S., Nguyen, L., Liu, J., in review. Satellite prediction of coastal hypoxia in the northern Gulf of Mexico. in review.
- Li, Y., Zhang, Y., Tiffany, L.A., Chen, R., Cai, M., Liu, J., 2021. Synthesizing social and environmental sensing to monitor the impact of large-scale infrastructure development. *Environmental Science & Policy* 124, 527–540. <https://doi.org/10.1016/j.envsci.2021.07.020>
- Liang, S., Stylianou, K.S., Jolliet, O., Supekar, S., Qu, S., Skerlos, S.J., Xu, M., 2017. Consumption-based human health impacts of primary PM_{2.5}: The hidden burden of international trade. *Journal of Cleaner Production* 167, 133–139. <https://doi.org/10.1016/j.jclepro.2017.08.139>
- Liao, C., Jung, S., Brown, D.G., Agrawal, A., 2016. Insufficient research on land grabbing. *Science* 353, 131–131. <https://doi.org/10.1126/science.aaf6565>
- Limburg, K.E., Breitburg, D., Swaney, D.P., Jacinto, G., 2020. Ocean Deoxygenation: A Primer. *One Earth* 2, 24–29. <https://doi.org/10.1016/j.oneear.2020.01.001>
- Lin, S., 2017. Climate change and algal blooms. Michigan State University, East Lansing.
- Lin, X., Ruess, P., Marston, L., Konar, M., 2019. Food flows between counties in the United States. *Environ. Res. Lett.* <https://doi.org/10.1088/1748-9326/ab29ae>
- Linderman, M.A., An, L., Bearer, S., He, G., Ouyang, Z., Liu, J., 2005. Modeling the spatio-temporal dynamics and interactions of households, landscapes, and giant panda habitat. *Ecological Modelling* 183, 47–65. <https://doi.org/10.1016/j.ecolmodel.2004.07.026>

- Liu, F., Page, A., Strode, S.A., Yoshida, Y., Choi, S., Zheng, B., Lamsal, L.N., Li, C., Krotkov, N.A., Eskes, H., A. R. van der, Veefkind, P., Levelt, P.F., Hauser, O.P., Joiner, J., 2020. Abrupt decline in tropospheric nitrogen dioxide over China after the outbreak of COVID-19. *Science Advances* 6, eabc2992. <https://doi.org/10.1126/sciadv.abc2992>
- Liu, J., 2020. Consumption patterns and biodiversity. *Biodiversity Programme of The Royal Society*.
- Liu, J., 2018. An integrated framework for achieving Sustainable Development Goals around the world. *Ecol. Econ. Soc.* 1, 11–17.
- Liu, J., 2017. Integration across a metacoupled world. *Ecology and Society* 22. <https://doi.org/10.5751/ES-09830-220429>
- Liu, Jianguo, Balmford, A., Bawa, K.S., 2022. Fuel, food and fertilizer shortage will hit biodiversity and climate. *Nature* 604, 425–425. <https://doi.org/10.1038/d41586-022-01061-y>
- Liu, Jing, Bowling, L., Kucharik, C., Jame, S., Baldos, U., Jarvis, L., Ramankutty, N., Hertel, T., 2022. Multi-scale Analysis of Nitrogen Loss Mitigation in the US Corn Belt. <https://doi.org/10.48550/arXiv.2206.07596>
- Liu, J., Dietz, T., Carpenter, S.R., Alberti, M., Folke, C., Moran, E., Pell, A.N., Deadman, P., Kratz, T., Lubchenco, J., Ostrom, E., Ouyang, Z., Provencher, W., Redman, C.L., Schneider, S.H., Taylor, W.W., 2007. Complexity of Coupled Human and Natural Systems. *Science* 317, 1513–1516. <https://doi.org/10.1126/science.1144004>
- Liu, J., Dou, Y., Batistella, M., Challies, E., Connor, T., Friis, C., Millington, J.D., Parish, E., Romulo, C.L., Silva, R.F.B., Triezenberg, H., Yang, H., Zhao, Z., Zimmerer, K.S., Huettmann, F., Treglia, M.L., Basher, Z., Chung, M.G., Herzberger, A., Lenschow, A., Mechiche-Alami, A., Newig, J., Roche, J., Sun, J., 2018a. Spillover systems in a telecoupled Anthropocene: typology, methods, and governance for global sustainability. *Current Opinion in Environmental Sustainability, System dynamics and sustainability* 33, 58–69. <https://doi.org/10.1016/j.cosust.2018.04.009>
- Liu, J., Herzberger, A., Kapsar, K., Carlson, A.K., Connor, T., 2019. What Is Telecoupling?, in: *Telecoupling*. Springer, pp. 19–48.
- Liu, J., Hull, V., Batistella, M., DeFries, R., Dietz, T., Fu, F., Hertel, T.W., Izaurrealde, R.C., Lambin, E.F., Li, S., Martinelli, L.A., McConnell, W.J., Moran, E.F., Naylor, R., Ouyang, Z., Polenske, K.R., Reenberg, A., Rocha, G. de M., Simmons, C.S., Verburg, P.H., Vitousek, P.M., Zhang, F., Zhu, C., 2013. Framing Sustainability in a Telecoupled World. *Ecol. Soc.* 18, 26. <https://doi.org/10.5751/ES-05873-180226>
- Liu, J., Hull, V., Godfray, H.C.J., Tilman, D., Gleick, P., Hoff, H., Pahl-Wostl, C., Xu, Z., Chung, M.G., Sun, J., Li, S., 2018b. Nexus approaches to global sustainable development. *Nature Sustainability* 1, 466. <https://doi.org/10.1038/s41893-018-0135-8>

- Liu, J., Hull, V., Luo, J., Yang, W., Liu, W., Viña, A., Vogt, C., Xu, Z., Yang, H., Zhang, J., An, L., Chen, X., Li, S., Ouyang, Z., Xu, W., Zhang, H., 2015a. Multiple telecouplings and their complex interrelationships. *Ecology and Society* 20. <https://doi.org/10.5751/ES-07868-200344>
- Liu, J., Hull, V., Moran, E., Nagendra, H., Swaffield, S.R., Turner, B.L., 2014. Applications of the telecoupling framework to land-change science. *Rethinking Global Land Use in an Urban Era* 119–140.
- Liu, J., Mooney, H., Hull, V., Davis, S.J., Gaskell, J., Hertel, T., Lubchenco, J., Seto, K.C., Gleick, P., Kremen, C., Li, S., 2015b. Systems integration for global sustainability. *Science* 347, 1258832. <https://doi.org/10.1126/science.1258832>
- Liu, J., Viña, A., Yang, W., Li, S., Xu, W., Zheng, H., 2018c. China's Environment on a Metacoupled Planet. *Annual Review of Environment and Resources* 43, 1–34. <https://doi.org/10.1146/annurev-environ-102017-030040>
- Liu, J., Yang, W., 2013. Integrated assessments of payments for ecosystem services programs. *Proceedings of the National Academy of Sciences* 110, 16297–16298. <https://doi.org/10.1073/pnas.1316036110>
- Liu, Jiajia, Zhang, T., Gibson, L., 2022. Transboundary conservation's rise. *Science* 375, 154. <https://doi.org/10.1126/science.abn5621>
- Liu, W., Li, X., Liu, H., Tang, Z., Guan, D., 2015. Estimating inter-regional trade flows in China: A sector-specific statistical model. *J. Geogr. Sci.* 25, 1247–1263. <https://doi.org/10.1007/s11442-015-1231-6>
- Mahjabin, T., Mejia, A., Grady, C., 2021. Virtual nitrogen and virtual water transfers embedded in food trade networks across the US. *Environ. Res. Lett.* 16, 045015. <https://doi.org/10.1088/1748-9326/abe06f>
- Malik, A., Egan, M., du Plessis, M., Lenzen, M., 2021a. Managing sustainability using financial accounting data: the value of input-output analysis. *Journal of Cleaner Production* 126128. <https://doi.org/10.1016/j.jclepro.2021.126128>
- Malik, A., Lafortune, G., Carter, S., Li, M., Lenzen, M., Kroll, C., 2021b. International spillover effects in the EU's textile supply chains: A global SDG assessment. *Journal of Environmental Management* 295, 113037. <https://doi.org/10.1016/j.jenvman.2021.113037>
- Marques, A., Verones, F., Kok, M.T., Huijbregts, M.A., Pereira, H.M., 2017. How to quantify biodiversity footprints of consumption? A review of multi-regional input–output analysis and life cycle assessment. *Current Opinion in Environmental Sustainability* 29, 75–81. <https://doi.org/10.1016/j.cosust.2018.01.005>
- Mason-D'Croz, D., Bogard, J.R., Herrero, M., Robinson, S., Sulser, T.B., Wiebe, K., Willenbockel, D., Godfray, H.C.J., 2020. Modelling the global economic consequences

- of a major African swine fever outbreak in China. *Nature Food* 1, 221–228.
<https://doi.org/10.1038/s43016-020-0057-2>
- Matli, V.R.R., Fang, S., Guinness, J., Rabalais, N.N., Craig, J.K., Obenour, D.R., 2018. A Space-Time Geostatistical Assessment of Hypoxia in the Northern Gulf of Mexico. *Environ. Sci. Technol.* <https://doi.org/10.1021/acs.est.8b03474>
- Matli, V.R.R., Laurent, A., Fennel, K., Craig, K., Krause, J., Obenour, D.R., 2020. Fusion-based hypoxia estimates: combining geostatistical and mechanistic models of dissolved oxygen variability. *Environ. Sci. Technol.* <https://doi.org/10.1021/acs.est.0c03655>
- Ménesguen, A., Lacroix, G., 2018. Modelling the marine eutrophication: A review. *Science of The Total Environment* 636, 339–354. <https://doi.org/10.1016/j.scitotenv.2018.04.183>
- Meter, K.J.V., Cappellen, P.V., Basu, N.B., 2018. Legacy nitrogen may prevent achievement of water quality goals in the Gulf of Mexico. *Science* 360, 427–430.
<https://doi.org/10.1126/science.aar4462>
- Mitsch, W.J., Day, J.W., Gilliam, J.W., Groffman, P.M., Hey, D.L., Randall, G.W., Wang, N., 2001. Reducing Nitrogen Loading to the Gulf of Mexico from the Mississippi River Basin: Strategies to Counter a Persistent Ecological Problem: Ecotechnology—the use of natural ecosystems to solve environmental problems—should be a part of efforts to shrink the zone of hypoxia in the Gulf of Mexico. *BioScience* 51, 373–388.
[https://doi.org/10.1641/0006-3568\(2001\)051\[0373:RNLTG\]2.0.CO;2](https://doi.org/10.1641/0006-3568(2001)051[0373:RNLTG]2.0.CO;2)
- Moran, D., Giljum, S., Kanemoto, K., Godar, J., 2020. From Satellite to Supply Chain: New Approaches Connect Earth Observation to Economic Decisions. *One Earth* 3, 5–8.
<https://doi.org/10.1016/j.oneear.2020.06.007>
- Moran, D.D., Lenzen, M., Kanemoto, K., Geschke, A., 2013. Does ecologically unequal exchange occur? *Ecological Economics* 89, 177–186.
<https://doi.org/10.1016/j.ecolecon.2013.02.013>
- Mou, N., Li, J., Sun, S., Yang, T., Zhang, L., Zhang, H., Liu, W., 2020. The impact of opening the Arctic Northeast Passage on the global maritime transportation network pattern using AIS data. *Arab J Geosci* 13, 419. <https://doi.org/10.1007/s12517-020-05432-5>
- Müller, M.F., Yoon, J., Gorelick, S.M., Avisse, N., Tilmant, A., 2016. Impact of the Syrian refugee crisis on land use and transboundary freshwater resources. *Proceedings of the National Academy of Sciences* 113, 14932–14937.
<https://doi.org/10.1073/pnas.1614342113>
- Munia, H.A., Guillaume, J.H.A., Wada, Y., Veldkamp, T., Virkki, V., Kummu, M., 2020. Future Transboundary Water Stress and Its Drivers Under Climate Change : A Global Study. *Earth's Future* 8, e2019EF001321. <https://doi.org/10.1029/2019EF001321>
- Munroe, D.K., Batistella, M., Friis, C., Gasparri, N.I., Lambin, E.F., Liu, J., Meyfroidt, P., Moran, E., Nielsen, J.Ø., 2019. Governing flows in telecoupled land systems. *Current*

- Opinion in Environmental Sustainability 38, 53–59.
<https://doi.org/10.1016/j.cosust.2019.05.004>
- Murphy, J.C., Hirsch, R.M., Sprague, L.A., 2013. Nitrate in the Mississippi River and its tributaries, 1980-2010: an update (USGS Numbered Series No. 2013–5169), Nitrate in the Mississippi River and its tributaries, 1980-2010: an update, Scientific Investigations Report. U.S. Geological Survey, Reston, VA. <https://doi.org/10.3133/sir20135169>
- Murphy, R.R., Kemp, W.M., Ball, W.P., 2011. Long-Term Trends in Chesapeake Bay Seasonal Hypoxia, Stratification, and Nutrient Loading. *Estuaries and Coasts* 34, 1293–1309. <https://doi.org/10.1007/s12237-011-9413-7>
- Murray, C.J., Muller-Karulis, B., Carstensen, J., Conley, D.J., Gustafsson, B., Andersen, J.H., 2019. Past, present and future eutrophication status of the Baltic Sea. *Front. Mar. Sci.* 6. <https://doi.org/10.3389/fmars.2019.00002>
- Naidoo, R., Fisher, B., 2020. Reset Sustainable Development Goals for a pandemic world. *Nature* 583, 198–201. <https://doi.org/10.1038/d41586-020-01999-x>
- Nepstad, D., McGrath, D., Stickler, C., Alencar, A., Azevedo, A., Swette, B., Bezerra, T., DiGiano, M., Shimada, J., Seroa da Motta, R., Armijo, E., Castello, L., Brando, P., Hansen, M.C., McGrath-Horn, M., Carvalho, O., Hess, L., 2014. Slowing Amazon deforestation through public policy and interventions in beef and soy supply chains. *Science* 344, 1118–1123. <https://doi.org/10.1126/science.1248525>
- Ning, X., Lin, C., Su, J., Liu, C., Hao, Q., Le, F., 2011. Long-term changes of dissolved oxygen, hypoxia, and the responses of the ecosystems in the East China Sea from 1975 to 1995. *J Oceanogr* 67, 59–75. <https://doi.org/10.1007/s10872-011-0006-7>
- NOAA, 2022. NOAA forecasts summer “dead zone” of nearly 5.4K square miles in Gulf of Mexico [WWW Document]. URL <http://www.noaa.gov/news-release/noaa-forecasts-summer-dead-zone-of-nearly-54k-square-miles-in-gulf-of-mexico> (accessed 7.31.22).
- NOAA, 2017. Gulf of Mexico ‘dead zone’ is the largest ever measured [WWW Document]. URL <https://www.noaa.gov/media-release/gulf-of-mexico-dead-zone-is-largest-ever-measured> (accessed 7.27.21).
- Norris, C., Norris, G., 2015. The Social Hotspots Database Context of the SHDB. pp. 52–73.
- Obenour, D.R., Michalak, A.M., Scavia, D., 2015. Assessing biophysical controls on Gulf of Mexico hypoxia through probabilistic modeling. *Ecological Applications* 25, 492–505. <https://doi.org/10.1890/13-2257.1>
- OECD, 2016. Environmental Labelling and Information Schemes.
- Oita, A., Malik, A., Kanemoto, K., Geschke, A., Nishijima, S., Lenzen, M., 2016. Substantial nitrogen pollution embedded in international trade. *Nature Geoscience* 9, 111–115. <https://doi.org/10.1038/ngeo2635>

- Oita, A., Wirasenjaya, F., Liu, J., Webeck, E., Matsubae, K., 2020. Trends in the food nitrogen and phosphorus footprints for Asia's giants: China, India, and Japan. *Resources, Conservation and Recycling* 157, 104752. <https://doi.org/10.1016/j.resconrec.2020.104752>
- Pastor, A.V., Palazzo, A., Havlik, P., Biemans, H., Wada, Y., Obersteiner, M., Kabat, P., Ludwig, F., 2019. The global nexus of food–trade–water sustaining environmental flows by 2050. *Nature Sustainability* 1. <https://doi.org/10.1038/s41893-019-0287-1>
- Pekel, J.-F., Cottam, A., Gorelick, N., Belward, A.S., 2016. High-resolution mapping of global surface water and its long-term changes. *Nature* 540, 418–422. <https://doi.org/10.1038/nature20584>
- Pelletier, C., Valero, S., Inglada, J., Champion, N., Dedieu, G., 2016. Assessing the robustness of Random Forests to map land cover with high resolution satellite image time series over large areas. *Remote Sensing of Environment* 187, 156–168. <https://doi.org/10.1016/j.rse.2016.10.010>
- Pitcher, G.C., Aguirre-Velarde, A., Breitburg, D., Cardich, J., Carstensen, J., Conley, D.J., Dewitte, B., Engel, A., Espinoza-Morriberón, D., Flores, G., Garçon, V., Graco, M., Grégoire, M., Gutiérrez, D., Martin Hernandez-Ayon, J., May Huang, H.-H., Isensee, K., Elena Jacinto, M., Levin, L., Lorenzo, A., Machu, E., Merma, L., Montes, I., Swa, N., Paulmier, A., Roman, M., Rose, K., Hood, R., Rabalais, N.N., Gro V. Salvanves, A., Salvatelli, R., Sánchez, S., Sifeddine, A., Wahab Tall, A., van der Plas, A.K., Yasuhara, M., Zhang, J., Zhu, Z., 2021. System controls of coastal and open ocean oxygen depletion. *Progress in Oceanography* 102613. <https://doi.org/10.1016/j.pocean.2021.102613>
- Poore, J., Nemecek, T., 2018. Reducing food's environmental impacts through producers and consumers. *Science* 360, 987–992. <https://doi.org/10.1126/science.aaq0216>
- Prag, A., Lyon, T., Russillo, A., 2016. Multiplication of Environmental Labelling and Information Schemes (ELIS): Implications for Environment and Trade. OECD, Paris. <https://doi.org/10.1787/5jm0p33z27wf-en>
- Puma, M.J., Bose, S., Chon, S.Y., Cook, B.I., 2015. Assessing the evolving fragility of the global food system. *Environ. Res. Lett.* 10, 024007. <https://doi.org/10.1088/1748-9326/10/2/024007>
- Puma, M.J., Konar, M., 2022. What the War in Ukraine Means for the World's Food Supply. *The New York Times*.
- Qin, S., Kuemmerle, T., Meyfroidt, P., Napolitano Ferreira, M., Gavier Pizarro, G.I., Periago, M.E., Reis, T.N.P. dos, Romero-Muñoz, A., Yanosky, A., 2022. The geography of international conservation interest in South American deforestation frontiers. *Conservation Letters* n/a, e12859. <https://doi.org/10.1111/conl.12859>

- Rabalais, N.N., Díaz, R.J., Levin, L.A., Turner, R.E., Gilbert, D., Zhang, J., 2010. Dynamics and distribution of natural and human-caused hypoxia. *Biogeosciences* 7, 585–619. <https://doi.org/10.5194/bg-7-585-2010>
- Rabalais, N.N., Turner, R.E., 2019. Gulf of Mexico Hypoxia: Past, Present, and Future. *Limnology and Oceanography Bulletin* n/a. <https://doi.org/10.1002/lob.10351>
- Rabalais, N.N., Turner, R.E., Díaz, R.J., Justić, D., 2009. Global change and eutrophication of coastal waters. *ICES Journal of Marine Science* 66, 1528–1537. <https://doi.org/10.1093/icesjms/fsp047>
- Rabotyagov, S.S., Kling, C.L., Gassman, P.W., Rabalais, N.N., Turner, R.E., 2014. The Economics of Dead Zones: Causes, Impacts, Policy Challenges, and a Model of the Gulf of Mexico Hypoxic Zone. *Review of Environmental Economics and Policy* 8, 58–79. <https://doi.org/10.1093/reep/ret024>
- Ray, R., Gallagher, K.P., Kring, W., Pitts, J., Simmons, B.A., 2021. Geolocated dataset of Chinese overseas development finance. *Sci Data* 8, 241. <https://doi.org/10.1038/s41597-021-01021-7>
- Reis, T.N.P. dos, Meyfroidt, P., zu Ermgassen, E.K.H.J., West, C., Gardner, T., Bager, S., Croft, S., Lathuillière, M.J., Godar, J., 2020. Understanding the Stickiness of Commodity Supply Chains Is Key to Improving Their Sustainability. *One Earth* 3, 100–115. <https://doi.org/10.1016/j.oneear.2020.06.012>
- Roley, S.S., Tank, J.L., Tyndall, J.C., Witter, J.D., 2016. How cost-effective are cover crops, wetlands, and two-stage ditches for nitrogen removal in the Mississippi River Basin? *Water Resour. Econ.* 15, 43–56. <https://doi.org/10.1016/j.wre.2016.06.003>
- Roy, E.D., Wagner, C.R.H., Niles, M.T., 2021. Hot spots of opportunity for improved cropland nitrogen management across the United States. *Environ. Res. Lett.* 16, 035004. <https://doi.org/10.1088/1748-9326/abd662>
- Sachs, J., Kroll, C., Lafortune, G., Fuller, G., Woelm, F., 2021. Sustainable Development Report 2021, The Decade of Action for the Sustainable Development Goals. Cambridge University Press, Cambridge.
- Sachs, J., Lafortune, G., Kroll, C., Fuller, G., Woelm, F., 2022. From Crisis to Sustainable Development: the SDGs as Roadmap to 2030 and Beyond. Sustainable Development Report 2022. Cambridge University Press, Cambridge.
- Sachs, J., Schmidt-Traub, G., Kroll, C., Durand-Delacre, D., Teksoz, K., 2017. SDG Index and Dashboards Report 2017. Bertelsmann Stiftung and Sustainable Development Solutions Network (SDSN), New York.
- Sachs, J., Schmidt-Traub, G., Kroll, C., Lafortune, G., Fuller, G., 2020. Sustainable Development Report 2020, The Sustainable Development Goals and COVID-19. Cambridge University Press, Cambridge.

- SafeGraph, 2022. SafeGraph Docs [WWW Document]. SafeGraph. URL <https://docs.safegraph.com/docs/about-safegraph> (accessed 7.17.22).
- Scavia, D., Bertani, I., Obenour, D.R., Turner, R.E., Forrest, D.R., Katin, A., 2017. Ensemble modeling informs hypoxia management in the northern Gulf of Mexico. *PNAS* 114, 8823–8828. <https://doi.org/10.1073/pnas.1705293114>
- Scavia, D., Evans, M.A., Obenour, D.R., 2013. A Scenario and Forecast Model for Gulf of Mexico Hypoxic Area and Volume. *Environ. Sci. Technol.* 47, 10423–10428. <https://doi.org/10.1021/es4025035>
- Schim van der Loeff, W., Godar, J., Prakash, V., 2018. A spatially explicit data-driven approach to calculating commodity-specific shipping emissions per vessel. *Journal of Cleaner Production* 205, 895–908. <https://doi.org/10.1016/j.jclepro.2018.09.053>
- Schipanski, M.E., Bennett, E.M., 2012. The Influence of Agricultural Trade and Livestock Production on the Global Phosphorus Cycle. *Ecosystems* 15, 256–268. <https://doi.org/10.1007/s10021-011-9507-x>
- Schirpke, U., Tappeiner, U., Tasser, E., 2019. A transnational perspective of global and regional ecosystem service flows from and to mountain regions. *Scientific Reports* 9, 6678. <https://doi.org/10.1038/s41598-019-43229-z>
- Schmidt-Traub, G., Kroll, C., Teksoz, K., Durand-Delacre, D., Sachs, J.D., 2017. National baselines for the Sustainable Development Goals assessed in the SDG Index and Dashboards. *Nature Geosci* 10, 547–555. <https://doi.org/10.1038/ngeo2985>
- Schröter, M., Koellner, T., Alkemade, R., Arnhold, S., Bagstad, K.J., Erb, K.-H., Frank, K., Kastner, T., Kissinger, M., Liu, J., López-Hoffman, L., Maes, J., Marques, A., Martín-López, B., Meyer, C., Schulp, C.J.E., Thober, J., Wolff, S., Bonn, A., 2018. Interregional flows of ecosystem services: Concepts, typology and four cases. *Ecosystem Services*, *Global Flows of Ecosystem Services* 31, 231–241. <https://doi.org/10.1016/j.ecoser.2018.02.003>
- Seegers, B.N., Stumpf, R.P., Schaeffer, B.A., Loftin, K.A., Werdell, P.J., 2018. Performance metrics for the assessment of satellite data products: an ocean color case study. *Opt. Express*, *OE* 26, 7404–7422. <https://doi.org/10.1364/OE.26.007404>
- Sethi, T., Custer, S., Turner, J., Sims, J., DiLorenzo, M., Latourell, R., 2017. Realizing Agenda 2030: Will Donor Dollars and Country Priorities Align with Global Goals. *AidData at the College of William & Mary, Williamsburg, VA*.
- Shao, Z., Cai, J., Fu, P., Hu, L., Liu, T., 2019. Deep learning-based fusion of Landsat-8 and Sentinel-2 images for a harmonized surface reflectance product. *Remote Sensing of Environment* 235, 111425. <https://doi.org/10.1016/j.rse.2019.111425>
- Shapiro, J.S., 2020. The Environmental Bias of Trade Policy. *The Quarterly Journal of Economics*. <https://doi.org/10.1093/qje/qjaa042>

- Shen, F., Tang, R., Sun, X., Liu, D., 2019. Simple methods for satellite identification of algal blooms and species using 10-year time series data from the East China Sea. *Remote Sensing of Environment* 235, 111484. <https://doi.org/10.1016/j.rse.2019.111484>
- Sikor, T., Auld, G., Bebbington, A.J., Benjaminsen, T.A., Gentry, B.S., Hunsberger, C., Izac, A.-M., Margulis, M.E., Plieninger, T., Schroeder, H., Upton, C., 2013. Global land governance: from territory to flow? *Current Opinion in Environmental Sustainability, Human settlements and industrial systems* 5, 522–527. <https://doi.org/10.1016/j.cosust.2013.06.006>
- Simas, M.S., Golsteijn, L., Huijbregts, M.A.J., Wood, R., Hertwich, E.G., 2014. The “Bad Labor” Footprint: Quantifying the Social Impacts of Globalization. *Sustainability* 6, 7514–7540. <https://doi.org/10.3390/su6117514>
- Sinha, E., Michalak, A.M., Balaji, V., 2017. Eutrophication will increase during the 21st century as a result of precipitation changes. *Science* 357, 405–408. <https://doi.org/10.1126/science.aan2409>
- Smith, M.D., Oglend, A., Kirkpatrick, A.J., Asche, F., Benneer, L.S., Craig, J.K., Nance, J.M., 2017. Seafood prices reveal impacts of a major ecological disturbance. *PNAS* 201617948. <https://doi.org/10.1073/pnas.1617948114>
- Söderström, J., 2008. Cultural Distance : An Assessment of Cultural Effects on Trade Flows.
- Sonderegger, G., Oberlack, C., Llopis, J., Verburg, P., Heinemann, A., 2020. Telecoupling visualizations through a network lens: a systematic review. *Ecology and Society* 25. <https://doi.org/10.5751/ES-11830-250447>
- Stokal, M., Kroeze, C., Wang, M., Bai, Z., Ma, L., 2016. The MARINA model (Model to Assess River Inputs of Nutrients to seAs): Model description and results for China. *Science of The Total Environment* 562, 869–888. <https://doi.org/10.1016/j.scitotenv.2016.04.071>
- Sun, J., Mooney, H., Wu, W., Tang, H., Tong, Y., Xu, Z., Huang, B., Cheng, Y., Yang, X., Wei, D., Zhang, F., Liu, J., 2018. Importing food damages domestic environment: Evidence from global soybean trade. *PNAS* 115, 5415–5419. <https://doi.org/10.1073/pnas.1718153115>
- Tadesse, B., White, R., 2010. Cultural distance as a determinant of bilateral trade flows: do immigrants counter the effect of cultural differences? *Applied Economics Letters* 17, 147–152. <https://doi.org/10.1080/13504850701719983>
- Takayama, P.B., 2013. Effects of the concept of cultural distance on the international trade of ‘telenovelas.’ *Latin America Research Review* 47, 61–78.
- Teluguntla, P., Thenkabail, P.S., Oliphant, A., Xiong, J., Gumma, M.K., Congalton, R.G., Yadav, K., Huete, A., 2018. A 30-m landsat-derived cropland extent product of Australia and China using random forest machine learning algorithm on Google Earth Engine

- cloud computing platform. *ISPRS Journal of Photogrammetry and Remote Sensing* 144, 325–340. <https://doi.org/10.1016/j.isprsjprs.2018.07.017>
- Tian, H., Xu, R., Pan, S., Yao, Y., Bian, Z., Cai, W.-J., Hopkinson, C.S., Justic, D., Lohrenz, S., Lu, C., Ren, W., Yang, J., 2020. Long-Term Trajectory of Nitrogen Loading and Delivery From Mississippi River Basin to the Gulf of Mexico. *Global Biogeochemical Cycles* 34, e2019GB006475. <https://doi.org/10.1029/2019GB006475>
- Tollefson, J., 2022. What the war in Ukraine means for energy, climate and food. *Nature* 604, 232–233. <https://doi.org/10.1038/d41586-022-00969-9>
- Tomasetti, S.J., Gobler, C.J., 2020. Dissolved oxygen and pH criteria leave fisheries at risk. *Science* 368, 372–373. <https://doi.org/10.1126/science.aba4896>
- Tromboni, F., Liu, J., Ziaco, E., Breshears, D.D., Thompson, K.L., Dodds, W.K., Dahlin, K.M., LaRue, E.A., Thorp, J.H., Viña, A., Laguë, M.M., Maasri, A., Yang, H., Chandra, S., Fei, S., 2021. Macrosystems as metacoupled human and natural systems. *Frontiers in Ecology and the Environment* 19, 20–29. <https://doi.org/10.1002/fee.2289>
- Tu, Q., Parvatker, A., Garedew, M., Harris, C., Eckelman, M., Zimmerman, J.B., Anastas, P.T., Lam, C.H., 2021. Electrocatalysis for Chemical and Fuel Production: Investigating Climate Change Mitigation Potential and Economic Feasibility. *Environ. Sci. Technol.* 55, 3240–3249. <https://doi.org/10.1021/acs.est.0c07309>
- Tukker, A., Dietzenbacher, E., 2013. Global Multiregional Input–Output Frameworks: An Introduction and Outlook. *Economic Systems Research* 25, 1–19. <https://doi.org/10.1080/09535314.2012.761179>
- Turner, J., 2019. Financing the SDGs: Evidence in Four Countries. AidData at William & Mary, Williamsburg, VA.
- Turner, J., Burgess, B., 2019. Estimating Financing to the Sustainable Development Goals, Version 2.0. Williamsburg, VA: AidData at William & Mary.
- Turner, R.E., Rabalais, N.N., Justić, D., 2012. Predicting summer hypoxia in the northern Gulf of Mexico: Redux. *Marine Pollution Bulletin* 64, 319–324. <https://doi.org/10.1016/j.marpolbul.2011.11.008>
- UN, 2019. Global indicator framework for the Sustainable Development Goals and targets of the 2030 Agenda for Sustainable Development.
- UN, 2018. Financing for SDGs breaking the bottlenecks of investment from policy to impact. Technical report. <https://www.un.org/pga/72/wp-content/uploads/sites/51/2018/05/Financing-for-SDGs-29-May.pdf>, New York.
- UNEP-DHI, U.N.E., UNEP, U.N.E., 2016. Transboundary River Basins: Status and Trends, Summary for Policy Makers. United Nations Environment Programme (UNEP), Nairobi.

- UNHCR, 2022. Ukraine Refugee Situation [WWW Document]. URL <https://data.unhcr.org/en/situations/ukraine> (accessed 7.18.22).
- US Census Bureau, U.C., 2020. Commodity Flow Survey Methodology [WWW Document]. Census.gov. URL <https://www.census.gov/programs-surveys/cfs/technical-documentation/methodologies.html> (accessed 7.5.22).
- U.S. Department of Transportation, B. of T.S., U.S. Department of Commerce, U.S.C.B., 2020. 2017 Commodity Flow Survey Datasets: 2017 CFS Public Use File (PUF) [WWW Document]. Census.gov. URL <https://www.census.gov/data/datasets/2017/econ/cfs/historical-datasets.html> (accessed 7.4.22).
- US EPA, 2008. Gulf Hypoxia Action Plan 2008 for Reducing Mitigating, and Controlling Hypoxia in the Northern Gulf of Mexico and Improving Water Quality in the Mississippi River Basin. Washington, DC.
- US EPA, O., 2015. Hypoxia Task Force Reassessment 2013: Assessing Progress Made Since 2008 (Reports and Assessments).
- USDA, 2022. Livestock and Meat Domestic Data [WWW Document]. U.S. Department of Agriculture website. URL <https://www.ers.usda.gov/data-products/livestock-and-meat-domestic-data/> (accessed 7.4.22).
- USDA ERS, 2022. State Agricultural Trade Data [WWW Document]. URL [https://www.ers.usda.gov/data-products/state-agricultural-trade-data/state-agricultural-trade-data/#State%20Trade%20by%20Country%20of%20Origin%20and%20Destination%20\(Fiscal%20Quarters\)](https://www.ers.usda.gov/data-products/state-agricultural-trade-data/state-agricultural-trade-data/#State%20Trade%20by%20Country%20of%20Origin%20and%20Destination%20(Fiscal%20Quarters)) (accessed 7.13.22).
- Vanham, D., Leip, A., Galli, A., Kastner, T., Bruckner, M., Uwizeye, A., van Dijk, K., Ercin, E., Dalin, C., Brandão, M., Bastianoni, S., Fang, K., Leach, A., Chapagain, A., Van der Velde, M., Sala, S., Pant, R., Mancini, L., Monforti-Ferrario, F., Carmona-Garcia, G., Marques, A., Weiss, F., Hoekstra, A.Y., 2019. Environmental footprint family to address local to planetary sustainability and deliver on the SDGs. *Science of The Total Environment* 693, 133642. <https://doi.org/10.1016/j.scitotenv.2019.133642>
- Verschuur, J., Koks, E., Li, S., Hall, J., 2022. Multi-Hazard Risk to Global Port Infrastructure and Resulting Trade and Logistics Losses.
- Verschuur, J., Koks, E.E., Hall, J.W., 2021. Observed impacts of the COVID-19 pandemic on global trade. *Nature Human Behaviour* 5, 305–307. <https://doi.org/10.1038/s41562-021-01060-5>
- Vinca, A., Parkinson, S., Riahi, K., Byers, E., Siddiqi, A., Muhammad, A., Ilyas, A., Yogeswaran, N., Willaarts, B., Magnuszewski, P., Awais, M., Rowe, A., Djilali, N., 2020. Transboundary cooperation a potential route to sustainable development in the Indus basin. *Nature Sustainability* 1–9. <https://doi.org/10.1038/s41893-020-00654-7>

- Walker, N.D., Rabalais, N.N., 2006. Relationships among satellite chlorophyll a , river inputs, and hypoxia on the Louisiana Continental shelf, Gulf of Mexico. *Estuaries and Coasts* 29, 1081–1093. <https://doi.org/10.1007/bf02781811>
- Wan, L., Kendall, A.D., Martin, S.L., Hyndman, D.W., 2019. Quantifying Nutrient Loads to the Great Lakes Coastline with a Spatially Explicit Nutrient Transport Model 2019, H41R-2000.
- Wang, J., Karakoc, D.B., Konar, M., 2022. The carbon footprint of cold chain food flows in the United States. *Environ. Res.: Infrastruct. Sustain.* 2, 021002. <https://doi.org/10.1088/2634-4505/ac676d>
- Wang, L., Justić, D., 2009. A modeling study of the physical processes affecting the development of seasonal hypoxia over the inner Louisiana-Texas shelf: Circulation and stratification. *Continental Shelf Research* 29, 1464–1476. <https://doi.org/10.1016/j.csr.2009.03.014>
- Wang, Y., Hong, S., Wang, J., Lin, J., Mu, H., Wei, L., Wang, Z., Bryan, B.A., 2022. Complex regional telecoupling between people and nature revealed via quantification of trans-boundary ecosystem service flows. *People and Nature* 4, 274–292. <https://doi.org/10.1002/pan3.10298>
- Wang, Z., Zhang, L., Li, X., Li, Y., Fu, B., 2021. Integrating ecosystem service supply and demand into ecological risk assessment: a comprehensive framework and case study. *Landscape Ecol* 36, 2977–2995. <https://doi.org/10.1007/s10980-021-01285-9>
- West, P.C., Gerber, J.S., Engstrom, P.M., Mueller, N.D., Brauman, K.A., Carlson, K.M., Cassidy, E.S., Johnston, M., MacDonald, G.K., Ray, D.K., Siebert, S., 2014. Leverage points for improving global food security and the environment. *Science* 345, 325–328. <https://doi.org/10.1126/science.1246067>
- Wezeman, P.D., Fleurant, A., Kuimova, A., Tian, N., Wezeman, S.T., 2018. Trends in International Arms Transfers, 2017.
- Wiedmann, T., Lenzen, M., 2018. Environmental and social footprints of international trade. *Nature Geosci* 11, 314–321. <https://doi.org/10.1038/s41561-018-0113-9>
- Wiedmann, T.O., Schandl, H., Lenzen, M., Moran, D., Suh, S., West, J., Kanemoto, K., 2015. The material footprint of nations. *Proceedings of the national academy of sciences* 112, 6271–6276.
- Wood, S.A., Smith, M.R., Fanzo, J., Remans, R., DeFries, R.S., 2018. Trade and the equitability of global food nutrient distribution. *Nature Sustainability* 1, 34–37. <https://doi.org/10.1038/s41893-017-0008-6>
- Wood, S.N., Bravington, M.V., Hedley, S.L., 2008. Soap film smoothing. *Journal of the Royal Statistical Society: Series B (Statistical Methodology)* 70, 931–955. <https://doi.org/10.1111/j.1467-9868.2008.00665.x>

- Xia, Z., Li, Y., Chen, R., Sengupta, D., Guo, X., Xiong, B., Niu, Y., 2022. Mapping the rapid development of photovoltaic power stations in northwestern China using remote sensing. *Energy Reports* 8, 4117–4127. <https://doi.org/10.1016/j.egyr.2022.03.039>
- Xiao, Y., Lenzen, M., Benoît-Norris, C., Norris, G.A., Murray, J., Malik, A., 2018a. The Corruption Footprints of Nations. *Journal of Industrial Ecology* 22, 68–78. <https://doi.org/10.1111/jiec.12537>
- Xiao, Y., Murray, J., Lenzen, M., 2018b. International trade linked with disease burden from airborne particulate pollution. *Resources, Conservation and Recycling* 129, 1–11. <https://doi.org/10.1016/j.resconrec.2017.10.002>
- Xiao, Y., Norris, C.B., Lenzen, M., Norris, G., Murray, J., 2017. How social footprints of nations can assist in achieving the sustainable development goals. *Ecological Economics* 135, 55–65.
- Xinhua News Agency, 2021. South-to-North Water Diversion Project transferred nearly 50 billion cubic meters of water to the north in seven years (In Chinese) [WWW Document]. URL http://www.gov.cn/xinwen/2021-12/12/content_5660275.htm (accessed 7.19.22).
- Xiong, C., Hu, S., Yang, M., Luo, W., Zhang, L., 2020. Mobile device data reveal the dynamics in a positive relationship between human mobility and COVID-19 infections. *PNAS* 117, 27087–27089. <https://doi.org/10.1073/pnas.2010836117>
- Xu, Z., Chau, S.N., Chen, X., Zhang, J., Li, Yingjie, Dietz, T., Wang, J., Winkler, J.A., Fan, F., Huang, B., Li, S., Wu, S., Herzberger, A., Tang, Y., Hong, D., Li, Yunkai, Liu, J., 2020a. Assessing progress towards sustainable development over space and time. *Nature* 577, 74–78. <https://doi.org/10.1038/s41586-019-1846-3>
- Xu, Z., Chau, S.N., Ruzzenenti, F., Connor, T., Li, Y., Tang, Y., Li, D., Gong, M., Liu, J., 2019a. Evolution of multiple global virtual material flows. *Science of The Total Environment* 658, 659–668. <https://doi.org/10.1016/j.scitotenv.2018.12.169>
- Xu, Z., Chen, X., Liu, J., Zhang, Y., Chau, S., Bhattarai, N., Wang, Y., Li, Yingjie, Connor, T., Li, Yunkai, 2020b. Impacts of irrigated agriculture on food–energy–water–CO₂ nexus across metacoupled systems. *Nature Communications* 11, 5837. <https://doi.org/10.1038/s41467-020-19520-3>
- Xu, Z., Li, Yingjie, Chau, S.N., Dietz, T., Li, C., Wan, L., Zhang, J., Zhang, L., Li, Yunkai, Chung, M.G., Liu, J., 2020c. Impacts of international trade on global sustainable development. *Nature Sustainability* 1–8. <https://doi.org/10.1038/s41893-020-0572-z>
- Xu, Z., Li, Yingjie, Herzberger, A., Chen, X., Gong, M., Kapsar, K., Hovis, C., Whyte, J., Tang, Y., Li, Yunkai, Liu, J., 2019b. Interactive national virtual water-energy nexus networks. *Science of The Total Environment* 673, 128–135. <https://doi.org/10.1016/j.scitotenv.2019.03.298>

- Yang, H., Lupi, F., Zhang, J., Chen, X., Liu, J., 2018. Feedback of telecoupling: the case of a payments for ecosystem services program. *Ecology and Society* 23. <https://doi.org/10.5751/ES-10140-230245>
- Yang, H., Simmons, B.A., Ray, R., Nolte, C., Gopal, S., Ma, Y., Ma, X., Gallagher, K.P., 2021. Risks to global biodiversity and Indigenous lands from China's overseas development finance. *Nat Ecol Evol* 5, 1520–1529. <https://doi.org/10.1038/s41559-021-01541-w>
- Yao, G., Zhang, X., Davidson, E.A., Taheripour, F., 2021. The increasing global environmental consequences of a weakening US–China crop trade relationship. *Nat Food* 2, 578–586. <https://doi.org/10.1038/s43016-021-00338-1>
- You, N., Dong, J., Huang, J., Du, G., Zhang, G., He, Y., Yang, T., Di, Y., Xiao, X., 2021. The 10-m crop type maps in Northeast China during 2017–2019. *Scientific Data* 8, 41. <https://doi.org/10.1038/s41597-021-00827-9>
- Yu, Y., Feng, K., Hubacek, K., 2013. Tele-connecting local consumption to global land use. *Global Environmental Change* 23, 1178–1186. <https://doi.org/10.1016/j.gloenvcha.2013.04.006>
- Zeng, Y., Runting, R.K., Watson, J.E.M., Carrasco, L.R., 2021. Telecoupled environmental impacts are an obstacle to meeting the sustainable development goals. *Sustainable Development* n/a. <https://doi.org/10.1002/sd.2229>
- Zhang, Q., Jiang, X., Tong, D., Davis, S.J., Zhao, H., Geng, G., Feng, T., Zheng, B., Lu, Z., Streets, D.G., Ni, R., Brauer, M., van Donkelaar, A., Martin, R.V., Huo, H., Liu, Z., Pan, D., Kan, H., Yan, Y., Lin, J., He, K., Guan, D., 2017. Transboundary health impacts of transported global air pollution and international trade. *Nature* 543, 705–709. <https://doi.org/10.1038/nature21712>
- Zhao, C., Liu, B., Piao, S., Wang, X., Lobell, D.B., Huang, Y., Huang, M., Yao, Y., Bassu, S., Ciais, P., Durand, J.-L., Elliott, J., Ewert, F., Janssens, I.A., Li, T., Lin, E., Liu, Q., Martre, P., Müller, C., Peng, S., Peñuelas, J., Ruane, A.C., Wallach, D., Wang, T., Wu, D., Liu, Z., Zhu, Y., Zhu, Z., Asseng, S., 2017. Temperature increase reduces global yields of major crops in four independent estimates. *PNAS* 114, 9326–9331. <https://doi.org/10.1073/pnas.1701762114>
- Zhao, H., Chang, J., Havlík, P., van Dijk, M., Valin, H., Janssens, C., Ma, L., Bai, Z., Herrero, M., Smith, P., Obersteiner, M., 2021. China's future food demand and its implications for trade and environment. *Nat Sustain* 1–10. <https://doi.org/10.1038/s41893-021-00784-6>
- Zhao, X., Liu, J., Liu, Q., Tillotson, M.R., Guan, D., Hubacek, K., 2015. Physical and virtual water transfers for regional water stress alleviation in China. *Proceedings of the National Academy of Sciences* 112, 1031–1035. <https://doi.org/10.1073/pnas.1404130112>
- Zhao, Z., Cai, M., Wang, F., Winkler, J.A., Connor, T., Chung, M.G., Zhang, J., Yang, H., Xu, Z., Tang, Y., Ouyang, Z., Zhang, H., Liu, J., 2020. Synergies and tradeoffs among

- Sustainable Development Goals across boundaries in a metacoupled world. *Science of The Total Environment* 141749. <https://doi.org/10.1016/j.scitotenv.2020.141749>
- Zhou, F., Chai, F., Huang, D., Wells, M., Ma, X., Meng, Q., Xue, H., Xuan, J., Wang, P., Ni, X., Zhao, Q., Liu, C., Su, J., Li, H., 2020. Coupling and Decoupling of High Biomass Phytoplankton Production and Hypoxia in a Highly Dynamic Coastal System: The Changjiang (Yangtze River) Estuary. *Frontiers in Marine Science* 7.
- Zhou, Y., Scavia, D., Michalak, A.M., 2014. Nutrient loading and meteorological conditions explain interannual variability of hypoxia in Chesapeake Bay. *Limnology and Oceanography* 59, 373–384. <https://doi.org/10.4319/lo.2014.59.2.0373>
- Zhu, Z.-Y., Zhang, J., Wu, Y., Zhang, Y.-Y., Lin, J., Liu, S.-M., 2011. Hypoxia off the Changjiang (Yangtze River) Estuary: Oxygen depletion and organic matter decomposition. *Marine Chemistry* 125, 108–116. <https://doi.org/10.1016/j.marchem.2011.03.005>
- zu Ermgassen, E.K.H.J., Bastos Lima, M.G., Bellfield, H., Dontenville, A., Gardner, T., Godar, J., Heilmayr, R., Indenbaum, R., dos Reis, T.N.P., Ribeiro, V., Abu, I., Szantoi, Z., Meyfroidt, P., 2022. Addressing indirect sourcing in zero deforestation commodity supply chains. *Science Advances* 8, eabn3132. <https://doi.org/10.1126/sciadv.abn3132>